Research of fuel injection and combustion control for maximum fuel efficiency and minimum emissions in a heavy-duty diesel engine

A thesis submitted for the degree of
Doctor of Philosophy

by
Wei Guan

Department of Mechanical and Aerospace Engineering
College of Engineering, Design and Physical Sciences
Brunel University London

February 2019

Abstract

The simultaneously requirements of ultra-low emissions and lower operating cost are driving the technology development of heavy-duty (HD) diesel engines. In order to meet the stringent emission regulations and maximise the fuel efficiency and thus minimise the greenhouse gases (GHG), significant efforts have been made to develop highly efficient and clean diesel combustion. In addition to the challenge of the trade-off between exhaust emissions and fuel efficiency, HD diesel engines experience low exhaust gas temperature (EGT) at low-load operation, which significantly reduces the effectiveness of the exhaust aftertreatment systems. In response to these issues, variable valve actuation (VVA)-based advanced combustion control technologies have been researched to curb engine-out emissions and maximise fuel efficiency as well as improving the low-load thermal management, helping to minimise total engine operational cost (EOC).

This research started with an investigation into the influence of injector nozzle designs on engine combustion, emissions, and performance. This was followed by the systematic study of Miller cycle operation over the engine speed-load map with and without exhaust gas recirculation (EGR). Experimental work was carried out in a single cylinder HD diesel engine equipped with a high pressure common rail fuel injection system, an external cooled EGR circuit, and a VVA system. The results showed that the injector geometry optimization is necessary to improve the trade-off between engine-out emissions and fuel efficiency. Special attention should be paid to the interaction of spray-bowl and spray-wall under different operating conditions. The introduction of residual gases via an intake valve re-opening during the exhaust stroke was demonstrated as an effective combustion control strategy for exhaust thermal management at the low load operation of 2.2 bar indicated mean effective pressure (IMEP). Additionally, the combined “Miller cycle + EGR + post injection” strategy was shown to beneficial for engine-out emission reduction and EGT control at 6 bar IMEP. Furthermore, the effectiveness of Miller cycle with or without EGR was examined from low to full engine loads at constant intake pressure and constant lambda conditions. A cost-benefit and the cycle-averaged results calculated over the World Harmonized Stationary Cycle (WHSC) were presented and analysed. The results showed that the “Miller cycle + EGR” strategy with a constant lambda attained the highest corrected net indicated efficiency over the WHSC by up to 8% in comparison to the baseline without EGR. Finally, the potentials of different combustion control strategies to meet the Euro VI emission regulation were assessed at different NOx aftertreatment efficiencies. Overall, this study has presented promising cost-effective emission control and fuel efficiency technologies that could be suitable for the “SCR-only” and “SCR + EGR” technical routes for the future HD diesel engines.

List of Contents

List of illustrations

List of tables

Publications related to this research

[1] Guan, W., Pedrozo, V., Zhao, H., Ban, Z., and Lin, T., “Investigation of EGR and Miller Cycle for NOx Emissions and Exhaust Temperature Control of a Heavy-Duty Diesel Engine,” SAE Tech. Pap., 2017, doi:10.4271/2017-01-2227.

[2] Guan, W., Zhao, H., Ban, Z., and Lin, T., “Exploring alternative combustion control strategies for low-load exhaust gas temperature management of a heavy-duty diesel engine,” *Int. J. Engine Res.* 146808741875558, 2018, doi:10.1177/1468087418755586.

[3] Guan, W., Pedrozo, V., Zhao, H., Ban, Z., and Lin, T., “Exploring the NOx Reduction Potential of Miller Cycle and EGR on a HD Diesel Engine Operating at Full Load,” SAE Tech. Pap. 2018–April:1–12, 2018, doi:10.4271/2018-01-0243.

[4] Guan, W., Pedrozo, B., Zhao, H., Ban, Z., and Lin, T., “Miller cycle combined with exhaust gas recirculation and post–fuel injection for emissions and exhaust gas temperature control of a heavy-duty diesel engine,” Int. J. Engine Res. 1468087419830019, 2019, doi:10.1177/1468087419830019.

[5] Guan, W., Pedrozo, B., Zhao, H., Ban, Z., and Lin, T., “Variable valve actuation – based combustion control strategies for efficiency improvement and emissions control in a heavy-duty diesel engine,” Int. J. Engine Res., 2019, doi:10.1177/1468087419846031.

[6] Guan, W., Pedrozo, V., Wang, X., Zhao, H., Ban, Z., and Lin, T., “Exploring the potential of Miller cycle with and without EGR for maximum efficiency and minimum exhaust emissions in a heavy-duty diesel engine” (Peer review in process)

[7] Guan, W., Ban, Z., Zhao, H., Lin, T., and Zheng, Z., “Effective Engine Technologies for Optimum Efficiency and Emission control of the Heavy-Duty diesel engine” (In the process of correction).

[8] Guan, W., Ban, Z., Zhao, H., and Lin, T., “Investigation of Miller cycle with high intake boosted for emissions and fuel consumption reduction on a heavy-duty diesel engine operating at different loads” (In the process of correction).

[9] Guan, W., Ban, Z., Zhao, H., and Lin, T., "Influence of injector nozzle geometry on achieving high efficiency and low emissions in a heavy-duty diesel engine" (In the process of correction).

Acknowledgements

My PhD study at Brunel University London has been a wonderful journey, which is memorable, challenging, and extremely rewarding experience. First and foremost, I would like to express my deep gratitude to my supervisor, Professor Hua Zhao, for providing me the fully funded position and support necessary to be able to follow my dreams, and all his help and invaluable guidance on my research.

I would like to acknowledge Guangxi Yuchai Machinery Company, without whose financial support my PhD studies would not have been possible. Special thanks to Dr Zhiqiang Lin, Dr Tiejian Lin, and Dr Zhibo Ban for their excellent supports and invaluable guidance on internal combustion engine testing. I would also like to thank all my friends and other engineers at Yuchai for share of experience and knowledge as well as their help.

I would like to thank my friends and colleagues in Brunel engines group, particularly Thompson, Yan, Yuanping, Reza, Ward, Mahmoud, Khalifa, Akira, Alessandro, Apostolos, Dengquan, Zinong, Meghna, Ray, and Enshen for providing support and their friendship. Special thanks to Vini and Xinyan for their professional advice that always helped to keep me motivated. I couldn't have asked for a better colleague and friend and I will never forget all the great moments we have shared together. I would also like to thank all my other colleagues and friends for their friendship and support that made this a meaningful time. I am appreciative for the assistance and indispensable help of all the technicians in the lab, particularly Andy, Eamon, William, and Chris.

I would also like to acknowledge several individuals that have helped me over last few years. I am deeply grateful to Professor Mingfa Yao, Dr Zunqing Zheng, and Dr Haifeng Liu at Tianjin University, as well as Professor Haozhong Huang and Dr Chunlan Mo at Guangxi University for helping and encouraging me to pursue my dream here. Thank you as well to academic visitors Professor Zhongshu Wang, Dr Defu Zhang, Dr Jie Zhang, Dr Xiuyong Shi, and Dr Zhaojie Shen for all the help you provided. Particular thanks to Ms Jady Wang and Professor Jianguo Lin for their kind help and encouragement.

Finally, my most sincere gratitude goes to my parents, my brothers and sister, for their endless love, unwavering support, and encouragement. Last and foremost, I am eternally and deeply grateful to my wife, Zilian Gan, for her love and support as well as daily encouragement and happiness, giving me the strength to overcome the difficulties encountered during the period of pursuing my dreams.

Nomenclature

1D: one-dimensional
2EVO: exhaust valve re-opening
2IVO: intake valve re-opening
ASC: ammonia slip catalyst
ATDC: after firing top dead centre
ATS: aftertreatment system
BMEP: brake mean effective pressure
C_p: specific heat at constant pressure
C_v: specific heat at constant volume
CA10: crank angle of 10% cumulative heat release
CA10-CA50: 10-50% cumulative heat release
CA10-CA90: combustion duration or 10-90% cumulative heat release
CA50: combustion phasing or crank angle of 50% cumulative heat release
CA90: crank angle of 90% cumulative heat release
CAD: crank angle degree
CARB: California air resource board
CDC: conventional diesel combustion
CFD: computational fluid dynamics
CI: compression ignition
CO: carbon monoxide
CO_2: carbon dioxide
$(CO_2\%)_{intake}$: CO2 concentration in the intake manifold
$(CO_2\%)_{exhaust}$: CO2 concentration in the exhaust manifold
$(NH_2)_2CO$: urea
COV_IMEP: coefficient of variation of IMEP
$C_xH_yO_z$: normalised molecular composition of the actual in-cylinder fuel mixture
D: valve reference diameter
DAQ: data acquisition
DEF: diesel exhaust fluid
DOC: diesel oxidation catalyst
DPF: diesel particulate filter
EC: European Commission
ECR: effective compression ratio
ECU: engine control unit
EEVC: early exhaust valve closing
EEVO: early exhaust valve opening
EGR: exhaust gas recirculation
EIA: energy information administration
EIVC: early intake valve closing
EGT: exhaust gas temperature
EPA: Environmental Protection Agency
ESC: European stationary cycle
ETA: electric turbocharger assist
EU: European Union
EVC: exhaust valve closing
EVO: exhaust valve opening
FID: flame ionisation detector
GHG: greenhouse gas
H_2O: water
H_a: ambient humidity
HC: hydrocarbons
HCCI: homogeneous charge compression ignition
HCLD: heated chemiluminescence detector
HD: heavy-duty
HHR: heat release rate
HPL: high pressure loop
IC: internal combustion
iEGR: internal exhaust gas recirculation

IMEP: net indicated mean effective pressure
IPCC: intergovernmental panel on climate change
ISCO: net indicated specific emissions of carbon monoxide
$ISCO_2$: net indicated specific emissions of carbon dioxide
ISHC: net indicated specific emissions of unburnt hydrocarbons
ISNOx: net indicated specific emissions of nitrogen oxides
ISsoot: net indicated specific emissions of soot
IVC: intake valve closing
IVO: intake valve opening
k_f: fuel specific factor of wet exhaust
k_{hG}: ambient humidity correction factor
k_w: dry-to-wet correction factor
k_{FID}: correction factor for the FID response to oxygenated fuels
L: valve lift
LHV: lower heating value
LHV_{CO}: lower heating value of carbon monoxide
LHV_{HC}: lower heating value of unburnt hydrocarbons
LHV_{fuel}, lower heating value of fuel
LHV_{diesel}: lower heating value of diesel
LIVC: late intake valve closing
LIVO: late intake valve opening
LNT: lean NOx trap
LTC: low temperature combustion
m/m: mass basis
$\dot{m}_{air}$: mass flow rate of fresh air
$\dot{m}_{diesel}$: mass flow rate of diesel
$\dot{m}_{dry\ air}$: mass flow rate of dry air
$\dot{m}_{exh}$: mass flow rate of exhaust gas
$\dot{m}_{fuel}$: in-cylinder fuel mass flow rate
$\dot{m}_{CO}$: mass flow rate of carbon monoxide
$\dot{m}_{HC}$: mass flow rate of unburnt hydrocarbons
$\dot{m}_{H_2O}$: mass flow rate of water-in-fuel
$\dot{m}_{NOx}$: mass flow rate of nitrogen oxides
$\dot{m}_{soot}$: mass flow rate of soot
$\dot{m}_{urea}$: mass flow rate of aqueous urea solution
m_{rg}: mass of residual gas trapped at exhaust valve closing
m_{total}: total in-cylinder mass
MFB: mass fraction burnt
MK: modulated kinetics
MAP: manifold air pressure
N: engine speed
N_2: nitrogen
NDIR: non-dispersive infrared absorption
N_2O: nitrous oxide
NH_3: ammonia
NHTSA: national highway traffic safety administration
NIE: net indicated efficiency
$NIE_{corr.}$: corrected NIE
NO: nitrogen oxide
NO_2: nitrogen dioxide
NOx: nitrogen oxides
n_{lo}: 50% of the speed at maximum net power
n_{hi}: 70% of the speed at maximum net power
O_2: oxygen
OBD: on-board diagnostics
OECD: organization for economic cooperation and development

p: pressure
p_a: ambient air pressure
p_{EVC}: in-cylinder gas pressure at exhaust valve closing
P_i: net indicated power
PCCI: premixed charge compression ignition
P_{inj}: injection pressure
P_{int}: intake pressure
PM: particle matter
P_{max}: maximum in-cylinder gas pressure
PMEP: pumping mean effective pressure
PN: particle number
PPCI: partially premixed charge compression ignition
ppm: parts per million
PREDIC: premixed lean diesel combustion
PRR: pressure rise rate
Q_{ch}: combustion energy release
Q_{ht}: heat transfer
Q_{net}: net heat release
$\tilde{R}$: universal gas constant
R: specific gas constant
R_c: compression ratio
RCCI: reactivity controlled compression ignition
REF: trigger signal
RGF: residual gas fraction
RH: relative humidity in ambient air
rpm: revolutions per minute
S: stroke
SCR: selective catalytic reduction
SDPF: SCR coated DPF
SI: spark ignition
SOC: start of combustion
SOF: soluble organic fraction
SOI: actual start of injection
SP: water saturation pressure
t: time
T: temperature
T_a: ambient air temperature
TCO: total cost of ownership
T_b: mean in-cylinder gas temperature
T_{EVC}: mean in-cylinder gas temperature at exhaust valve closing
T_{inj}: main diesel injection
TDC: firing top dead centre
TTG: transport task group
u_{gas}: gas molar fraction
UNIBUS: uniform bulky combustion system
US: United States
v/v: volume basis
V: volume
V_{clr}: clearance volume
V_d: displaced volume
V_{EVC}: in-cylinder volume at exhaust valve closing
V_{ins}: instantaneous in-cylinder volume
VGT: variable geometry turbine
VVA: variable valve actuation
W_{ALF}: hydrogen mass content in the fuel
W_{EPS}: oxygen mass content in the fuel

$W_{c,i}$: net indicated work per cycle
WHTC: world harmonized transient driving cycle
WHSC: world harmonized steady state cycle
x: molar carbon to carbon ratio
y: molar hydrogen to carbon ratio
z: molar oxygen to carbon ratio

[CO]: concentration of carbon monoxide in the exhaust gas

[CO_2]: concentration of carbon dioxide in the exhaust gas

[FSN]: filter smoke number

[HC]: concentration of unburnt hydrocarbons in the exhaust gas

[NOx]: concentration of nitrogen oxides in the exhaust gas

[soot]: concentration of soot in the exhaust gas

γ: ratio of specific heats (c_p/c_v)

Φ: global fuel/air equivalence ratio

θ: crank angle position

λ: lambda or relative air/fuel ratio

ρ: density

ρ_{diesel}: diesel density

ρ_{exh}: exhaust gas density

Chapter 1
Introduction

1.1 Preface

The first internal combustion (IC) engines can date back to 19th century, initially by means of a four-stroke cycle engine commonly known as Otto cycle engine or spark ignition (SI) engine, which was put forwarded by Nicolaus Otto. Followed by the revolutionary design of the first compression ignition (CI) engine developed by a German engineer called Rudolph Diesel who gave his name to the 'Diesel' engine. Since the first IC engine was invented, the IC engine has achieved great success and has become the principal power plant for road transportation, stationary power plant, and marine, attributed to the development of innovative engine technologies over the last century.

Although the automotive products equipped with IC engine produce many positive influences on human's activities and have become an essential part of a country's industry and economy, the steep increase in the huge number of global automobiles in the last few decades also lead to some severe issues, raised concerns about the pollutants such as nitrogen oxides (NOx), particular matter (PM), carbon monoxide (CO) and hydrocarbon (HC) from IC engines and their impact on the environment and human health. Besides, the issue of natural resources depletion which was first recognized by the oil crisis in the USA in the mid-1970s, as well as the climate warming have attracted global attention and caused increasing concerns with sustainable development of humans. Much effort is being made to develop new energy resources and expect to significantly improve the fuel efficiency of conventional IC engines, which are necessary for the control of GHG and harmful emissions.

Demands for fuel savings and environment protection as well as human health have led to the adoption of emissions and fuel efficiency standards. Emission legislation has been initially proposed in the early 1960s by the California Air Resource Board (CARB) and Environmental Protection Agency (EPA) in the USA, followed by the European Union (EU) in the 1990s. Since then, the emission legislation has been continuously reviewed and updated, particularly in the HD sector which typically equipped with a diesel engine, as they hold 4% of on-road vehicles but account for 18% of fuel consumption and characterised one of the largest contributors of global CO_2 emissions within the transportation sector.

Motivated by the high efficiency of CI diesel engines, many engine manufacturers decided to offer a diesel option, not only to conserve energy, but also to allow their customers to capitalize on reduced fuel consumption and operating costs. However, compared to their gasoline counterparts, it has become increasingly difficult for diesels to meet diesel emission regulations since 1990s. The main focus in diesel regulation has been on emissions of NOx and PM, the most perilous emissions produced by diesel engines. Consequently, many advanced technologies have been developed and applied to modern diesel engines mainly for the control of NOx and PM as well as to maximize fuel conversion efficiency. Among them optimization in the injector design, implementation of ultra-high injection pressure (P_{inj}), as well as introduction of cooled external EGR have been identified as effective technologies to either reduce fuel consumption or exhaust emissions. However, more progress is still required, as the levels of NOx and PM remain too higher to meet the increasingly stringent emission regulations, which requires the introduction of exhaust gas aftertreatment technologies for further emissions reduction.

One of the main challenges encountered by modern diesel engines are insufficient high exhaust gas temperature (EGT) for efficient conversion of exhaust gases in the aftertreatment systems (ATS) at low engine loads, as well as significant high NOx emissions and peak in-cylinder pressure due to higher diesel combustion temperature and pressure at high engine loads. Miller cycle achieved by advancing or delaying intake valve closing (IVC) timing, has the ability to enhance EGT at low loads and reduce effective compression ratio (ECR) and consequent peak cylinder pressure at high engine loads to optimise combustion phasing and reduce the level of NOx. In this work, the injector geometry optimization and relevant injection strategies were initially optimized for the best trade-off between fuel efficiency and exhaust emissions on a HD diesel engine equipped with a VVA system on the intake camshaft. This is followed by the investigation of VVA-based technologies and EGR over the HD diesel engine speed-load map. The total engine operating cost was then estimated and compared among different combustion control strategies. The potentials of Miller cycle with EGR (SCR + EGR) and without EGR (SCR-only) under constant intake pressure or constant air/fuel ratio as the baseline engine operations to meet the Euro VI emission regulations were assessed at different NOx aftertreatment efficiencies.

1.2 Project objectives

The aim of this project is to maximise the fuel efficiency and minimise the exhaust emissions of a HD diesel engine via the optimisation of fuel injection and the investigation of Miller cycle strategy from low to full engine loads. Furthermore, to explore a cost-

effective emission control and fuel efficiency technology incorporated in the “SCR-only” and “SCR + EGR” technical routes for future HD diesel engines by combining with and/or without EGR. The main objectives of this work comprise:

i. To investigate the influence of injector nozzle geometry such as nozzle hole shape, fuel mass flow rate, and spray cone angle in order to achieve the optimum trade-off between fuel efficiency and emissions as well as to provide a sensible starting point (baseline) for the investigation of Miller cycle.
ii. To determine the effectiveness of Miller cycle as a technical measure to enhance exhaust gas temperature management at low engine loads as well as to minimise engine-out emissions and improve fuel efficiency at high engine loads.
iii. To explore the potential of Miller cycle operation with or without EGR under constant intake pressure and constant air/fuel ratio from low to full engine loads.
iv. To identify the optimum combustion control strategies for the “SCR-only” and “SCR + EGR” technical routes that can be applied to meet EURO VI NOx emissions targets of < 0.4 g/kWh and analyse their potential to minimizing EOC.

1.3 Thesis outline

Chapter 1 provides a brief context for this work and delimit the scope of the research objectives. Chapter 2 presents a literature review relevant to this work. The history and evolution of heavy-duty diesel engine technologies along with the corresponding regulatory standards are described. Afterward, the current development and application of Miller cycle on diesel engine are discussed. Chapter 3 gives a detail description of the research engine and test cell facilities used to carry out the experimental work. The equations required for the experimental data acquisition and analysis in both real-time and post-processing are described.

An investigation of diesel fuel injector parameters including fuel flow rate, nozzle hole-shape and injection cone angle is discussed in Chapter 4, which is aimed to identify the injector geometry parameters optimised for diesel engine combustion, performance, and emissions. The focus of Chapter 5 and 6 are on the characterisation of the Miller cycle operation from low to full engine loads. Chapter 5 evaluates the effect of fuel injection characteristics, internal and external exhaust gas recirculation, as well as intake pressure on Miller cycle operation at low to medium loads. The exploration of Miller cycle combined with internal EGR as a means for a light load exhaust gas temperature management is also presented. Chapter 6 characterises the effect of Miller cycle operation at high engine loads and assesses the EOC at full engine load.

An analysis of overall engine efficiency and emissions over engine speed-load map is discussed in chapter 7. The cycle-averaged results calculation of different combustion control strategies over the WHSC test cycle was carried out as well as their potential to meet Euro VI emission regulations. Chapter 8 summarises the main findings in terms of engine performance and emissions as well as EOC from the experimental work, which is followed by the proposed recommendations for future work.

Chapter 2

Literature review

2.1 Introduction

2.1.1 Energy and environment issues

Energy consumption in the transportation sector is evolving. According to the Energy Information Administration's (EIA) International Energy Outlook (IEO) 2017, the Organization for Economic Cooperation and Development (OECD) countries' transportation energy consumption will remain relatively flat in the next 25 years. However, the levels in non-OECD countries will increase even higher than in OECD countries by the early 2020s. This rapid growth in non-OECD growth leads to continued transportation energy consumption growth through at least 2040 [1,2]. The data presented in Figure 2.1 describes the energy transition through three different aspects: sectors, regions, and fuels, each of which reveals different aspects of the transition [3]. The energy growth for the transport sector is much slower than in the past, reflecting faster gains in vehicle efficiency. Even though the energy supply by 2040 is the most diversified ever seen, the dominants fuel in the transportation sector is still by fossil fuels, which represents 55% of the worldwide oil consumption [1]. By region, the fast-growing developing economies such as China, India and other emerging Asian countries account for around two-thirds of the growth in energy consumption.

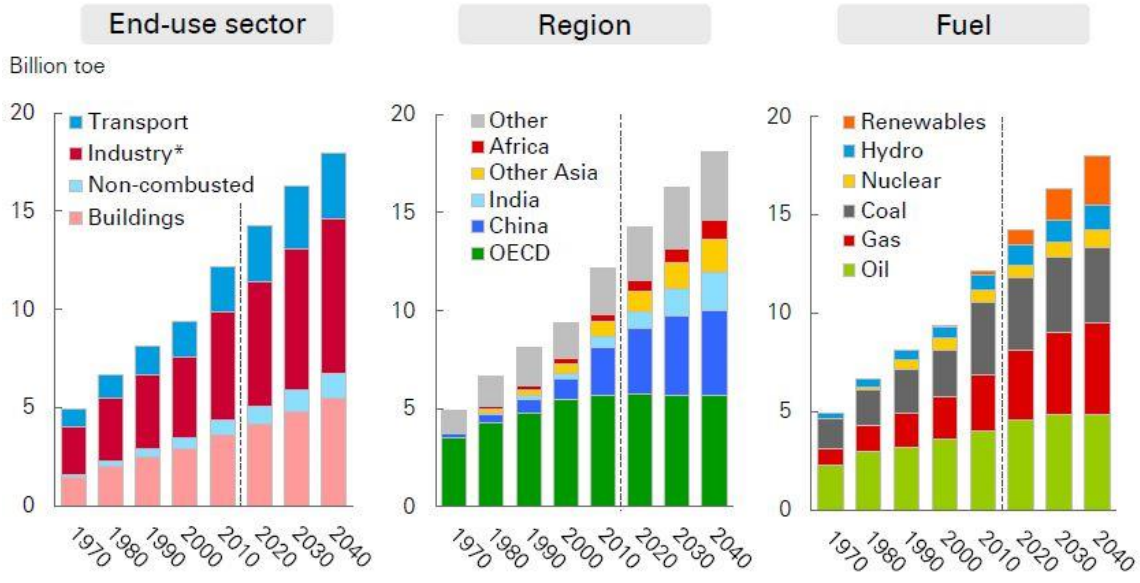

Figure 2.1: Global primary energy demand by sector, region and fuel. Adapted from [3].

Figure 2.2 shows the global transportation fuel demand breaking down in different transportation means. Over next 25 years, global transportation demand is expected to grow about 25%. Although personal mobility demands continue to increase, the more efficient vehicles result in a peak and eventual decline in the energy demand of light duty vehicles. However, the heavy-duty segment (mostly trucks and buses) is the largest growth by volume and the highest fraction of energy demand in 2040.

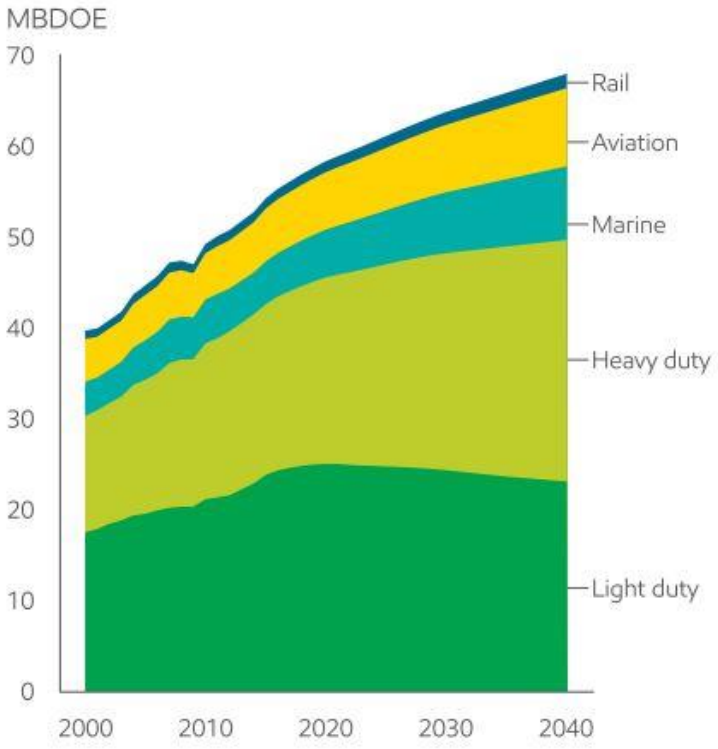

Figure 2.2: Fuel demand varies by transportation sector. Adapted from [1].

According to the most comprehensive assessment of climate change undertaken by the Intergovernmental Panel on Climate Change (IPCC) [4], the global warming is strongly related to the burning of fossil fuels, which add a substantial amount of heat-trapping green-house gases such as CO_2 and methane into the atmosphere [5]. The data presented in Figure 2.3 compares the current global atmospheric concentrations of CO_2 with the past 800,000 years. Since the beginning of the industrial era, CO_2 concentrations have increased approximately 43% from an annual average of 280 ppm in the late 1700s to 401 ppm as measured at Mauna Loa in 2015, primarily due to human activities [6]. Figure 2.4 presents the CO_2 emissions varies by sources. In 2016, CO_2 emissions produced by transport was the largest sector, having surpassed the energy supply sector. Since there is no specific CO_2 capture device employed on a vehicle to filter out the CO_2 from cars, the most effective way to reduce CO_2 produced from cars is to improve the fuel efficiency. This is the aim to introduce fuel efficiency regulations.

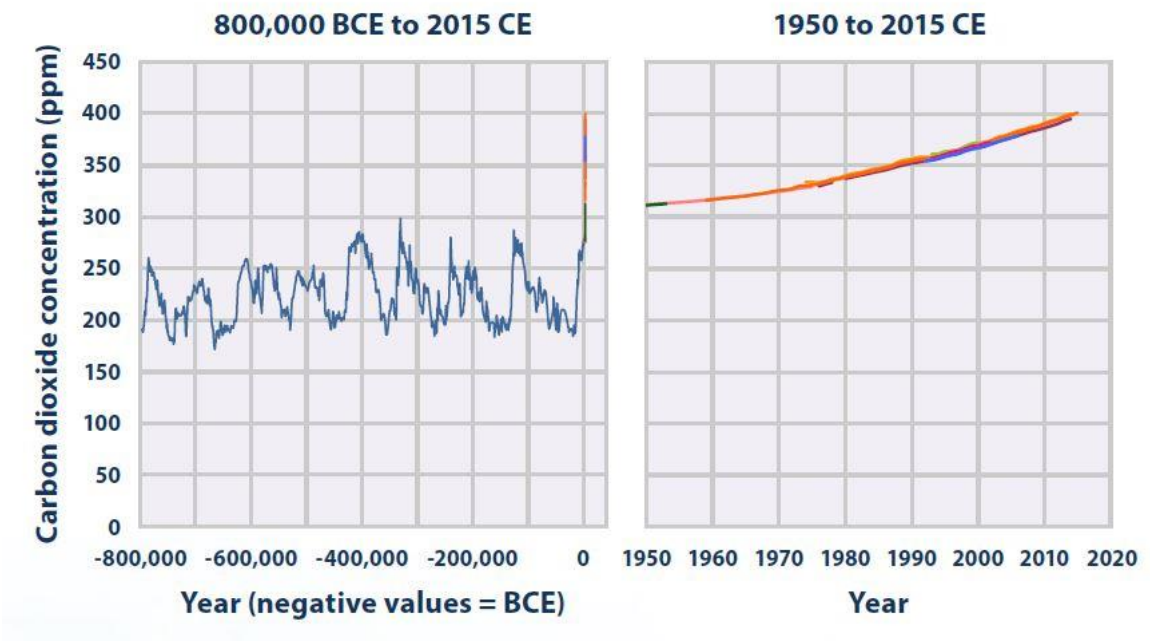

Figure 2.3: Global atmospheric concentrations of CO_2 over time. Adapted from [6].

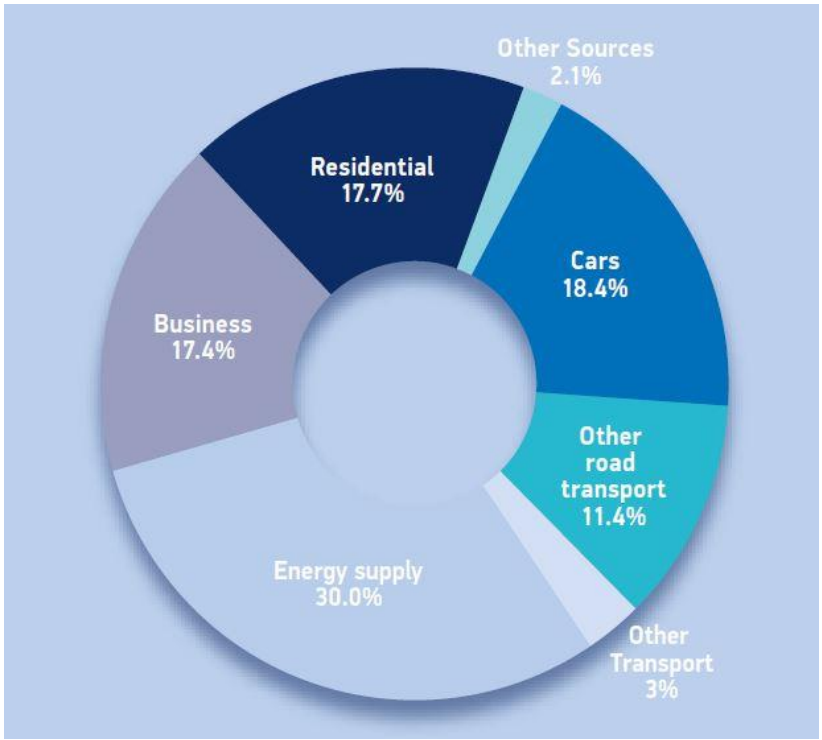

Figure 2.4: CO_2 emissions by sources. Adapted from [7].

In response to the concerns with the global climate change, many countries have established mandatory fuel efficiency or CO_2 emission regulations [8,9]. Recently, the Paris Agreement have entered into force on 4th November 2016 with the aim to deal with the global temperature rise through reducing the global GHG emissions.

With the increase in the number of automotive vehicles, the CO_2 emissions from such vehicle has become one of the major sources of global CO_2 concentration. In particular, the commercial sector, namely HD trucks, with 4% of the total number of on-road vehicles, account for 18% of the fuel consumption and CO_2 emissions within the transportation sector [10]. Moreover, nearly half of the CO_2 emissions in the road transport sector and one-third of the global greenhouse gases in the global transportation sector are produced by HD vehicles, which comprises 11% of the vehicles around the world [11,12]. For these reasons, attention has to be paid to improve the engine design and more research has to be performed to develop a high efficiency and clean combustion HD vehicles, in order to minimize the fuel consumption and emissions of the HD engines. This helps curb the GHG emissions and thus the impact on the global warming.

2.1.2 Emission and fuel efficiency regulations

The aforementioned increasingly concern over the environmental impacts caused by vehicles related pollutants, requires worldwide stringent emission and fuel efficiency regulations to be introduced. In addition to the GHG emissions, the other gaseous emissions such as carbon monoxide (CO), unburnt hydrocarbon (UHC), nitrogen oxides (NOx) and particulate matter (PM) have significantly harmful impact on human health and environment. This has prompted the emissions regulations, which was first introduced by the California Air Resource Board in the early 1960s [13]. Followed by the implementation of emission regulations for HD on-road vehicles began in the early 1970s in North America and Japan and in the 1980s in Europe [14]. From then all main countries and regions worldwide began to establish related emission regulations for environmental protection. Shown in Figure 2.5 is an overview of NOx and PM emissions limits for HD engines in the EU, US, and China. The trade-off between NOx and PM emissions and the differences in regulatory emissions limits in the EU and the US result in different technical pathways in these two regions. In China, the emissions levels are set equivalent to those of EU and therefore resulted in a similar emission control strategy.

Euro VI emission standards, the most strict emission limits for on-road HD vehicles in Europe, were introduced by regulation 595/2009 [15]. This emission limits were comparable in stringency to the US 2010 standards and came into effect for new type-approvals in 2013 and for all registrations in 2014. As depicted in Table 2.1, the Euro VI HD emission Regulation not only set tougher emission limits for pollutants, but also adopted the worldwide harmonized drive cycles which includes the World Harmonized Transient Driving Cycle (WHTC) and the WHSC [16]. Moreover, the particle number (PN) emission limit and stricter on-board diagnostics (OBD) requirements were introduced.

Additional provisions of the Euro VI regulation also include a new limit for ammonia (NH_3) concentration in order to control the aqueous urea solution injection in the SCR systems.

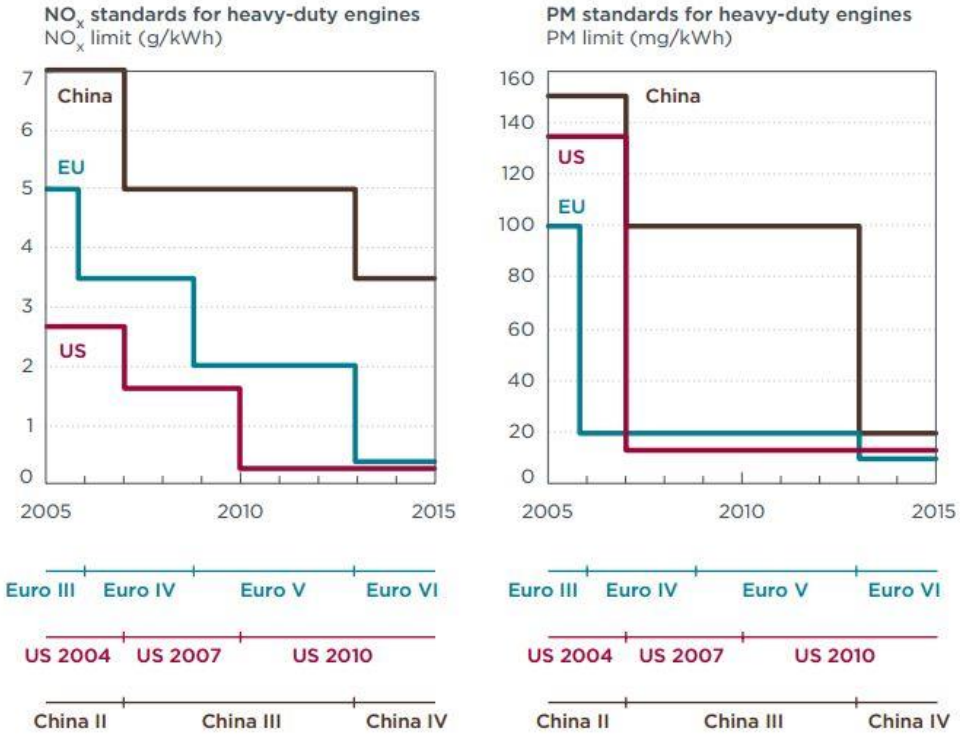

Figure 2.5: NOx and PM emissions standards for Heavy-Duty CI engines in the EU, US, and China. Adapted from [17].

Table 2.1: EURO VI emission standards for on-road HD engines and vehicles. Adapted from [16].

Test cycle	Pollutant limits							
	NOx (g/Kwh)	CO (g/Kwh)	HC (g/Kwh)	CH4 (g/Kwh)	NMHC (g/Kwh)	PM (g/Kwh)	PN (#/Kwh)	NH3 (ppm)
WHSC (CI)	0.40	1.50	0.13	n/a	n/a	0.010	$8.0x10^{11}$	10
WHTC (CI)	0.46	4.00	0.16	n/a	n/a	0.010	$6.0x10^{11}$	10
WHTC (PI)	0.46	4.00	n/a	0.50	0.16	0.010	$6.0x10^{11}$	10

In the case of US, the regulation of NOx and PM emissions for HD on-road diesel engines was first discussed in the 1970s. As shown in Table 2.2, the first emission regulations became effective in 1974, since then substantial reduction in the emissions have been obtained in a number of steps [18]. Prior to the 1988s, the focus of the US regulations was NOx, HC, CO and smoke. The limits for PM were introduced in 1988 [14]. A more stringent NOx and PM limits was the first phased-in which began in 1988 and was completed in 1998, reducing NOx by 62% and PM by 83% compared to the former standards [19]. The

current emissions standards for HD engines were phased-in over the period of 2007-2010, which limits the NOx level lower than those of the Euro VI standards.

Table 2.2: An overview of US EPA and California Emission standards for HD diesel engines. Adapted from [18].

Year	CO	HC[a]	HC[a]+NOx	NO_x	PM	
					General	Urban Bus
1974	40	-	16	-	-	
1979	25	1.5	10	-	-	
1985	15.5	1.3	-	10.7	-	
1987	15.5	1.3	-	10.7[d]	0.60[f]	
1988	15.5	1.3[b]	-	10.7[d]	0.60	
1990	15.5	1.3[b]	-	6.0	0.60	
1991	15.5	1.3[c]	-	5.0	0.25	0.25[g]
1993	15.5	1.3[c]	-	5.0	0.25	0.10
1994	15.5	1.3[c]	-	5.0	0.10	0.07
1996	15.5	1.3[c]	-	5.0[e]	0.10	0.05[h]
1998	15.5	1.3	-	4.0	0.10	0.05[h]
2004[j]	15.5	-	2.4[i]	-	0.10	0.05[h]
2007	15.5	0.14[k]	-	0.20[k]	0.01	
2015	15.5	0.14	-	0.02[l]	0.01	

a. NMHC for 2004 and later standards
b. For methanol-fueled engines, the standard is for total hydrocarbon equivalent (THCE).
c. California: NMHC = 1.2 g/bhp·hr, in addition to the THC limit.
d. California: NOx = 6.0 g/bhp·hr
e. California: Urban bus NOx = 4.0 g/bhp·hr
f. California only, no federal PM limit.
g. California standard 0.10 g/bhp·hr
h. In-use PM standard 0.07 g/bhp·hr
i. Alternative standard: NMHC+NOx = 2.5 g/bhp·hr and NMHC = 0.5 g/bhp·hr
j. Under the 1998 Consent Decrees, several manufacturers supplied 2004 compliant engines from October 2002.
k. NOx and NMHC standards were phased-in on a percent-of-sales basis: 50% in 2007-2009 and 100% in 2010. Most manufacturers certified their 2007-2009 engines to a NOx limit of about 1.2 g/bhp·hr, based on a fleet average calculation.
l. Optional. Manufacturers may choose to certify engines to the California Optional Low NOx Standards of 0.10, 0.05 or 0.02 g/bhp·hr

In parallel to the evolution of emissions standards set for pollutants control, attention is being increasingly put on CO_2 emission in the last decade. The first mandatory targets for GHG emissions or fuel efficiency was introduced by United States (US) and Japan and became effective in the mid-2010s [14]. In order to further reduce the fuel consumption and GHG emissions from new heavy-duty vehicles, tractors, trailers, and engines, the U.S. EPA and the U.S. Department of Transportation's National Highway Traffic Safety Administration (NHTSA) jointly proposed a new Phase 2 regulations, which is built upon the last standards and cover model years between 2014 and 2018 [20]. In the EU, the CO_2 emissions and fuel consumption for HD vehicles will be obtained from the future monitoring and reporting scheme. In 2016, the European Commission (EC) revealed that the EU is working on the legislative proposal for HD vehicles efficiency standards [21]. Other Transport Task Group (TTG) members such as Canada, China, and Japan have

already established corresponding CO_2 and fuel efficiency standards of HD vehicles for their countries [22].

2.2 Heavy-duty diesel engine emissions

Diesel engines have been the main power source in transportation sectors owing to their high torque output and superior thermal efficiency. However, conventional diesel combustion produces significant pollutants, particularly NOx and soot emissions. This is due to the existence of locally fuel-rich and high combustion temperature zones resulted from the non-premixed diffusion-controlled combustion [13]. The mixing challenges and incomplete fuel combustion in diesel engines lead to the formation of engine pollutants such as PM, HCs, and CO, while NOx emissions are formed primarily due to the high-temperature combustion conditions. The reduction of these pollutants from engines are of particular important because they contributed to a serious health and environmental threats [23]. In addition, according to the chemical and medical investigations the suspension of fine particles in ambient air linked to the potential health risk [24]. More attentions should be focused on the detail investigation of fuel-air mixing and in-cylinder combustion process in order to better understand the formation mechanisms of the abovementioned emissions.

Figure 2.6 schematically illustrated the particle structure composition. The principal constituent of PM is composed of sulphate particles, soluble organic fraction (SOF), and dry carbon referred to as soot [25][26]. The majority of the particles are burned before the remaining soot is exhausted to form particulates with unburnt fuel and engine oil.

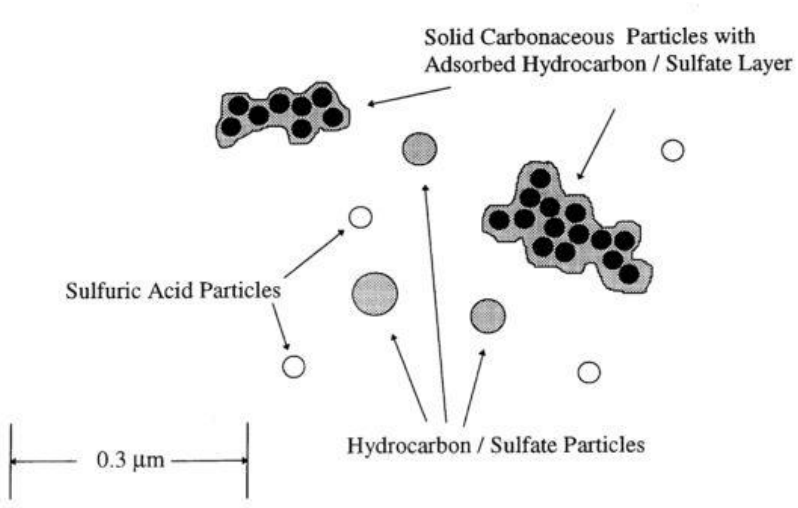

Figure 2.6: Typical particle structure for a HD diesel engine. Adapted from [25].

Shown in Figure 2.7 is the typical particle composition for a HD diesel engine by testing on a US HD Transient Test [25]. The fuel sulfur content is almost equivalent to the sulfuric acid/sulfate fraction. The fraction associated with unburned fuel and lube oil varies with engine design and operating condition.

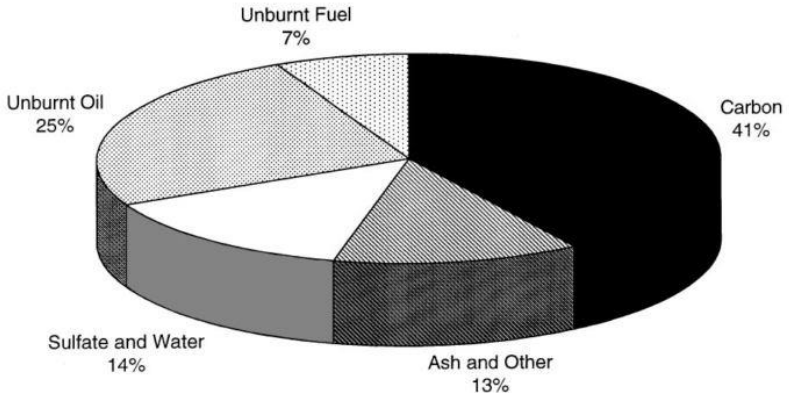

Figure 2.7: Typical composition of engine exhaust particles. Adapted from [25].

NOx emissions present in the exhaust gas consist of approximately 70-90% nitrogen monoxide (NO) and 10-30% nitrogen dioxide (NO_2). The formation of NO is typically in the premixed and diffusion-controlled combustion phases as a function of the flame temperature and in-cylinder oxygen availability [27]. Zeldovich and “prompt” are the two major mechanisms associated with the NO formation process [28]. Presented in reaction (2.1), (2.2), and (2.3) below are the Zeldovich mechanism:

$$N_2 + O \rightarrow NO + N \tag{2.1}$$

$$N + O_2 \rightarrow NO + O \tag{2.2}$$

$$N + OH \rightarrow NO + H \tag{2.3}$$

Reaction (2.1) is highly dependent on combustion temperature as the reaction requires high activation energy. It is also a determine step for the reaction rate and has significant effect on the amount of NO formation. Although NO accounts for the majority of NOx species formed in the combustion chamber, massive NO_2 can also be formed at a certain conditions.

Figure 2.8 shows the conceptual model of diesel combustion plume, which characterizes various combustion phases starting from the liquid fuel injection in the injector nozzle orifice to the edge of the combustion plume. According to the conceptual model, the understanding of the in-cylinder combustion process and emissions formation

mechanisms can be advanced considerably. A locally rich mixture is formed in the interior of the diffusion flame via injecting liquid fuel into the combustion chamber, which leads to high equivalent ratio combustion inside the plume and produces particles. Afterward, these particles are oxidized in the exterior edge of the diffusion flame where temperature is significantly high (2700K). As a result, the soot emissions emitted from the engines are the net result of soot formation and oxidation. Since soot formation requires combustion heating to pyrolyze the fuel, soot concentrations are very high on the fuel side of the diffusion flame. This is differed from the formation of NOx emissions, which are formed on the high temperature periphery.

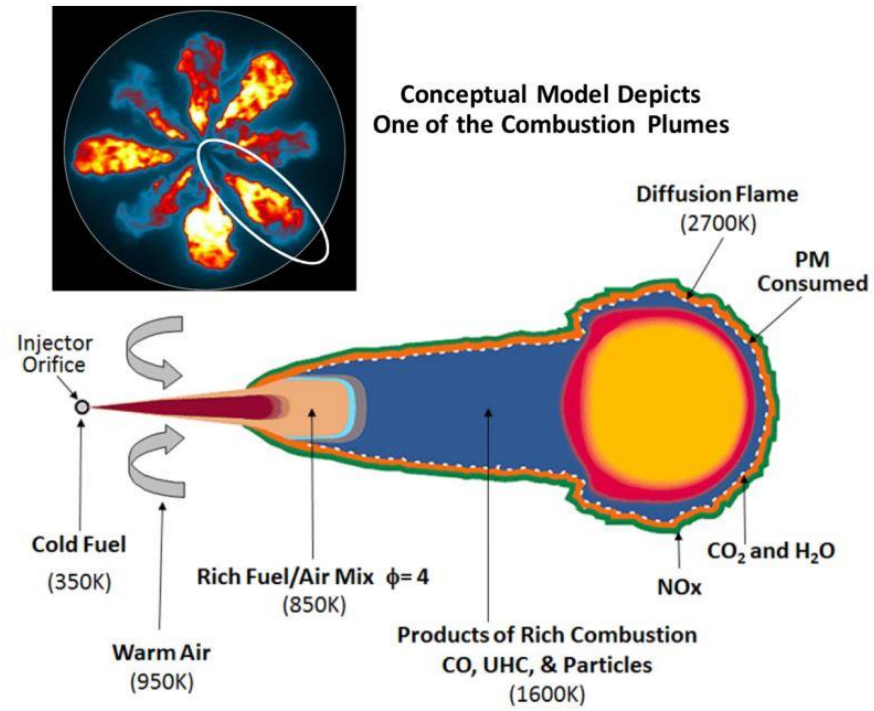

Figure 2.8: Conceptual model of quasi-steady diesel diffusion flame combustion. Adapted from [29].

Compared to the gasoline counterpart, diesel engines typically produce relatively lower unburnt HC and CO emissions due to operating in lean conditions. The oxygen availability and in-cylinder gas temperature play significant roles for HC and CO formation [30]. Unburnt HC is mainly produced from unburned fuel and partially decomposed fuel molecules. Research has also shown that poor mixture formation, lubricating oil combustion, and quenching are significantly contribute to the HC emissions. CO emissions are the intermediate combustion product of hydrocarbon and primarily formed in the over-rich combustion where incomplete combustion is occurred [13].

2.3 Heavy-duty diesel engine emission control technologies

2.3.1 Combustion system optimization

In most recent years, increasingly concerns over air pollution and the stringent emission norms have forced engine researchers and manufacturers to further optimise the combustion system in all areas of the engine design. Advanced engine design allows for improving in-cylinder air motion and therefore curb the formation of in-cylinder emissions. During the combustion system design of modern diesel engines, significant effort has been put on the optimization of piston bowl geometry, swirl motion of the air, injection strategy, and fuel injector nozzle configuration, which includes diameter and number of orifices, fuel injection angle, and spray targeting, in order to improve fuel conversion efficiency and engine-out emissions [29].

In diesel engines, in-cylinder air motion which characterized by squish, swirl, and turbulence, has significant effect on the air/fuel mixing process and consequently, the combustion and emission characteristics, particularly near the top dead centre (TDC) during the compression stroke [13]. The swirling motion in the cylinder is typically generated via a special intake port design or a fully variable inlet valve system [31,32]. The effect of swirl ratio on combustion and emissions has been extensively investigated by many researchers in last decades [31,33–35]. Generally, a higher swirl ratio can help improve combustion and thus lower engine-out emissions [32,36]. However, an increased swirl ratio can also lead to higher fuel consumption and NOx emissions. This is due to the enhanced mixing and higher gas motion near the cylinder wall surfaces, contributing to higher heat losses [32,37]. Furthermore, high swirl ratio increases the possibility of trapping more partially-burned fuel into the piston bowl [38]. Therefore, there exists an optimal in-cylinder swirl level for achieving minimum emissions and optimum efficiency, beyond this level the mixing rates could be deteriorated. Some research also demonstrated that a higher swirl level usually beneficial for the soot emissions reduction at risk of higher NOx levels [31,39].

Another means of controlling the mixture distribution and enhancing air/fuel mixing for a better combustion is the optimisation of piston bowl geometry. In recent years, huge efforts have been made by numerous researchers on the improvement of engine combustion via the optimization of engine design parameters. This mainly includes the following three different types of piston bowl geometry: re-entrant, toroidal, and stepped [40–42]. Figure 2.9 shows the piston bowl geometries of conventional and stepped types.

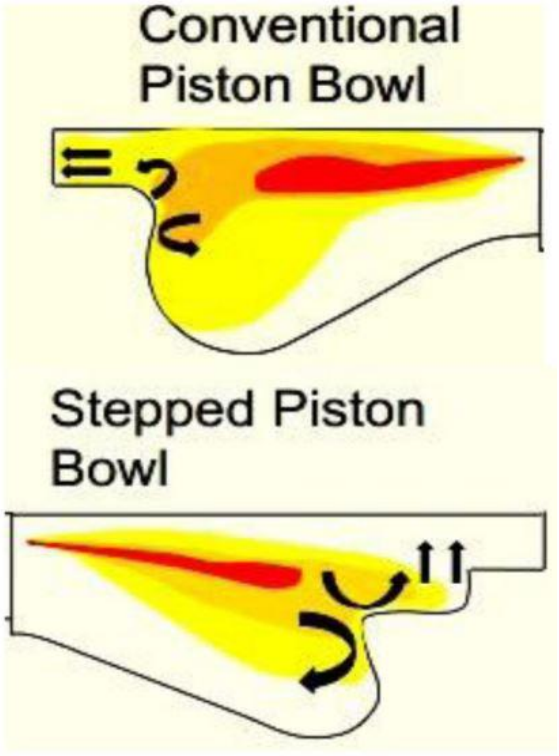

Figure 2.9: Piston bowl geometries of conventional and stepped types. Adapted from [34].

Generally, the stepped piston bowl allows for a better mixture preparation and demonstrates a reduction in soot and CO emissions as well as better fuel conversion efficiency when compared to the conventional piston bowl type [42]. A relatively open bowl geometry can produces an earlier combustion phasing and higher NOx and CO emissions, whereas a vertical side-wall bowl lead to lower CO and HC emissions, as shown in the computational work by Cao et al. [43]. Similar results have been reported by Splitter et al. [44] through experimentally study the effect of piston geometry and compression ratio on the load limits and efficiency of Reactivity Controlled Compression Ignition (RCCI) combustion. Furthermore, Quazi et al. [34] demonstrated that a large shallow piston bowl usually can result in lower soot emissions and better fuel conversion efficiency at the same

compression ratio. By contrast, the smaller piston bowl design tends to curb NOx formation at the expense of higher fuel consumption and soot emissions.

In addition to the important effect on combustion of air motion, fuel spray characteristics such as the injector geometry structure and injection strategies are also play a very significant role on diesel engine combustion and emissions. Therefore, it is important to match well the fuel injection with the piston bowl geometry in order to achieve the optimum engine performance and engine-out emissions.

Injector design parameters such as orifice diameter and number, nozzle hole-shape, and spray cone angle have a direct effect on the fuel atomization, vaporization and consequent air/fuel mixing. In recent years, the diameter of nozzle orifice tends to be decreased with the aim to reduce the fuel droplet size. At higher injection pressures, a smaller orifice diameter can be used to decrease the fuel penetration and can also reduce the liquid fuel impingement on the cylinder walls [45]. Other advantages of using a smaller nozzle hole are to enhance the fuel atomization and increase the air entrainment, etc. This can help increase the mixing rate and form a more uniform air/fuel mixture, yielding lower soot emissions and fuel consumption with an increase in NOx emissions [46]. However, a smaller nozzle hole increases the fuel injection duration and become increasingly difficult to achieve enough high injection rate, which could result in lower combustion efficiency. This can be improved by increasing injection pressure to accelerate the injection rate [47,48]. Increasing the number of injector nozzle holes will contribute to the occurrence of spray overlap and reduce the length of spray penetration, which deteriorates the soot oxidation [49,50]. Some studies also reported that the larger number of holes with smaller diameter has an adverse effect on the fuel efficiency in a HD diesel engine due to the poor spray penetration [51].

The orifice cross-sectional area is another important characteristics for a nozzle as it has a direct impact on the injector internal flow field characteristics and the evolution of cavitation and turbulence over the nozzle length. As shown in Figure 2.10 the classic cylindrical hole and two conical holes with a progressive reduction in the cross-sectional area between inlet and outlet. The k-hole can be defined by

the nozzle conicity or the so-called k-factor, which was demonstrated in equation (2.4) as

$$K - factor = 100 * \frac{(D_{in} - D_{out})}{L} \quad (2.4)$$

where D_{in} is the inlet hole diameter, D_{out} is the outlet hole diameter, and L is the length of nozzle.

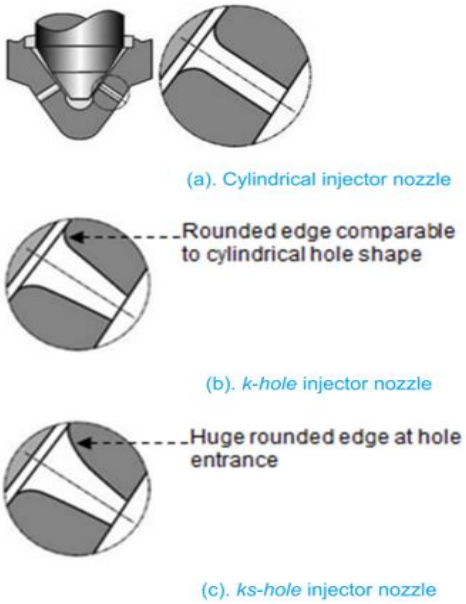

Figure 2.10: Layouts of cylindrical, K, and ks nozzle holes. Adapted from [52].

Compared to cylindrical hole-shape, the k-hole injector produces smaller spray angle, stronger penetration, slower injection rate and more stable spray characteristics. While the ks-hole characterised by a relatively bigger rounded edge at the hole entrance, is the upgrade version of the k-hole by Konisch Strömungsoptimiert [52]. The advantages over k-hole are the higher efficiency in transforming the fuel pressure into spray velocity across the inlet section and lower flow separation downstream of the hole entrance [53,54]. An experimental work performed by Benajes et al. [55] investigated the flow characteristics of two different nozzle hole shapes (cylindrical and conical). It found that the conical nozzle achieve higher value of discharge coefficient than the one with a cylindrical shape. They also revealed that the flow collapsed at high injection pressures only occurred at cylindrical nozzle due to cavitation. Desantes et al. [56] analysed the impact of nozzle conicity on the formation of cavitation. Results revealed that an increase in K-factor value can effectively reduce the possibility of cavitation. Research has also demonstrated the potentials of conical nozzle in reducing soot emissions due to enhanced atomization and better air–fuel mixing, although the ignition delay was reduced. However, it yielded higher NOx emissions due to higher level of diffusion combustion [57].

Early injection strategy has been widely used in the direct injection engines, particularly HCCI diesel engines, in order to allow for enough time to form a homogeneous air/fuel mixture [58,59]. The spray cone angles for a conventional diesel fuel injectors are typically between 120 and 160 degrees with vertical centerline direct injected fuel towards the cylinder liner. However, they will increases the risk of fuel spray impinging on the cylinder walls [60]. The resulting wall-wetting has negative effect on combustion efficiency, oil dilution, and soot emissions [61]. Numbers of studies have proved that limiting the spray cone angle is an effective way to reduce or avoid wall-wetting by targeting the fuel within the combustion bowl [62–64]. Additionally, a better air/fuel mixing process can be realized with the use of a narrow spray angle as it demonstrates a better spray-wall interaction [65]. By using narrow angle injectors with optimized injection strategy, simultaneous low levels of NOx and soot emissions can be achieved with small penalty on fuel efficiency [66]. Thus, it can be seen that the spray targeting plays a very important role in controlling engine-out emissions by improving the mixing process and mixture distribution.

Previous studies have also revealed that there exists an optimum combination between bowl geometry, swirl ratio, and spray targeting to maximize fuel efficiency and minimize engine-out emissions [33–36]. Thus, it is important to carry out an investigation of combustion chamber geometry along with swirl ratio and fuel injector geometry structure to achieve an optimum combustion system in terms of emissions and fuel efficiency.

2.3.2 High pressure common rail fuel system

The development of diesel fuel systems has been accelerated with the advent of advanced common rail fuel system. Currently, the common rail system along with unit injector and unit pump are used widely in HD vehicles [19]. In diesel engines, the combustion characteristics and emissions formation are heavily influenced by spray atomization and its mixing with in-cylinder air flow. Thus, modern diesel systems have tended to rely on advanced fuel injection systems with capability of high injection pressures. This is because fuel injection pressure is one of the most important injection parameters and has significant impact on the performance of air/fuel mixing process [67,68]. Figure 2.11 shows the typical efficiency results of diesel fuel injection technologies for HD engines over the last 30 years.

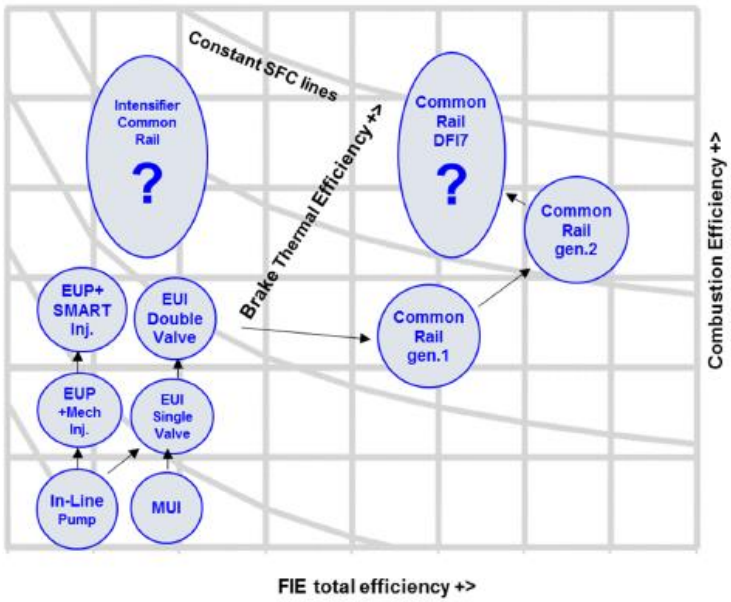

Figure 2.11: Comparison of typical HD engine fuel systems in terms of efficiency results. Adapted from [69].

The main drivers for the development of fuel injection system with the capability of high injection pressure are to increase the tolerance for high EGR rate, to minimize emissions, and to improve engine performance and efficiency [70]. High fuel injection pressure has been regarded as one of the most efficient technologies to meet the current and future stringent emissions regulations. Studies have showed that the use of high injection pressure improves spray atomization and fuel–air mixing, leading to a faster heat release rate [71,72]. This can directly influence engine performance and emissions characteristics. Fuel injection pressure has great impact on the spray droplet diameter distribution, which fundamentally affects the combustion characteristics. When the fuel injection pressure is increased, the spray droplet become smaller and vaporize faster. This is the reason for the improvement of fuel-air mixture and thus leads to lower soot and CO emissions [73,74]. Besides, a longer lift-off length can be realized by using higher pressure injection, which is beneficial for the soot reduction. This is a result of the lower equivalence ratio at the flame base and shorter residence time for soot formation [75,76]. The earlier end of injection resulted from higher fuel injection pressure is also one of the major reasons for the reduction of soot formation. This can be explained by the prolonged mixing time before combustion and hence higher degree of premixed combustion [75]. However, using over-high fuel injection pressure in some cases also has negative effect on combustion. As it could reduce the ignition delay and thus the formation of inhomogenous mixture, resulting in lower combustion efficiency [77]. Furthermore, although using ultra-high pressure injection can effectively realize fast spray vaporization and high air entrainment rate, it is undesirable at low load operation due to increased parasitic work for pressurizing the high pressure fuel and probably lead to fuel spray over-penetration [70,78].

2.3.3 Boosting technology

In diesel engines, turbocharger systems play an important role for achieving high power output and low exhaust emissions. The early development of turbochargers is primarily based on marine engines and stationary. Since from the late 1930s to the present day, almost all turbocharged automotive engines have been built with a pulse turbocharger [79]. A conventional turbocharger consists of a turbine and a compressor, both of which are connected by a shaft. It uses the exhaust gas from the engine to drive the turbine, which then powers the air compressor to increase intake pressure and thus the amount of in-cylinder air charge.

Increasing engine power output and thermal efficiency are the main reasons of using turbocharger as it can significantly increase the cylinder charge density to burn more fuel at each cycle. However, the amount of air can be compressed is rely on the swallowing capacity and isentropic efficiency of turbine. The swallowing capacity determines the overall flow restriction in the turbine while the isentropic efficiency represents the actually power achieved in the turbine stage. The waste-gate turbocharger is the first commercially used turbocharger, which was limited to working properly at part loads. The turbine power can be modulated by controlling the waste-gate to adjust the swallowing capacity. Consequently, high intake pressure and low possibility of surge problems can be realised by closing waste-gate at low engine speeds. On the contrary, the waste-gate is kept opening to avoid over-boosting at high engine speeds [80].

In a two-stage turbocharger, a relatively lager low pressure turbocharger along with a smaller high pressure turbocharger are deployed in series, both of which are optimized to ensure properly operation either at low speed or high speed conditions. Typically, a two-stage turbocharger demonstrates lots of advantages over a single-stage turbocharger, such as higher isentropic efficiency, better low-end torque, and faster transient response [81,82]. The higher intake pressure provided by a two-stage turbocharger can also significantly enhance engine power density [83] and beneficial for the performance of soot oxidation during the diffusion-controlled combustion period [84]. In addition, the utilization of a two-stage turbocharger can provide desired intake pressures to compensate the in-cylinder fresh air loss caused by some strategies such as EGR and Miller cycle, and therefore improve combustion process. As a result, two-stage turbocharger system has been widely used to overcome the restrictions of Miller cycle and EGR technologies in recent years [85,86].

However, the main challenge of applying a fixed geometry turbocharger with a wastegated type turbine to a diesel engine is the so called “turbo-lag” problem at low speed and low load conditions and the capability of introducing desired EGR with minimal fuel efficiency penalty at all engine operation conditions [87,88]. This has severely limited the development of diesel engine downsizing [89]. Alternatively, a Variable geometry turbocharger (VGT) can be employed to improve engine transient respond, allowing the turbine power to be adjusted according to the real-time engine operating conditions, without the need to bypass the turbine flow via a waste-gate. Consequently, the benefits of VGT over wastegated turbines include providing higher air-fuel ratio and higher peak torque at low engine speeds and improved vehicle accelerations without the need to resort to turbines with high pumping loss at high engine speeds [29,90]. In modern diesel engines, more attention is being paid on the VGT system design as an enabling technology for the improvement upon torque and performance, the introduction and control of EGR, as well as the aftertreatment regeneration [91–93]. Additionally, the hybrid turbocharger, which includes an Electric Turbocharger Assist (ETA) device and a VGT system demonstrates greater potential in the development of engine downsizing over other boosting technologies. This is mainly because the ETA technology can provide additional boost to enhance the full load performance of downsized engine, particularly at low engine speeds. It can also reduce pumping loss by supply power to turbocharger [94–98]. Shown in Figure 2.12 is the engine layout with an electrically-assisted turbocharger device.

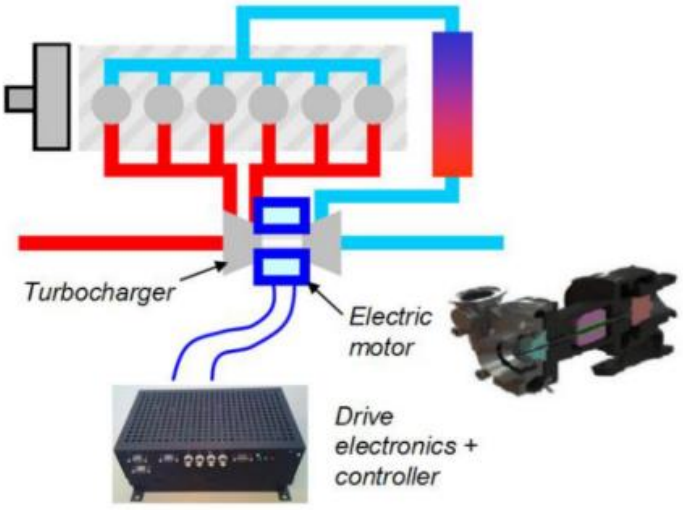

Figure 2.12: The layout of an electrically-assisted turbocharging engine system. Adapted from [94].

Therefore, with the increasing demand for engine downsizing, the hybrid turbocharger technology remains an efficient option due to the capability of simultaneous improvement

in transient response and fuel efficiency, although the extra cost and weight of the entire system as well as relative technology challenges.

2.3.4 Exhaust gas recirculation

The dominant factor leading to the NOx formation is the peak combustion temperatures, which also referred to as flame temperatures. Thus, it is necessary to reduce the flame temperatures by means of some combustion control technologies in order to suppress the NOx formation. Recirculating exhaust gas is an effective means to decrease the flame temperatures. There are two different pathways to introduce the exhaust gas back to the cylinder.

The first one is the external EGR (eEGR), which is an effective and well established technology for NOx emissions control from internal combustion engines. It can be simply realized by introducing a proportion of the exhaust gas from exhaust manifold to the inlet side. As intake air temperature has significant effect on engine combustion, performance, and emissions, EGR cooler is deployed to cool down the high temperature exhaust gases before mixing with fresh air. This design is commonly known as cooled EGR and can effectively reduce the thermal loading in the engine [29]. Figure 2.13 is a schematic representative of EGR system used in a passenger car, which complied with Euro 3 emissions standard and was introduced in 1999.

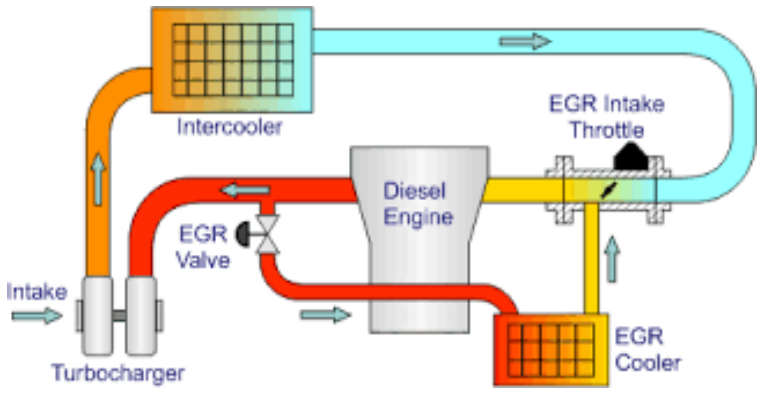

Figure 2.13: Layout of the EGR/intake throttle system for Euro 3 application on Audi 3.3L V8 TDI engine. Adapted from [99].

The main reasons for efficient NOx emissions control by the use of EGR can be summarized as follows:

- Dilution of the inlet air via the introduced inert gases to reduce the oxygen concentration (dilution effect).
- Increase of the total in-cylinder heat capacity as CO_2 and water (H_2O) existed in

the recirculated exhaust gas have higher specific heat capacity (thermal effect).

- Modification of the combustion process due to the dissociation of water vapour and CO_2 (chemical effect).

Among them, the dilution is the most effective EGR effect in reducing NOx emissions at a constant intake pressure as it introduces higher impact on the flame temperatures than others [80]. However, the thermal effect becomes the most significant one when increasing the boost pressure to maintain a constant in-cylinder air/fuel ratio [100,101]. Owing to these important EGR effects on the composition of mixture and the consequent flame temperatures, EGR has become almost essential to meet current and future HD diesel engine NOx limits [102].

Particularly, high EGR levels are regarded as an enabler for low temperature combustion (LTC) strategy, which allows for simultaneous low levels of NOx and soot [103,104]. In recent years, extensive theoretical and empirical studies have been carried out in order to understand thoroughly the fundamental influence of EGR on diesel engine combustion [100,105–107]. Nevertheless, EGR also demonstrates adverse effect on fuel efficiency and PM to some extent. The lower combustion temperature and slower rate of combustion introduced by EGR can deteriorate the engine combustion characteristics. Besides, aggressive use of EGR could considerably increase the smoke emissions when in-cylinder oxygen concentration becomes insufficient to maintain a complete combustion. Moreover, the use of EGR would raise some practical considerations. At higher engine loads, a significant higher intake pressure is required to maintain in-cylinder air/fuel ratio to avoid excessive smoke, which poses great challenge on the turbocharger. Moreover, the higher intake pressure required at higher engine loads is limited by the maximum peak cylinder pressure [106]. Reliability, packaging, and maintenance cost are the main concerns as well [108].

The other method used to trap exhaust gases back to the cylinder is by means of the internal EGR (iEGR) which can be achieved through a VVA system. Such a system can either enables the intake valve re-opening during the exhaust stroke (2IVO) or capable of exhaust valve re-opening during the intake stroke (2EVO). Also, the iEGR can be realized by an early exhaust valve closing (EEVC) event along with modulate the valve overlap on a conventional camshaft [109]. Compared to other methods, the 2IVO strategy has been demonstrated the potential to obtain the best fuel efficiency and smoke [110,111].

The iEGR strategy shows great advantages over the eEGR method such as simpler packaging, lower maintenance cost and higher reliability, as well as a better cycle-to-cycle

control for the exhaust gas fraction [112]. Moreover, the introduction of iEGR with higher exhaust back pressures enabled lower unburnt HC and CO, and higher EGT at low engine loads [113]. The increased EGT at these operating conditions with low exhaust gas enthalpy is typically important for increasing the performance of ATS [114,115]. However, the iEGR plays a less significant role on the NOx formation than the eEGR as the recirculated exhaust gas via iEGR is uncooled. The hot exhaust gas can reduce the intake air flow density, leading to higher smoke emissions and fuel consumption, and may cause power loss at full engine loads. Thus, the iEGR is generally turned off at high engine loads [112,116].

Despite these in-cylinder techniques described above have demonstrated great potential in reducing engine-out emissions and improving engine thermal efficiency, diesel engines are facing the challenge of the trade-off between exhaust emissions and fuel efficiency. Therefore, it is necessary to research alternative in-cylinder combustion and engine control technologies coupled with aftertreatment control strategy in order to achieve a fuel and cost-efficient solution [117].

2.3.5 Aftertreatment technologies

To meet the stringent emissions regulations such as Euro VI and US 2010, significant reduction in these pollutants is required by using in-cylinder combustion technologies and aftertreatment control. Over the past decades, these diesel engine ATSs have been developed rapidly and have been combined with advanced engine combustion control technologies aforementioned to enable an optimum trade-off between engine-out emissions and total fluid consumption [118].

Typical ATS including selective catalytic reduction (SCR), Lean NOx Trap (LNT), diesel particulate filter (DPF), and diesel oxidation catalyst (DOC) allow for NOx, PM, CO and HC emissions reduction accordingly. Figure 2.14 depicts a representative of aftertreatment systems integrated on a modern HD diesel engine. The conversion efficiency of these ATS is strongly dependent on the EGT. A minimum EGT of approximately 200°C is required for catalyst light-off and to initiate the emissions control. This is extremely challenging at low-load conditions when the EGT is too low to provide sufficient emissions reduction. Therefore, a suitable control strategy to raise EGT while maintaining high engine efficiency is significantly important at low engine loads.

The DPF technology dated back to 1999 when it was first commercially used in light-duty engine, while in the HD truck in 2005 [119]. The primary goal of using DPF is to remove or reduce the particulate matter from the exhaust gases emitted from the engines. The

main concern for DPF in practical use is the required periodical regeneration, which is the process of removing the accumulated soot from the filter in order to avoid blocking [120]. DPF regeneration can be fulfilled passively and actively. The former is achieved via using the exhaust enthalpy or with the assistance of a catalyst using in the filter, while the latter need to use external heating measures to accomplish the regeneration process. The DOC system is generally installed upstream of a wall-flow DPF system. The primary purposes of the DOC are to oxidize hydrocarbons and carbon monoxide in the exhaust, but also promote the oxidation of NO to NO_2 to improve the SCR conversion efficiency [121] and supply oxidation exotherm to allow passive regeneration for the DPF [119,122].

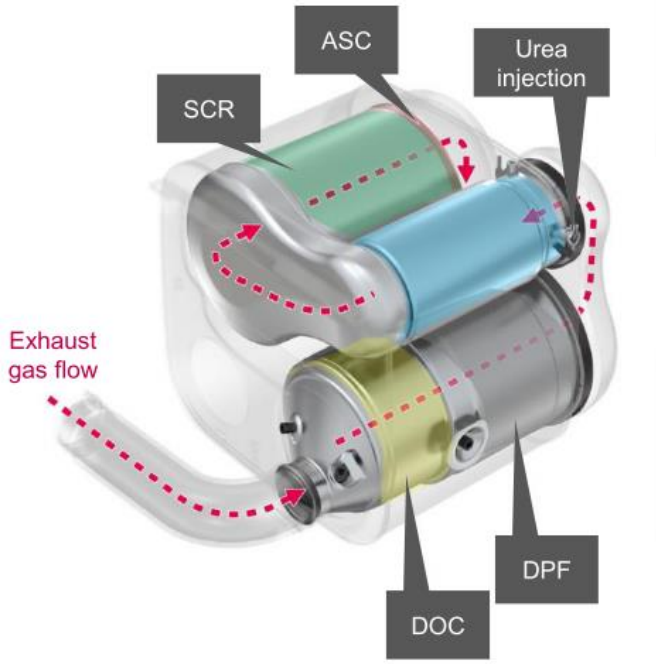

Figure 2.14: A layout of an aftertreatment system integrated on a modern HD diesel engine. Adapted from [123].

SCR is an efficient technology for NOx reduction based on ammonia and has now been used more widely than the other aftertreatment control techniques [124]. Typically, SCR system includes a urea storage and dosing system and an ammonia slip catalyst (ASC) since the use of urea ($(NH_2)_2CO$)/water solution has become common for SCR system. Aqueous urea (typical a mixture of 32.5% high purity urea), used as the chemical reduction agents, has been known as commercial names of Diesel Exhaust Fluid (DEF) and AdBlue in North American and Europe, respectively. The relative prices between diesel fuel and urea are different in different countries and regions, which determines the optimum engine-out NOx level should be controlled by the in-cylinder technologies [29,125].

The urea mixture reacts and decomposes into ammonia and water when being injected to the exhaust stream where the EGT is more than 300°C [79]. The impact of the urea decomposition on the performance of SCR catalyst can be neglected when the EGT is above 250 °C [126]. The nitrogen oxides mainly including NO and NO_2 are reduced by ammonia to form nitrogen gas and water vapour. An ASC is typically equipped downstream of the SCR system in the Euro VI and US 2010 systems to remove excess NH_3 slip from the dosing system. However, the reaction between ASC and NH_3 may produce harmful gases such as nitrous oxide (N_2O) and NOx [127].

The primary challenges for SCR system are the complex processes of ammonia storage, SCR-catalyst heating-up strategy, as well as the reliable urea injection and ammonia slip, which poses great challenge on SCR system to optimizing control algorithms in order to achieve efficient SCR conversion rate with a minimum ammonia slip at all engine operating conditions [124]. Alternatively, SCR coated DPF (SDPF) is one of the potential technologies capable of reducing the packaging space and improving the light-off performance of SCR system [128]. Recent studies have also been focused on the investigation of catalysts used in the SCR system mainly including vanadia, Fe-zeolite, and Cu-zeolite [129–131]. Moreover, there is an optimum balance between in-cylinder control and aftertreatment control for NOx emissions, which requires further investigation to reduce the engine running cost by minimizing the diesel fuel consumption and the aqueous urea solution consumption in the SCR system [125].

2.4 Heavy-duty diesel engine combustion strategies

2.4.1 Conventional diesel combustion

Diffusion combustion enables conventional diesel engines to operate with high torque output, high reliability and durability, as well as superior thermal efficiency, making diesel engines the dominant powertrain in HD vehicles. However, diesel engines are confronted with great challenge when it comes to emissions. The mixing-controlled diesel combustion produces significant PM in the fuel-rich burning region and high concentration of NOx in the high-temperature zones. To better understand how emissions are formed, Figure 2.15 shows the details of the conventional diesel combustion (CDC) process.

The diesel combustion consists of four combustion phases: ignition delay, premixed combustion, mixing-controlled combustion, and late combustion, as described in Figure 2.15. The ignition delay is defined as the period between start of injection (SOI) and start of combustion (SOC). Followed by the premixed combustion phase where the fuel and air well-mixed during the ignition delay period. These prepared mixture burns rapidly and

intensely once the auto-ignition temperature is reached. This phase is characterised by high peak of heat release and high combustion temperature, and therefore beneficial for the NOx formation. The mixing-controlled combustion, also referred to as diffusion combustion, is primarily controlled by the fuel injection rate and the fuel-air mixing rate. Compared to premixed combustion phase, lower heat release peak is observed in this phase and thus lower flame temperature, but it contributes to the majority of soot formation owing to the fuel-rich combustion. Finally, the remaining fuel continues to mixing with air and is consumed in the late combustion phase. A significant lower heat release rate is recorded in this phase as the in-cylinder temperature is relatively low during the expansion stroke.

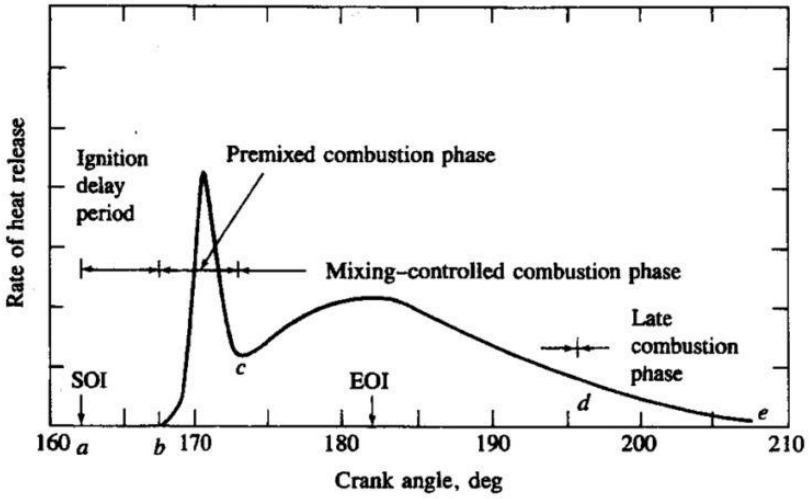

Figure 2.15: Typical diesel engine combustion heat release rate. Adapted from [13].

2.4.2 Alternative combustion strategies

Increasingly stringent emissions regulations and fuel prices are driving the development of more efficient internal combustion engines. Nowadays, HD diesel engines have to depend heavily on the complex and expensive ATS in order to meet current and future emissions regulations. Advanced combustion modes such as homogeneous charge compression ignition (HCCI), premixed charge compression ignition (PCCI), and LTC have shown great potential to significantly reduce engine-out NOx and smoke emissions through reducing the peak in-cylinder combustion temperatures and the local equivalence ratios, as show in Figure 2.16. This can greatly reduce the demand on costly ATS [132,133].

HCCI combustion mode is one of the LTC technologies, which involves a prolong ignition delay and enables a premixed and sufficiently lean air/fuel mixture prior to the SOC. Typically, early injection strategy during the compression stroke is used to achieve HCCI

combustion. However, HCCI combustion tends to suffer from wall-wetting phenomenon due to early injection, high unburnt HC and CO attributed to the low combustion temperature, and high excessive pressure rise rates. The greatest challenge for HCCI combustion strategy is still the direct control of SOC and combustion phasing, especially at transient conditions as the conventional link between fuel injection and combustion process is not able to be maintained [134–136].

To overcome the disadvantages of HCCI combustion aforementioned, the PCCI type combustions are proposed, such as the Premixed Charge Compression Ignition [134,137], Partially Premixed Charge Compression Ignition (PPCI) [132,138], Premixed Lean Diesel Combustion (PREDIC) [139], as well as Modulated Kinetics (MK) [140] and Uniform Bulky Combustion System (UNIBUS) [141]. Differ from HCCI combustion, the PCCI type combustions use a less early fuel injection strategy to reduce or avoid wall-wetting. However, the charge homogeneity is lower and tend to produce lower power output, although the PCCI type combustions can maintain the link between fuel injection and combustion at part loads. In addition, the PCCI combustions tend to produce higher unburnt HC and CO emissions and its operating range is limited to partial load. The high EGR level used in the PCCI combustions also impose great demand on the boosting system.

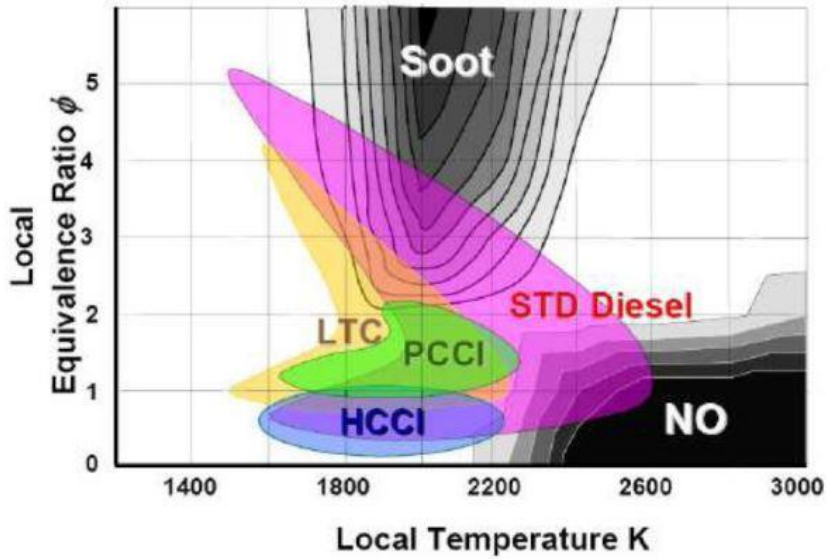

Figure 2.16: Local equivalence ratio versus temperature map for the classification of combustion strategies. Adapted from [134].

In order to successfully apply PCCI combustion strategies in practical HD diesel engines and realize the commercialization of HD diesel PCCI engines, extending the PCCI to higher engine load regions is necessary. However, the PCCI combustions are characterized by fast heat release and high peak cylinder pressure at higher engine loads,

an effective combustion control strategy to overcome these issues is required. A lower compression ratio achieved via a VVA system is one of the most promising technologies due to its fast response time and the capability of controlling in-cylinder gas pressure and temperature at TDC [142,143]. Moreover, the resulting lower in-cylinder temperature can reduce the requirement of EGR rate for NOx emissions control [144]. A number of experimental and computational studies have been carried out to explore the potential of late intake valve closing (LIVC) for the application of PCCI combustion in HD diesel engines [145–148].

2.5 Miller cycle engine operation

2.5.1 Principle of Miller cycle operation

Engine cycles can be referred to as over-expansion cycles when its effective expansion ratio (EER) is higher than the ECR. Atkinson cycle, the first four stroke internal combustion engine process with a relatively longer effective expansion stroke compared to the compression stroke, was invented by the English engineer James Atkinson in 1880s [149,150]. A complex linkage crank mechanism was deployed to realize the unequal compression and expansion strokes in the Atkinson engine, in which all four engine strokes are completed during one single revolution of the crankshaft.

Aside from the Atkinson cycle engine, Miller cycle engine is another type of over-expansion cycle engine achieved by means of adjusting valve timing to control ECR, which was built upon the former one. In 1950s, Miller cycle was patented by an American engineer, Ralph Miller [151–153]. In the beginning, the primarily interest of using Miller cycle is to reduce the cylinder temperature at TDC by modulating IVC timings. With lower in-cylinder temperature at the end of the compression stroke, more fuel can be burned at full load to increase engine power density while maintaining the limits of the supercharged engine components within acceptable levels, which was mentioned in the 1954 patent [151]. While in the patent of 1956, the main objective was particularly focus on the boosted spark ignition engines in an attempt to control auto-ignition and enable a proper air/fuel mixture at high engine load with a higher degree of over-expansion cycle [152].

Despite both EIVC and LIVC strategies are commonly used to realize Miller cycle, the EIVC was the preferred embodiment as it could achieve the “internal cooling”. This happen because the EIVC can create an extra expansion during the intake stroke, which helps reduce the initial compression temperature and pressure [154,155]. As shown in Figure 2.17, the EIVC was used to achieve Miller cycle operation at engine loads between 50% and 100% in a boosted diesel engine. The in-cylinder gas temperature was reduced

apparently with an EIVC strategy, but required higher intake pressure to maintain in-cylinder air/fuel ratio [151]. Figure 2.18 shows an ideal process of Miller cycle performed with EIVC and LIVC strategies against conventional diesel combustion in terms of “Miller loss”.

However, the terms of Miller cycle and Atkinson cycle used in the literature are not consistent. The over-expansion cycle by means of LIVC is commonly referred as the Atkinson cycle while the use of EIVC strategy is often associated with the Miller cycle [156–158]. Some literature, however, believed that the primary difference between these two terms is whether the over-expansion cycle equipped with boosting systems, considering Miller cycle engine is generally employed a supercharger or a turbocharger to recover the fresh air loss [159,160]. There are also some studies considered the Miller cycle is essentially same as the Atkinson cycle or the Miller cycle is a boosted Atkinson cycle with a boosting system [161–163].

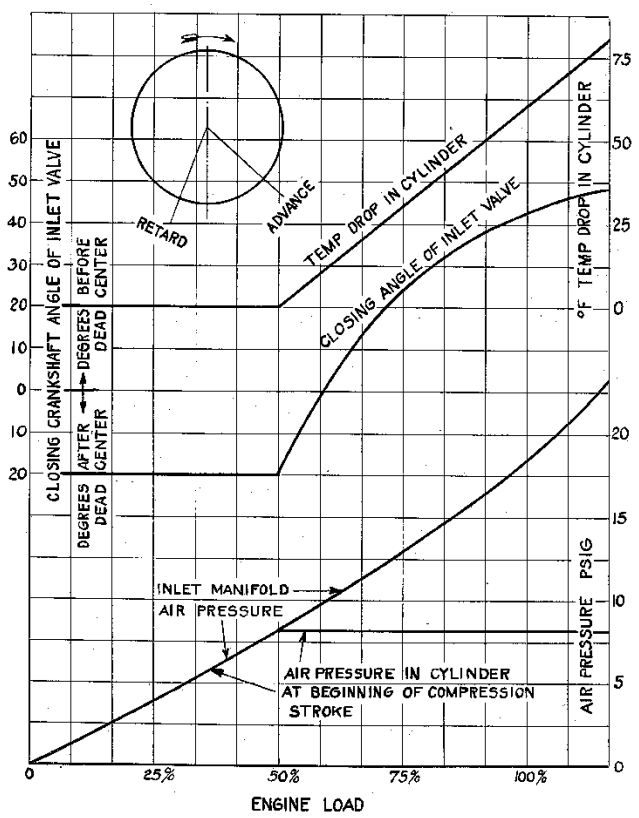

Figure 2.17: Effect of Miller cycle with EIVC strategy on in-cylinder gas temperature and its requirement on the intake pressure for a boosted diesel engine. Adapted from [151].

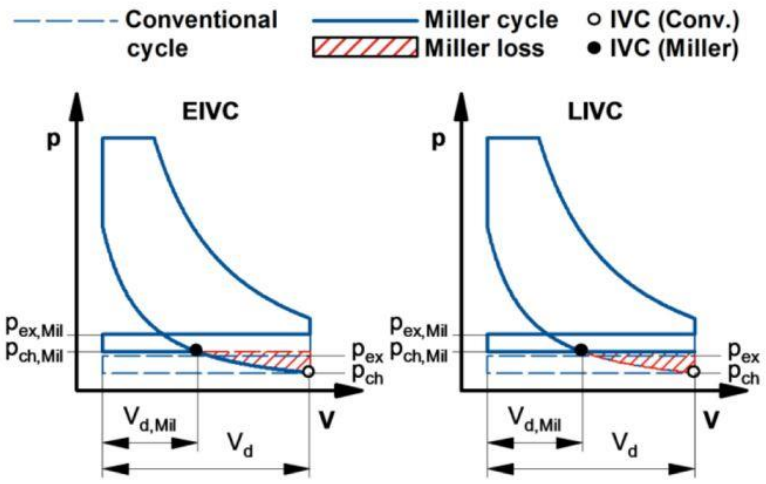

Figure 2.18: Idealized process of the Miller cycle with EIVC and LIVC for the “Miller loss”. Adapted from [164,165].

In this work, as the original patents of Atkinson cycle used a crankshaft mechanism instead of a VVA system to achieve lower ECR, the author regard any over-expansion cycles achieved by means of either EIVC or LIVC as the Miller cycle, regardless of the air induction is naturally aspirated or boosted. While those over-expansion cycles accomplished via a linkage crank mechanism should be considered as the Atkinson cycle. The typical representatives of using Atkinson cycle and Miller cycle concepts in commercial applications can be the Honda EXlink engine [166] and Mazda SKYACTIV-G engine [167], respectively.

2.5.2 Development and application of Miller cycle in IC engines

The Miller cycle concept has been well known since from the 1950s, and has found a number of commercial applications for different types of engines such as gasoline, diesel, and gas engines [168–170]. Initially, the main interest of applying Miller cycle in diesel engines is for emissions control in marine applications by lowering the in-cylinder gas temperatures at the end of the compression stroke [153,169,171]. In recent years, however, the main research focus have been on the reduction of NOx emissions from on-road diesel vehicles as the emissions regulation become increasingly stringent [172–175].

In comparison, the Miller cycle technology has been widely applied in gasoline engines. A number of studies have shown the great potential of Miller cycle in reducing pumping losses at part loads and can reduce the risk of knocking at high engine loads, which thus improving the overall fuel efficiency and engine performance. This is significantly important when applied this combustion concept in an increasingly downsizing turbocharged gasoline engine. Thus, many automotive companies have been mainly attracted by the fuel efficiency benefits of Miller cycle technology and have commercially

applied it on the gasoline engines in passenger vehicles [176–180]. Among them, Mazda is the first automotive company in mass production of Miller cycle engine and introduced to the market in 1993 [168].

From the perspective of some practical applications, the potential of Miller cycle technology is being studied in diesel engine field for marine engine emissions control [171]. In recent years, the main research focus have been put on the reduction of NOx and PM emissions from on-road diesel vehicles as the emissions regulation become increasingly stringent. Thus, Miller cycle has received more attention on both high-speed and heavy-duty diesel engines due to the potential benefit in the reduction of NOx emissions obtained by lowering the in-cylinder gas temperature at the end of the compression stroke and hence the peak combustion temperature.

Many studies have recent been performed on the investigation of Miller cycle in diesel engines. Experimental and numerical studies by Rinaldini et al. [181] showed the Miller cycle strategy could led to simultaneous reduction in NOx and soot emissions by 25% and 60% respectively, but with a fuel efficiency penalty of 2% in a light-duty diesel vehicle in the European Driving Cycle. The NOx emissions reduction observed in the Miller cycle was mainly because of the lower combustion temperatures, while significant soot reduction was explained by the higher values of air/fuel ratio as a consequence of the higher boost pressure. Wang et al. [182] experimentally investigated the application of Miller cycle in a diesel engine for NOx emissions control, decreasing NOx emissions by up to 17.5%. Wu et al. [183] investigated the influence of Miller cycle and variable geometry turbocharger in steady and transient operation of a HD diesel engine. The peak NOx emissions were reduced by 10% with a quick dynamic torque response when compared to the diesel conventional cycle. Gonca et al. [184] carried out experimental and simulation analysis to evaluate the influence of Miller cycle on engine performance and emission parameters. A maximum NOx reduction of 30% was obtained by Miller cycle at the expense of lower torque and brake efficiency. Further experimental studies by Gonca et al. [185] showed that the Miller cycle combined with turbo-charging can effectively minimize NOx emissions by 27% while increasing the engine torque by 1%.

Despite many studies have demonstrated the capability of Miller cycle for NOx emissions control, the level of NOx reduction achieved by Miller cycle alone is limited in diesel engines, particularly at low engine loads [16]. This is primarily due to the relatively small impact on the peak in-cylinder gas temperature at low load operations [32,33]. External EGR, however, is a proven technology for NOx formation control [34]. Some studies [35–

38] have investigated the combined use of Miller cycle and EGR and have demonstrated that this strategy is effective in minimizing engine-out NOx emissions.

Verschaeren et al. [186] evaluated the effect of EGR with Miller cycle via EIVC on engine efficiency and NOx emissions in a medium speed heavy-duty diesel engine. The results showed a significant increase in the ignition delay when combining EGR with more advanced intake valve closure timing. This led to a delayed combustion phasing, resulting in longer combustion duration and lower engine efficiency. NOx emissions were reduced by up to 70% at different loads. CO and PM increased whereas HC emission decreased due to the higher exhaust temperature which allowed for more oxidation of HC emission during the expansion stroke. Kim et al. [16] investigated the effects of LIVC with EGR on engine performance and emissions of a single cylinder diesel engine operating at low load conditions. The LIVC strategy alone demonstrated a limited NOx emissions reduction. With appropriate combination of LIVC and EGR, a reduction in the NOx emissions from more than 10 g/kWh to less than 1 g/kWh was obtained with slight penalty on the IMEP.

Benajes et al. [187] studied the impact of EIVC with a constant intake pressure in a HD diesel engine. The EGR rate was varied to keep the in-cylinder oxygen concentration constant. An increase in the in-cylinder combustion temperatures was observed due to the lower total heat capacity of the in-cylinder gas, while the lower compressed gas temperatures prior to the start of combustion reduced the flame temperature which plays the dominant role on the NOx formation. Additionally, the use of EGR rates were more effective in reducing the flame temperature than the use of EIVC. Further studies by Benajes et al. [159] through CFD simulation showed that both EIVC and EGR lowered the combustion temperatures and led to leaner local equivalence ratios. This effectively suppressed NOx and soot formation at the expense of lower engine efficiency.

In addition to the challenges observed in curbing the NOx emissions, peak in-cylinder pressure limitation is another constraint for modern turbocharged HD diesel engines when operating at high engine loads. Miller cycle reduces the maximum in-cylinder pressure by delaying the initiation of the compression process. This allows for the application of more advanced diesel injection timing, higher fuel injection pressures, and boost pressures to improve the engine efficiency. Kovács et al. [164] investigated the Miller cycle in the upper load range of a HD diesel engine in order to reduce the peak cylinder pressure. The pressure reserve was used to combine with advanced measures while maintaining the maximum in-cylinder pressure of the baseline case. When applied with higher fuel injection pressure, Miller cycle increased the engine efficiency by up to 10%. In the combination of Miller cycle with higher boost pressure at constant CA50 and/or NOx

emission by adjusting the start of injection and EGR rate respectively, soot and CO emissions were significantly reduced, and thus a significant improvement in the trade-offs between NOx, soot, and CO.

Moreover, in modern diesel engines, advanced combustion control technologies such as higher injection pressure, two-stage turbocharger, and multiple fuel injection strategy have been developed to increase engine thermal efficiency, but these technologies typically accompanied with a decrease in EGT and the NOx-soot and NOx-CO trade-offs remain. In addition, these strategies would increase the total engine operational cost when considering the total fluid consumption including diesel fuel and the estimated urea consumption in the SCR system. For these reasons, a number of studies have explored various techniques to increase EGT and improve fuel efficiency and emissions. One of the effective ways to increase EGT is using VVA device to realize Miller cycle and internal EGR, which provides a number of other benefits as well. Ratzberger et al. [188] carried out an experimental and numerical study to evaluate the ability of an early exhaust valve opening (EEVO) and LIVC for exhaust thermal management. An increase in EGT was realized by LIVC. However, the decreased pressure and temperature at the start of combustion led to poor combustion stability and problematic unburnt HC emission. The results also showed that EEVO enabled a distinct increase in exhaust enthalpy at the expense of higher fuel consumption.

Garg et al. [189] investigated the influence of cylinder throttling with EIVC and LIVC timings. The results showed that both delaying and advancing IVC reduced the volumetric efficiency, resulting in a reduction of in-cylinder air mass flow. This contributed to an increase in EGT. The reduction in piston motion–induced compression resulted in a lower in-cylinder gas temperature and higher degree of premixed combustion, which can simultaneously curb NOx and soot formations. The higher EGT and lower unburnt HC and CO were attained at low-load conditions by trapping internal exhaust gas recirculation with higher exhaust back pressures [113,115]. Other research into the use of a VVA to improve upon exhaust thermal management can be found in literatures [190,191].

The previous investigations have shown that Miller cycle with iEGR or eEGR strategies can be effective in increasing EGT and minimizing the engine-out NOx emissions from diesel engines. The lower ECR and oxygen availability, however, can adversely affect the soot emissions and fuel conversion efficiency and thus the total EOC. In addition to the fuel efficiency, the total EOC will be also affected by the urea consumption in the ATS. Therefore, the optimization of the combustion process with Miller cycle and EGR is

necessary in order to explore the NOx reduction capability while decreasing the EOC of a SCR equipped vehicle.

Despite all the previous studies on Miller cycle applied in diesel engines, the practical application of the Miller cycle into automotive diesel engines is still significant challenge. The main reasons can be summarized as follow [174,181,192]:

- The diesel engines are typically unthrottled and have better scavenging performance, so the Miller cycle technology used in diesel engines is more difficult to improve fuel efficiency compared to operating in gasoline engines.
- The Miller cycle strategy applied in diesel engines is limited only at partial load. This is because there is little interest for NOx reduction at full load where requires significant higher demands on boosting systems and intercoolers and the Miller cycle would also reduce the volumetric efficiency at full load [193,194].
- Constant switching the IVC timings when engines running continuously requires a highly reliable and durable VVA system to realize Miller cycle.
- A high compression ratio is commonly used in diesel engine, thus, the clearance between the piston and valve can be an issue.
- At medium to low engine speeds, the standard turbocharger is not able to provide the required air flow rate when Miller cycle is applied, which requires a sophisticated boosting system to supply the high boost pressures.
- Furthermore, a variable valvetrain and the high performance turbocharging system to maintain power density would increase the engine initial cost [168].

In the most recent years, however, the growing concerns over the GHG such as CO_2 and continuing push for emission control are driving the development of advanced combustion and engine control technologies for HD vehicles. Miller cycle has been shown as an effective engine control technology and is being considered as a mainstream technology to be adopted into HD diesel engines by engine manufacturers. One example is the recent development of the IAV SlideCam system for the HD engines. This device is able to accomplish two goals. The first one is to enhance the combustion process and thus improve the fuel conversion efficiency by means of Miller cycle. The other is increasing EGT at low operation loads through earlier exhaust valve opening (EVO), which can improve the conversion efficiency of ATS with insignificant penalty on the engine efficiency [174].

2.6 Summary

This chapter has presented the challenges faced by internal combustion engines and the necessity of developing highly efficient and clean HD engines to comply with the increasingly stringent fuel efficiency and exhaust emissions regulations in the transportation sector. The primary exhaust emissions from diesel engines and their respective formation mechanisms have been presented. Development of HD diesel engine emission control technologies have been mainly driven by the continuing push of legislations. The potentials and limits of alternative diesel combustion strategies in reducing exhaust emissions and fuel consumption have been discussed.

Miller cycle has been studied previously and identified as a promising technology for reducing exhaust emissions and enhancing low-load exhaust temperature management, and thus help to meet the current and future emission regulations. The main benefits and challenges of using Miller cycle in a HD diesel engine were demonstrated while the potential of Miller cycle with internal and external EGR were explored regarding the engine-out emissions and fuel efficiency, as well as exhaust temperature management. However, there is not detailed and comprehensive analysis of different parameters contributing to the overall influence observed with the employment of Miller cycle technology. Research and development works are necessary to explore the potential synergy of Miller cycle with other techniques and identify the optimum engine control technologies for the best trade-off between emissions and engine thermal efficiency. Moreover, investigations should be conducted to assess the effect of Miller cycle technology on the total engine fluid consumption of a SCR equipped HD diesel engines over the entire engine operation map.

Chapter 3
Experimental methodology

3.1 Introduction

The research work was conducted on a single-cylinder four-stroke HD diesel engine equipped with a VVA system and coupled to an eddy current dynamometer. This chapter firstly describes the experimental setup and test cell facilities used during the engine testing to acquire all measurements and research data in section 3.2. Followed by the description of the data acquisition and analysis methods, as well as the equations used in both real-time and post-processing analysis in section 3.3, while described in section 3.4 is the engine testing methodology.

3.2 Experimental setup

Figure 3.1 shows the schematic of the experimental setup in this work, which comprises of a single cylinder engine, the engine test bench, a boosting system, as well as measurement devices and a data acquisition system. Specifically, the research engine was a 2.026 dm^3 HD diesel engine unit, which includes a common rail diesel injection system, an external supercharger with closed loop control, a High Pressure Loop (HPL) cooled EGR and a hydraulic lost motion VVA system on the intake camshaft. An overview of the engine test bed and experimental facilities is depicted in Figure 3.2. An electric starter motor mounted on the dynamometer was powered by a battery with voltage of 12V and was used to start the engine. In order to absorb the work inputted from the engine, a Froude-Hofmann AG150 Eddy current dynamometer with a rated power of 150kW and maximum torque of 500 Nm was deployed. The principle is that a Texcel V4-EC controller was used to varying the magnetic field generated by coils in order to control the power absorption. The resulting eddy currents act to oppose the engine rotation and generating heat in the loss plates, which was dissipated by external cooling water. Additionally, a Thames Side Sensors U4000 load cell was used to measure the engine torque. Engine coolant and lubrication oil were supplied externally and their temperatures along with the intake air and EGR flow temperatures were controlled by the water cooled heat exchangers. All the equipment in the test cell have been calibrated before carrying out the experimental test and a daily check was taken every day before starting formal testing. The specifications of the measurement equipment can be found in Appendix A.

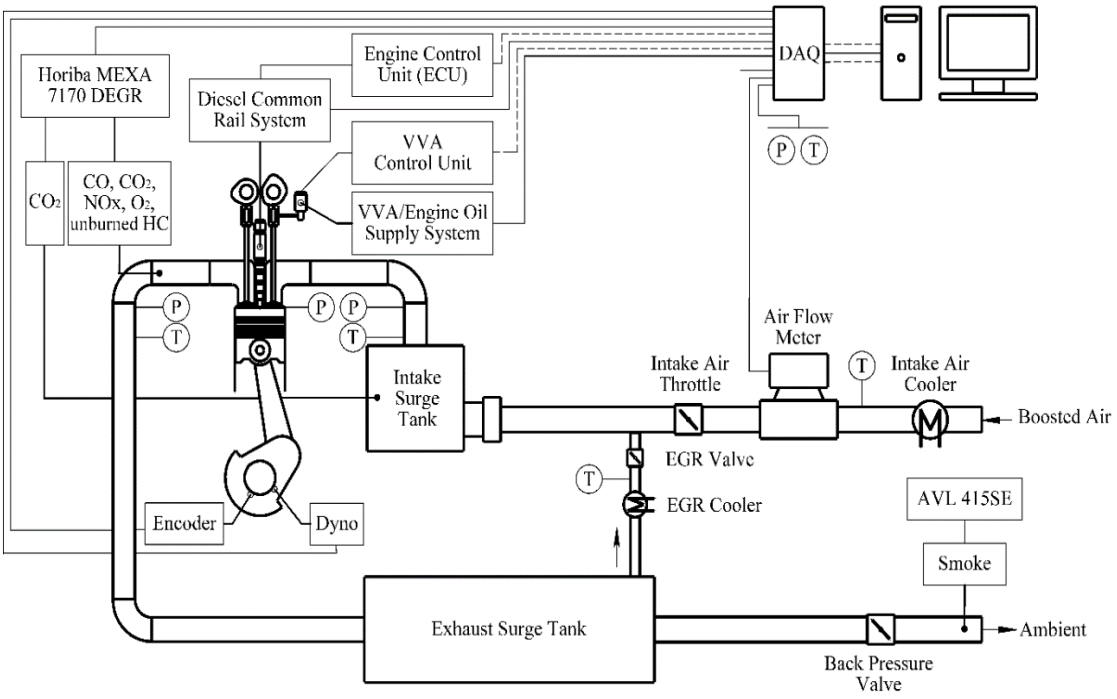

Figure 3.1: Layout of the engine experimental setup.

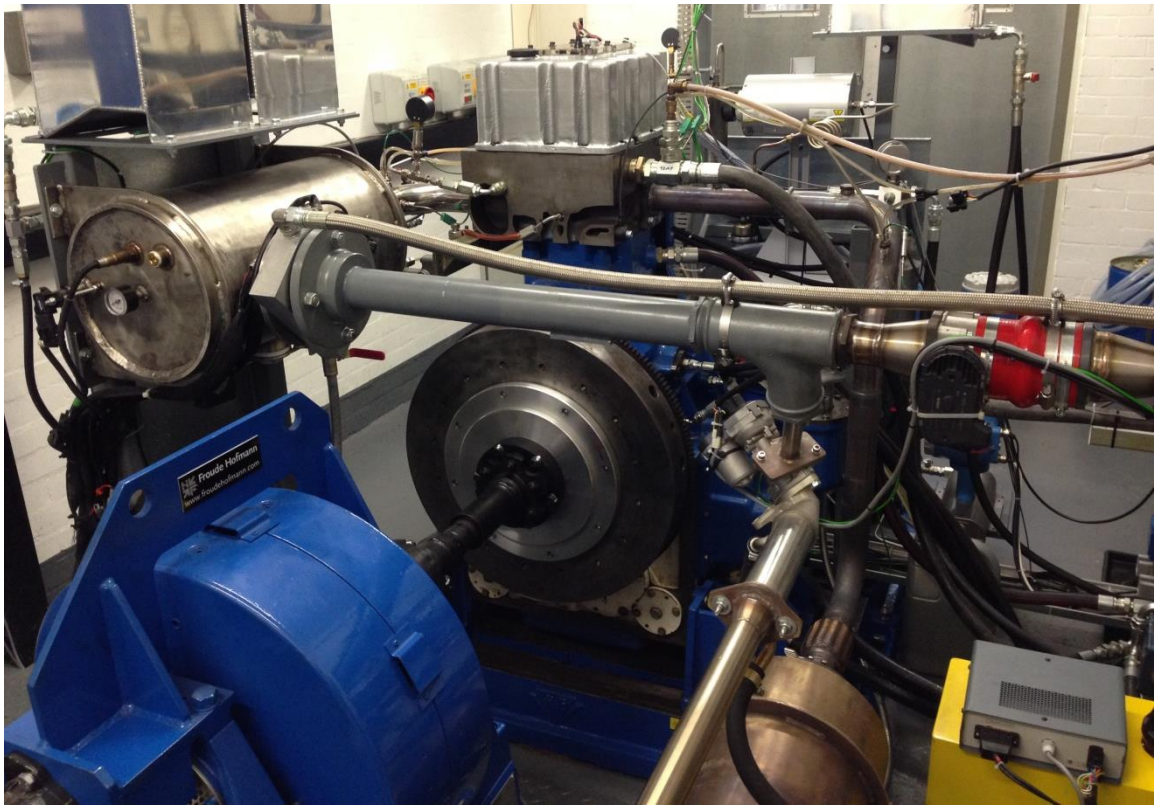

Figure 3.2: Overview of the engine test bed and experimental facilities.

3.2.1 Engine specifications

The testing engine is typically developed for a modern truck. The key specifications of the engine are listed in Table 3.1. Amid the composition of the engine, the design of the cylinder head with 4-valve and a stepped-lip piston bowl were based on the Yuchai YC6K six-cylinder engine, while the bottom end/short block was AVL-designed with two counter-rotating balance shafts. It should be also noted that the combustion chamber was swirl-oriented with the aim to enhance in-cylinder air motion.

Table 3.1: Specifications of the single cylinder HD diesel engine.

Parameter	Value
Bore x Stroke	129 x 155 mm
Displaced Volume	2.026 dm^3
Clearance volume	0.128 dm^3
Connecting Rod Length	256 mm
Geometric Compression Ratio	16.8
Piston Type	Stepped-lip bowl
Number of Valves	4
Intake Valve Diameter	43.9 mm
Exhaust Valve Diameter	40.4 mm
Intake valve opening/closing	Variable
Exhaust valve opening/closing	144/360 CAD ATDC (at 0.5mm valve lift)
Maximum Intake/Exhaust valve lift	14 mm
Maximum Cylinder Pressure	180 bar
Maximum Engine Speed	1900 rpm
Diesel Injection system	Bosch Common Rail
Diesel Injector	Central DI Bosch CRIN 3-22, 8 Holes, 150° Spray Angle, 0.18 mm hole diameter
Maximum Fuel Injection Pressure	2200 bar

3.2.2 Variable valve actuation system

Overhead camshafts were installed on the cylinder head, as shown in Appendix B. The intake camshaft of the engine was equipped with a Jacobs hydraulic lost motion VVA system, in which a collapsing tappet on the valve side of the rocker arm was incorporated to realize the required valve events such as LIVC and 2IVO [195]. Figure 3.3 depicts the high speed solenoid assembly, which was controlled with engine oil and calibrated TTL

signal, combining with a special design of intake cam to enable the modification of the intake valve lift height.

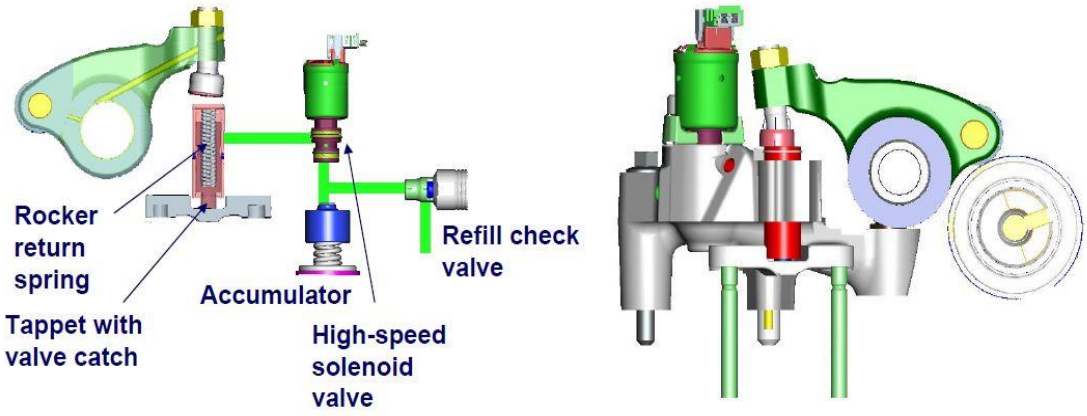

Figure 3.3: Research engine and lost-motion VVA system with collapsing tappet on the intake valve side [195].

Figure 3.4 shows the fixed exhaust camshaft timing and variable intake valve profiles. A mechanical failsafe partial intake valve lift was provided as shown by the green dash line, which represented the “Tappets Collapsed” mode where the VVA system is switched off. In this scenario, the high oil pressure in the tappet was released and thus the oil was free to flow out of the tappets, which led to a minimum intake valve lift of 9.6 mm.

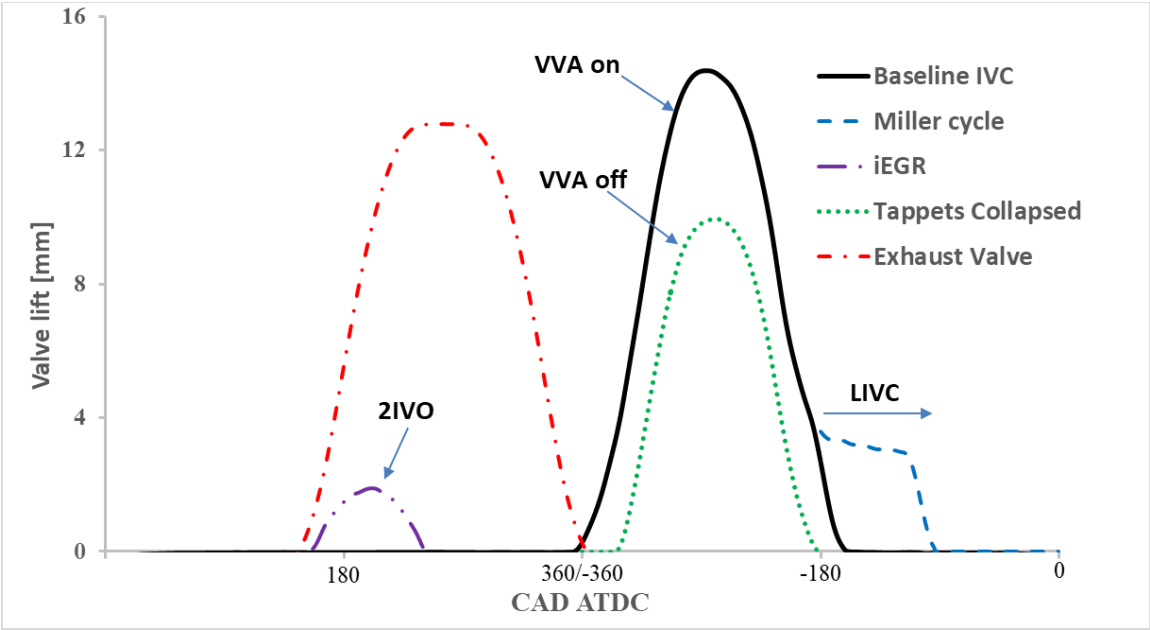

Figure 3.4: Engine fixed exhaust and variable intake valve lift profiles with VVA.

The VVA system enabled a variable IVC timings to obtain the required ECR and also a 2IVO event to trap the residual gas. The maximum lifts of intake valve and 2IVO event were 14 and 2 mm, respectively. All valve opening and closing events in this study were

considered at 1 mm valve lift. A LORD MicroStrain S-DVRT-24 displacement sensor was installed on the top of the intake valve spring retainer and was used to measure the intake valve lift.

3.2.3 Intake and exhaust systems

The fresh air inside the test cell was supplied either with naturally aspirated or with boosted, as shown in Figure 3.1. In particular, the compressed air flow was supplied by an AVL 515 sliding vanes compressor unit with closed-loop control, which was coupled to an electric motor. The range of absolute intake pressure can be adjusted between 1.1 and 3.2 bar and the accuracy can be maintain within ± 0.015 bar. The intake flow rate was measured by an Endress+Hauser Proline t-mass 65F thermal mass flow meter. The working principle is based on the cooling effect of the mass flow when it passes over a heated transducer. There are two PT 100 RTD transducers fitted to the air stream, one is used as a temperature sensing device while the other is used as a heater. Power was provided to the sensor to maintain a constant temperature differential between these two transducers. In addition, the higher mass flow, the higher cooling effect and power consumed. Finally, the total consumption of heater power was therefore the measurement of the gas mass flow rate. The intake manifold pressure was fine adjusted by means of an electronic intake throttle valve with a diameter of 74 mm.

Two piezo-resistive pressure transducers were installed to measure the instantaneous pressures of both intake and exhaust ports. The exhaust back pressure was independently controlled through a butterfly valve located downstream of the exhaust surge tank. Two large surge tanks were installed in the intake and exhaust systems to damp out the strong pressure fluctuations in the intake and exhaust manifolds resulted from the gas exchange dynamics of the engine. The one for intake was a 24 liter surge tank while the other one for exhaust was a 54 liter surge tank. High-pressure loop cooled external EGR was introduced into the engine upstream of the intake surge tank using a pulse width modulation-controlled EGR valve and the pressure differential between the intake and exhaust manifolds.

3.2.4 Fuel delivery system

During the experiments, the diesel fuel was firstly delivered by an independent low-pressure system to a Bosch CP4-S2 high-pressure pump by means of a pressure regulator, as schematically shown in Figure 3.5. Afterward, the diesel fuel was supplied by the high-pressure pump driven via an ABB electric motor to a Bosch common rail system. Finally, it was injected into the cylinder by an 8-hole Central DI Bosch CRIN 3-22

solenoid injector with fuel pressure up to 2200 bar. A bespoke CR.8 electronic control unit (ECU) provided by ECE Engine Control Electronics GmbH was used to control fuel injection parameters such as the injection pressure, start of injection, and the number of injection per cycle.

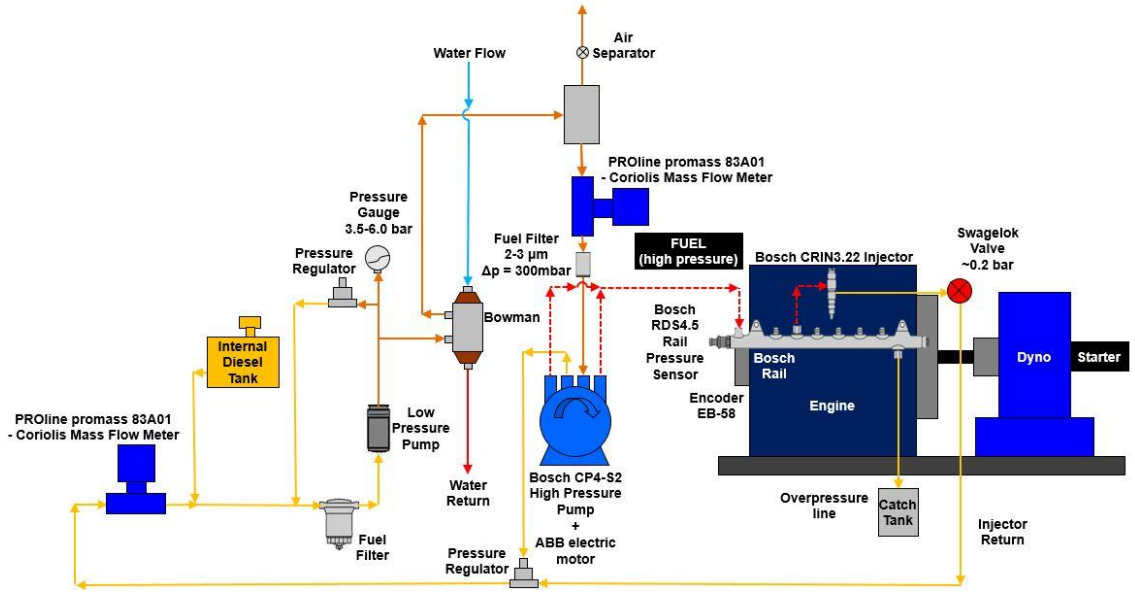

Figure 3.5: Overview of the diesel fuel supply diagram.

Figure 3.6 is a picture of the fuel flow meter used in the test bed. Due to the constraints faced by the high pressure pump and diesel injector regarding the fuel returning, it was necessary to use two Endress+Hauser Promass 83A Coriolis mass flow meters to measuring the fuel consumption during the test. This method could also minimize the effect of fuel pressure drop across the suction line and reduce the cycle variation of the mass flow measurements. The top one was used for measuring the total fuel supplied while the bottom one was used for measuring the fuel return from the high-pressure pump and injector.

In addition, there is an air separator connected to this loop with another top end connected to the entrance of the total mass flow meter at atmospheric pressure. The pipe of the air separator goes upwards and the top end is higher than all other pipes and parts in the system, which helps to remove any air bubbles in the low pressure fuel circuit before the fuel is delivered to the high pressure fuel circuit, as shown in Figure 3.5.

The fuel flow meter is working on the principle of the oscillations amplitude generated by the Coriolis forces, which is independent of the physical fluid properties including temperature, pressure, viscosity, and density. The mass flow through the measuring tube produces Coriolis forces, which leads to a phase shift in the oscillating frequency. The greater mass flow, the greater phase difference and therefore the amplitude of the

oscillations. Two electrodynamic sensors are used to measure the tube oscillations between the inlet and outlet and thus to determine the actual mass flow. The detail of the fuel mass flow meter calibration and the diesel fuel specification were demonstrated in Appendix C and D, respectively.

Figure 3.6: Endress+Hauser Promass 83A Coriolis Flow Meters.

3.2.5 Emissions measurement system

The Horiba MEXA-7170 DEGR emission analyser was used to measure the EGR rate and the gaseous exhaust emissions such as NOx, CO, CO_2, oxygen (O_2), and total unburnt HC. An AVL 415SE Smoke Meter was used to measure the smoke concentration, which was collected from downstream of the back pressure valve after the exhaust gases passed the exhaust surge tank. This was because a more homogeneous and steady gases flow could be achieved in this location. In addition, a high-pressure sampling module and a heated line were deployed between the exhaust sampling point and the emission analyser in order to allow for high-pressure sampling closed to the exhaust port and avoid condensation with a gas temperature above 464 K, respectively. To ensure the repeatability and consistence of emissions measurement in different days, the exhaust analyser was calibrated using standard span gases prior to engine tests. Moreover, all gaseous emissions were measured by the emission analyser with an error below 1% of full scale and a repeatability within 0.5% of full scale.

With the use of the analyser system, gases including CO and CO_2 were measured on a dry basis through a non-dispersive infrared absorption (NDIR) analyser. The

measurement principle was relied on the different radiation absorption of each constituent gas in a sample at a particular wavelength. The measurement range for CO and CO_2 were set to 0-120000 ppm 0-200000 ppm volume by volume (v/v), respectively. The total unburnt HC was measured on a wet basis using a FIA-725A heated flame lonization detector (FID) and the measurement range was set to 0-50000 ppm v/v. This detector was working on the principle that the sample gas was introduced in a burner and mixing with hydrogen-helium and high purify air provided. Electrons and positive ions were generated when the hydrocarbon in the sample were burnt. There were two electrodes on each sides of the burner, which were used to detect the ions in the form of an electric current. The electric current across the collector was closely proportional to the rate of ionization, which in turn determined the number of carbon atoms and thus the concentration of hydrocarbons in the sample. The free O_2 concentration in the exhaust sample was measured using a MPA-720 magneto-pneumatic detector with an operation range between 0 and 250000 ppm v/v dry. This method was based on the nonhomogeneous magnetic field where the sample was immersed in. The differential pressure created by the O_2 concentration in the sample and the reference gas with a given O_2 concentration enabled the detection of O_2 concentration in the sample using a microphone. Finally, NOx emissions comprised of NO and NO_2 were measured on a dry basis using a CLA-720MA heated chemiluminescence detector (HCLD) with an operation range between 0 and 10000 ppm v/v. NO_2 emissions in the sample were first converted to NO by means of a catalyst because the detector can only measure NO instead of NO_2. The total NO and ozone react to form electrically excited NO_2 in the first reaction, then immediately return back to the ground state along with emitting red light. The intensity of the red light measured is proportional to the total NO concentration in the sample.

In addition to the measurement of those exhaust gases discussed above, the smoke concentration in the exhaust was measured by an AVL 415SE Smoke Meter. The known volume of exhaust sample was drawn through the filter paper and led to filter paper blackening. This was due to the captured soot and could be measured by an optical reflectometer head. The resulting blackening level was converted to a range between 0 and 10 which in accordance with Filter Smoke Number (FSN). The higher number value was corresponded to the higher light absorption and therefore higher soot levels. According to the calibrated results, the sampling time set to 30 seconds with a sample volume collection of 5 liters can achieve higher measurement accuracy.

In this study, Horiba emissions analyser was also used to measure the external cooled EGR through using an additional AIA-722 NDIR gas analyser to sample CO_2 concentration from the intake surge tank. The EGR rate was defined as the ratio of the

measured CO_2 concentration in the intake surge tank ($(CO_2\%)_{intake}$) to the CO_2 concentration in the exhaust manifold ($(CO_2\%)_{exhaust}$) as

$$EGR\ rate\ = \frac{(CO_2\%)_{intake}}{(CO_2\%)_{exhaust}} \times 100\% \quad (3.1)$$

3.2.6 Data acquisition and control systems

The data acquisition and control systems were primarily comprised of an ECU, a VVA control unit, a data acquisition (DAQ) board, and a personal computer. The ECU-CR.8 provided by ECE Engine Control Electronics GmbH was responsible for controlling injection characteristics such as SOI, amount of injection, and injection pressure, while the amount of fuel flow supplied at a certain load was adjusted automatically by the ECU based on the principle of engine speed governor. A Bosch RDS4.5 high-pressure sensor mounted on the common rail was used for the measurement of fuel injection pressure. Additionally, the injector current signals sent by the ECU were captured by a LEM PR30 current probe. Finally, the communication from ECU to personal computer was realized through an USB-CAN interface and a specific running program.

Two National Instruments data acquisition cards were used, which include a high speed USB-6251 with a maximum sampling rate of 1.25 Mega samples per second (MS/s) and a low speed USB-6210 with a sampling rate of 250 kilo samples per second (kS/s). The former one was used to capture high speed signals such as the intake valve timings and the crank angle resolved data which was synchronized with encoder. The low speed one was used for low frequency signals generated from the measurement equipment. In addition, the communication between the exhaust analyser and the computer was realized via Ethernet cable. These data collected together with the ECU feedback to the DAQ card were processed in real-time and displayed lively on a transient combustion analyser software developed by Dr Yan Zhang [196], as displayed in Figure 3.7. Parameters shown in the screenshot were recorded and averaged over 100 engine cycles.

Engine load was controlled in real-time by a TEXCEL V4 dynamometer controller and measured by a Thames Side Sensors U4000 Universal tension load cell with an error below ±0.03% of full scale load. Engine speed was measured using an electromagnetic pulse pick up and a toothed wheel mounted on the shaft half coupling hub. The Encoder Technology EB58 optical encoder with 1440 pulse per revolution was mounted to the engine crankshaft, which detected the position of crank angle and also determined the resolution of crank angle by 0.25 crank angle degrees. A Hall-effect unit camshaft sensor was used to monitor the camshaft position by installing it to the vicinity of camshaft gear.

The set IVC timings were sent to the VVA control unit via an analogue output channel in the high speed DAQ card. A LORD MicroStrain DEMOD-DVRT temperature compensated signal conditioner and an S-DVRT-24 displacement sensor were employed to measure the displacement of the valve spring retainer in order to capture the intake valve lift profile in real-time, as shown in Figure 3.8.

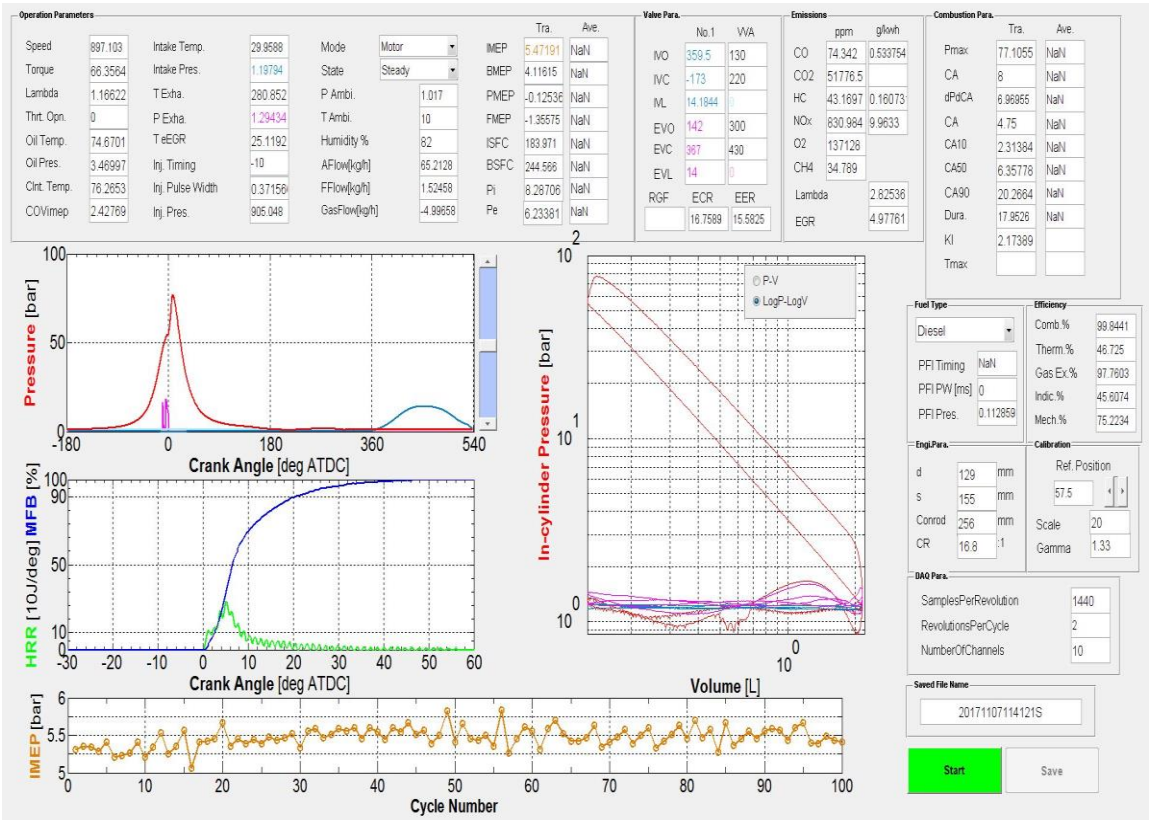

Figure 3.7: Experimental data displayed lively on the transient combustion analyser software.

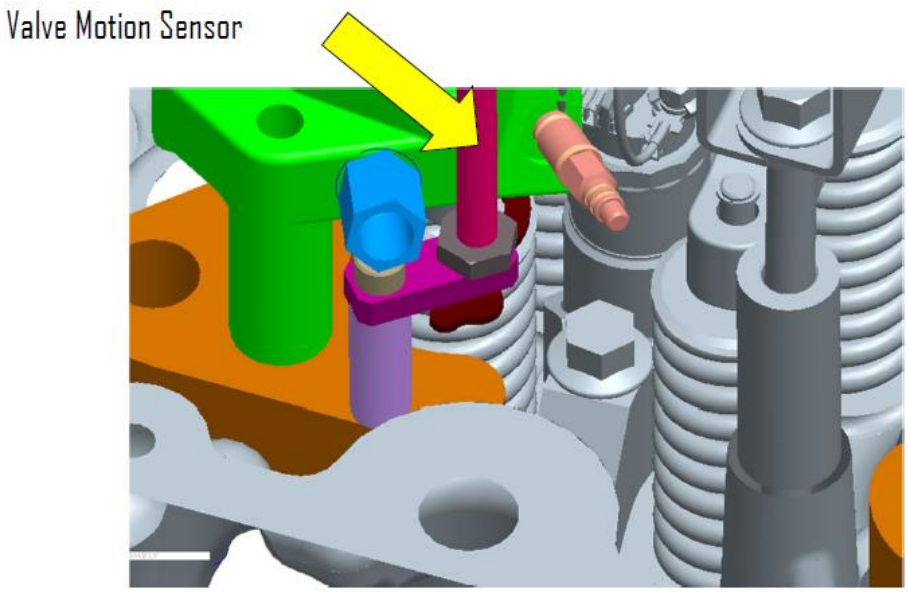

Figure 3.8: Intake valve displacement sensor in the VVA system.

The in-cylinder pressure which enabled the calculation of the IMEP, indicated specific fuel consumption (ISFC) and other important combustion parameters, was measured by a Kistler 6125C piezoelectric pressure sensor with an accuracy of ±0.4% full scale. The pressure sensor was capable of measuring pressure range to 300 bar with a sensitivity of -31.22 pC/bar. In addition, this sensor made with a shoulder sealing allowed it to be mounted in the cylinder head with its front flush. The electrostatic charge produced by the PiezoStar crystals in the sensor was processed and converted into electric potential difference by an AVL FI Piezo charge amplifier, which was proportional to the sustained pressure. To avoid zero point drift and phase shift errors, the charge amplifier was set to a cyclic drift compensation mode with a filter frequency of 100 kHz. It should be noted that the measurement of the piezoelectric sensor is only the variations of pressure. Therefore, the in-cylinder pressure signals were pegged to the average intake manifold pressure at around the bottom dead center (BDC) of intake stroke for all test cycles. A trigger signal (REF) was used to adjust the TDC position to keeping the motored peak cylinder pressure phased within a range of -1.0 ~ -0.5 CAD ATDC.

The measurement of the intake and exhaust pressures were performed via two Kistler water cooled piezoresistive absolute pressure sensors Type 4049A with analog temperature compensation, which enabled a measure range between 0 and 10 bar and were typically coupled to Kistler amplifiers Type 4622A. In addition, engine oil pressures were measured with GE UNIK 5000 pressure sensors. Finally, K- type thermocouples and pressure gauges were located at relevant locations for the measurement of other general temperatures and pressures.

3.3 Data analysis

This subsection briefly describes the analysis process of the data acquired by the DAQ program. During the engine test, every test point was saved twice and thus 200 cycles were recorded. Some of the data such as net heat release rate (HRR), pressure rise rate (PRR), IMEP, and ISFC were processed by the transient combustion analyser software in real-time while others like combustion efficiency, net indicated efficiency (NIE), and specific emissions were post-processed. The important equations and procedures for the post-processing are illustrated as follows along with the acronyms and symbols defined in the notation section. Another point should be noted for the post-processing was that the international system of units was used unless otherwise stated.

3.3.1 Heat release analysis

To calculate the HRR, a single zone heat release model was used and thus the internal energies of both products and reactants into this combustion system were considered uniform. In this case, the heat release rate of the fuel's chemical energy was in accord with the variation of in-cylinder pressure. Therefore, the net heat release rate analysis could be carried out according to the first law of thermodynamics along with the in-cylinder pressure and crankshaft position measured. In a combustion process, fuel and oxidizer in a combustion system react to produce different forms of energy, which was shown in the energy balance equation (3.2) as

$$dQ_{ch} = dW + dUs + dQ_{ht} + \sum h_i dm_i \tag{3.2}$$

where (Q_{ch}) is the heat chemical energy released from the fuel, (W) is the work done on the piston by the combustion system and (Q_{ht}) is the heat transfer across the system boundary into the chamber walls, (Us) is the internal energy change of the cylinder contents due to the chemical reaction. A small amount of in-cylinder gas (burnt and unburnt) flows into the crevice spaces or leaves the system was represented by the mass flux term ($h_i dm_i$). According to ideal gas law ($pV = \frac{m}{M}RT$), the cylinder charge temperature in the whole combustion system is assumed uniform and the variation in the ideal gas constant is negligible. Thus, it allows for the calculation of the HRR according to [13]:

$$dQ_{ch} = \left(\frac{c_v}{R}\right) V\, dP + \left(\frac{c_v}{R} + 1\right) p\, dV + dQ_{ht} + (h_{cr} - u + c_v T) dm_{cr} \tag{3.3}$$

In addition, Equation (3.3) can be further modified when combining the energy released term with the mass flux term and heat transfer. This means that only both the work done on the piston and the internal sensible energy change of the cylinder contents are considered and thus the output becomes the apparent net heat release (Q_{net}). In order to clearly display the heat release rate, all combustion data was divided by the crank angle position. Furthermore, the term ($\frac{c_v}{R}$) can be simplified by replacing with ($\frac{1}{\gamma-1}$), allowing Equation (3.3) becomes:

$$HRR = \frac{dQ_{net}}{d\theta} = \frac{1}{\gamma - 1} V \frac{dp}{d\theta} + \frac{\gamma}{\gamma - 1} p \frac{dV}{d\theta} \tag{3.4}$$

where $d\theta$ is the crank angle of 0.25 CAD as set by encoder resolution, γ is the ratio of specific heats, while p and V are the in-cylinder pressure and volume at any crank angle position. According to [197], the ratio of specific heats was suggested to assume constant at 1.33 throughout the engine cycle, although its value varies as the mixture composition and temperature change. The in-cylinder volume V at any crank angle position was calculated by the following equation (3.5):

$$V_{ins} = V_{clr} 0.5(R_c + 1) \left[\frac{2L}{S} + 1 - cos\theta - \left(\left(\frac{2L}{S} \right)^2 - sin^2\theta \right)^{\frac{1}{2}} \right] \tag{3.5}$$

The mass fraction burnt (MFB) was derived from the integration of Equation (3.4) and its maximum cumulation of heat release. With the analysis of the MFB curve, the important combustion parameters can be estimated, such as the combustion phasing (50% of the MFB), combustion duration (10-90% of the MFB), and ignition delay defined as the period between the SOI and the SOC (0.3% of the MFB).

The PRR expressed in bar/CAD, is one of the important indicators of combustion noise, as it is able to indicate how quick the heat release rate occurs. The magnitude of PRR was primarily determined by the engine robustness and human noise perception. In Equation (3.6) below, the maximum pressure variations correlated to the crank angle position were averaged over 200 engine cycles to calculate the PRR. It should be also noted that a FFT Filter with a window size of five data points was used to remove the signal noise from the apparent net HRR and the average in-cylinder pressure during the period of data post-process.

$$PRR = \sum_{n=1}^{200} PRR_{max} \Big/ n = \sum_{n=1}^{200} \left(\frac{dp}{d\theta_{max}} \right) \Big/ n \tag{3.6}$$

3.3.2 Overall engine parameters analysis

The pressure data for the in-cylinder gas over the cylinder volume of entire engine cycle was used to calculate the work done on the piston. The Equation (3.7) below was the integration of pressure signal over the corresponding cylinder volume throughout the engine cycle with the firing TDC defined at a zero crank angle position for the calculation of the net indicated work per cycle ($W_{c,i}$).

$$W_{c,i} = \int_{-180}^{540} p_i \; dV \tag{3.7}$$

The net indicated power (P_i) was defined as the rate of the net indicated work per cycle transfer from the in-cylinder gas to the piston, which was shown in Equation (3.8).

$$P_i = \frac{W_{c,i}\, N}{2} \tag{3.8}$$

A valuable relative engine performance parameter for comparing engines with different sizes is the net indicated mean effective pressure (IMEP), which was obtained by dividing the net indicated work per cycle by the swept volume (V_d), as presented in Equation (3.9).

$$IMEP = \frac{\int_{-180}^{540} p_i \, dV}{V_d} = \frac{W_{c,i}}{V_d} \tag{3.9}$$

While the gross indicated mean effective pressure ($IMEP_{gross}$) was obtained by dividing the gross indicated work during the compression and expansion cycles by the swept volume as

$$IMEP_{gross} = \frac{\int_{-180}^{180} p_i \, dV}{V_d} \tag{3.10}$$

The pumping mean effective pressure (PMEP), defined as the work performed on in-cylinder gas by the piston during the intake and exhaust stroke cycles, was given by

$$PMEP = IMEP - IMEP_{gross} \tag{3.11}$$

The engine cyclic variation during combustion, represented by the coefficient of variation of IMEP (COV_IMEP), was analysed by the ratio of the standard deviation of the IMEP to its averaged value obtained over 200 engine cycles as

$$COV\_IMEP = \frac{IMEP_{std}}{IMEP_{average}} * 100 \tag{3.12}$$

In single cylinder engines, the evaluation of NIE was greatly important for comparing the engine relative performance as the mechanical losses was not considered. The engine NIE was defined by the ratio of the work done to the amount of fuel energy supplied to the engine every cycle, as seen in Equation (3.13).

$$Net\ Indicated\ Efficiency = \frac{W_{c,i}}{m_{fuel} LHV_{fuel}} = \frac{P_i}{\dot{m}_{fuel} LHV_{fuel}} \tag{3.13}$$

The working fluids in the combustion chamber was usually treated as ideal gases. According to the ideal gas law [13], the average gas temperature in the cylinder at a given crank angle position was given by

$$T_{cyl,i} = \frac{p_i\, V_i\, M}{m\, R} = \frac{p_i\, V_i}{m\, r} \tag{3.14}$$

where m is the mass of gas, $\tilde{R}$ is the universal gas constant of 8.31432 J/mol.K, R is the gas constant for the gas, and *M* is the molecular weight. In addition, the mass of gas (m) is the total mass per cycle in the cylinder, as shown in Equation (3.15).

$$m = m_{fuel} + m_{air} + m_{rg} \tag{3.15}$$

where m_{fuel} is the amount of fuel mass and m_{air} is the air mass in every engine cycle. Particularly, the term m_{rg} is the mass of residual gas in the cylinder per cycle, which can be calculated using Equation (3.16) when there is not positive valve overlap.

$$m_{rg} = \frac{p_{EVC}\, V_{EVC}}{T_{EVC}\, R} \tag{3.16}$$

where p_{EVC} is the cylinder gas pressure at exhaust valve closing and V_{EVC} is the cylinder volume at EVC, while the T_{EVC} is the average exhaust gas temperature.

3.3.3 Engine-out exhaust emissions analysis

The exhaust emissions data given by the Horiba emissions analyser was in the form of parts per million (ppm), which was required to convert to specific exhaust gas emissions

in the unit of g/kWh when considering the relative engine exhaust flow. This was performed according to the methodology provided by the UN Regulation number 49 [16]. As described in subsection 3.2, the emission analyser provided the measured results of NOx and CO gases on a dry basis, which should be converted to a wet basis. In addition, a humidity correction was used for the calculation of specific NOx emissions as the ambient conditions played an important role. Equations (3.17), (3.18), and (3.19) were used to calculate the net indicated specific emissions of NOx, CO, and unburnt HC, respectively.

$$ISNOx = \frac{\dot{m}_{NOx}}{P_i} = \frac{u_{NOx}\,[NOx]k_w k_{hG}\dot{m}_{exh}}{P_i} \tag{3.17}$$

$$ISCO = \frac{\dot{m}_{CO}}{P_i} = \frac{u_{CO}\,[CO]k_w\dot{m}_{exh}}{P_i} \tag{3.18}$$

$$ISUHC = \frac{\dot{m}_{HC}}{P_i} = \frac{u_{CO}\,[UHC]\dot{m}_{exh}}{P_i} \tag{3.19}$$

where $\dot{m}_{gas}$ is the flow rate of each component in g/h, $[gas]$ is the concentration of each component in the exhaust gas in ppm, $\dot{m}_{exh}$ is the exhaust mass flow rate per cycle determined by the sum of air and fuel mass flow rate in kg/h, and u_{gas} is the fuel dependent molar mass fraction, as shown in Table 3.2.

Table 3.2: Molar mass fractions of exhaust gases for diesel [16].

Exhaust gas	Molar mass fractions
u_{CO}	0.000966
u_{NOx}	0.001586
u_{HC}	0.000482

To convert the NOx and CO emissions from dry basis to wet basis, a correction factor (k_w) was used, as presented in Equation (3.20). The correction factor was strongly dependent on ambient conditions as well as air and fuel mass flow rates. In addition, the fuel specific factor (k_f) was calculated considering the percentage mass of hydrogen (W_{ALF}) and oxygen (W_{EPS}) contents in the fuel as seen in Equation (3.21).

$$k_w = 1.008\left(1 - \frac{1.2442H_a + 111.19W_{ALF}\left(\frac{\dot{m}_{fuel}}{\dot{m}_{dry\ air}}\right)}{773.4 + 1.2442H_a + 1000\left(\frac{\dot{m}_{fuel}}{\dot{m}_{dry\ air}}\right)k_f}\right) \tag{3.20}$$

$$k_f = 0.055594W_{ALF} + 0.0070046W_{EPS} \tag{3.21}$$

An additional correction was performed for NOx emissions for compression-ignition engines using the factor k_{hG} as given by

$$k_{hG} = 0.6272 + 0.04403H_a - 0.000862{H_a}^2 \tag{3.22}$$

The term H_a is the ambient humidity, given in grams of water per kilogram of dry air, as calculated in Equation (3.23).

$$H_a = \frac{6.211 * RH * SP}{p_a - \frac{(RH * SP)}{100}} \tag{3.23}$$

where RH is the relative humidity in ambient air, p_a is the ambient air pressure, and SP is the water saturation pressure, which was derived from the ambient temperature (T_a) according to the methodology suggested by [198].

$$\begin{aligned} SP = {} & 604.8346 + 45.9058(T_a - 273.15) \\ & +1.2444(T_a - 273.15)^2 \\ & +0.0352248(T_a - 273.15)^3 \\ & +0.00009322061(T_a - 273.15)^4 \\ & +0.000004181281(T_a - 273.15)^5 \end{aligned} \tag{3.24}$$

The smoke concentration provided by AVL 415SE smoke meter was FSN values, which was converted to mg/m^3 and corrected to a standard condition of 273.15 K as seen in Equation (3.25) [199].

$$smoke\ concentration\ [soot] = \frac{1}{0.405} * 5.32 * [FSN] * e^{0.3062*[FSN]} * \frac{298}{273.15} \tag{3.25}$$

The net indicated specific soot emissions calculated from the soot emissions in mg/m^3, were a function of the fuel mass flow rate ($\dot{m}_{fuel}$), the air mass flow rate ($\dot{m}_{air}$), the net indicated power (P_i), and the exhaust gas density (ρ_{exh}) as given by

$$ISsoot = \frac{[soot]}{1000}\left(\frac{\dot{m}_{fuel} + \dot{m}_{air}}{\rho_{exh} * P_i}\right) \tag{3.26}$$

The exhaust gas density (ρ_{exh}) was calculated using Equation (3.27) provided by the UN Regulation number 49 [16].

$$\rho_{exh} = \frac{1000 + H_a + 1000\left(\frac{\dot{m}_{fuel}}{\dot{m}_{dry\ air}}\right)}{773.4 + 1.2434H_a + 1000k_f\left(\frac{\dot{m}_{fuel}}{\dot{m}_{dry\ air}}\right)} \quad (3.27)$$

Finally, the combustion efficiency was estimated after all exhaust gases and soot emissions were converted to net indicated specific emissions. The calculation of combustion efficiency was based on the unburnt exhaust products during combustion which mainly comprised of HC and CO for compression-ignition engines, as seen in Equation (3.28).

$$Combustion\ Efficiency = \frac{Q_{ch}}{m_{fuel}LHV_{fuel}} = 1 - \frac{\dot{m}_{HC}LHV_{HC} + \dot{m}_{CO}LHV_{CO}}{\dot{m}_{fuel}LHV_{fuel}} \quad (3.28)$$

where LHV_{CO} is the lower heating value of CO, given by 10.1 MJ/kg [13], and LHV_{HC} is the lower heating value of HC, which was assumed the same as the diesel fuel of 42.9 MJ/kg.

3.4 Method of engine testing

The study of various injector geometry parameters was performed over the European Stationary Cycle (ESC), which is a 13-mode, steady-state test procedure, introduced initially by the Euro III emission legislation [200]. Differed from ESC test cycle, the WHSC test cycle applied in the investigation of Miller cycle operation, is characterised with a reduction of average operational engine speed and load as well as the exhaust gas temperature, which has been adopted in the Euro VI emission regulation. Figure 3.9 shows the operating conditions in WHSC and ESC test cycles, as well as a light load test point located at a typical low exhaust gas temperature operating condition of a heavy-duty drive cycle. The size of the circle represents the weighting factor. A bigger size indicates a higher relative weighting of the engine operation condition in the corresponding test cycle.

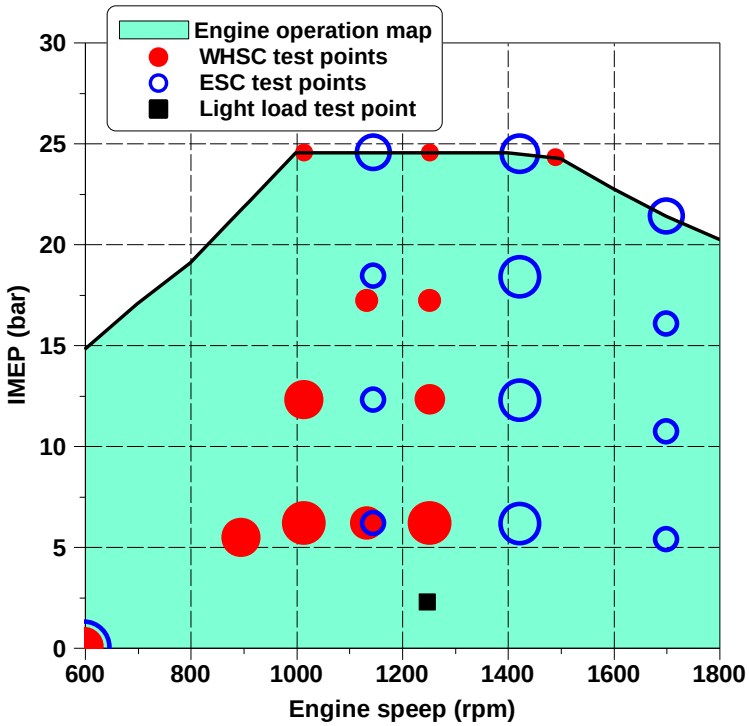

Figure 3.9: The WHSC and ESC test cycle points as well as a light load test point over the experimental engine speed-load map.

3.5 Summary

This chapter comprehensively describes the research engine, the experimental test cell facilities, and the measurement systems. The methodology is shown of how the data was collected, processed, and analysed by means of data acquisition system and both real-time and post-processing analysis. Followed by the description of the mathematical methods and related equations used to analyse the combustion heat release, overall engine performance parameters, and exhaust emissions. Finally, the test cycles used for the investigation of injector geometric parameters and the Miller cycle operation as well as a light load test point located at a typical low EGTs' operating conditions of a HD drive cycle are presented alongside the experimental engine speed-load map.

Chapter 4
Experimental study of the influence of injector geometric parameters

4.1 Introduction

As the intrinsic diesel fuel features of low viscosity and poor vaporization, the diesel engine performance and emission characteristics are strongly affected by the characteristics of the fuel spray development, such as fuel atomization, vaporization, and fuel-air mixing process. The fuel spray development processes are in turn determined by the injector geometry. Nowadays, in addition to introducing EGR, installing costly and complex aftertreatment devices, as well as employing alternative fuels, the diesel injector geometry is also considered as an important parameter for the compliance of the stringent emission legislations while maintaining high engine efficiency. Therefore, the injector geometry optimization plays an indispensable role to achieve highly efficient and clean combustion engine. In order to better understand the influence of injector geometric parameters on engine operations under different injection pressures and injection timings, a comprehensive investigation was carried out in this chapter.

4.2 Test methodology

In this chapter, injector geometric parameters including the injector Ks factor, fuel mass flow rate, and spray cone angle were experimentally investigated. Table 4.1 depicts the specifications of different test injectors. The study was performed at six operation points selected from European Steady-state Cycle (ESC), as depicted in Table 4.2. The operation conditions consist of three speeds (25%, 50%, and 75%, which are abbreviated as A, B, and C, respectively) and two engine loads (50% and 100%). The three engine speeds of A, B, and C are determined according to [200] as

$$A = n_{lo} + 25\% * (n_{hi} - n_{lo}) \tag{4.1}$$

$$B = n_{lo} + 50\% * (n_{hi} - n_{lo}) \tag{4.2}$$

$$C = n_{lo} + 75\% * (n_{hi} - n_{lo}) \tag{4.3}$$

where n_{hi} is the high speed, determined by calculating 70% of the speed at maximum net power, while n_{lo} is the low speed, defined by calculating 50% of the speed at maximum net power.

The primary objective of this study is to identify the optimum injector in terms of engine performance and emissions by comparing the test results of five injectors with different nozzle geometries. In doing so, the injector can be better matched with the combustion chamber of the engine before conducting the investigation of Miller cycle operation in the following chapters. This helps to better explore the potential of Miller cycle operation over the estimated HD diesel engine speed-load map. The intake pressure set point of the baseline operation was taken from a corresponding multi-cylinder HD diesel engine, which complies with the Euro V emission regulations. The exhaust pressures were adjusted to provide a constant pressure differential of 0.10 bar above the intake pressure.

Table 4.1: Specifications of the different test injectors.

Sequence	Injector	Hole number	fuel flow rate (ml/min)	Cone angle (°)	K-factor (-)	Hole layout	Hole diameter (mm)
1	#482	8	1600	150	1	Ks	0.176
2	#484		1700	146	1	Ks	0.180
3	#485		1700	150	1	Ks	0.180
4	#486		1700	153	1	Ks	0.180
5	#487		1700	150	0	Cylindrical	0.189

Table 4.2 Engine testing conditions.

No.	Name	Speed	IMEP	Engine load	Intake temperature	Intake pressure
	-	r/min	bar	%	°C	bar
1	A50	1147	12.8	50	31	1.73
2	A100	1147	24.2	100	42	2.16
3	B50	1425	12.6	50	34	2.00
4	B100	1425	23.6	100	47	2.68
5	C50	1702	11	50	33	2.06
6	C100	1702	20	100	46	2.54

At each test point, three different injection pressures were employed with a single injection. The maximum in-cylinder pressure was limited to 180 bar. Stable engine operation was determined by controlling the maximum PRR and COV_IMEP below 30 bar/CAD and 3%, respectively.

4.3 Effects of injector Ks factor

As mentioned in Chapter 2, the diesel injectors are mainly characterized by three different nozzle hole-shapes: cylindrical, K-hole, and Ks-hole. In this section, a comparison was performed between injectors with cylindrical-hole and Ks-hole regarding the engine performance and exhaust emissions.

4.3.1 Combustion characteristics

Figure 4.1 shows the ignition delay of both hole-shape injectors for all test conditions. It can be seen that the ignition delay of Ks-hole injector was relatively shorter than that of the cyl-hole injector. This was due to the higher value of discharge coefficient and the lower possibility of cavitation resulted from the Ks-hole injector, which enhanced the atomization of the injected fuel and enabled a better air/fuel mixing. As a result, these combustion conditions advanced the SOC.

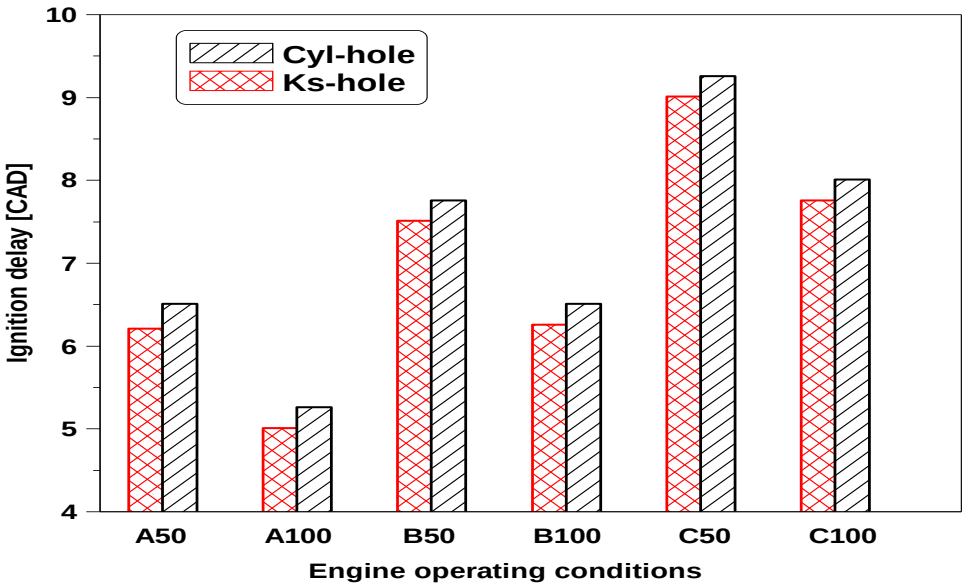

Figure 4.1: Ignition delay of the cyl-hole and Ks-hole injectors for all test points.

Figure 4.2 and Figure 4.3 show the in-cylinder pressures and heat release rates of the two different hole-shape injectors at both medium and full engine loads and a constant speed of 1147 rpm. The comparison was performed at two injection pressures while keeping the injection timing constant for each load. Both hole-shape injectors presented a similar trend of in-cylinder pressure and HRR at two test points. The shorter ignition delay in the Ks-hole injector advanced the initiation of heat release and thus the pressure rise rate. Consequently, this led to a lower peak HRR due to the lower degree of premixed combustion. A relatively higher injection pressure improved the air/fuel mixing, resulting in a higher peak HRR than that of lower injection pressure.

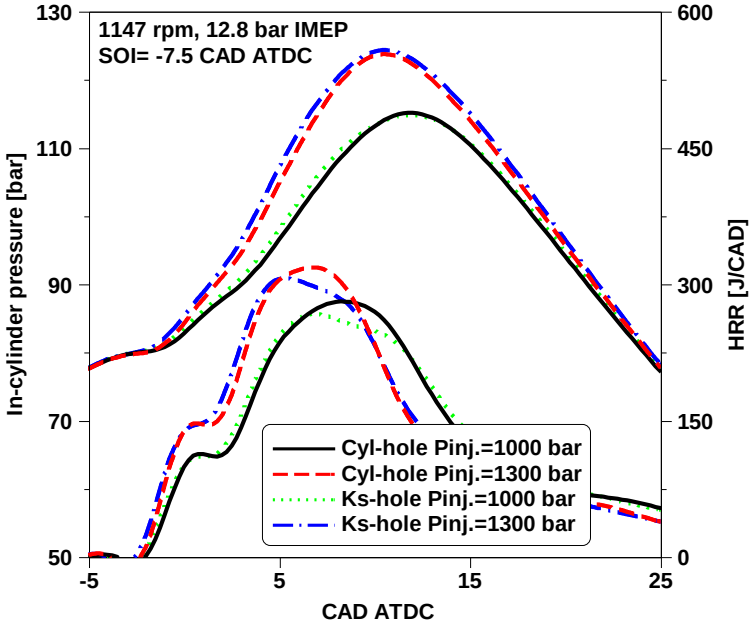

Figure 4.2: In-cylinder pressure and HRR of the two different hole-shape injectors at 1147rpm, 12.8 bar IMEP.

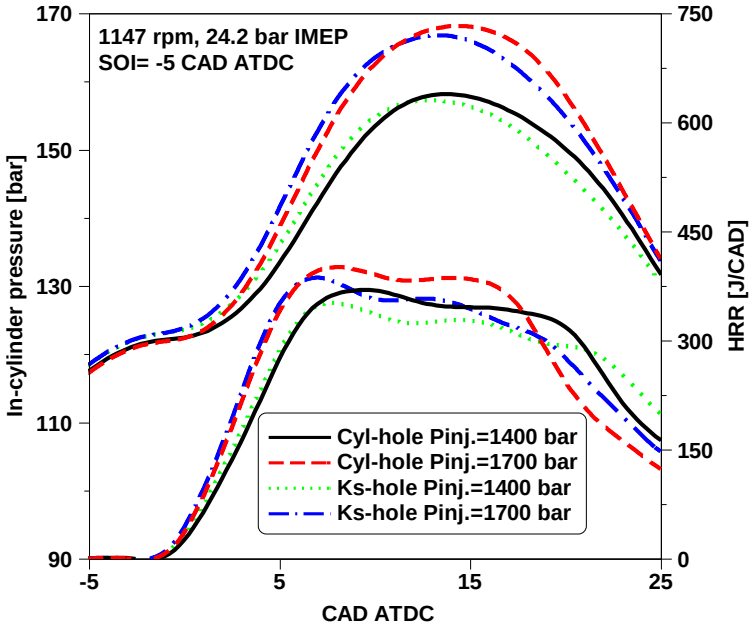

Figure 4.3: In-cylinder pressure and HRR of the two different hole-shape injectors at 1147 rpm, 24.2 bar IMEP.

4.3.2 Engine performance and gaseous emissions

Figure 4.4 shows the engine performance as a function of the injection pressure for the two hole-shape injectors at a speed of 1147 rpm and 50% of full engine load. Compared to cyl-hole injector, the Ks-hole injector showed higher lambda value at a constant SOI and injection pressure, particularly at a lower injection pressure as less fuel was burned

to maintain the same IMEP when the NIE was increased. The higher lambda value along with an earlier SOC contributed to a lower EGT.

Apparently, advanced SOI and higher injection pressure helped improve the NIE and fuel consumption owing to the resulting earlier combustion phasing and higher degree of premixed combustion. The Ks-hole injector presented a similar effect on the NIE to that of a higher injection pressure, increasing the NIE by 1.6% with the use of Ks-hole compared to the cyl-hole.

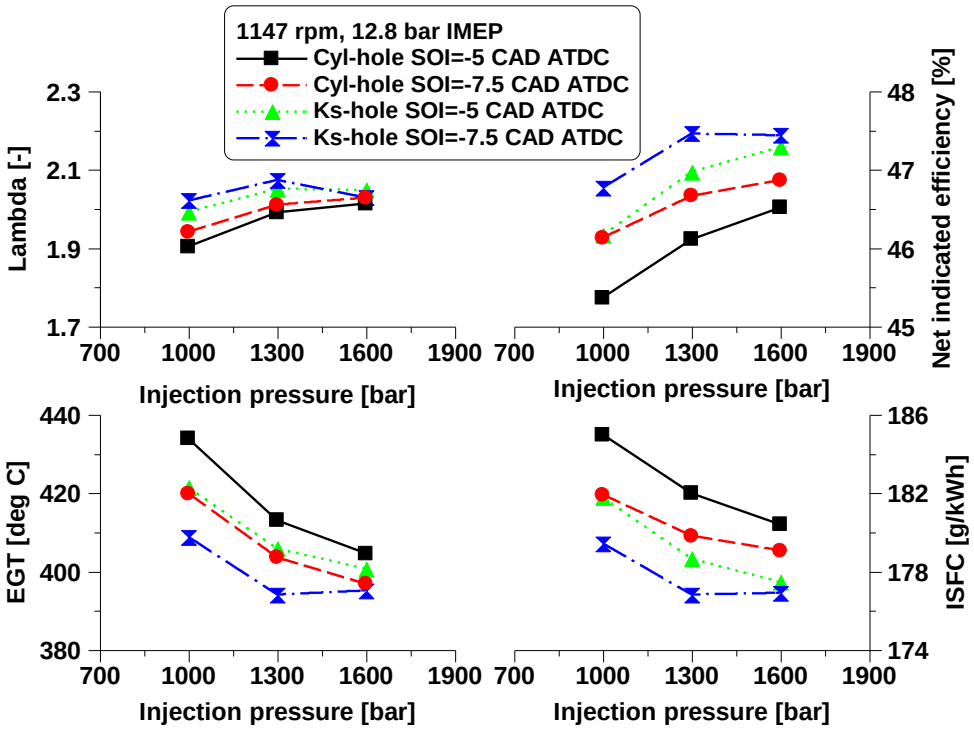

Figure 4.4: Engine performance of the two different hole-shape injectors at 1147rpm, 12.8 bar IMEP.

Figure 4.5 depicts the engine-out emissions for the two hole-shape injectors with various injection pressure and SOI, shown as the net indicated specific values of NOx, soot, unburned HC and CO. Earlier SOI and higher injection pressure decreased soot emissions at the expense of higher NOx emissions, regardless of the injector hole shape. In comparison with the cyl-hole, the use of Ks-hole shape showed higher impact on the soot emissions, maintaining a lower level of soot emissions and demonstrating less sensitivity to the injection timing and injection pressure. This was because the resulting higher lambda value and the enhanced air/fuel mixing. The NOx emissions were slightly lower than the cyl-hole injector at a given SOI, likely due to the lower peak combustion temperatures resulted from the relatively lower degree of premixed combustion.

The CO emissions exhibited a similar trend to that of soot emissions, decreased with Ks-hole injector and reduced rapidly as injection pressure was increased from 1000 to 1300

bar. This was the result of the improved in-cylinder air/fuel ratio, which played an important role on the CO emissions. The variations in SOI and injection pressure presented little impact on the unburnt HC emissions. However, the Ks-hole injector produced higher HC emissions than the cyl-hole injector. This was likely because of the higher air/fuel ratio and the higher risk of flame quenching, as well as the lower EGT which allowed for a lower oxidation of HC during the late combustion phase.

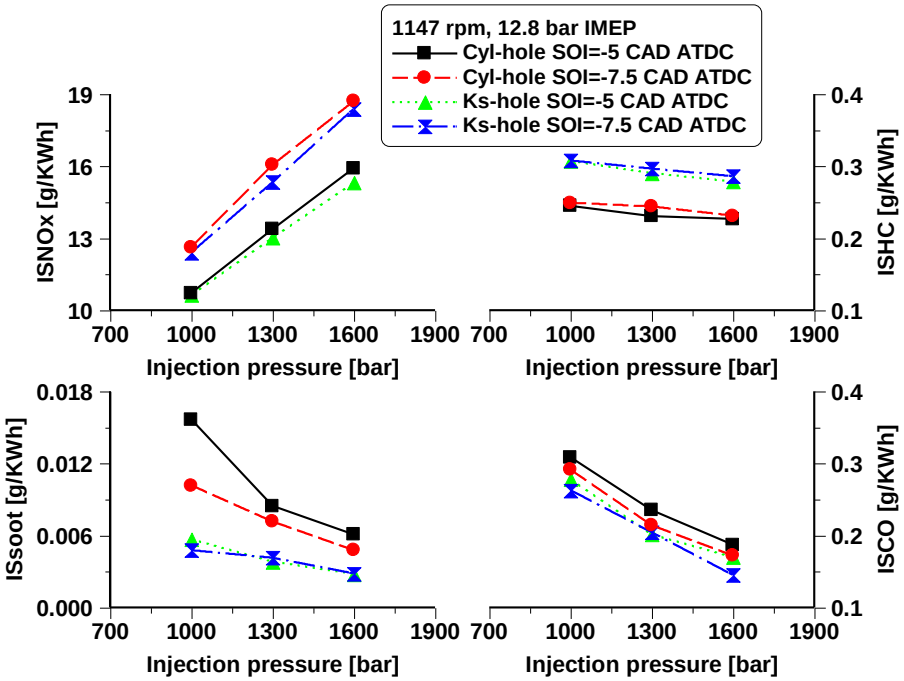

Figure 4.5: Exhaust emissions of the two different hole-shape injectors at 1147rpm, 12.8 bar IMEP.

Figure 4.6 compares the trade-off relationships of exhaust emissions and fuel consumption between Ks-hole and cyl-hole injectors. Compared to the cyl-hole injector, the Ks-hole injector achieved an improvement in the trade-off relationships between ISNOx, ISFC, ISsoot, and ISCO. It also can be seen that the Ks-hole injector decreased the fuel consumption by 1.8% and soot emission by 66.7% at the same NOx level of 10.5 g/kWh. However, the use of Ks-hole injector showed adverse effect on the ISNOx-ISHC trade-off attributed to an increase in HC emissions.

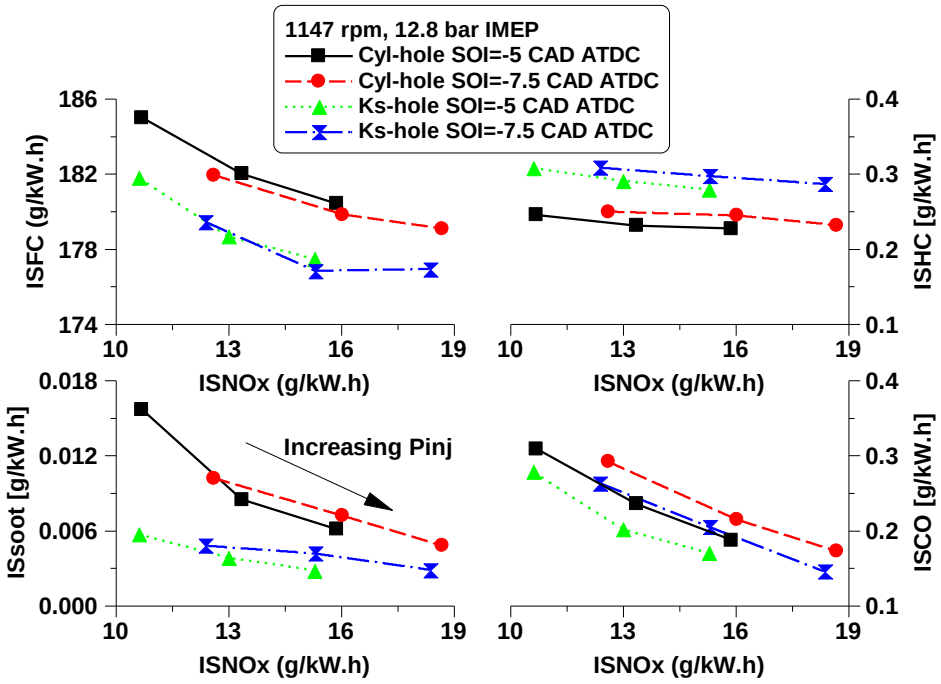

Figure 4.6: Trade-off relationships of two injectors with different hole-shape at 1147rpm, 12.8 bar IMEP.

4.3.3 Comparison of the two different hole-shape injectors over the operating conditions

This subsection estimates the benefit of Ks-hole injector over the cyl-hole injector in terms of fuel consumption and engine-out emissions at the six test points. The analysis was performed at a constant SOI as well as injection pressure for each engine load. Figures 4.7 and 4.8 show the NOx and soot emissions while Figure 4.9 depicted the fuel consumption.

There was small difference in NOx emissions of the two different hole-shape injectors. By using the Ks-hole injector, NOx emissions were slightly decreased at a lower engine speed while increased at higher engine speed. However, the soot emissions were reduced significantly via the use of Ks-hole injector at all operating conditions. This was attributed to a better fuel atomization and the resulting higher lambda value. The Ks-hole injector demonstrated a reduction in fuel consumption at most test points due to a better combustion process and lower combustion temperature and EGT. Therefore, the Ks-hole shape injector was determined as the optimum one for further analysis in the following study.

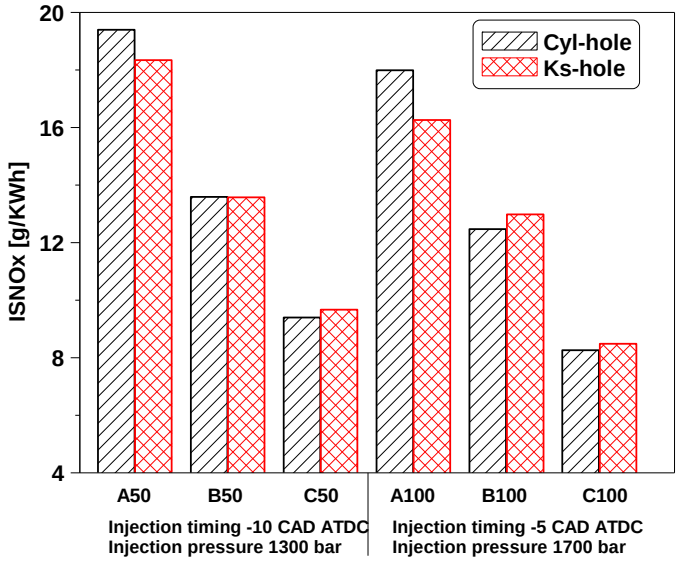

Figure 4.7: Comparison of NOx emissions for the two hole-shape injectors.

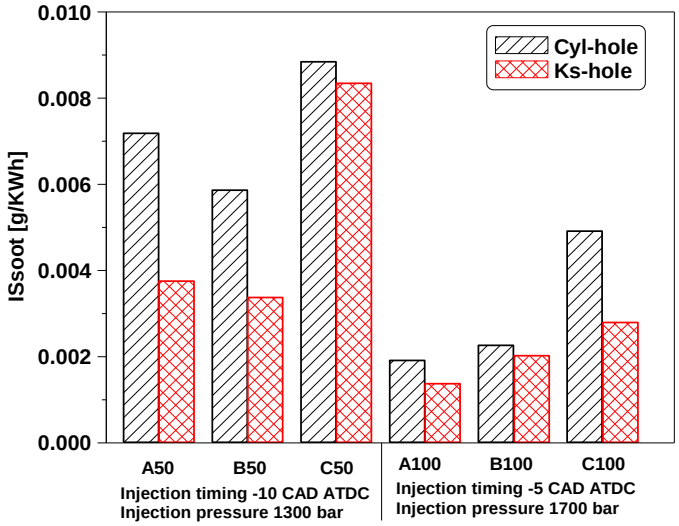

Figure 4.8: Comparison of soot emissions for the two hole-shape injectors.

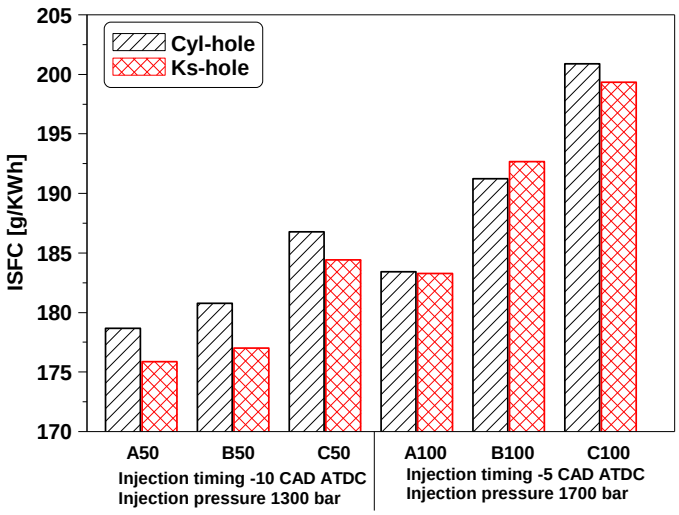

Figure 4.9: Comparison of fuel consumption for the two hole-shape injectors.

4.4 Effects of injector fuel flow rate

There is a strong connection between pollutant emissions and the characteristics of fuel injection, especially the instantaneous fuel flow rate and the evolution of the spray as well as its interaction with fresh air in the combustion chamber. In this subsection, a comparison will be made between two injectors with different fuel flow rates resulted from the different injector orifice diameters. The higher fuel flow rate represents a bigger injector orifice diameter. The aim of this study was to analyse the effect of injector fuel flow rate on engine combustion, performance, and emissions.

4.4.1 Combustion characteristics

Figure 4.10 compares the measured in-cylinder averaged pressure and HRR for the two different fuel flow rate injector at a speed of 1147 rpm and engine load of 12.8 bar IMEP. In comparison with a higher fuel flow rate injector, the lower fuel flow rate injector led to an earlier SOC at a constant SOI. This was because the orifice size of the lower fuel flow rate injector was smaller and thus produced smaller droplets which were atomizing, evaporating, and mixing faster than the larger droplets. Therefore, the time required to form ignitable mixture was shorter for a smaller orifice. The less premixed combustion resulted in a lower peak HRR while the earlier SOC contributed to higher peak cylinder pressure. A similar trend of the variations in the cylinder pressure and HRR was observed at a higher speed of 1703 rpm and engine load of 20 bar IMEP, as depicted in Figure 4.11.

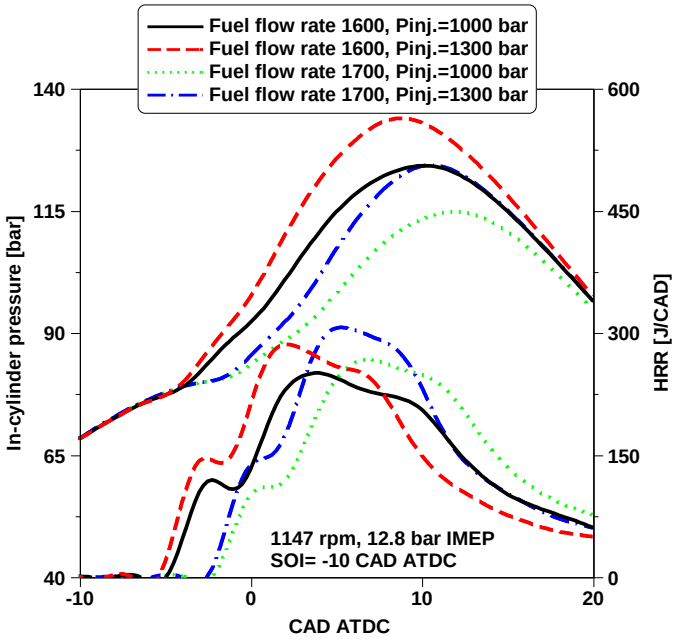

Figure 4.10: In-cylinder pressure and HRR for the two injectors with different fuel flow rate at 1147 rpm, 12.8 bar IMEP.

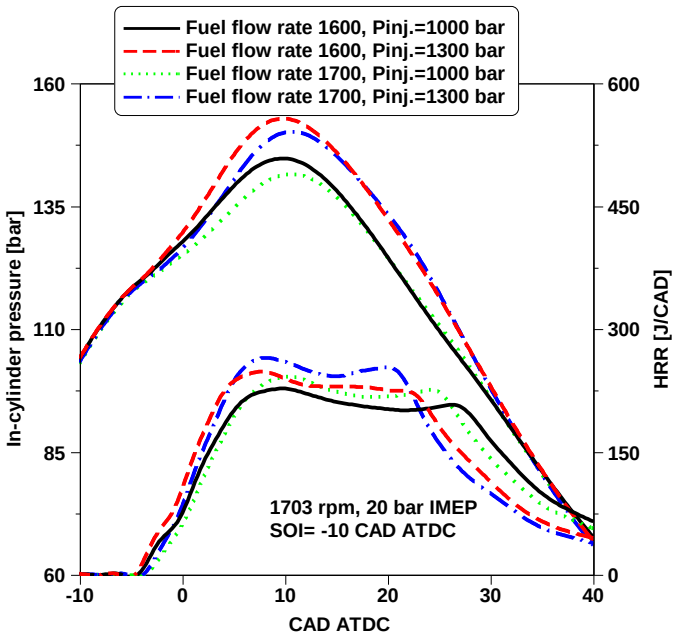

Figure 4.11: In-cylinder pressure and HRR for the two injectors with different fuel flow rate at 1703 rpm, 20 bar IMEP.

Figure 4.12 and Figure 4.13 show the resulting heat release characteristics for the two injectors with different fuel flow rates and different injection pressures and SOI. The injection pressure and SOI showed higher impact on the ignition delay at the lower speed medium load compared to that of higher speed full load conditions. The ignition delay was very sensitive to the orifice diameter at both operating conditions, reducing noticeably by means of a smaller orifice due to the resulting better ignition conditions by improving fuel atomisation.

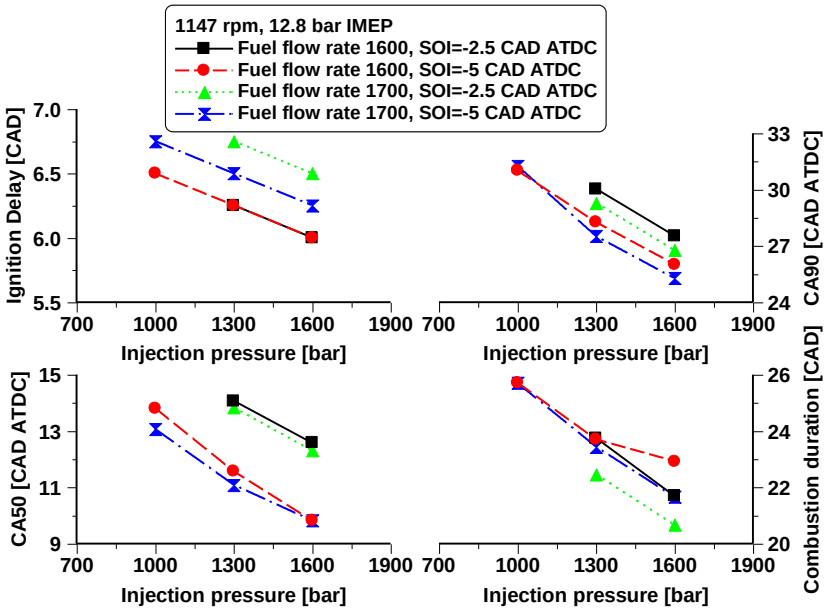

Figure 4.12: Combustion characteristics for the two injectors with different fuel flow rate at 1147 rpm, 12.8 bar IMEP.

The combustion phasing (CA50) was slightly delayed at the lower flow rate injector owing to the relatively lower degree of premixed combustion. The smaller orifice in the lower fuel flow rate injector increased the injection duration. As a result, more fuel combustion is shifted later in the expansion stroke as represented by the later CA90, leading to a longer period of combustion duration.

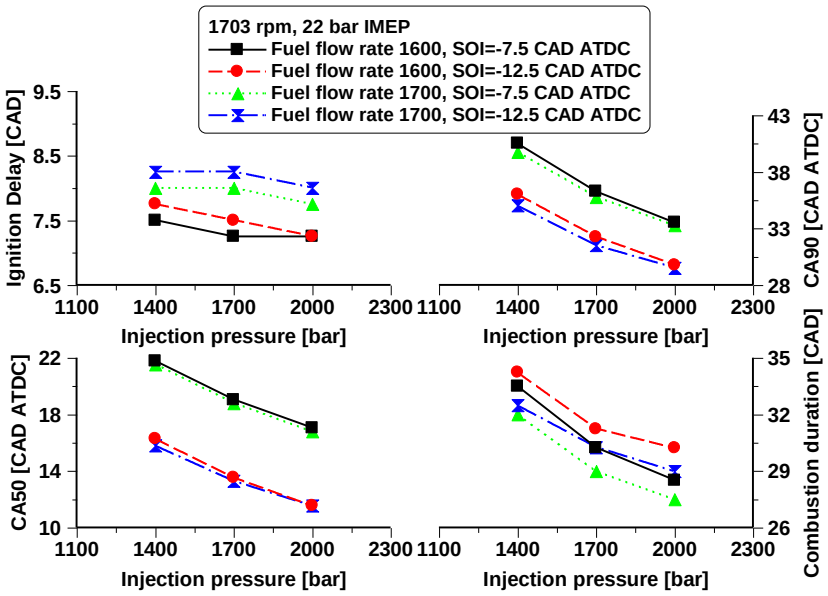

Figure 4.13: Combustion characteristics for the two injectors with different fuel flow rate at 1703 rpm, 20 bar IMEP.

4.4.2 Engine performance and gaseous emissions

Figure 4.14 and Figure 4.15 show the effect of injector fuel flow rate on engine performance characteristics at various injection pressures and SOIs. The relative air/fuel ratio (lambda) was increased with the use of a higher fuel flow rate injector. This was because a bigger orifice produced longer fuel penetration and a shorter injection duration, allowing more time for mixing. The EGT reduced linearly with an increase in lambda at all test points. It can be also seen that the NIE and fuel consumption were improved slightly with a higher fuel low rate injector. This can be explained by the shorter combustion duration and the lower in-cylinder average combustion temperatures resulted from the higher lambda value and thereby lower heat losses to the cylinder walls.

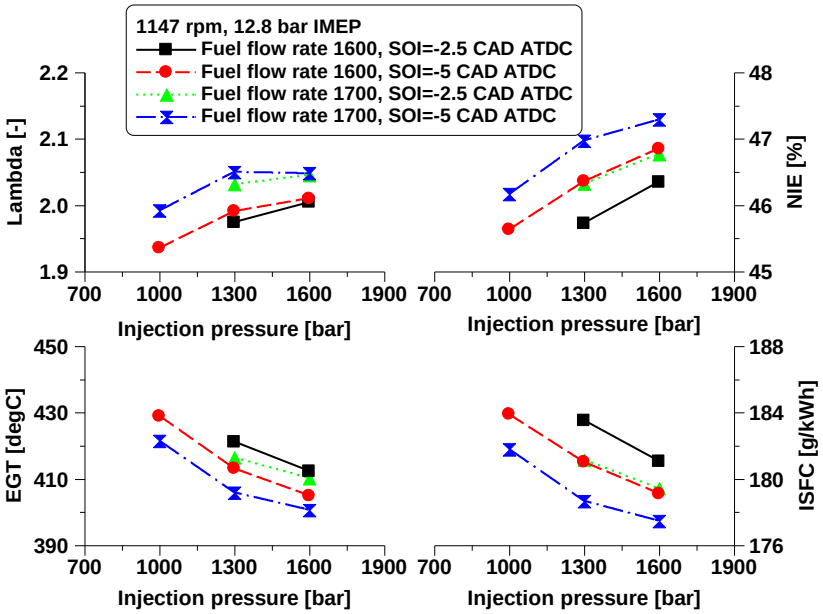

Figure 4.14: Engine performance for two injectors with different fuel flow rate at 1147 rpm, 12.8 bar IMEP.

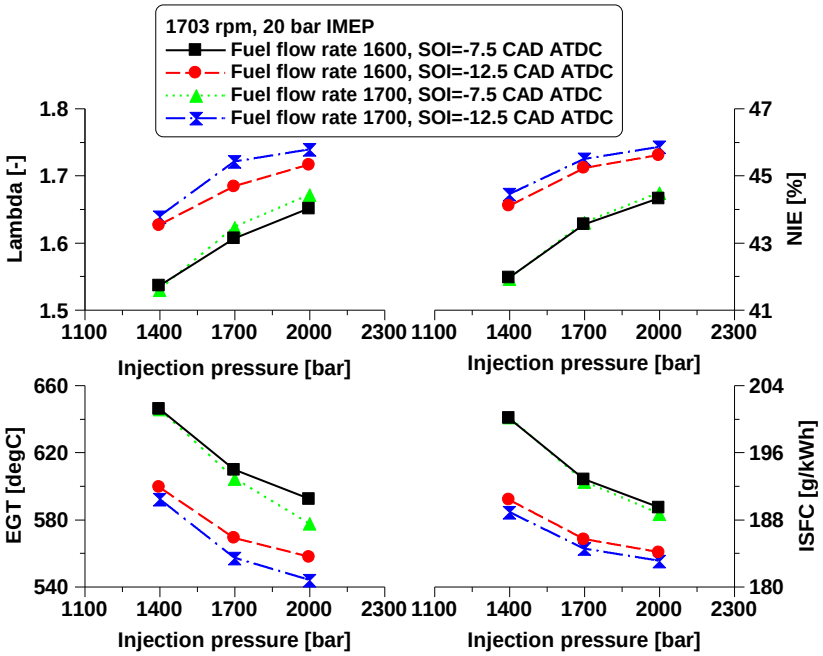

Figure 4.15: Combustion characteristics for two injectors with different fuel flow rate at 1703 rpm, 20 bar IMEP.

The indicated specific engine-out emissions for different fuel flow rate injectors operating with various injection pressures and SOI were depicted in Figure 4.16 and Figure 4.17. The NOx and soot emissions were lower when using a lower fuel flow rate injector at 1147 rpm, 12.8 bar IMEP. This was a result of the decreased lambda value and relatively better air entrainment into the spray core.

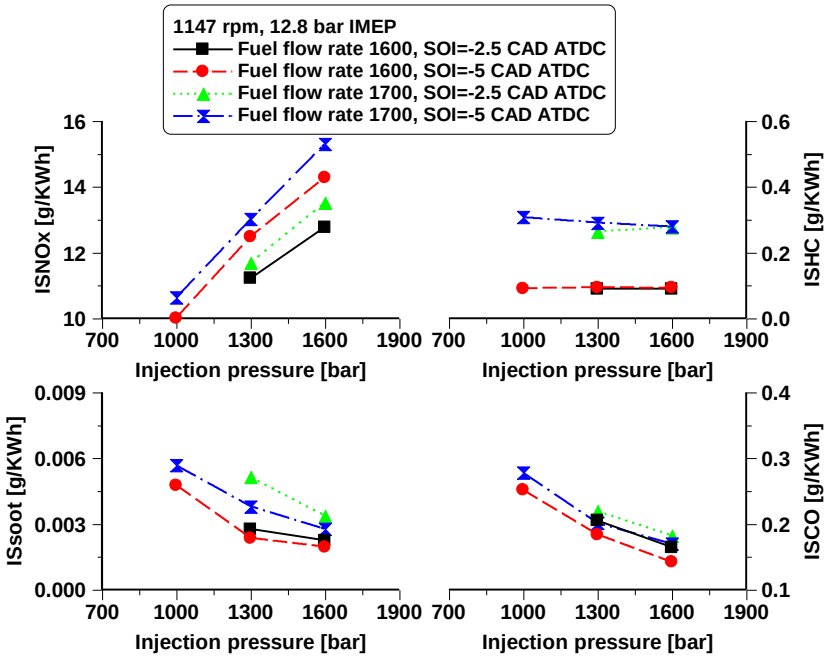

Figure 4.16: Engine-out emissions for the two injectors with different fuel flow rate at 1147 rpm, 12.8 bar IMEP.

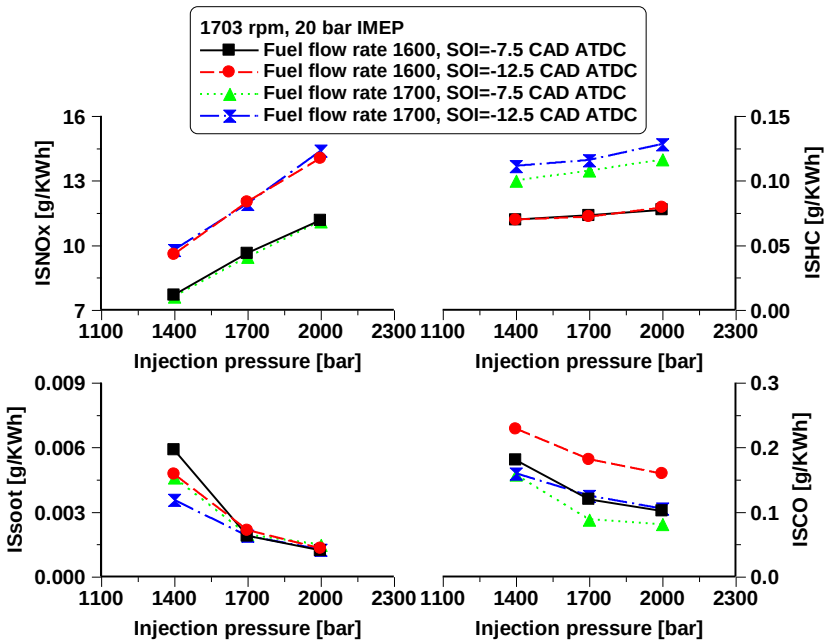

Figure 4.17: Engine-out emissions for the two injectors with different fuel flow rate at 1703 rpm, 20 bar IMEP.

At a higher load, however, the orifice diameter showed little impact on NOx emissions and the smaller orifice produced slightly higher soot emissions, especially when operating with lower injection pressures. This was likely due to the poor air utilization as more fuel was injected at higher load and the smaller orifice led to shorter spray penetration, resulting in a richer local mixture. The CO emissions followed the trend observed in soot emissions, the smaller orifice injector produced less CO emissions at low speed and medium load

while increased CO emissions at higher speed and full load condition. It also can be seen that HC emissions were significantly lower at the smaller orifice diameter injector at both operating conditions. One of the major reasons for the lower HC level was because the smaller orifice injected the fuel with a shorter spray penetration. The shorter ignition delay was believed to be another reason as the over-lean mixture could be partly avoided, which was the main source of unburnt HC emissions.

Figures of 4.18 and 4.19 show the trade-off relations between fuel consumption and engine-out emissions for the two different fuel flow rate injectors. An improvement in the trade-off of NOx-ISFC was observed in the higher fuel flow rate injector, regardless of the engine operating conditions. The smaller orifice injector presented a better trade-off of NOx-soot at 1147 rpm and 12.8 bar IMEP. However, a reverse trend was found at 1703 rpm, 20 bar IMEP. The higher fuel flow rate injector achieved better trade-off of NOx and soot emissions. The observed trend of NOx-CO trade-off for various injection pressures and SOI was similar to that of NOx-soot. The lower HC emissions resulted from the smaller orifice diameter, contributing to an improvement in the trade-off between NOx and HC emissions.

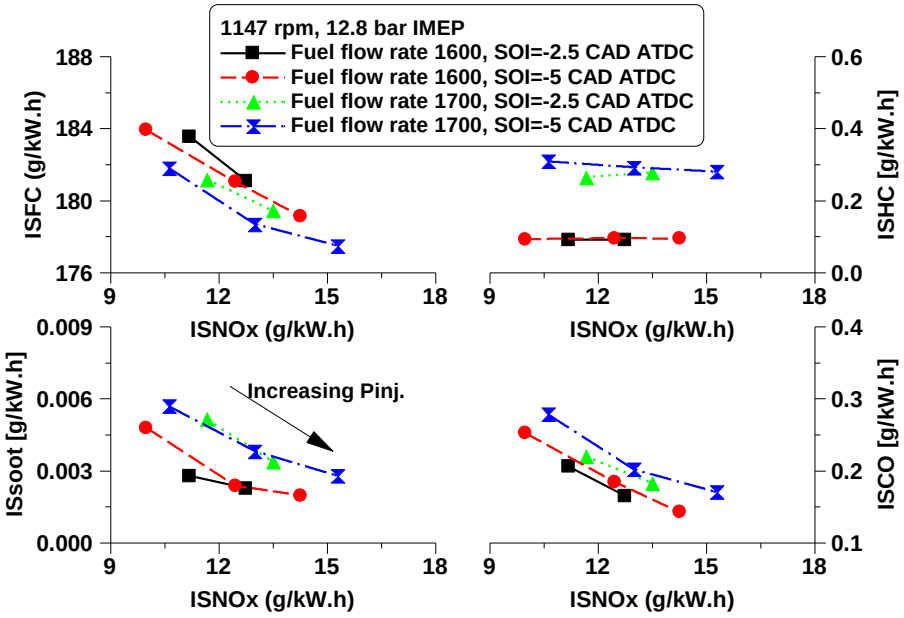

Figure 4.18: Trade-off relationships for the two injectors with different fuel flow rate at 1147 rpm, 12.8 bar IMEP.

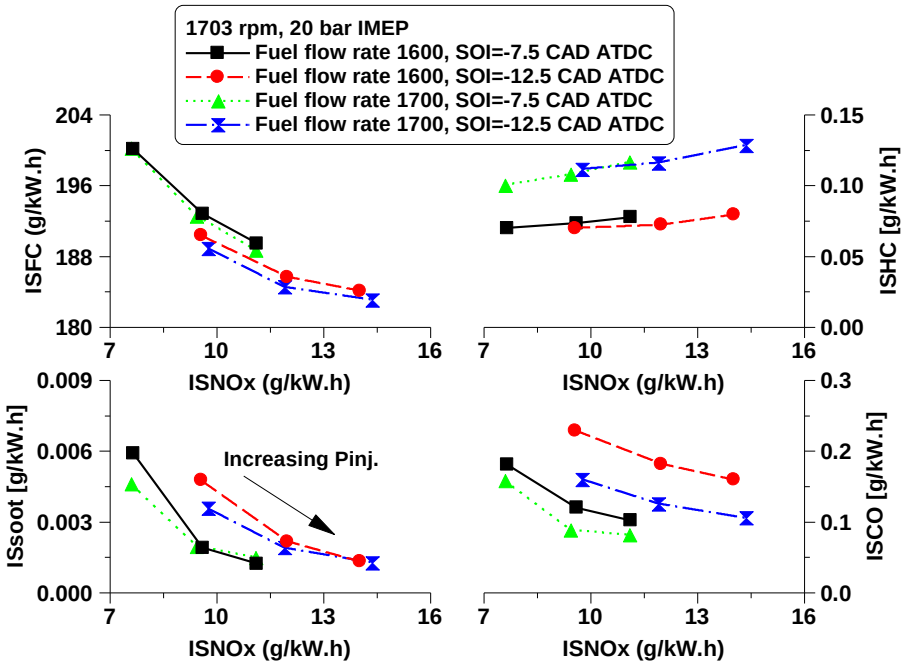

Figure 4.19: Trade-off relationships for the two injectors with different fuel flow rate at 1703 rpm, 20 bar IMEP.

4.4.3 Comparison of the two injectors with different fuel flow rates over the operating conditions

In order to better compare injectors with different fuel flow rates regarding engine performance and emissions, an overview of fuel consumption and exhaust emissions for all test points was performed. As shown in Figure 4.20, 4.21, and 4.22, the injection pressures employed for 50% and 100% of full engine loads were 1300 and 1700 bar with corresponding injection timings at -10 and -5 CAD ATDC, respectively.

Figure 4.20 shows that a slightly lower NOx level was achieved with a lower fuel flow rate injector at the majority test points. As displayed in Figure 4.21, the soot emissions of a smaller orifice injector decreased at medium loads while increased at full engine loads. This was a result of the improved air entrainment at 50% of full engine loads but poor air utilization at 100% of full engine loads. The data depicted in Figure 4.22 is a comprehensive comparison of the fuel consumption for the two injectors with different fuel flow rates. The higher fuel flow rate injector demonstrated a slight reduction in fuel consumption at most test points, which was mainly attributed to the longer spray penetration, higher lambda value, and shorter combustion duration. Overall, the lower fuel flow rate injector produced relatively lower exhaust emissions while the injector with relatively higher fuel flow rate obtained slightly better fuel economy. In this study, the injector with high fuel flow rate of 1700 ml/min was selected for the following analysis.

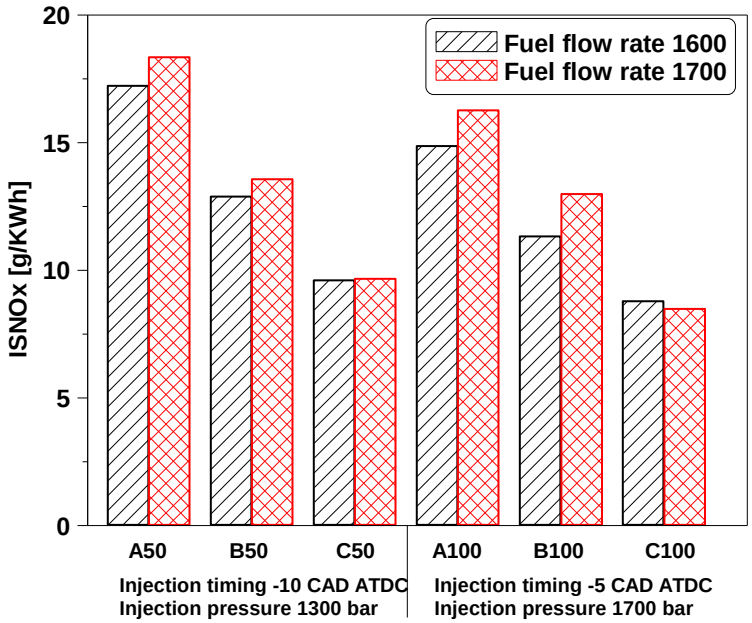

Figure 4.20: Comparison of NOx emissions for the two injectors with different flow rates.

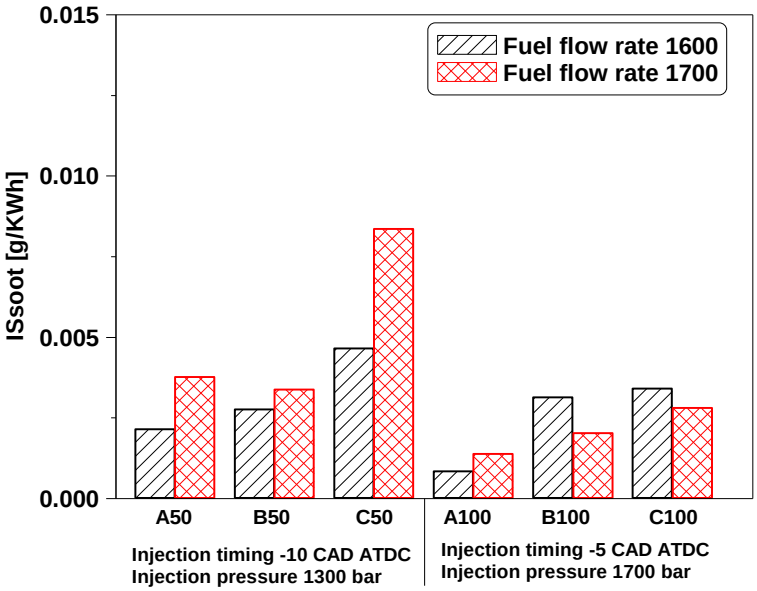

Figure 4.21: Comparison of soot emissions for two the injectors with different flow rates.

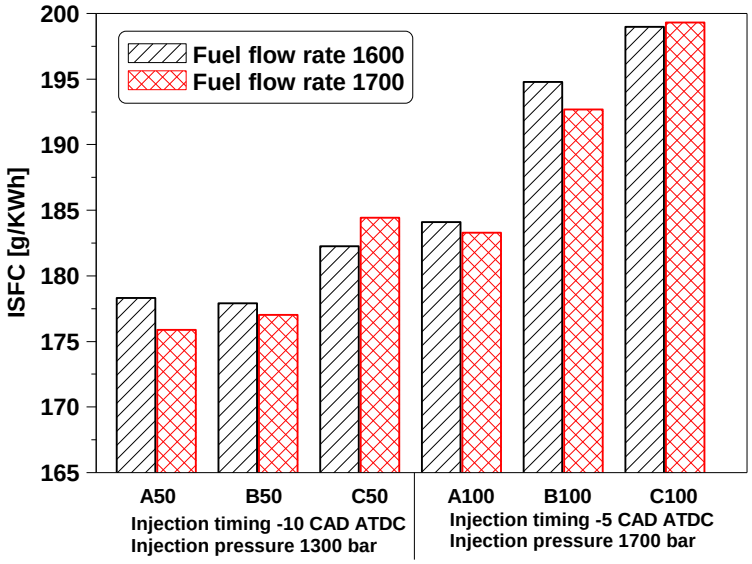

Figure 4.22: Comparison of fuel consumption for the two injectors with different flow rates.

4.5 Effects of injector cone angle with different washer thickness

The interaction between the fuel spray and the combustion chamber is extremely important since the fuel targeting directly affect the mixture formation and thus the combustion process. The wall wetting regions resulted from the impinging fuel on cylinder walls contribute most to the total engine-out soot emissions. Narrow spray cone angle injector is capable of avoiding the fuel spray missing the combustion bowl hence allow early injection timing without much wall film formed. On the other hand, it can lead to poor fuel vaporization and high liquid fuel penetration, increase the risk of impinging liquid fuel on the piston surface.

In addition, the spray targeting is affected strongly by the injection timing, as shown in Figure 4.23 the position of the fuel spray in the piston bowl for the three different cone angle injectors performed at two injection timings. It can be seen that the injection timing had great impact on the spray targeting on the piston surface. The narrower spray angles could target more fuel into the piston bowl compared to the wider spray angles. Therefore, the spray-bowl interaction played important role in the formation of air/fuel mixture and hence the combustion and emissions characteristics.

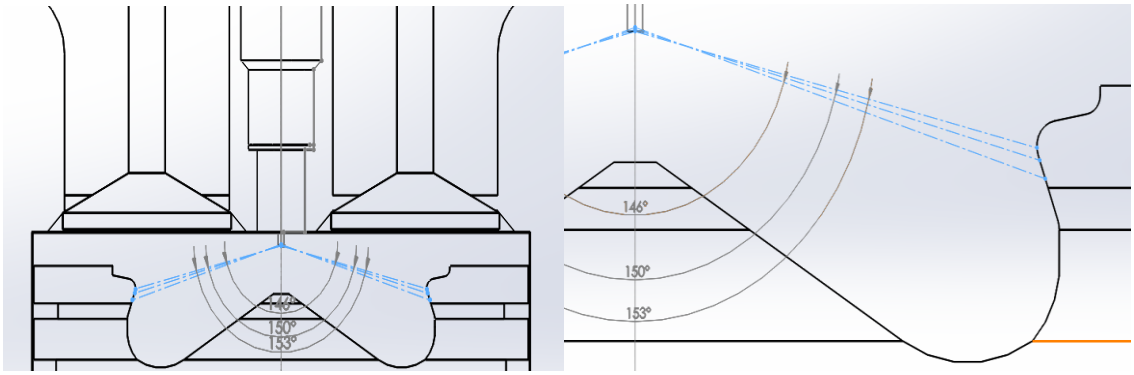

(a) Injection timing at -20 CAD ATDC

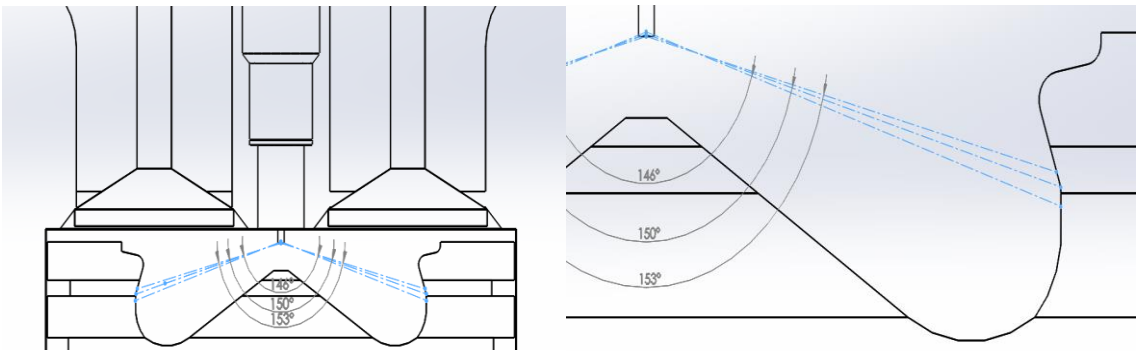

(b) Injection timing at -10 CAD ATDC

Figure 4.23: Fuel spray position at -20 CAD ATDC (a) and -10 CAD ATDC (b) for the three different spray cone angle injectors.

Since the distance from the nozzle tip to the piston bowl, which also called injector protrusion, can be adjusted via a washer mounted between the injector and the cylinder head. The thicker the washer, the less the injector protrusion, as shown in Figure 4.24. Therefore, this subsection analysed the influence of the combination of spray cone angle with washer thickness to explore the optimum washer thickness for each injector, in order to match it well with the combustion chamber and the applied injection strategy. In doing so, the optimum injectors can be determined through comparing the three injectors with their corresponding optimum washer thicknesses. Table 4.3 depicts the specifications of the three different spray angle injectors. The washer thicknesses for the testing injectors were between 1.6 and 2.0 mm.

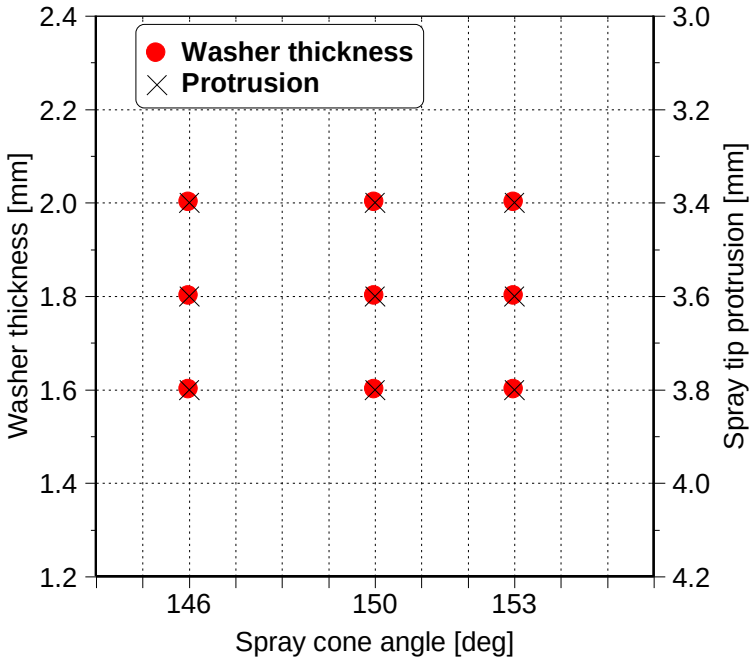

Figure 4.24: Spray tip protrusion for the three injector cone angles with different washer thicknesses.

Table 4.3: Testing injector specifications and corresponding washer thickness.

injector	Mass flow rate (ml/min)	Cone angle	Washer thickness
#484	1700	146°	1.6, 1.8, 2.0mm
#485	1700	150°	1.6, 1.8, 2.0mm
#486	1700	153°	1.6, 1.8, 2.0mm

4.5.1 Analysis of spray cone angle with different washer thickness

Figure 4.25 shows the NIE and engine-out emissions for the injector spray angle of 146° with different washer thicknesses at 1147 rpm and 12.8 bar IMEP. The use of the smallest washer thickness produced the lowest soot emissions at the cost of higher NOx emissions. This was due to the smallest washer thickness decreased the distance between the spray tip and piston bowl, allowing more fuel spray injected or impinged close to the piston bowl and thus led to a better mixture formation [65]. However, soot emissions increased significantly at a lower injection pressure as the washer thickness was increased to 1.8 mm, which could be improved by further increased the washer thickness to 2.0 mm. The increased risk of higher possibility of spray impinging on the cylinder walls and piston bowl resulted in higher unburnt HC emissions. There was small difference in NIE between the three different washers. The smallest washer thickness achieved slightly higher efficiency at lower injection pressure, however, the highest efficiency was obtained by the biggest washer thickness as the injection pressure increased.

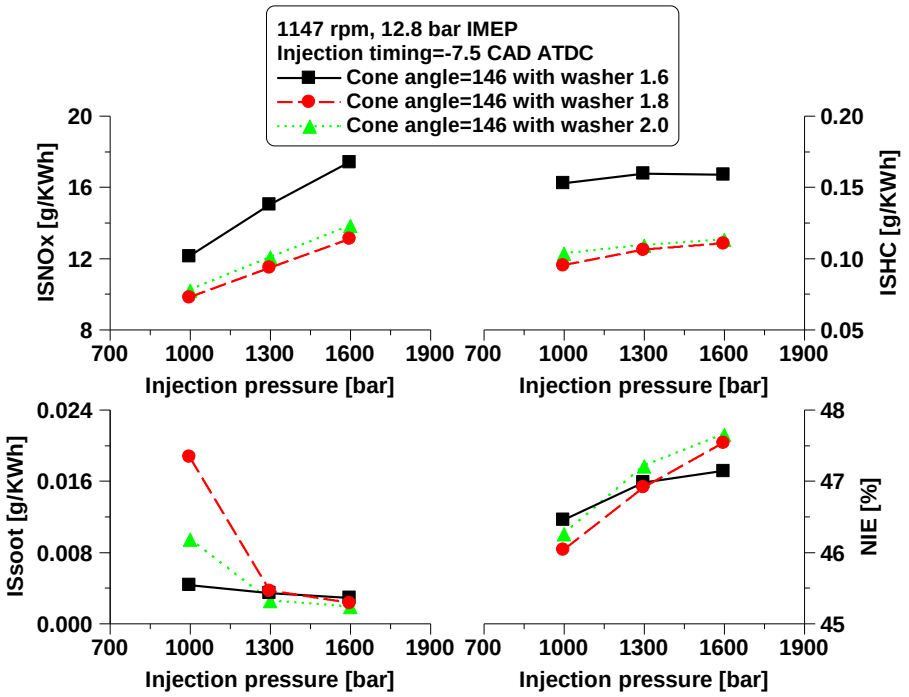

Figure 4.25: Engine-out emissions and efficiency for the injector spray angle of 146°with different washer thickness at 1147 rpm, 12.8 bar IMEP.

Figure 4.26 shows the emissions and engine efficiency for the injector spray cone angle of 150° with different washer thicknesses. This injector has a wider spray angle than the previous, indicating the spray tip penetration was relatively shorter and less fuel spray was injected into the piston bowl at a constant washer thickness. The use of smaller washer thickness increased the possibility of spray impinging in the squish region to form a richer air/fuel mixture. As a result, the HC emissions were higher and the NIE was lower. In addition, the soot emissions were deteriorated at a low injection pressure of 1000 bar, particularly with washer thickness of 1.6 mm. The NOx emissions were increased when using a washer thickness of 2 mm. In contrast, the use of washer thickness of 1.8 mm achieved the optimum exhaust emissions and efficiency. Compared to the two aforementioned injectors, the injector with a spray cone angle of 153° has a wider spray angle and shorter spray tip penetration. Thus, the distance between spray tip and the piston bowl should be decreased to avoid wall wetting. As shown in Figure 4.27, this injector with the smallest washer thickness of 1.6 mm achieved the optimum balance between engine efficiency and exhaust emissions.

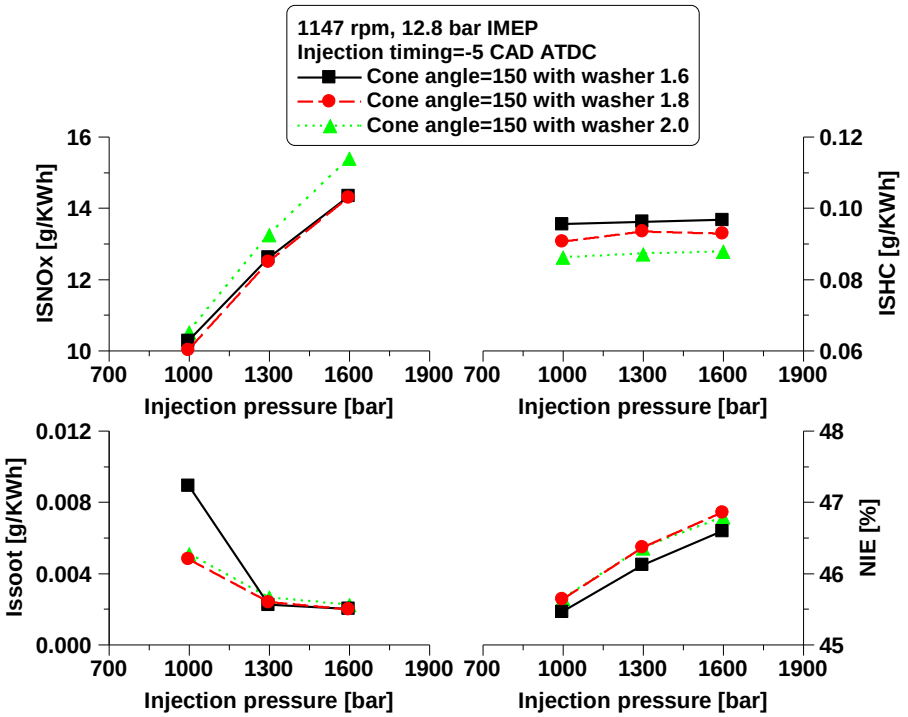

Figure 4.26: Engine-out emissions and efficiency for the injector spray angle of 150°with different washer thickness at 1147 rpm, 12.8 bar IMEP.

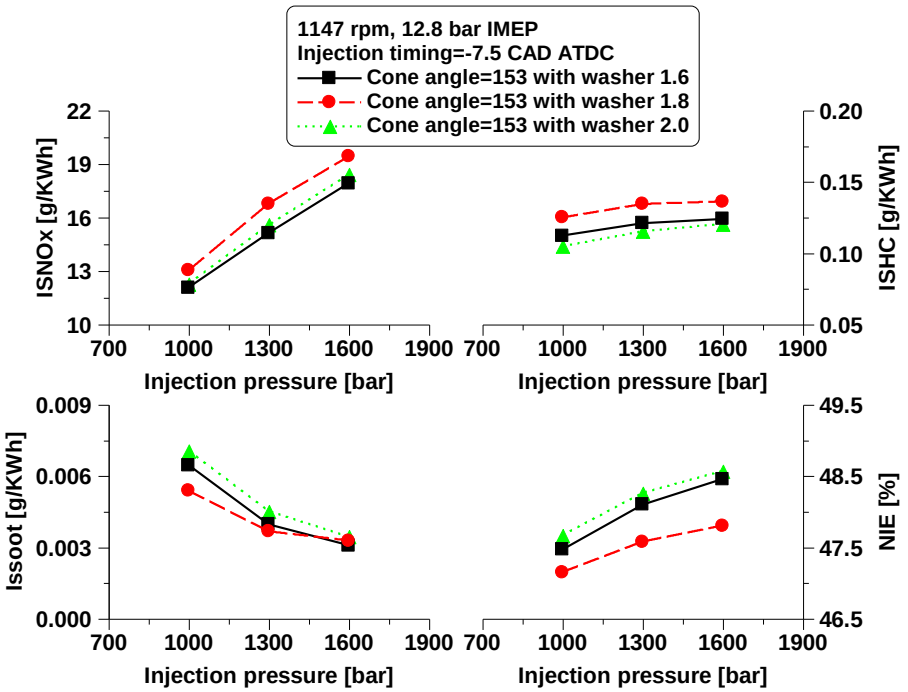

Figure 4.27: Engine-out emissions and efficiency for the injector spray angle of 153°with different washer thickness at 1147 rpm, 12.8 bar IMEP.

To better identify the optimum washer thickness for every injector, engine efficiency and emissions of the three different spray cone angle injectors as a function of the washer thickness were plotted. As shown in Figure 4.28, the comparison was performed at 1147 rpm and 12.8 bar IMEP. The results showed that the bigger spray angle injector with

deeper protrusion by using thinner washer achieved the best results regarding the engine efficiency and exhaust emissions.

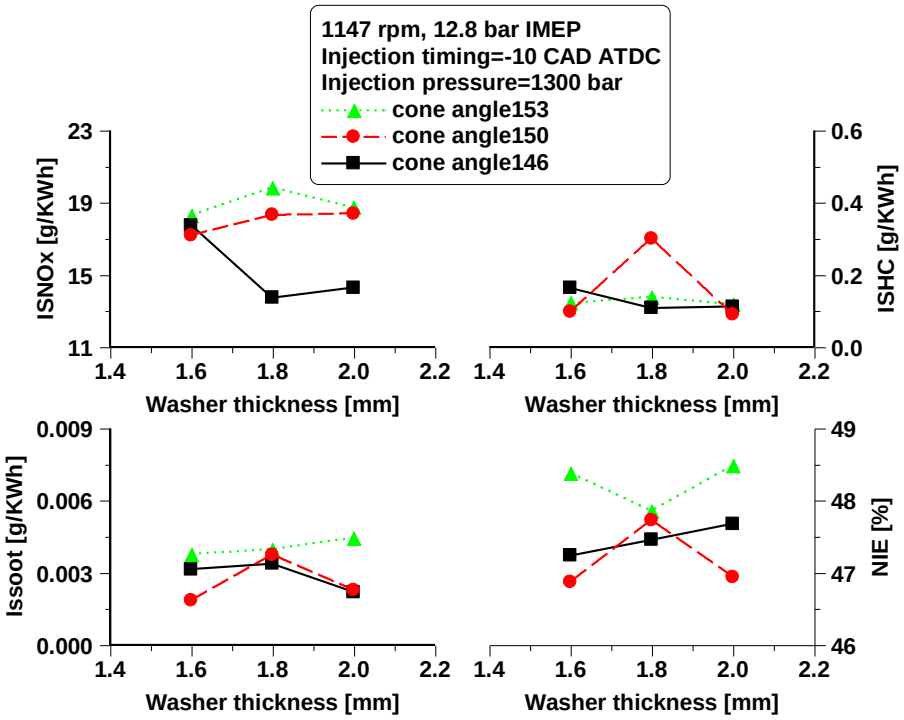

Figure 4.28: Comparison of the three spray angle injectors with different washer thickness at 1147 rpm, 12.8 bar IMEP.

4.5.2 Comparison of different spray cone angle injectors with corresponding optimum washer thickness

A comparison of the three injectors with different spray cone angles and corresponding optimum washer thickness was carried out over the six test points. Figure 4.29 shows the fuel consumption while the data in Figure 4.30 and Figure 4.31 demonstrate the NOx and soot emissions at 50% and 100% of full engine load, respectively. The results revealed the injector with spray angle of 153° and washer thickness of 1.6 mm demonstrated a higher potential in minimizing the fuel consumption than the other two injectors at all operating conditions. However, the narrowest spray angle injector matched a washer thickness of 2.0 mm produced the lowest NOx emissions, regardless of the injection pressure used.

The variations of soot emissions were not consistent for all test points. At a relatively lower injection pressure, the injector with the narrowest spray angle produced significantly higher soot emissions, particularly at 100% of full engine load. This could be improved apparently as the injection pressure was increased. Both injectors with spray angle of 150° and 153° generated similar NOx and soot emissions at most test points.

Overall, injectors with different geometry parameters presented different advantages over the fuel efficiency and exhaust emissions. Therefore, the optimum injectors should be selected carefully according to the objective of the research work.

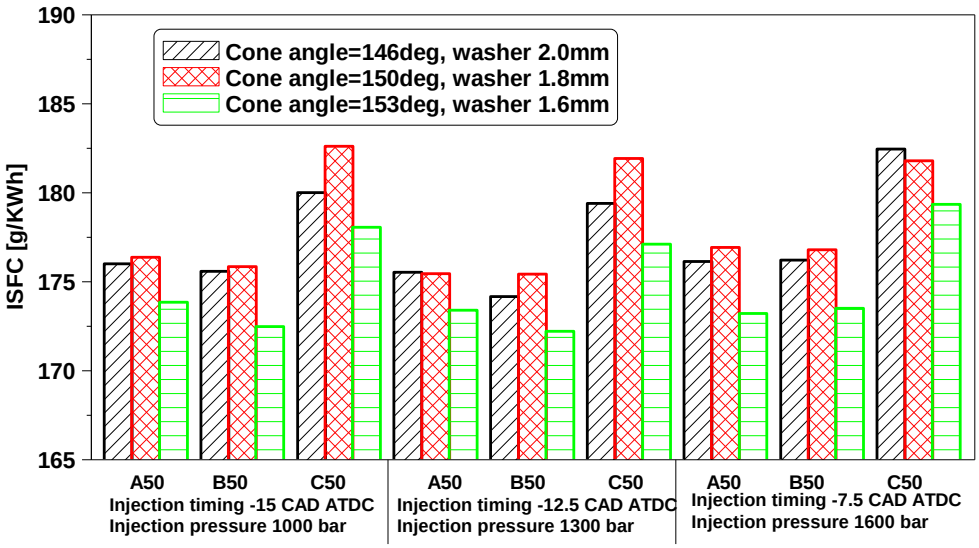

(a) 50% of full engine load;

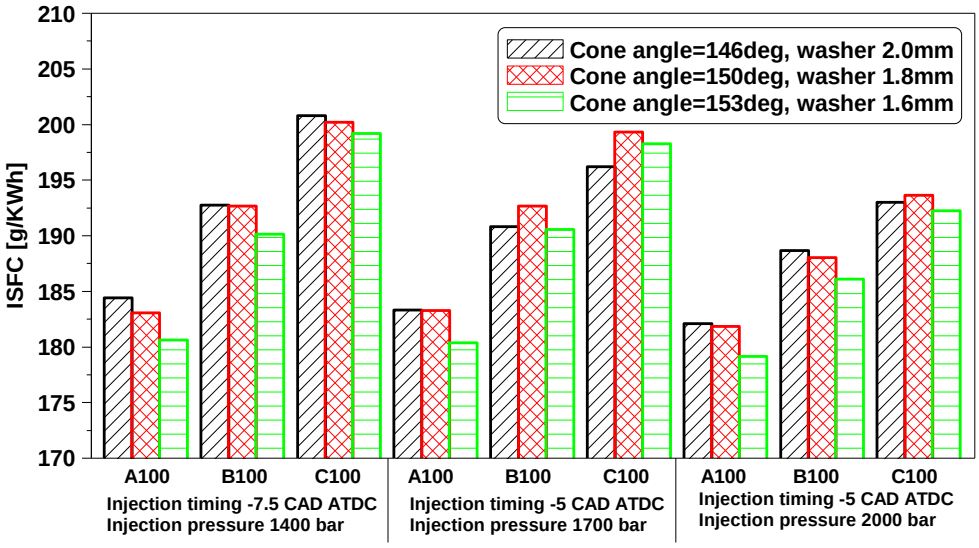

(b) 100% of full engine load;

Figure 4.29: Comparison of fuel consumption for the three different spray angle injectors with their optimum washer thickness.

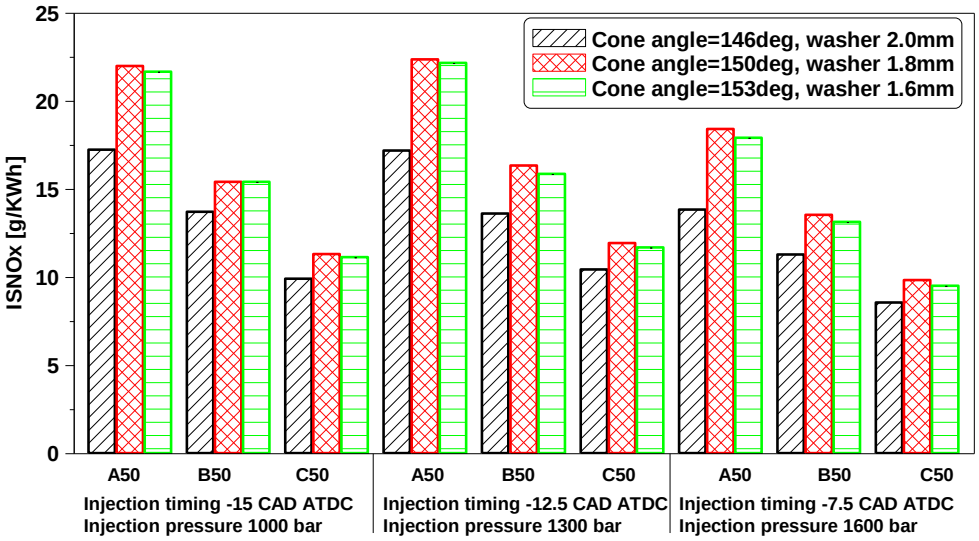

(a) 50% of full engine loads;

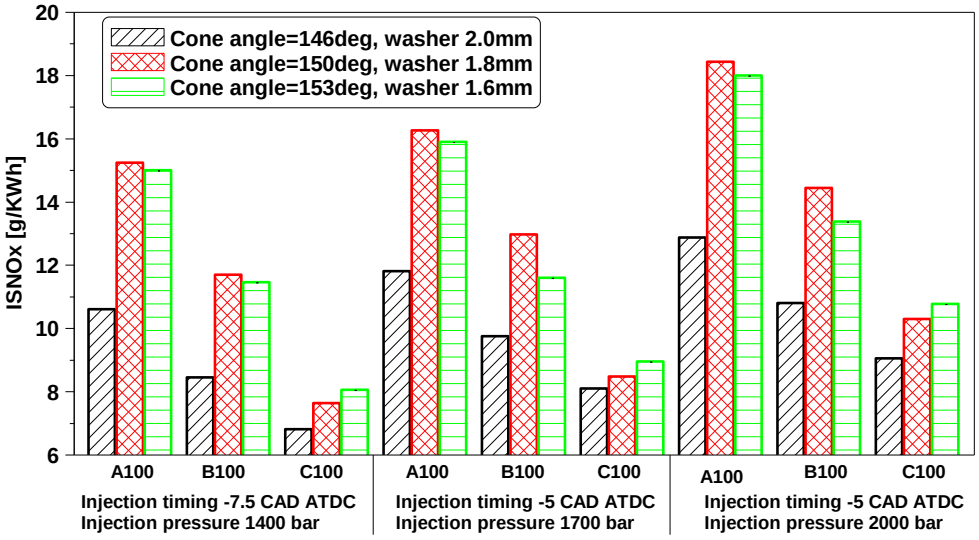

(b) 100% of full engine loads;

Figure 4.30: Comparison of NOx emissions for the three different spray angle injectors with their optimum washer thickness.

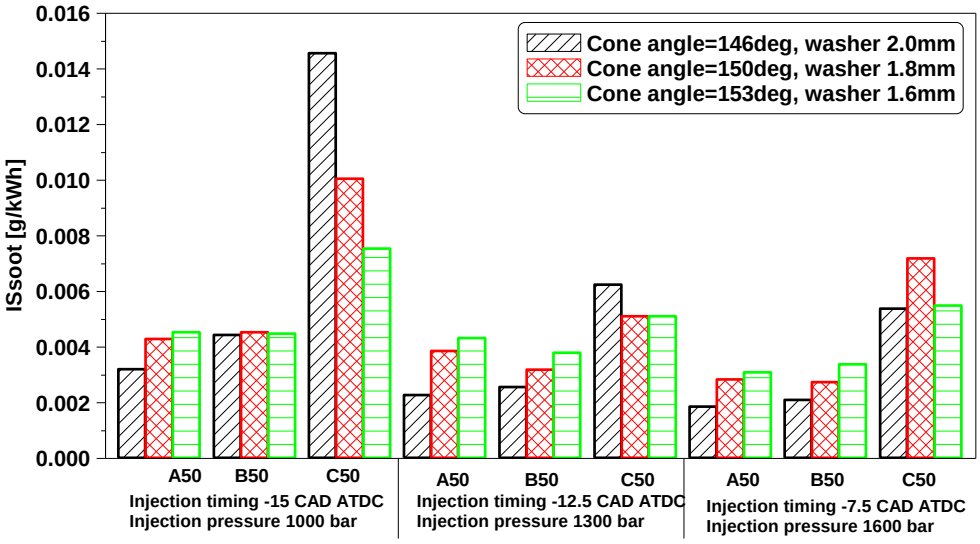

(a) 50% of full engine loads;

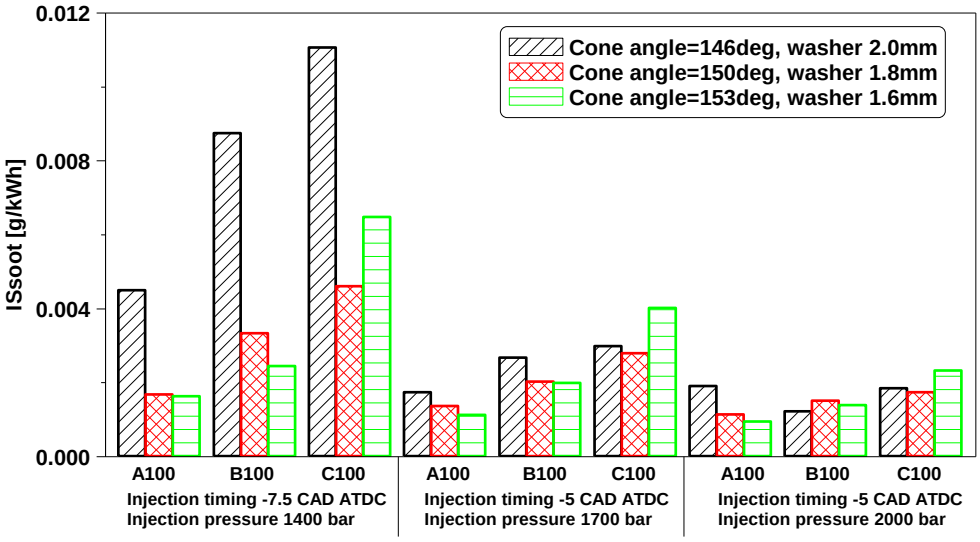

(b) 100% of full engine loads;

Figure 4.31: Comparison of soot emissions for the three different spray angle injectors with their optimum washer thickness.

4.5.3 Overall engine efficiency analysis

In this study, the main focus of the injector geometry optimization was put on the trade-off between engine efficiency and engine-out NOx emissions, as the practical use of SCR-equipped HD diesel engine will consider the aqueous urea solution consumption in the SCR system. Thus, an overall engine efficiency analysis over the six test points was carried out in order to determine the optimum injector configuration in terms of overall engine operating cost (EOC).

Particularly, the corrected Net Indicated Efficiency (NIE) was used in order to take into account both the measured diesel flow rate ($\dot{m}_{diesel}$) and the aqueous urea solution consumption in an SCR system ($\dot{m}_{urea}$). This allowed for a cost-benefit analysis of the total cost of the different injector configuration. As the urea consumption in the SCR system depends on the operating conditions as well as engine-out NOx emissions, reductions in the levels of engine-out NOx can help minimise the urea flow rate. According to [125,201–203], the urea consumption in the SCR system can be estimated as 1% of the diesel equivalent fuel flow per g/kWh of NOx reduction necessary to meet the Euro VI limit (NOx_{EuroVI}) of 0.4 g/kWh.

$$\dot{m}_{urea} = 0.01 * \left(NOx_{Engine-out} - NOx_{EuroVI}\right) * \dot{m}_{diesel} \tag{4.4}$$

As the relative prices between diesel fuel and urea are different in different countries and regions, the price and property of urea was simulated to be the same as diesel fuel in this study [125,202]. By adding the diesel fuel consumption to the estimated urea usage allowed for the calculation of total fluid consumption.

$$\dot{m}_{total} = \dot{m}_{urea} + \dot{m}_{diesel} \tag{4.5}$$

Therefore, the $\dot{m}_{total}$ allowed for the calculation of the corrected net indicated efficiency ($NIE_{corr.}$), which was defined as

$$NIE_{corr.} = \frac{P_i}{\dot{m}_{total}\, LHV_{diesel}} \tag{4.6}$$

where P_i is the net indicated power and LHV_{diesel} is the diesel lower heating value of 42.9 MJ/kg.

Figure 4.32 and 4.33 provide an overall assessment of the influence of the three injectors with different spray cone angles on the total fluid consumption and $NIE_{corr.}$ at 50% and 100% of full engine load, respectively. At 50% of full engine load, injectors with spray angle of 146° and 153° enabled lower total fluid consumption and higher $NIE_{corr.}$ than the injector with spray angle of 150° at most test points. This was attribute to the lower NOx emissions in the smallest spray angle injector and higher engine efficiency in the biggest spray angle injector accordingly. When comparing at 100% of full engine load, the injector with smallest spray angle presented a higher potential in reducing NOx emissions and thus the total fluid consumption, which led to an increase in the $NIE_{corr.}$. It can be also seen from Figures 4.32 and 4.33 that the lowest engine speed denoted as “A” produced noticeably lower total fluid consumption than the other two engine speeds of “B” and “C”. This was mainly because of the lower fuel mass flow rate at a lower engine speed.

The overall results have demonstrated the potential benefit of the optimization of injector spray angle with an appropriate washer thickness in improving the $NIE_{corr.}$ and thus the EOC via lower total fluid consumption. According to this study, the injector with spray cone angle of 146° and a washer thickness of 2.0 mm was determined as the optimum injector configuration to achieving the best balance between in-cylinder and aftertreatment NOx emissions control.

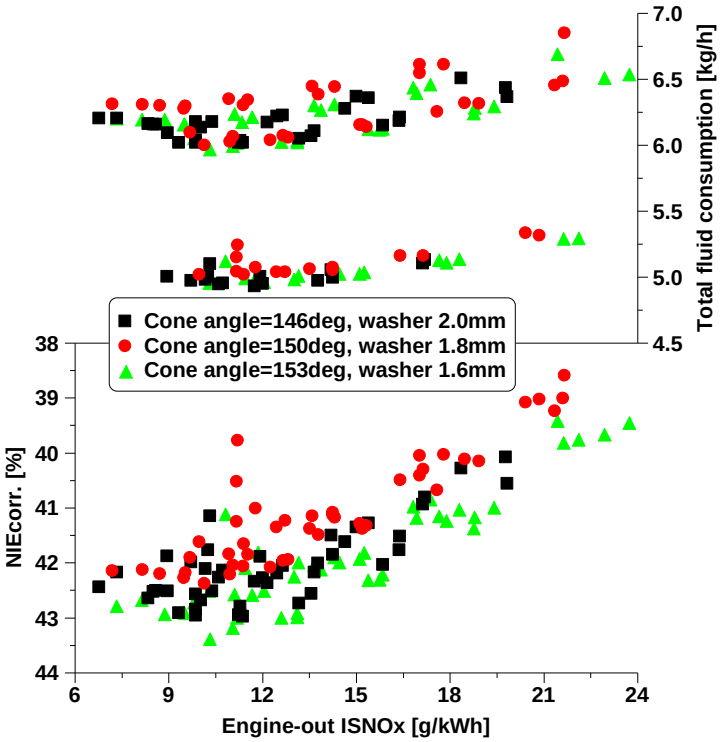

Figure 4.32: Overall engine efficiency analysis for injectors with different spray angles at 50% engine loads.

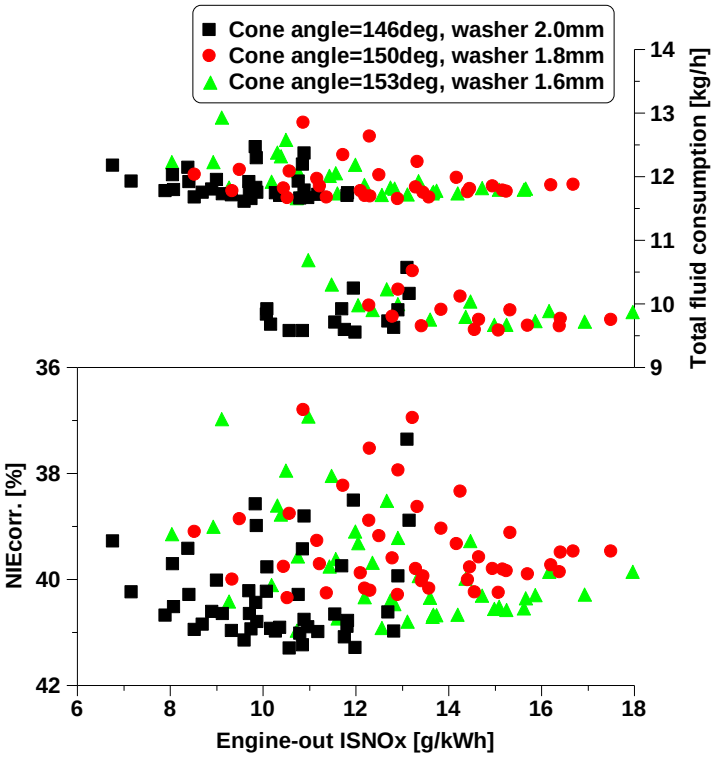

Figure 4.33: Overall engine efficiency analysis for injectors with different spray angles at 100% engine loads.

4.6 Summary

In this chapter, engine experiments were carried out to study the influence of injector specifications including nozzle shape, fuel mass flow rate, and spray cone angle in the research engine. Additionally, the optimum washer thicknesses for different spray cone angles were estimated in order to match well with the combustion chamber. Finally, the total engine efficiency was analysed by considering the urea consumption in the SCR system. The research was performed at six test points selected from the ESC test cycle. Injection pressure and SOI were varied to provide a better analysis of the influence of injector parameters on combustion characteristics, exhaust emissions, and engine performance. The main findings of the injector geometry study can be drawn as follows:

i. Injector with Ks-hole shape improved the fuel atomization quality owing to the relatively higher discharge coefficient and longer spray tip penetration than the cyl-hole shape, which yielded a similar impact on the mixture formation to that of a higher injection pressure. Consequently, the fuel consumption and soot emissions were reduced. However, the NOx emissions were slightly increased at most test points except at the lower engine speeds.

ii. In comparison to a higher fuel flow rate injector, the lower fuel flow rate injector

decreased the NOx and soot emissions at most test points due to improved fuel atomization. The HC emissions were lower likely due to a shorter spray tip penetration and hence reduced the possibility of the liquid spray impingement. However, the fuel consumption was increased due to the longer injection duration and shorter spray penetration, which shifted the combustion process later in the expansion stroke and led to poor air utilization.

iii. Both Ks-hole shape and a relatively higher fuel mass flow rate injectors allowed for an improvement in the trade-off relationships of NOx-soot and NOx-FC. Therefore, these injector geometric parameters were employed for the subsequent studies.

iv. The injector washer thickness (injector tip protrusion) showed strong effect on the interaction between the fuel spray and combustion bowl. The bigger spray angle matched with a thinner washer or the smaller spray angle matched with a thicker washer presented a better trade-off relationships of NOx-soot and NOx-ISFC.

v. Injector with the biggest spray cone angle obtained the highest fuel efficiency while the injector with the smallest spray cone angle produced the lowest level of NOx. The medium spray angle injector demonstrated a slightly lower soot emissions at most test points. Overall, injector with the biggest spray cone angle achieved the best NOx-ISFC trade-off.

vi. The injection timing and injection pressure also showed important impact on the injector geometry optimization as the injection timing could change the spray targeting position in the piston bowl while the injection pressure had great impact on the spray penetration.

vii. The overall engine efficiency analysis demonstrated that injector with the smallest spray angle of 146° and a washer thickness of 2.0 mm reduced the NOx emissions and therefore the aqueous urea solution consumption in the SCR system. This resulted in a lower total fluid consumption and contributed to a higher $NIE_{corr.}$, helping to minimise the EOC.

Overall, the results reveal that the investigation of injector orifice shape, fuel flow rate, and spray cone angle is needed to achieve a better balance between engine efficiency and engine-out emissions. Moreover, the optimum injector should be selected carefully according to the operating conditions and other combustion control strategies such as advanced injection strategy, EGR, and Miller cycle, which will be presented and discussed in the following chapters.

Chapter 5
Experimental assessment of the Miller cycle operation at low and medium engine loads

5.1 Introduction

When it was first proposed by Ralph Miller in 1950s, Miller cycle was intended to improve the thermal efficiency by avoiding knocking combustion in a spark ignition engine through the reduction of ECR. In recent years, it has received more attention in diesel engines due to its potential in reducing NOx emissions by lowering the peak combustion temperatures. Miller cycle is typically achieved by lowering the ECR while maintaining the expansion ratio via early or late IVC timings. In most Miller cycle engines, boosting technologies are applied to compensate the in-cylinder charge loss caused by the early or late IVC timings in order to maintain the power performance. The Miller cycle operation needs to be optimized in order to improve the remains trade-off between the actual engine efficiency and NOx emissions and minimize the EOC. In addition, the lower EGT at low engine load operations can reduce the conversion efficiency and performance of the diesel ATS, which plays an important role on the NOx emissions control. Reduction in the engine-out NOx emissions and maintaining a sufficiently higher EGT are required to meet the NOx targets and minimise the EOC.

In this chapter, experimental works have been performed on a single cylinder diesel engine to investigate the characteristics of Miller cycle at low and medium loads (between 6 and 12 bar IMEP) as well as to explore an optimum combustion control strategy for efficient EGT management at the light engine load (2.2 bar IMEP). Presented in Section 5.2 is the overview of the low-medium load Miller cycle operation while the influence of intake pressure on Miller cycle is shown in Section 5.3. The investigation of Miller cycle with EGR for NOx emissions and EGT control at low and medium loads is presented in Section 5.4. Section 5.5 explores the potential of Miller cycle combined with EGR and post fuel injection for emissions and exhaust gas temperature control at low load. Finally, Section 5.6 shows the exploration of the alternative combustion control strategies for EGT management at a light load. The specific test conditions are given in the “Test methodology” of each subsection.

5.2 Characterisation of Miller cycle operation at low and medium loads

This section will present the methodology used in this study to define the effective compression ratio. This is followed by an analysis and discussion of the Miller cycle operating with different combustion control technologies such as injection strategy, intake pressure, and external cooled EGR at low and medium loads.

5.2.1 Test methodology

Experimental investigation was carried out to demonstrate the characterization of low-medium load Miller cycle operation at 1250 rpm and two engine loads of 6 and 12 bar IMEP. These two test points represents high residency areas in a typical HD drive cycle. Figure 5.1 indicates the WHSC test cycle operating conditions as well as the two test points over an estimated HD diesel engine speed-load map. The size of the circle represents the weighting factor. A bigger size indicates a higher relative weighting of the engine operation conditions over the WHSC test cycle. The pressure differential across the cylinder was maintained at 10 kPa for all test points by varying the exhaust back pressure at a given intake pressure, which can maintain a comparable PMEP and hence a fair comparison for various cases. The PRR and COV_IMEP were limited to 20 bar/CAD and 3%, respectively.

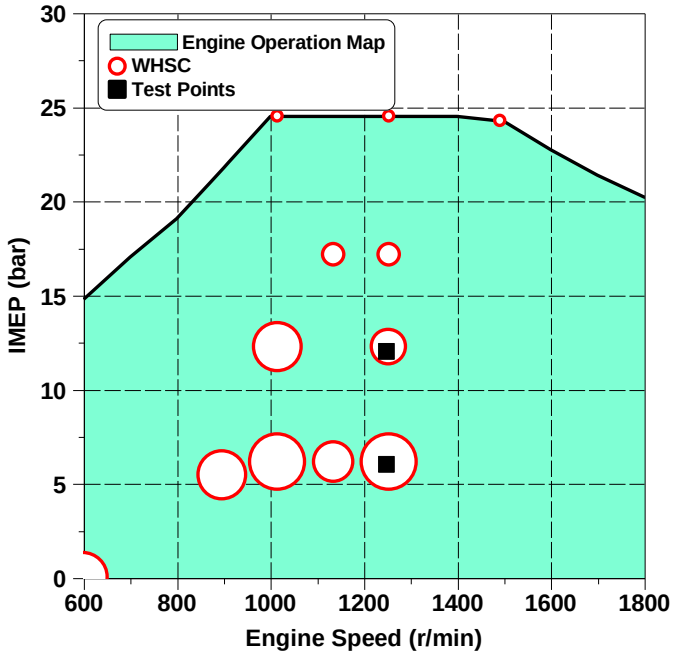

Figure 5.1: Test points and WHSC operation conditions over an estimated HD diesel engine speed-load map.

Table 5.1 summaries the engine operating conditions for the different variables swept. The injection timings and injection pressures were varied and a constant pre-injection of 3 mm^3 and a dwell timing of 1ms were used to maintain an acceptable level of PRR at low-medium loads. In some cases, higher intake pressure was applied to compensate the lower in-cylinder mass trapped. The role of cooled external EGR was tested with Miller cycle strategy, varied between 0 and 20% for low load while between 0 and 15% for medium load.

Table 5.1: Engine testing conditions for the characterization of low-medium load Miller cycle operation.

Parameter	Value	
Speed	1250 rpm	
IMEP	6 bar	12 bar
Injection timing	Varied between -7.5 and -15.5 CAD ATDC	Varied between -16 and -21.5 CAD ATDC
Injection pressure	1100 and 1300 bar	1400 and 1600 bar
Intake pressure	Varied between 1.44 and 2.14 bar	Varied between 1.70 and 2.30 bar
Exhaust pressure	Maintain 0.1 bar higher than intake pressure	Maintain 0.1 bar higher than intake pressure
EGR rate	0, 15, 20%	0, 10, 15%
Baseline IVC	-178 CAD ATDC	-178 CAD ATDC
Late IVC (Miller cycle)	-140,-130,-120,-110,-100 CAD ATDC	-130, -120, -110 CAD ATDC

The IVC timing was delayed to allow for the Miller cycle operation along with a reduction in the ECR. This is detailed in Figure 5.2 with the engine valve lift profiles used at a speed of 1250 rpm and a load of 6 bar IMEP. The IVO and IVC timings of the baseline case were set at 367 and -178 CAD ATDC, respectively. The tested IVC timings were delayed gradually from -178 CAD ATDC in the baseline to -93 CAD ATDC in the latest IVC timing, while maintaining the maximum lift of 14 mm constant.

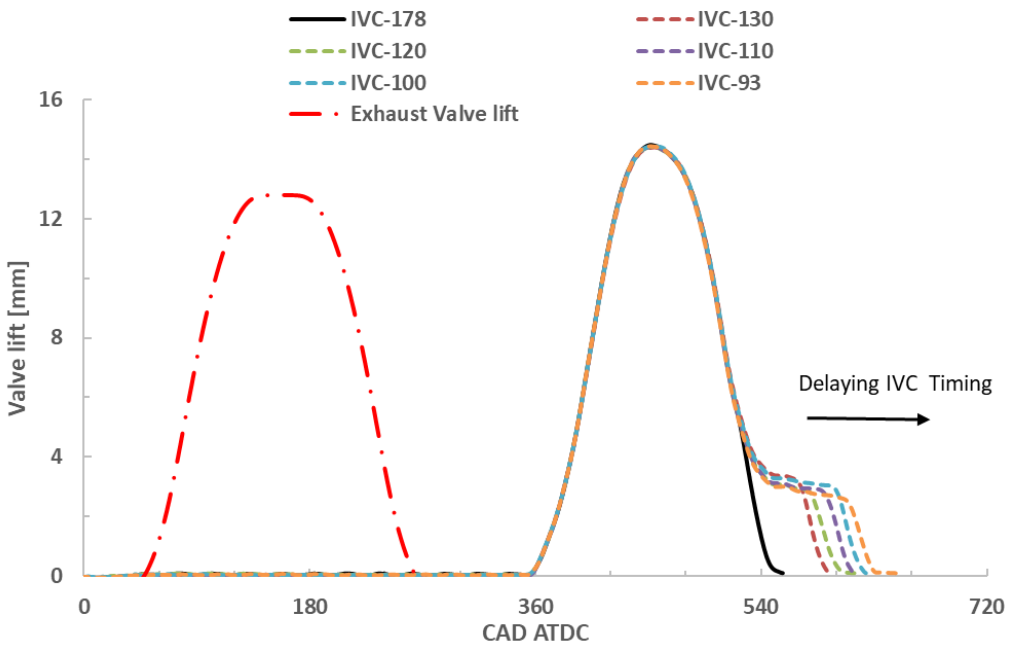

Figure 5.2: Engine fixed exhaust and variable intake valve lift profiles.

5.2.2 Definition of the effective compression ratio

The intake camshaft of the research engine was equipped with a VVA system, in which a hydraulic tappet on the valve side of the rocker arm was incorporated to realize the desired LIVC events [195]. During the period of late intake valve timing in the compression stroke, the upward piston motion will cause backflow into the intake manifold by pushing the air charge out of the cylinder before the IVC, which reduced the actual in-cylinder mass trapped.

The ECR is a commonly used parameter for effectively indicating the extent of compression and qualifying the effect of LIVC, which was reduced by the delayed initiation of the compression process. One of commonly used ECR definitions is based on the volumetric ratio, which is geometrically calculated as the ratio of the cylinder volume at the specified IVC to the cylinder clearance volume at TDC. The actual compression process, however, does not occur exactly when the intake valve close [204]. Figure 5.3 shows the illustration of the definition of volume-based and pressure-based ECR at a speed of 1250 rpm and 6 bar IMEP. The cylinder charge has already been partially compressed before the IVC. This is primarily due to the flow resistance across the intake valves and the gas-momentum-induced compression [205]. Therefore, the volume-based geometric ECR is inadequate to explain the experimental results.

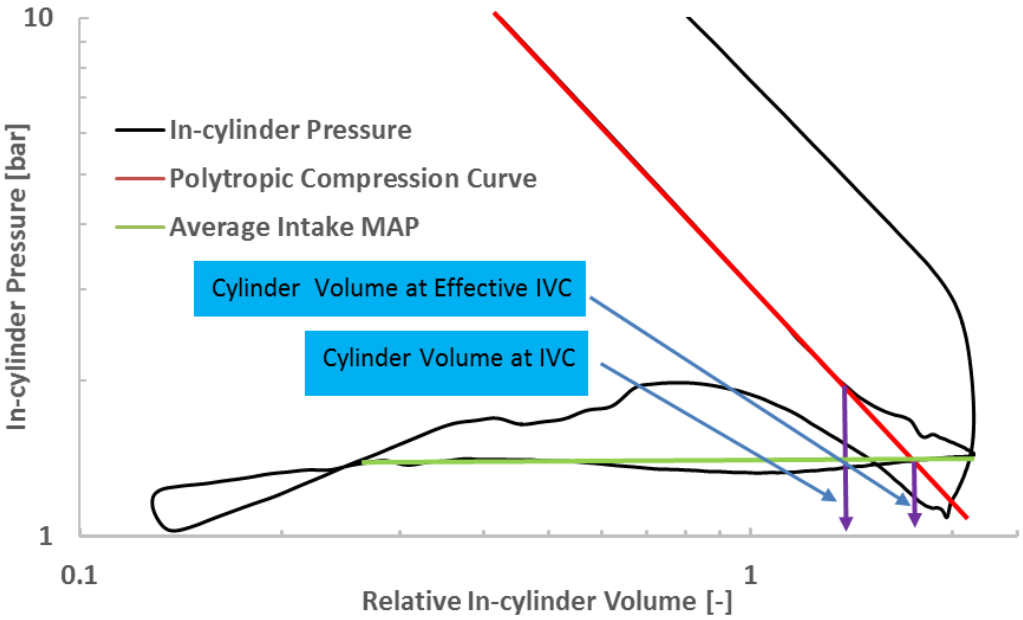

Figure 5.3: The illustration of volume-based and pressure-based methods for ECR calculation at 1250rpm and 6 bar IMEP.

In this work, the pressure-based method considers the cylinder volume at the start of gas compression for ECR calculation. The effective IVC volume is taken as the volume corresponding to the intersection point by extrapolating the polytropic compression process curve linearly down to intersect the average intake manifold air pressure (MAP). The pressure-based ECR is then defined as the ratio of the volume at effective IVC to the volume at TDC [204–207]. This method can be more accurately characterize the actual in-cylinder compression process than the volume-based method. Table 5.2 and Figure 5.4 depict the volume-based and pressure-based ECRs for all testing IVC timings. It can be seen that the volume-based geometric ECR is generally lower than the pressure-based ECR. This is because the volume-based method does not considering the influence of the in-cylinder flow momentum and the flow resistance across the intake valves during the compression stroke. Additionally, the difference between both ECRs is increased with later IVC.

Table 5.2: The variation of volume-based and pressure-based ECR at different IVC timings operating at 1250rpm and 6 bar IMEP.

IVC Timing	Volume-based Geometric ECR	Pressure-based ECR
CAD ATDC	-	-
-178	16.7	16.8
-140	15.3	16.5
-130	15.1	16.3
-120	14.4	15.9
-110	13.3	15.3
-100	12.3	14.7
-93	11.2	13.8

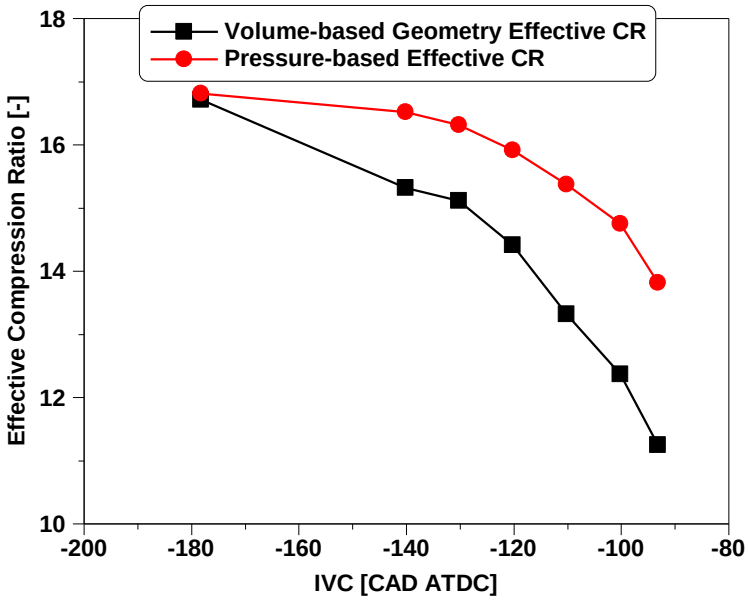

Figure 5.4: The volume-based geometric ECR and pressure-based ECR as a function of the IVC at 1250rpm and 6 bar IMEP.

5.2.3 Overview of the Miller cycle operation at low and medium loads

Figure 5.5 and 5.6 show the in-cylinder pressure and HRR for various IVC timings at a speed of 1250 rpm and two engine loads of 6 and 12 bar IMEP. The injection timing and injection pressure were maintained constant when varying IVC timing at both loads.

A similar trend in combustion characteristics was observed in both low and medium loads as IVC timing was delayed. Compared to the baseline IVC at -178 CAD ATDC, the Miller cycle via LIVC strategy decreased the compression pressure as a result of the reduction

of in-cylinder mass trapped. The lower compression pressure led to a significant reduction in peak in-cylinder pressure during the combustion process.

A later heat release (e.g. SOC) was observed as IVC timing was delayed from -178 to -100 CAD ATDC due to reduced initial in-cylinder pressure and temperature prior to combustion. The increased ignition delay allowed more time for a better mixing of the fuel and air, which resulted in a higher degree of premixed combustion as suggested by the appearance of the first peak HRR. The peak HRR was reduced with later IVC as a result of lower in-cylinder pressure and in-cylinder oxygen availability. This would lead to longer combustion duration and therefore could adversely affect the engine efficiency.

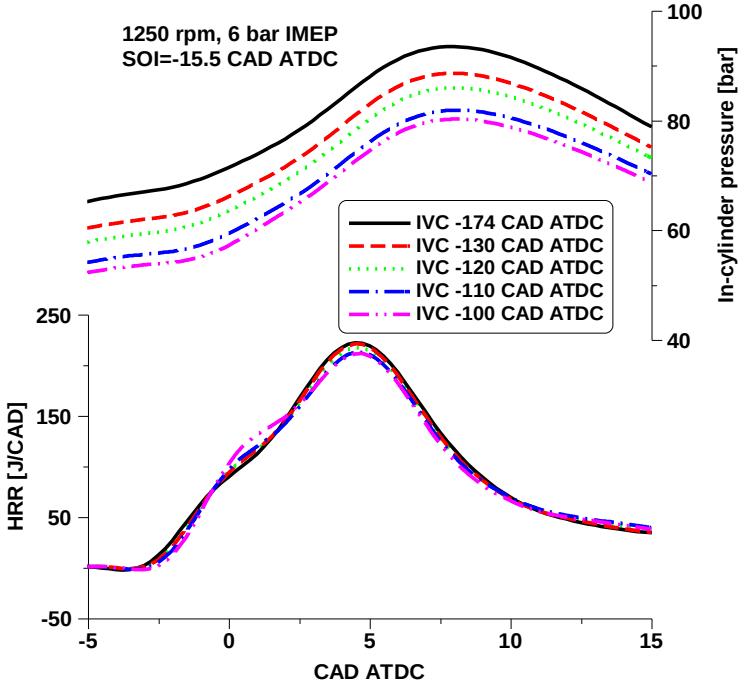

Figure 5.5: In-cylinder pressure and HRR for different IVC timings at 6 bar IMEP.

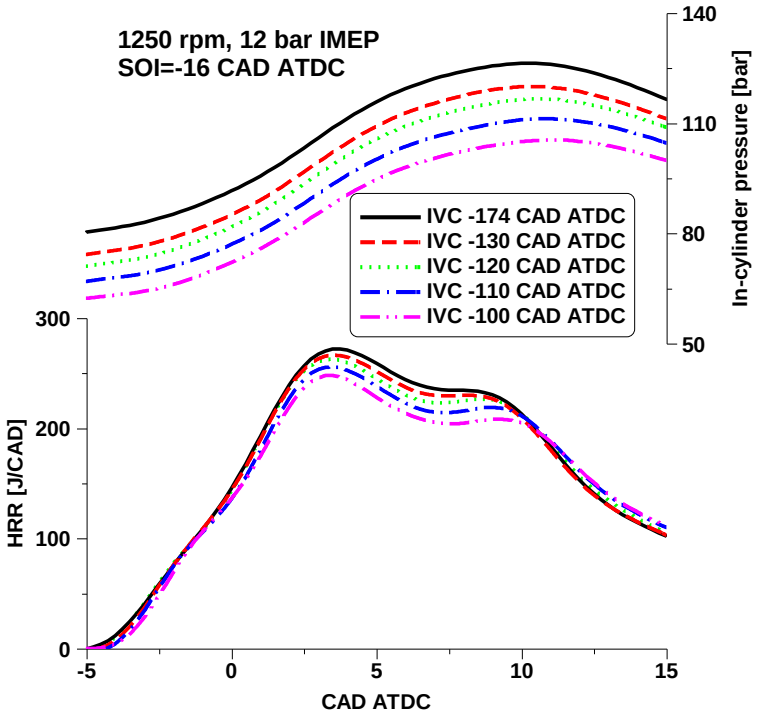

Figure 5.6: In-cylinder pressure and HRR for different IVC timings at 12 bar IMEP.

5.2.4 Effects of Miller cycle on the combustion phasing at low and medium loads

The SOI was swept to vary the CA50 between 5 and 18 CAD ATDC at 6 bar IMEP while between 4 and 20 CAD ATDC at 12 bar IMEP, in order to explore the sensitivity of Miller cycle operation to the combustion phasing. Figure 5.7 and 5.8 show the in-cylinder pressure and HRR as well as the diesel injector signal for both baseline and Miller cycle operations at 6 bar and 12 bar IMEP, respectively.

At a constant main SOI, the Miller cycle delayed the SOC as the lower ECR reduced the initial in-cylinder pressure and temperature prior to ignition. When compared at the same CA50, the heat release was delayed by Miller cycle at 6 bar IMEP while was reversed at 12 bar IMEP due to the use of more advanced SOI to maintain the same CA50. Overall, the Miller cycle significantly decreased the peak in-cylinder pressure and peak HRR when operating with same SOI or same CA50 condition.

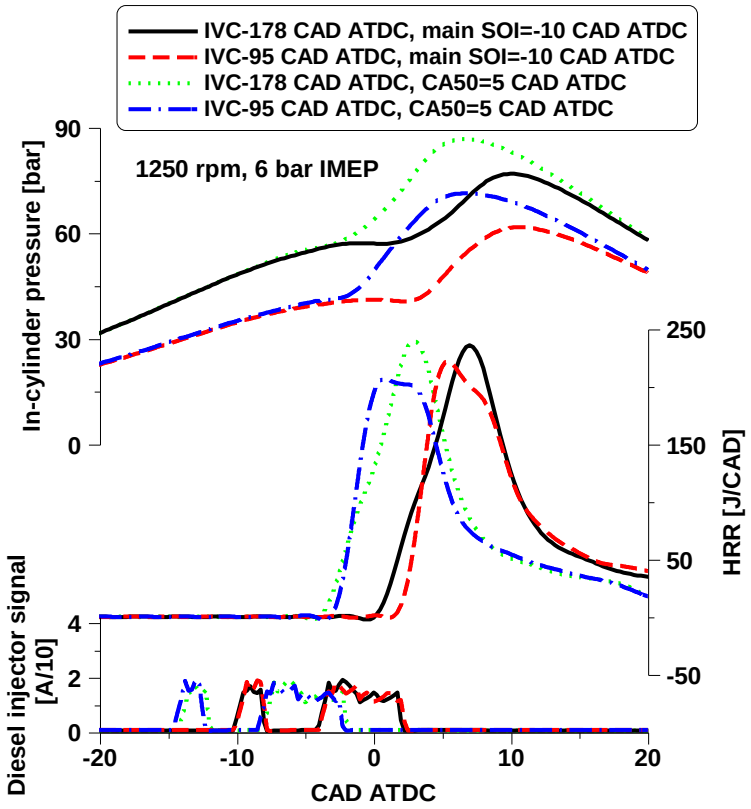

Figure 5.7: In-cylinder pressure, HRR, and injection signal of the baseline and Miller cycle strategies at 6 bar IMEP.

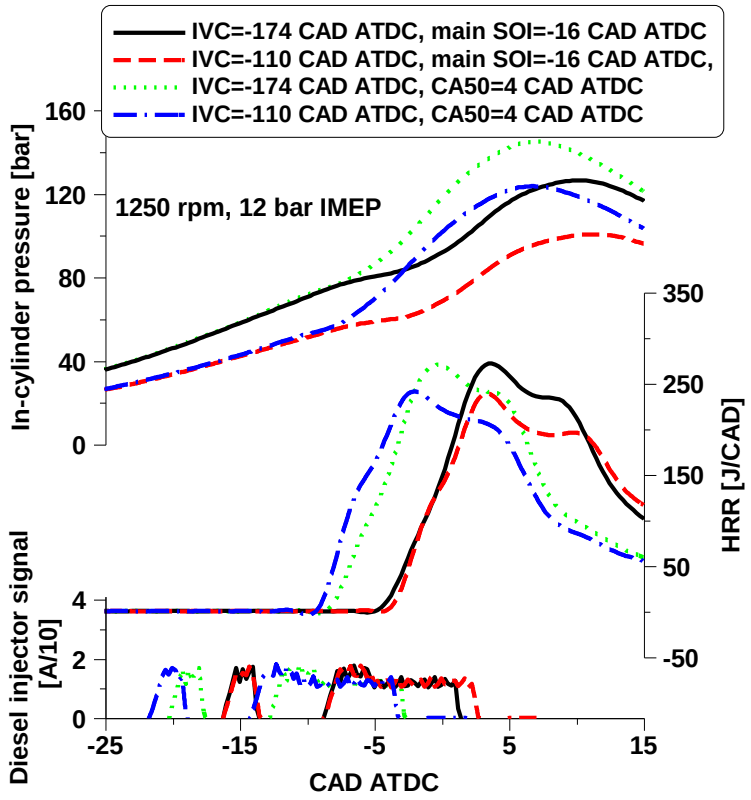

Figure 5.8: In-cylinder pressure, HRR, and injection signal of the baseline and Miller cycle strategies at 12 bar IMEP.

To explore the effect of Miller cycle on the trade-off between exhaust emissions and engine performance as well as evaluate its potential in reducing NOx emissions, a sweep of CA50 and IVC timing was performed at two test points. Figure 5.9 shows the variation of smoke number against CA50 and IVC timing with various NOx levels. Compared to a late CA50 strategy, Miller cycle enabled a relatively earlier CA50 to achieve the same NOx levels at the expense of slightly higher smoke number. The impact on the smoke number was higher at a relatively higher engine load, especially when comparing at the lower NOx levels. This was mainly due to the lower in-cylinder oxygen availability.

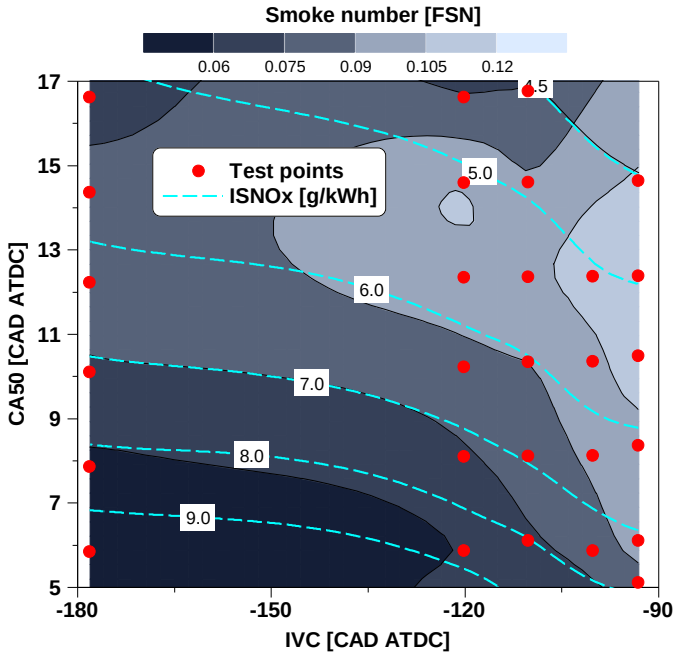

(a) 6 bar IMEP

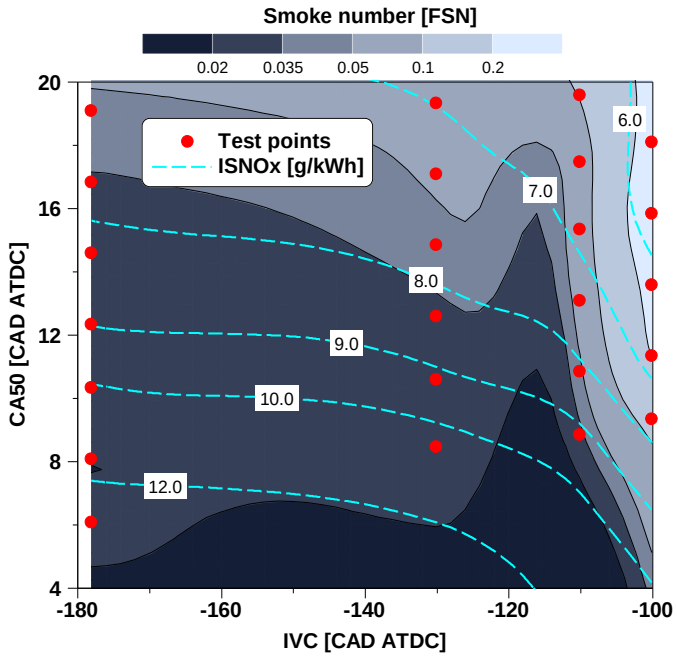

(b) 12 bar IMEP

Figure 5.9: Effects of Miller cycle and combustion phasing on smoke number.

Figure 5.10 shows the ISFC as a function of the CA50 and IVC timing with various NOx emissions at the low and medium loads. It can be seen that both later IVC and CA50 decreased NOx emissions with a penalty on ISFC. At 6 bar IMEP, the Miller cycle strategy resulted in a lower penalty on ISFC than a later CA50 strategy when comparing at the same NOx emissions, which was more pronounced at the lower NOx levels. This was attributed to the relatively earlier CA50 in the Miller cycle, which helped improve the fuel conversion efficiency. However, the fuel consumption penalty of Miller cycle strategy was comparable to the late CA50 strategy as the engine load was increased. This was a result of the lower lambda at a relatively higher load and therefore the combustion was more sensitivity to the variation of in-cylinder oxygen availability than that at the lower load.

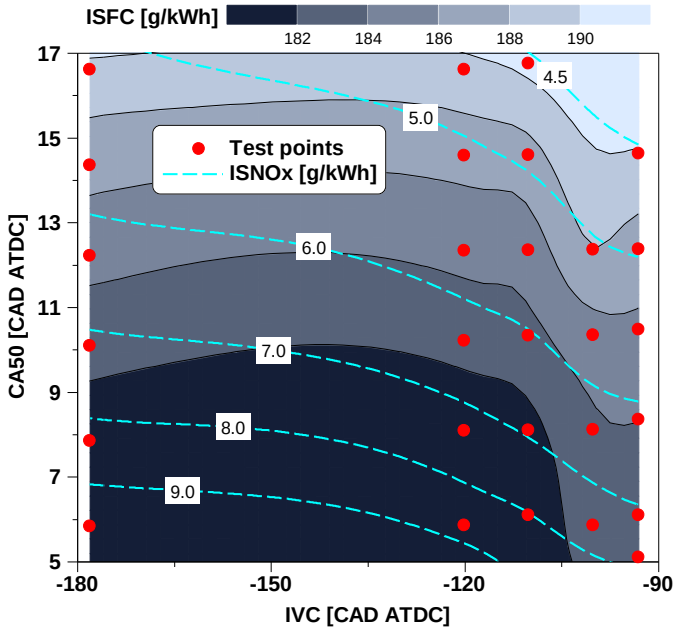

(a) 6 bar IMEP

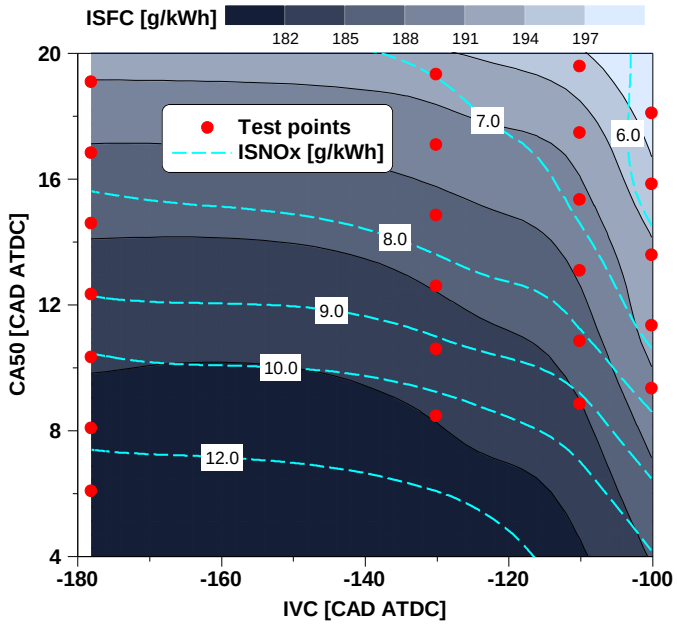

(b) 12 bar IMEP

Figure 5.10: Effects of Miller cycle and combustion phasing on ISFC.

Figure 5.11 depicts the EGT as well as the resulting fuel consumption penalty in percentage. As the EGT is mainly determined by the amount of charge trapped in the cylinder, a reduction in the cylinder mass flow allowed for a higher EGT due to the lower total in-cylinder gas heat capacity. The Miller cycle strategy showed a significant effect on EGT at a lower load, increasing EGT from 275°C in a baseline case to 345°C in an IVC at -110 CAD ATDC. This improvement was attained with a reduction of 2.5% in ISFC. However, the use of a late CA50 strategy was less effective in increasing EGT, achieving an increase of 40°C in EGT with a penalty of 5.5% in fuel consumption. At 12 bar IMEP, the effect of Miller cycle and combustion phasing on EGT exhibited a similar trend to that of the low load condition.

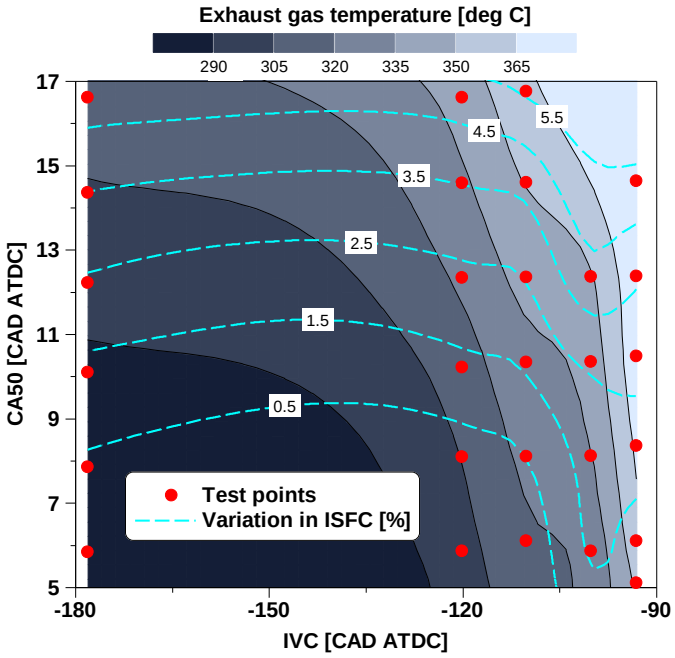

(a) 6 bar IMEP

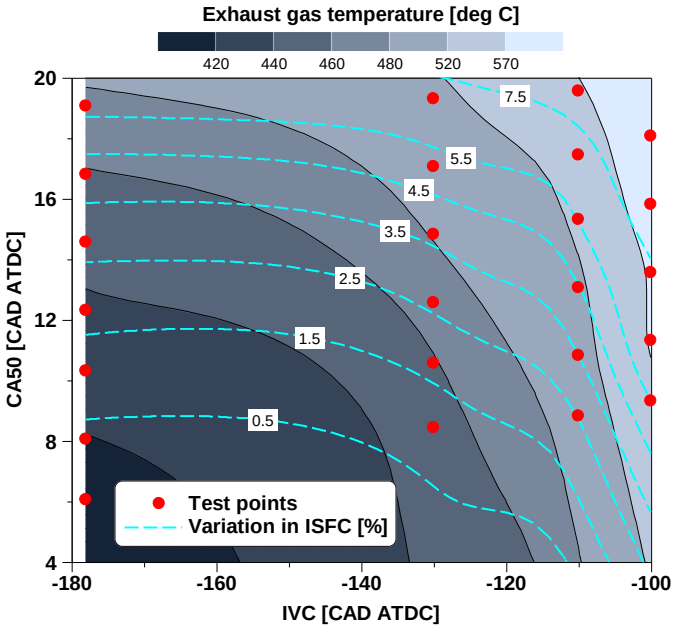

(b) 12 bar IMEP
Figure 5.11: Effects of Miller cycle and combustion phasing on EGT.

5.2.5 Effects of fuel injection pressure on Miller cycle operation at low and medium loads

A higher fuel injection pressure is generally employed for achieving higher efficiency and lower smoke emissions via improving the fuel-air mixing process. Figure 5.12 and 5.13 show the in-cylinder pressure, HRR, and the injector current signal for baseline and Miller cycle at low and medium loads, respectively. The diesel injection timings were optimised to obtain the optimum fuel efficiency for all test points. The comparison was carried out at the baseline IVC and Miller cycle with two different fuel injection pressures. The introduced EGR rate was 20% at 6 bar IMEP while 15% at 12 bar IMEP for both the baseline and Miller cycle strategies.

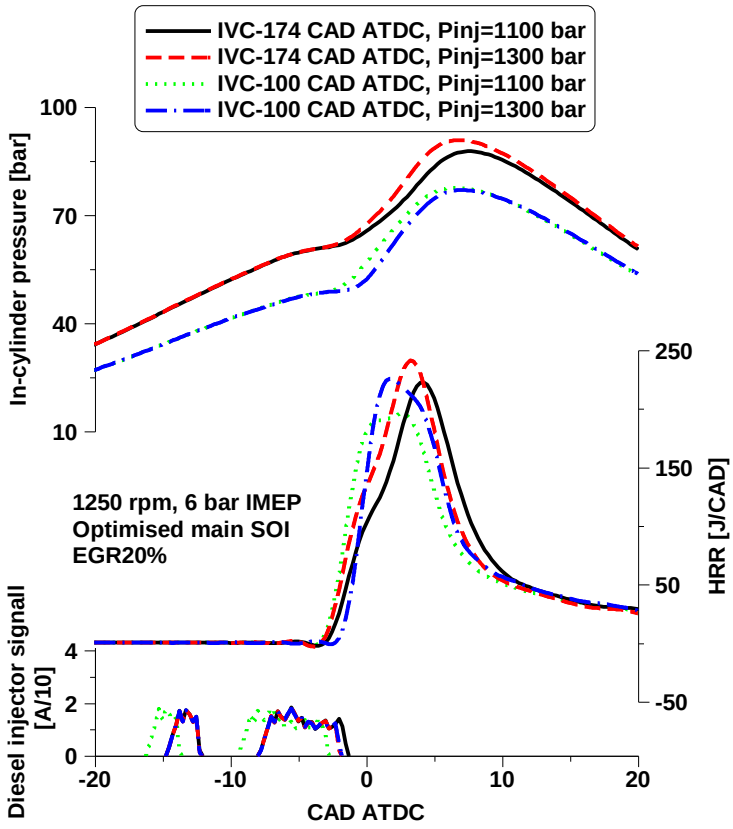

Figure 5.12: The effect of fuel injection pressure on low load Miller cycle operation with optimised SOI.

Results revealed that the optimised main SOI need to be retarded when a higher P_{inj} was applied in order to achieve the optimum fuel efficiency. This led to a later initiation of heat release. As a result, a similar peak in-cylinder pressure was observed at baseline and Miller cycle with different P_{inj}. However, the use of a higher P_{inj} caused higher peak HRR,

despite a later main SOI. Overall, the Miller cycle with a lower P_{inj} enabled the most advanced main SOI, leading to the earliest heat release as well as the lowest peak HRR.

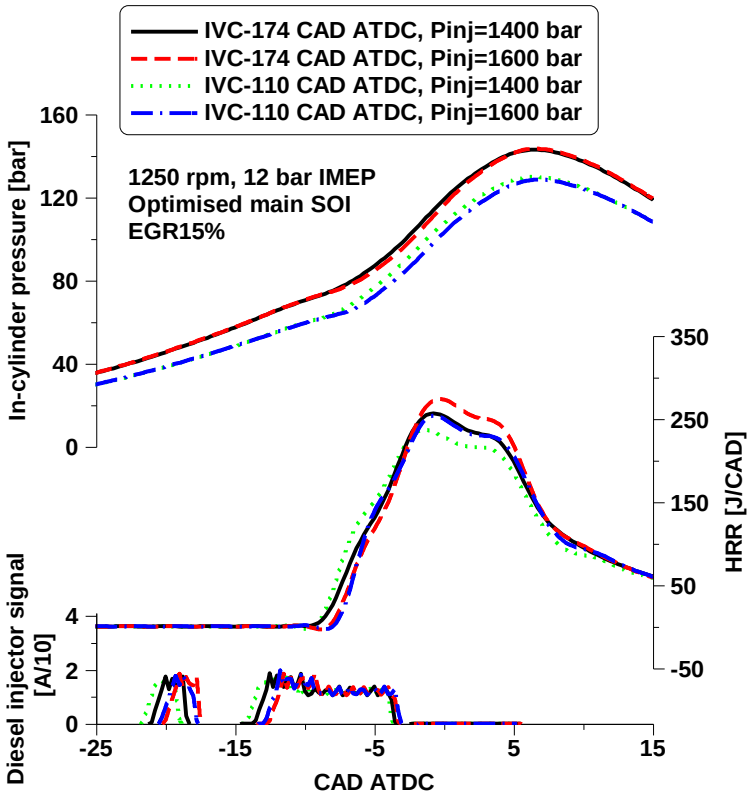

Figure 5.13: The effect of fuel injection pressure on medium load Miller cycle operation with optimised SOI.

To evaluate the effect of injection pressure on engine performance and emissions of various IVC timings, a comparison was performed and shown in Figure 5.14 and 5.15 for low and medium loads, respectively.

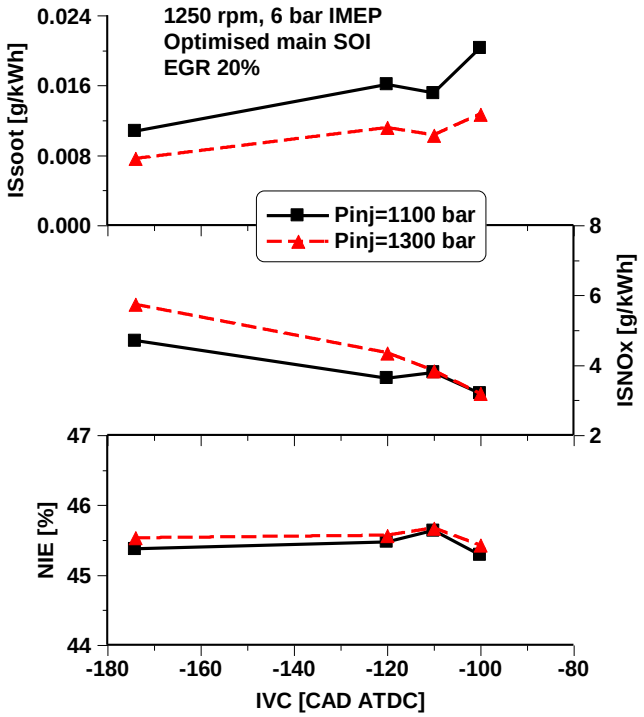

Figure 5.14: The effect of injection pressure on emissions and performance of low load Miller cycle operation with optimised injection timings.

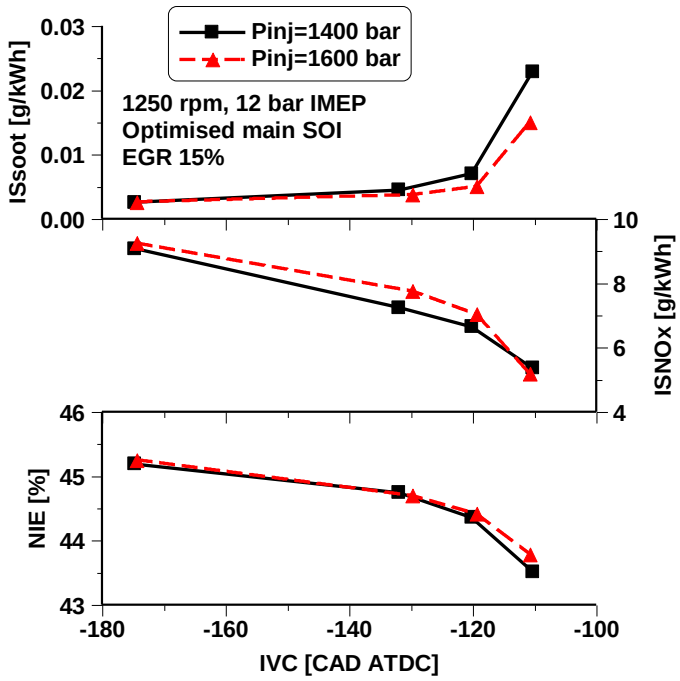

Figure 5.15: The effect of injection pressure on emissions and performance of medium load Miller cycle operation with optimised injection timings.

The higher P_{inj} with a delayed main SOI achieved lower soot emissions, especially at a later IVC. This was attained with a slight improvement in NIE and a higher NOx emissions. Therefore, a relatively lower P_{inj} (e.g. 1100 bar for low load and 1400 bar for medium load) was selected for the low-medium load Miller cycle operation in order to achieve a better trade-off between NOx and NIE.

5.3 The effect of intake pressure on Miller cycle operation at low and medium loads

This subsection aims to explore the potentials and challenges of the low-medium load Miller cycle operation at constant boost pressure and higher boost pressure. The investigation was performed at the same test points as those used in section 5.2, at a constant speed of 1250 rpm and two different engine loads of 6 and 12 bar IMEP.

5.3.1 Test methodology

Table 5.3 summaries the engine operating conditions for the baseline and Miller cycle operations. The experiments were carried out without EGR while varying the main SOI to maintain a constant CA50 for every test point. The intake pressure (P_{int}) for the Miller cycle

operation was varied between the same P_{int} and the same lambda as the baseline. The P_{inj} was maintained constant and the exhaust manifold pressure was adjusted according to the intake pressure and thus, maintaining a constant pressure differential of 0.1 bar across the cylinder with higher exhaust manifold pressure. A small pre-injection of an estimated volume of 3 mm^3 and a constant dwell timing of 1ms was employed in order to maintain PRR below 20 bar/CAD.

Table 5.3: Engine operating conditions for the baseline and Miller cycle operation with different intake pressures.

Parameter	Value	
Speed	1250 rpm	1250 rpm
IMEP	6 bar	12 bar
CA50	Varied between 7.5 and 14.5 CAD ATDC	Varied between 7.5 and 17 CAD ATDC
Injection pressure	1100 bar	1400 bar
Intake pressure	Varied between 1.44 and 1.84 bar	Varied between 1.7 and 2.3 bar
Exhaust pressure	0.1 bar higher than the P_{int}	0.1 bar higher than the P_{int}
Baseline IVC	-178 CAD ATDC	-178 CAD ATDC
LIVC (Miller cycle)	-95 CAD ATDC	-95 CAD ATDC

5.3.2 Combustion characteristics

Figures 5.15 and 5.16 show the in-cylinder pressure and HRR for the baseline case and Miller cycle operation with different P_{int} at 6 and 12 bar IMEP, respectively. The comparisons were performed at a constant CA50 in order to isolate the effect of combustion phasing on Miller cycle operation.

The intake pressure demonstrated a similar effect on the in-cylinder pressure and HRR for the two engine loads. The Miller cycle case with a constant P_{int} (red dashed line) was characterised by a significantly lower in-cylinder pressure and a higher degree of premixed combustion as suggested by the formation of a first peak heat release, especially at the lower load. This was the result of the lower ECR, which decreased the compressed air pressure and temperature. With increased P_{int}, higher in-cylinder pressure and peak HRR were observed due to the higher in-cylinder charge density. The first peak heat release disappeared as a result of the higher compression pressure and earlier SOC. The Miller cycle strategy achieved a similar HRR profile to the baseline case when operating with the same lambda. It can be also seen that the in-cylinder gas pressure was

slightly lower than that of the baseline case. This was a result of the lower in-cylinder gas temperatures achieved via a LIVC strategy.

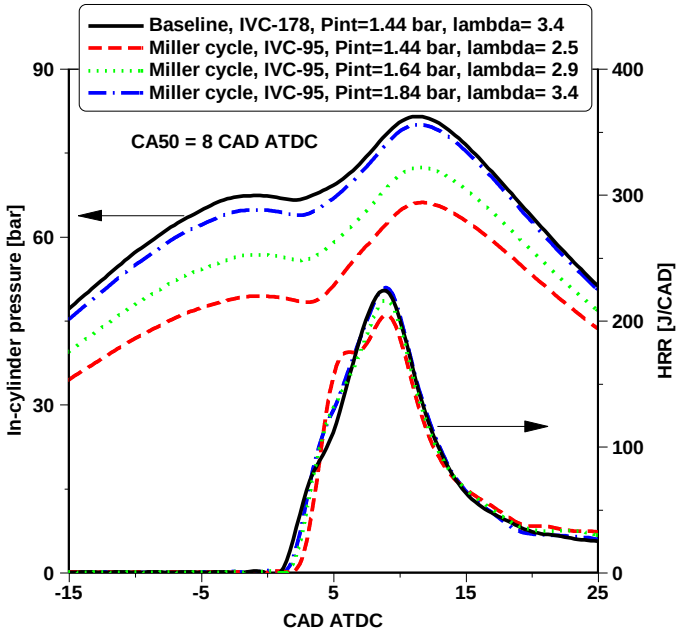

Figure 5.16: In-cylinder pressure and HRR for the baseline and Miller cycle cases at the low load.

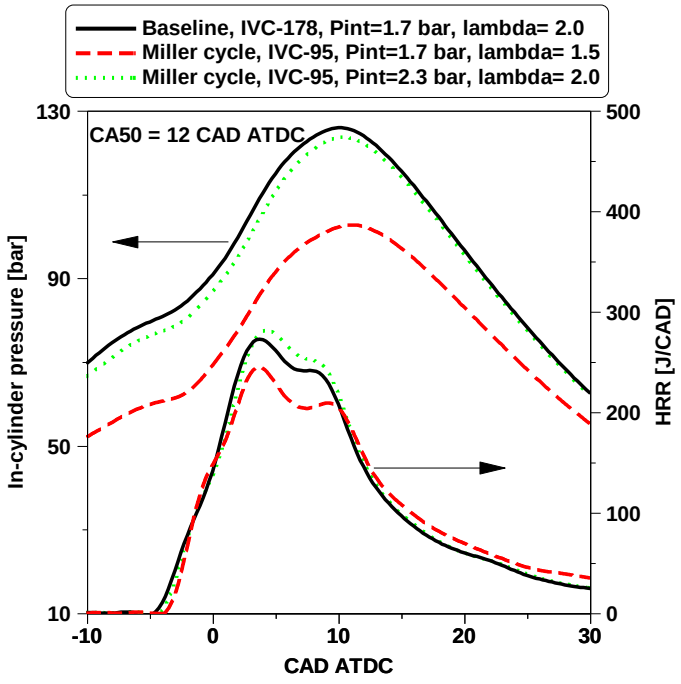

Figure 5.17: In-cylinder pressure and HRR for the baseline and Miller cycle cases at the medium load.

Figure 5.18 shows the ignition delay, CA90, CA50-CA90, and combustion duration (CA10-CA90) over a sweep of CA50 via varying the main SOI for low and medium loads, respectively. The Miller cycle with a P_{int} of 1.44 bar increased the ignition delay due to the lower compressed gas pressure and temperatures. The later ignition and slowed down

combustion process in the late combustion phase delayed the CA90. This resulted in a relatively longer period time of CA50-CA90 as well as combustion duration. A higher P_{int} improved the in-cylinder oxygen availability, which helped accelerate the combustion process. As a result, the ignition delay was shortened and the CA90 was advanced, which led to a shorter period time of CA50-CA90 and CA10-CA90. In particular, the combustion characteristics of the Miller cycle was similar to that of the baseline condition when operating with a constant lambda.

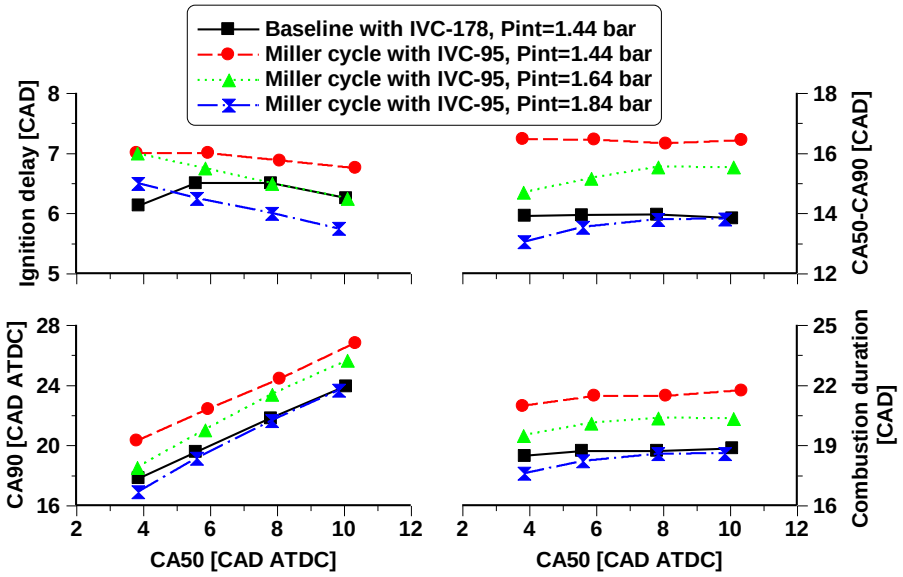

Figure 5.18: Heat release characteristics for the baseline and Miller cycle cases at the low load.

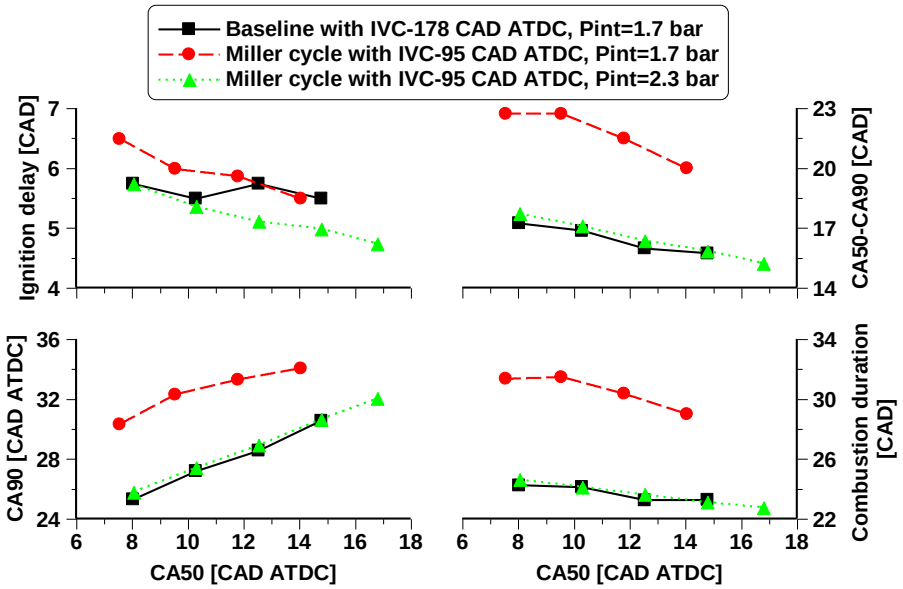

Figure 5.19: Heat release characteristics for the baseline and Miller cycle cases at the medium load.

5.3.3 Engine performance and gaseous emissions

Figure 5.20 and 5.21 show the engine performance parameters and net indicated specific emissions. At 6 bar IMEP, the use of Miller cycle with a constant P_{int} of 1.44 bar significantly reduced the lambda value due to lower in-cylinder mass trapped. This was also the reason for the increase of 75°C in the EGT, which is an important achievement considering that the EGT of 265°C in the baseline case was probably insufficiently high for efficient aftertreatment operation. This is because the optimum performance of the ATS can be achieved when the system inlet temperature is maintained between 250°C and 450°C [208], It is also important to note that the EGT showed in this study is the engine-out temperature, which will likely be reduced downstream of the turbocharger in a production multi-cylinder engine. At a higher load of 12 bar IMEP, the EGT was more sensitive to the use of Miller cycle with constant P_{int} due to the significantly lower lambda.

In comparison with the baseline engine operation, the NIE of the Miller cycle with constant P_{int} were decreased by approximately 1% at both engine loads. This was attributed to the slower CA50-CA90 period, longer combustion duration, as well as higher heat losses to cylinder walls due to higher mean in-cylinder gas temperatures (T_m) with LIVC [187,209]. The use of higher P_{int} helped increase the NIE due to the higher in-cylinder oxygen availability (e.g. lambda), but adversely affect the gains obtained in terms of EGT and NOx emissions. Miller cycle operation with constant lambda achieved a NIE as high as the baseline case at 6 and 12 bar IMEP.

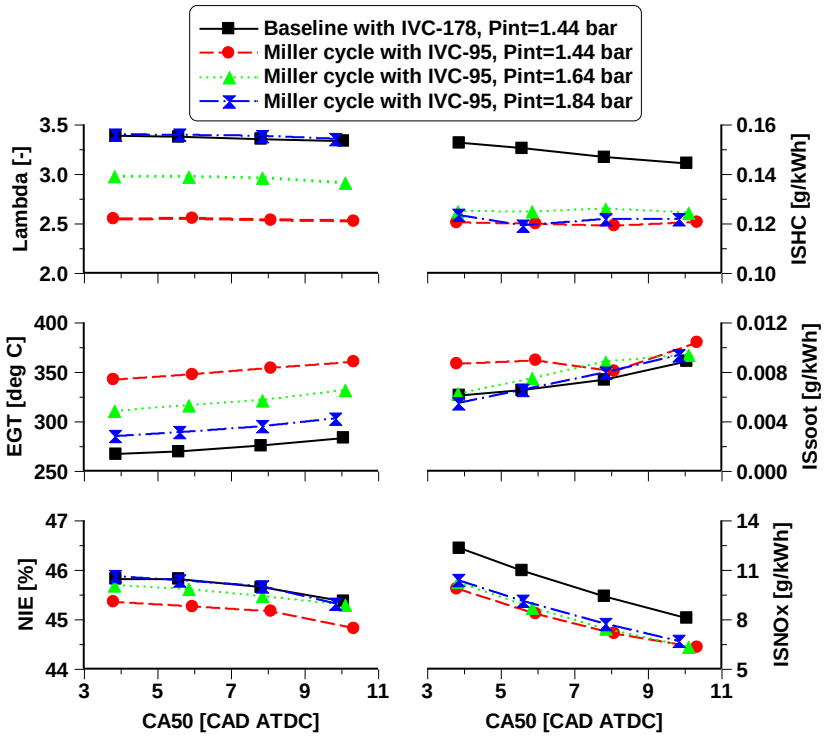

Figure 5.20: The effect of intake pressure on engine performance and exhaust emissions of low load Miller cycle operation.

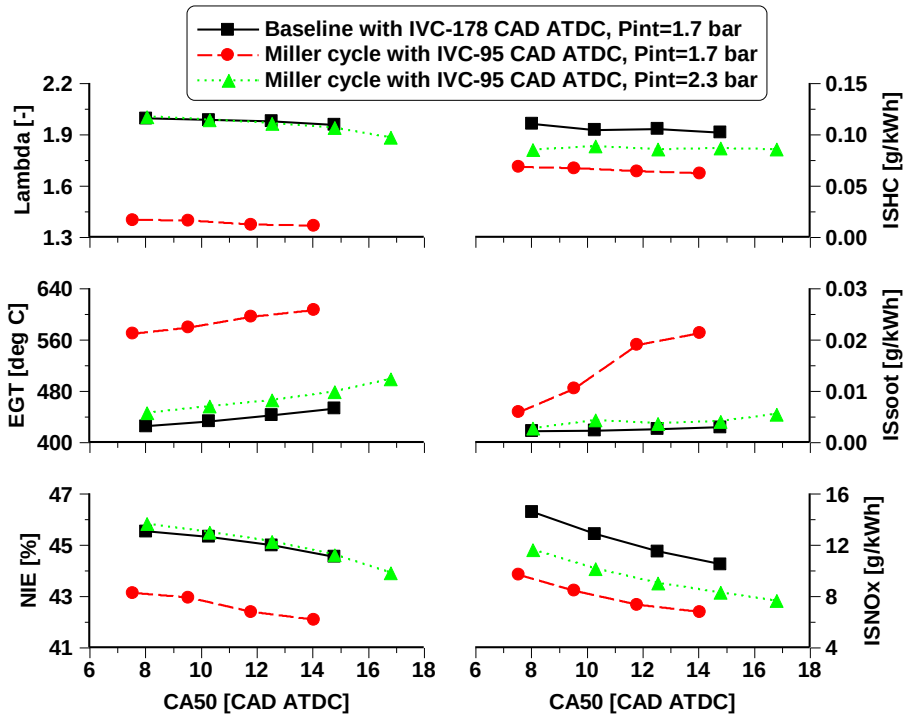

Figure 5.21: The effect of intake pressure on performance and exhaust emissions of medium load Miller cycle operation.

It can be also seen from Figure 5.20 and Figure 5.21 the intake pressure had a great impact on net indicated specific emissions. At 6 bar IMEP, the Miller cycle operation reduced the NOx emissions by 21% at the expense of slightly higher soot emissions. This was primarily a result of the lower in-cylinder air mass trapped and reduced initial burned zone gas temperature. At 12 bar IMEP, however, excessive soot emissions were observed by the use of Miller cycle, despite a decrease in NOx emissions by 36% on average. This was due to the significantly lower lambda at a higher engine load. A later CA50 effectively decreased combustion temperatures and therefore NOx emissions of all cases. As the P_{int} of the Miller cycle cases was increased, soot emissions were reduced and NOx emissions increased. Additionally, the application of Miller cycle decreased unburned HC emissions, regardless of the intake pressure used. This was possibly attributed to the relatively lower lambda and higher T_m, which can improve the HC oxidation during the combustion and expansion stroke. This characteristics was demonstrated by Verschaeren et al. [186] when applying Miller cycle on a medium speed heavy-duty diesel engine.

Overall, Miller cycle was the key enabler for effective EGT management and NOx emissions control at low-medium load condition. Despite the improvements in NIE

obtained when increasing the P_{int}, a higher lambda can impair the EGT and the NOx emissions benefits which were achieved by the use of Miller cycle.

5.4 Investigation of EGR and Miller Cycle for NOx emissions and exhaust temperature Control

The potential of the Miller cycle with EGR for NOx emissions control and exhaust temperature management have been investigated at 1250 rpm and both loads of 6 and 12 bar IMEP. The use of Miller cycle has previously been shown can curbed NOx emissions and elevated EGT simultaneously by lowering the compression pressure and temperature. EGR was used to dilute in-cylinder charge and increased the total in-cylinder heat capacity. This can help achieve better trade-off between the actual engine efficiency and NOx emissions. A one-dimensional engine simulation model was used to calculate the T_m and burned zone gas temperatures (T_b) based on the pressures measurement. Moreover, the results of an “EGR- only” and an “EGR + Miller” strategy at the same NOx reduction levels were compared to a baseline case with conventional IVC timing and no EGR.

5.4.1 Test methodology

Table 5.4 depicts the engine operating conditions for the different combustion control strategies investigated. Various EGR rates and ECRs were tested independently with constant intake and exhaust pressures at a given engine load. The pressure-based ECR was decreased from 16.8:1 to 12.4:1 at 6 bar IMEP and 14.8:1 at 12 bar IMEP. The main injection timing (T_{inj}) and injection pressure have been swept and optimized. However, the main injection timing and the injection pressures were kept constant for a given load to remove the effects introduced by the optimization process. A pilot injection was used before the main injection at all test conditions to keep the maximum of PRR below 20 bar/CAD. In this section, the steady state combustion was quantified by controlling the COV_IMEP below 3%.

Table 5.4: Engine test conditions for the baseline and Miller cycle at two test points.

Parameter	Value	
Speed	1250 r/min	1250 r/min
IMEP	6 bar	12 bar
T_{inj}	-11.5 CAD ATDC	-14 CAD ATDC
P_{inj}	1150 bar	1400 bar
P_{int}	1.4 bar	1.7 bar
Exhaust pressure	1.5 bar	1.8 bar
EGR	0, 7, 14, 19%	0, 9, 12, 16%
Baseline IVC	-178 CAD ATDC	-178 CAD ATDC
Miller cycle	-138, -120, -110 CAD ATDC	-148, -130 CAD ATDC
ECR	15.3, 13.5, 12.5	15.8, 14.8

5.4.2 Engine modelling

A one-dimensional (1D) thermodynamic simulation has been carried out using simulation software to calculate the mean in-cylinder gas temperature and burned zone gas temperature. The software is a computer-aided engineering code developed by Ricardo Software to analyse the dynamics of pressure waves, mass flows, and energy losses of various systems and machines. It provides a fully integrated treatment of time-dependent fluid dynamics and thermodynamics by means of a one-dimensional formulation which enables performance simulations to be carried out based on virtual intake, combustion, and exhaust system configuration. Shown in Figure 5.22 is the layout of the 1D model for single cylinder engine.

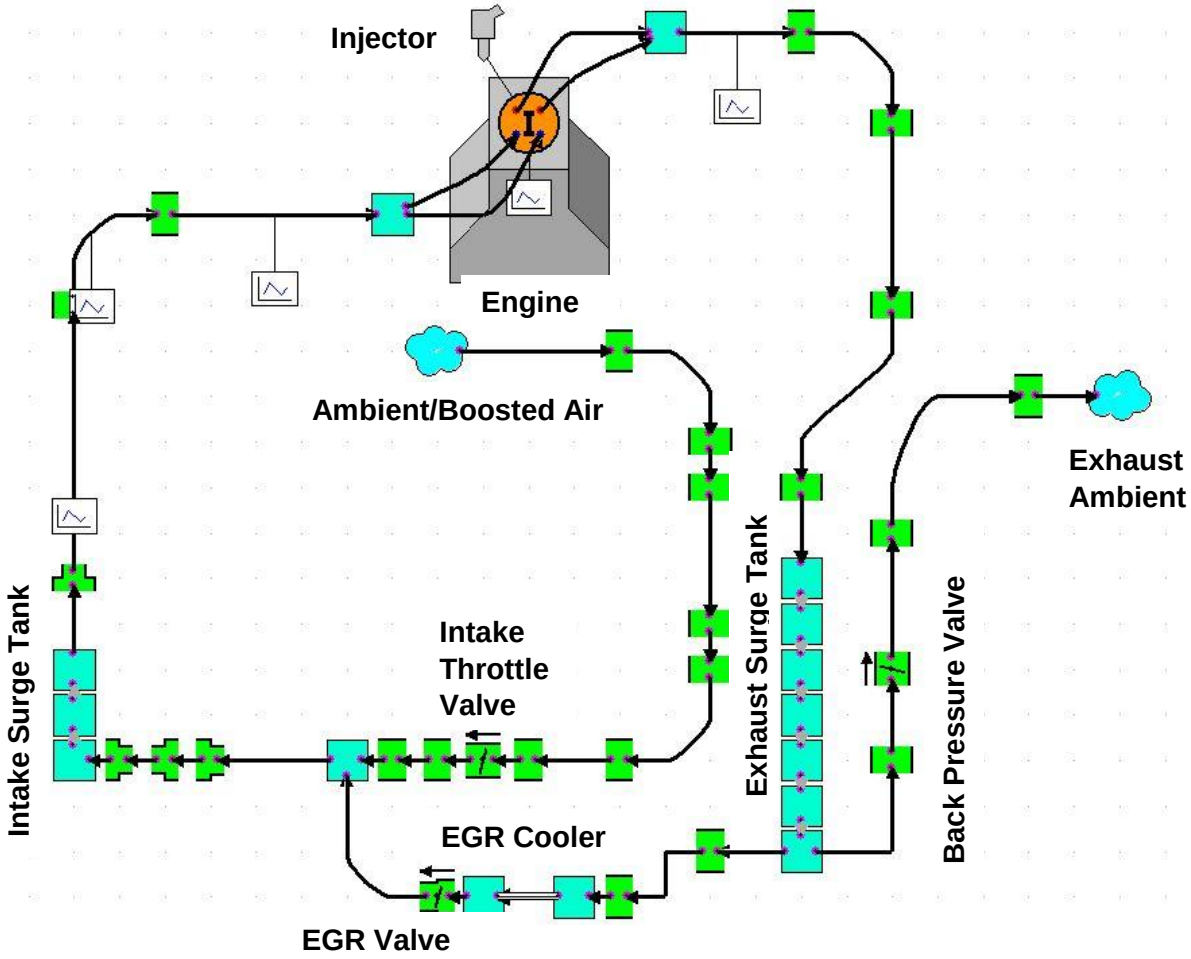

Figure 5.22: Layout of the one-dimensional model developed from Ricardo Wave.

The basic principle of this engine model is to solve the 1D unsteady compressible flow equations including conservation of mass, momentum and energy through finite difference method. The geometric dimensions of intake and exhaust pipes were measured from the engine bench while the ports and valve flow coefficients were provided by the engine supplier.

Figure 5.23 shows the flow coefficients at various Lift/Diameter for the intake and exhaust ports. The Lift/Diameter is the ratio of valve lift to the reference diameter obtained from the valve inner seats, which were equivalent to 39.2 mm and 35.8 mm for intake and exhaust sides, respectively. The data including initial temperatures for piston, liner, cylinder head, and valves, initial intake and exhaust pressures, injection timing and rail pressure, and fuel flow rates were taken from experiment and were imposed in the engine model.

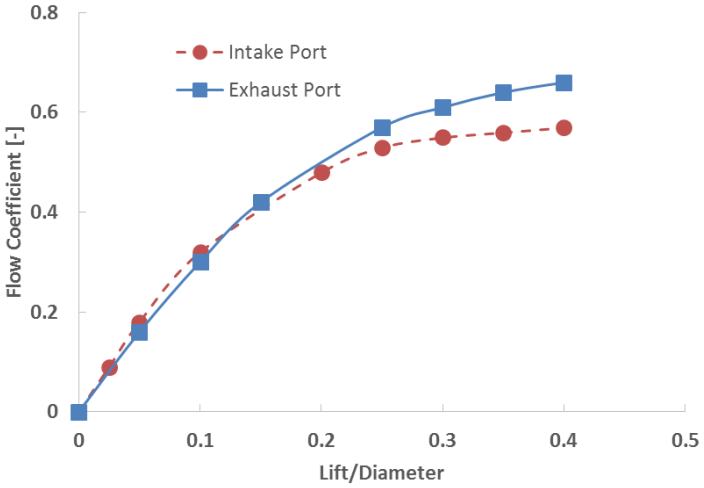

Figure 5.23: Flow coefficient of intake and exhaust ports as a function of Lift/Diameter.

The basic engine model is a time-dependent simulation of in-cylinder processes, based upon the solution of equations for mass and energy. In this study, the combustion process was simulated by using the profile combustion model, which is an alternative to Wiebe combustion models. The model required to enter a complete profile of combustion, which is equivalent to the experimentally derived heat release rate profile based on the measured in-cylinder pressure. In addition, the start of combustion angle must be prescribed, as shown in Figure 5.24.

Figure 5.25 depicts the panel for heat transfer model. The heat transfer was calculated by a Woschni heat transfer model, which assumes a simple convective heat transfer from a confined volume surrounded on all sides by cylinder walls. The thermodynamic state of the in-cylinder gas was estimated considering the interactions among the enthalpy of fluxes in and out of the chamber, heat transfer, and piston work by using a two zone model. The mixture was divided into burnt and unburnt zones, as proposed by Saegusa et al. The simulation duration and the standard tolerance for convergence were set to 80 cycles and 0.1%, respectively. The operating case would run one additional cycle if the settings of convergence was reached before the end of simulation duration.

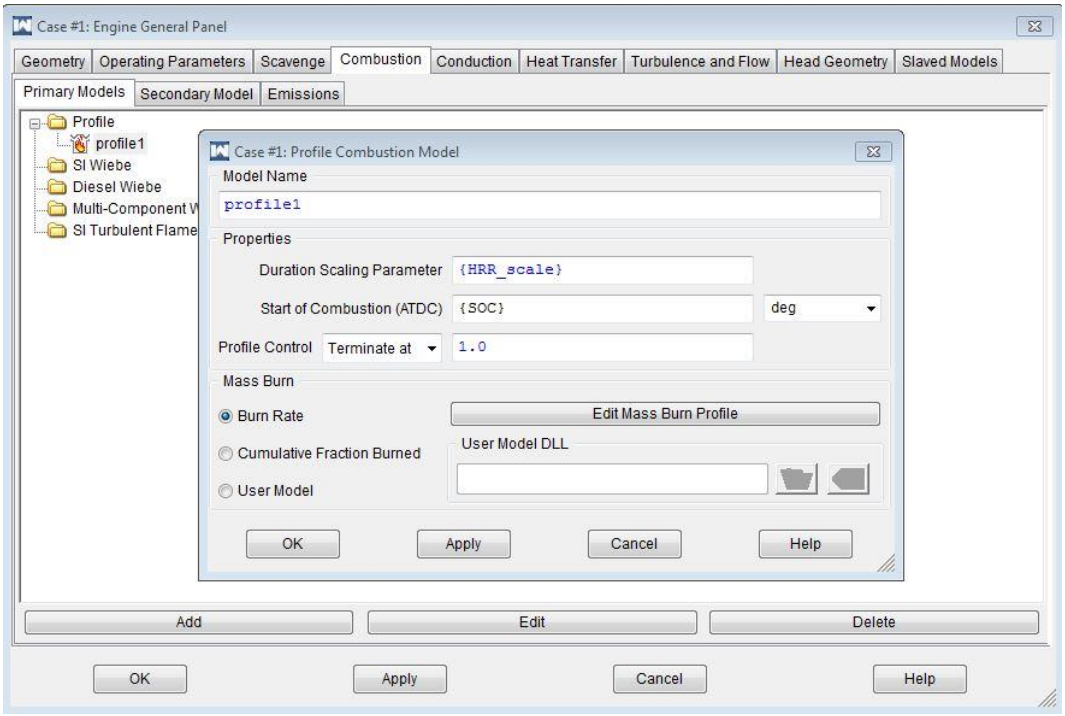

Figure 5.24: The Profile combustion model panel.

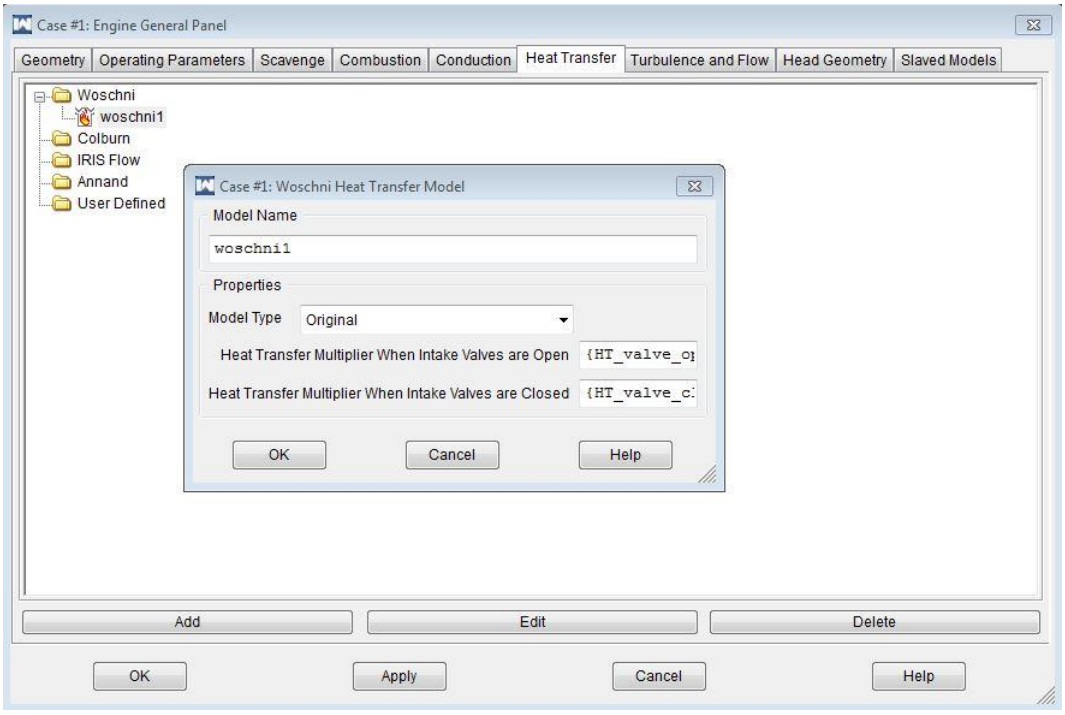

Figure 5.25: The Woschni heat transfer model panel.

5.4.3 Engine model validation

In all cases, the intake air mass flow rate, IMEP, in-cylinder pressure, intake and exhaust manifold pressures of all test points including “EGR-only”, “Miller cycle”, and “Miller cycle + EGR” strategies were calibrated against the experimental data in order to validate the

1D engine model. Figure 5.26 and 5.27 show that there is a good agreement between the simulated and experimental results of in-cylinder pressure as well as intake and exhaust pressures for the “Miller cycle + EGR” strategy at 12 bar IMEP.

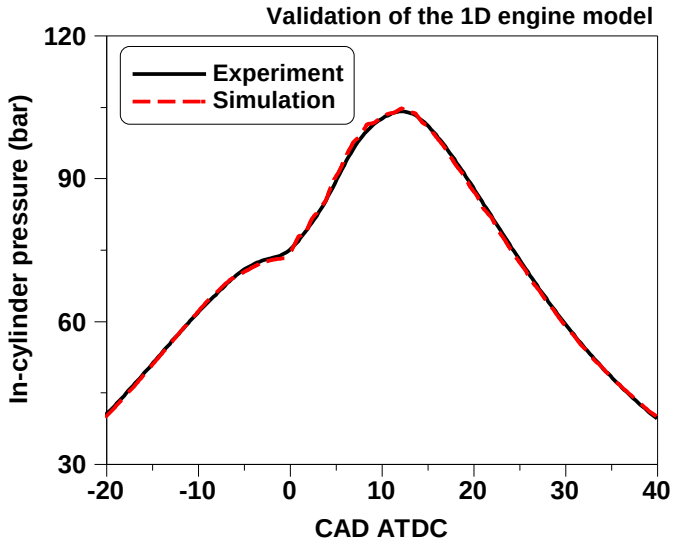

Figure 5.26: Experimental and simulated in-cylinder pressure for the “Miller cycle + EGR” strategy at 12 bar IMEP.

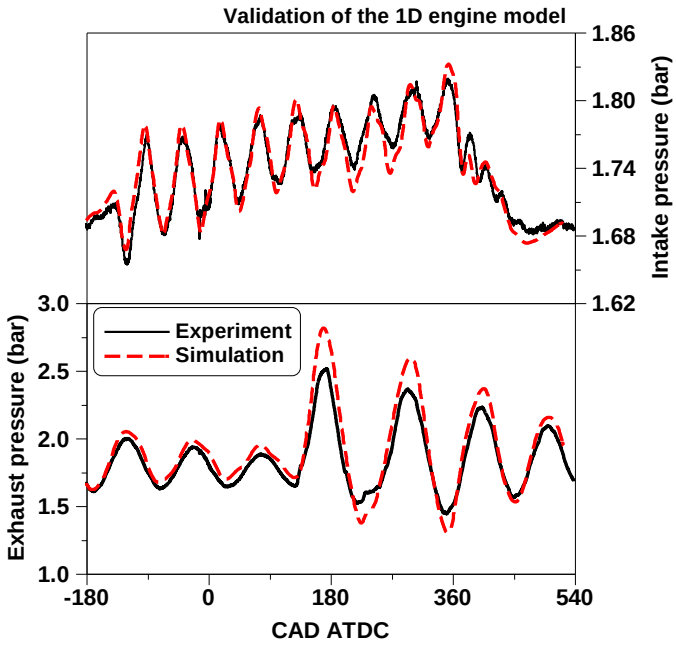

Figure 5.27: Experimental and simulated intake and exhaust manifold pressures for the “Miller cycle + EGR” strategy at 12 bar IMEP.

Figure 5.28 shows that the predictions of the intake air mass flow rate agrees well with experimentally acquired data at both engine loads of 6 bar and12 bar IMEP. Thus, the validated 1D engine model could be used to calculate T_m and T_b.

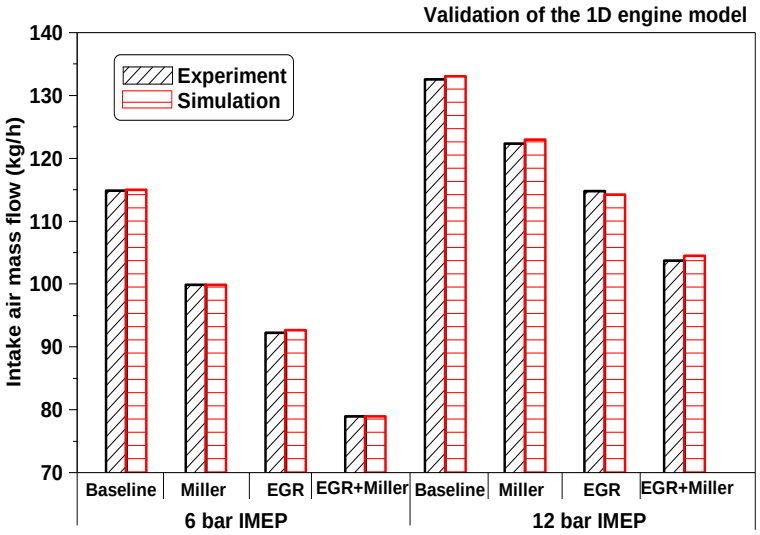

Figure 5.28: Validation of intake air mass flow rate at 6 and 12 bar IMEP.

5.4.4 Combustion characteristics

Figure 5.29 compares the measured in-cylinder averaged pressure and HRR for different strategies at 6 and 12 bar IMEP. Compared to the baseline case with an ECR of 16.8:1 and no EGR, the introduction of EGR led to longer ignition delay due to the dilution and thermal effects of the EGR, resulting in slightly lower peak in-cylinder pressure. It is noted that the delay of the IVC timing with a constant P_{int} yielded significantly lower in-cylinder pressures and slightly longer ignition delay due to the reduced ECR.

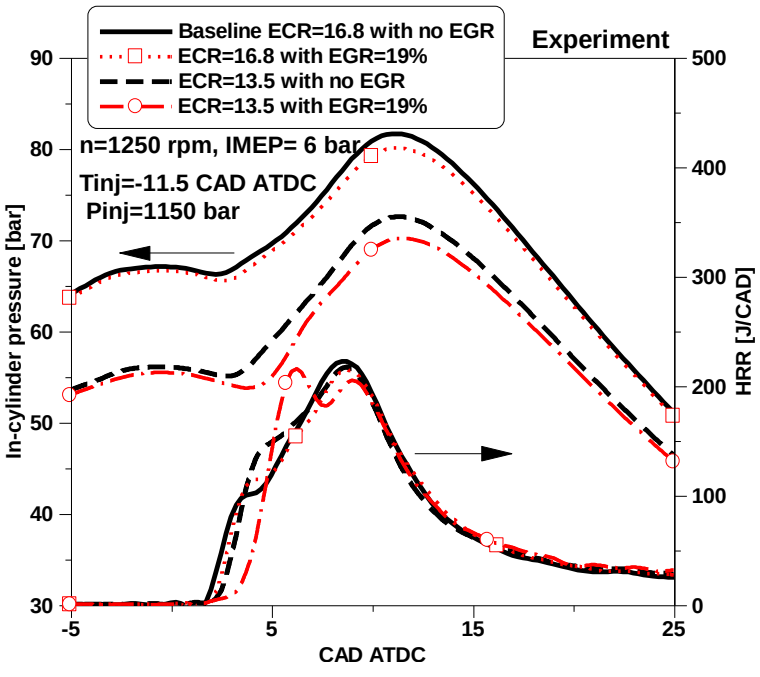

(a) 6 bar IMEP;

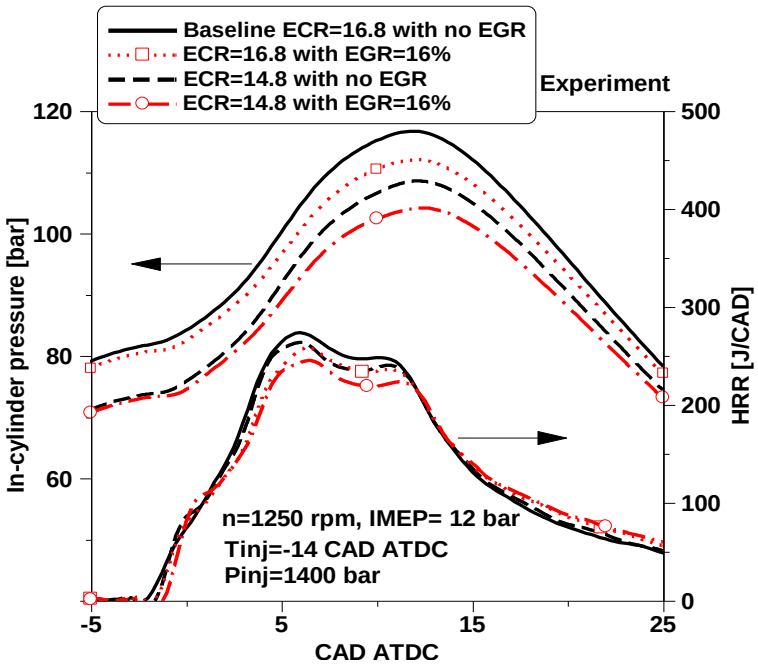

(b) 12 bar IMEP;

Figure 5.29: Experimental in-cylinder pressure and resulting HRR for different strategies.

Figure 5.30 compares the resulting T_m and T_b obtained from a 1D engine model. The use of EGR decreased the T_b significantly, which helped curb NOx formation. The T_b was slightly reduced by applying a late IVC timing due to the lower compression temperature. This shows that the introduction of EGR was much more effective in reducing the T_b than a Miller cycle strategy.

At 6 bar IMEP, the later IVC timing reduced the in-cylinder fresh charge and the total heat capacity, leading to a higher T_m. At the medium load of 12 bar, there was no significant difference between the T_m of the baseline and late IVC cases. This was likely a result of the lower impact of the LIVC timing on the in-cylinder mass trapped when compared to the effect of Miller cycle at a lower load of 6 bar IMEP.

For the combined strategy with both EGR and Miller cycle, the dilution and higher heat capacity introduced by EGR and the reduced compression ratio obtained by a LIVC timing increased the ignition delay, resulting in a higher degree of premixed combustion and two distinct heat release peaks, as depicted in Figure 5.29. Meanwhile, the T_m and T_b were reduced. These factors contributed to the reduction in both smoke and NOx emissions, as shown in the next subsection. However, Figure 5.30 indicates that the reduction of NOx emissions at various strategies was primary attributed to the lower local combustion temperatures (e.g. T_b).

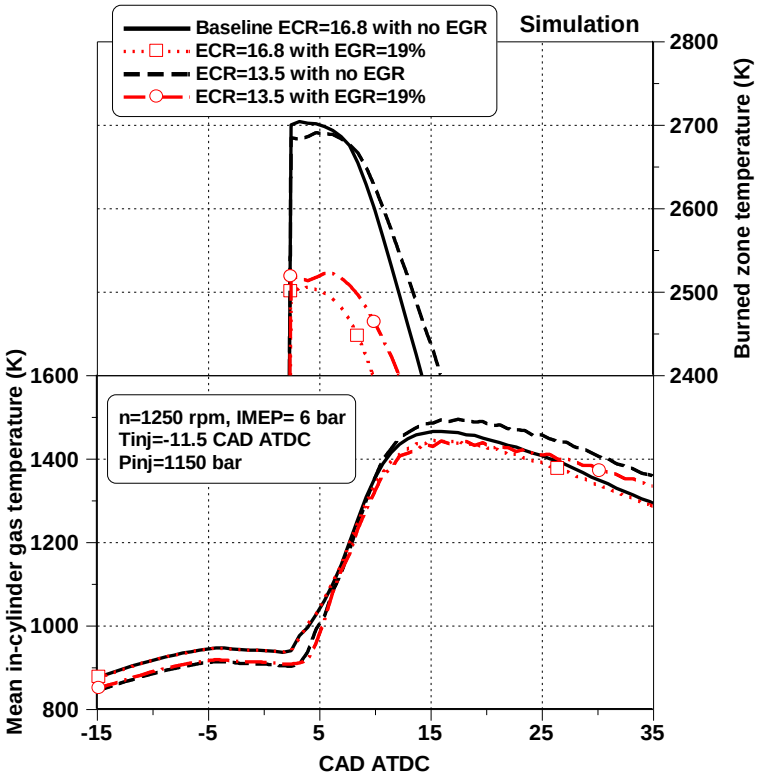

(a) 6 bar IMEP;

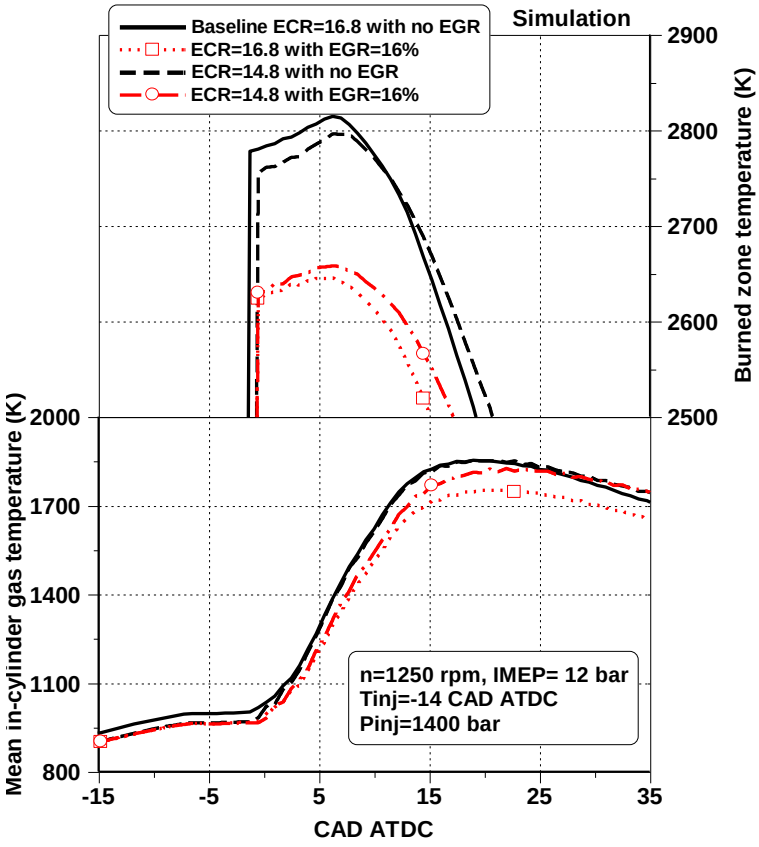

(b) 12 bar IMEP;

Figure 5.30: Simulated results of mean in-cylinder gas temperatures and burned zone temperatures for different strategies.

Figure 5.31 depicts the combustion duration as a function of the EGR rate and ECR. The use of EGR in the Miller cycle strategy led to longer CA10-CA90 due to a delayed combustion phasing and slower heat release rate of the mixing-control combustion. The combination of EGR and a LIVC timing produced the longest combustion durations, which would adversely affect the engine efficiency.

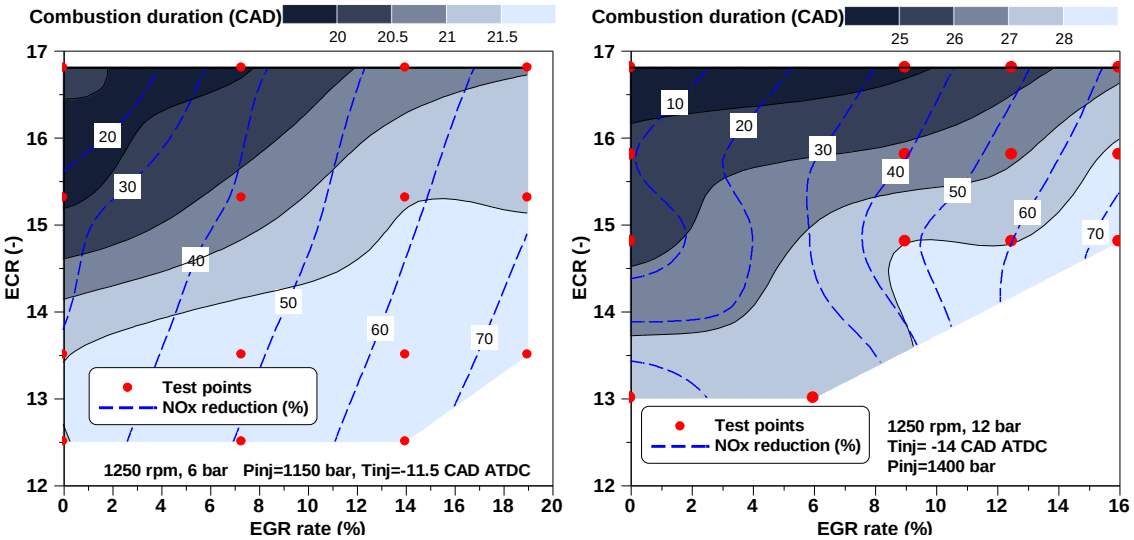

Figure 5.31: The effect of Miller cycle and EGR on combustion duration.

5.4.5 Engine performance and gaseous emissions

In addition to the burned zone gas temperature, the excess air ratio (lambda) is another dominant factor for the pollutant formation. Figure 5.32 shows the variation of lambda against EGR rate and ECR at 6 bar and 12 bar IMEP.

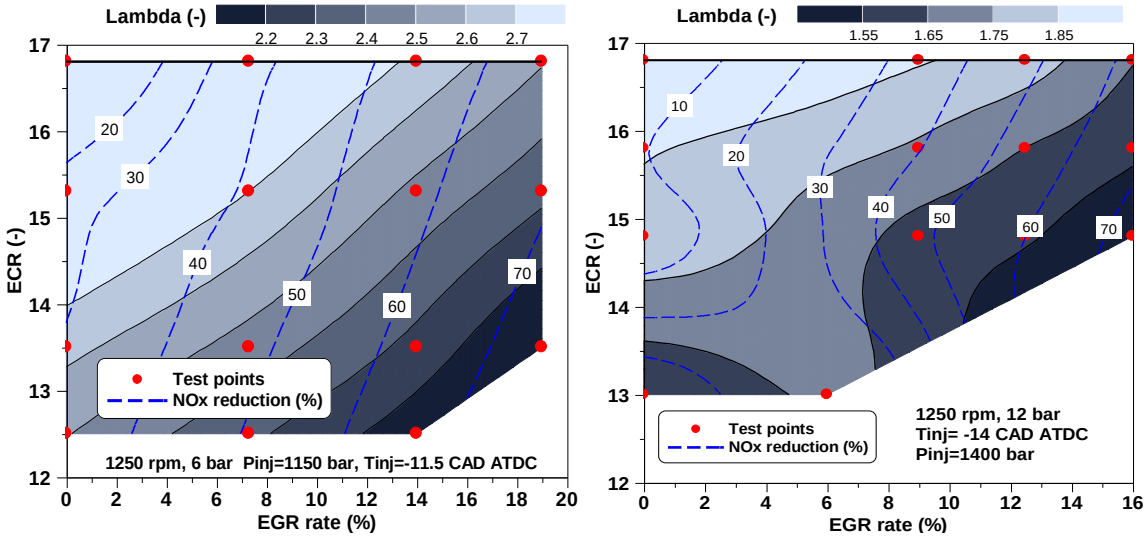

Figure 5.32: The effect of Miller cycle and EGR on lambda.

The lambda was gradually reduced with increased EGR rate and lowered ECRs due to the dilution effect of EGR and reduced in-cylinder mass trapped for the later IVC timings.

The EGR strategy maintained higher lambda than a Miller cycle strategy when controlling the NOx emissions at the same levels. The lowest lambda was achieved when increasing the EGR rate and delaying the IVC timing simultaneously.

The resulting lambda for different levels of EGR and ECR was different at the two loads investigated in this study. At a low load condition (see Figure 5.32 (a)), a reduction in NOx emissions of 70% could be achieved while maintaining lambda above 2, which was sufficiently high to avoid local fuel rich zones. Thus, the negative effect on combustion was relatively small. However, the lambda changed rapidly with the introduction of EGR and lower ECR at the medium load of 12 bar IMEP. Figure 5.32(b) shows that a 70% reduction in NOx emissions could only attained at the right-bottom corner, where the lambda was reduced to below 1.5. The fuel-rich combustion with a reduced lambda will likely deteriorate fuel consumption and smoke emissions.

As aforementioned the EGT has a huge effect on the ATS. Figure 5.33 depicts the EGT measurements at different EGR rates and ECRs. Figure 5.33(a) shows a significant change in EGT with a variation in EGR rate and ECR at 6 bar IMEP.

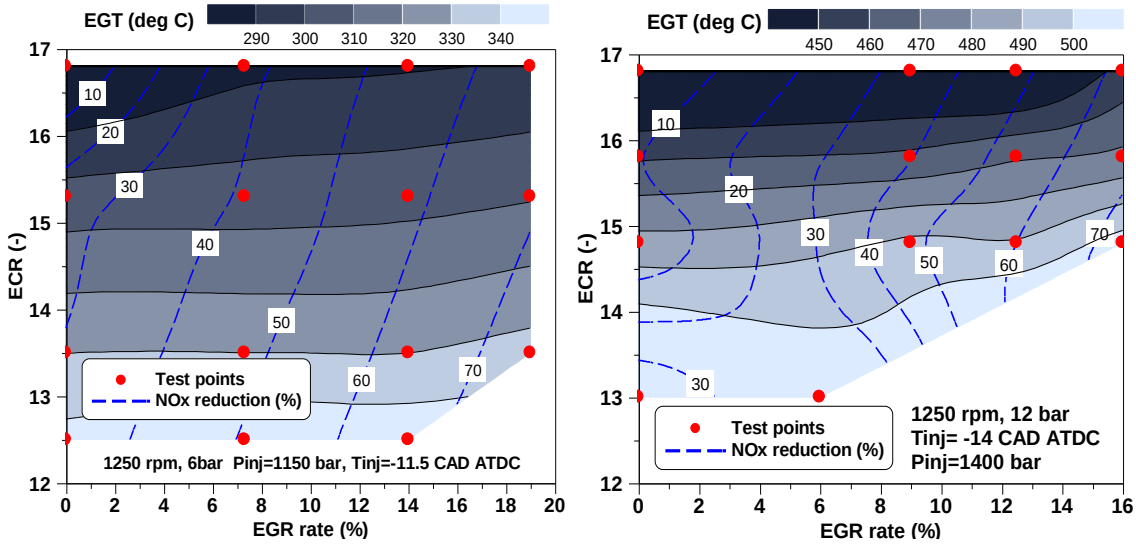

Figure 5.33: The effect of Miller cycle and EGR on exhaust gas temperature.

As the EGT is affected by the amount of charge in the cylinder, a decrease in intake mass flow allowed for higher EGTs. This was due to the reduced total in-cylinder gas heat capacity achieved when the IVC timing was delayed, leading to an increase in EGT up to 60°C. A similar relation between EGT and the lambda was presented by Garg et al. [189] using cylinder throttling via the IVC modulation at lower engine loads. In comparison, the use of EGR showed little impact on the EGT. This was possibly due to the replacement of the fresh air with recirculated exhaust gas, which increases the in-cylinder heat capacity.

At 12 bar IMEP, the effect of EGR on EGT presented a similar trend to that of the low load condition. However, any increase in EGT at the medium load is less significant to the SCR system as the EGT was sufficiently high for efficient NOx reduction.

Figure 5.34 shows the ISFC increased rapidly with reduced ECR at low load operation, while the effect of EGR on fuel consumption was relatively small. Factors such as combustion efficiency, heat transfer loss, combustion duration and pumping loss play important roles in the ISFC results.

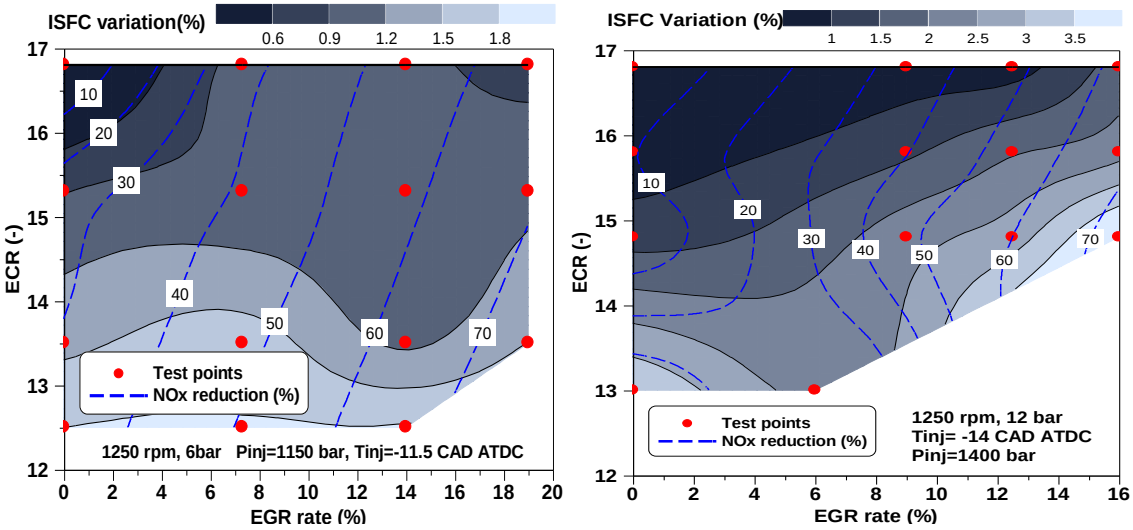

Figure 5.34: The effect of Miller cycle and EGR on ISFC.

At the low load, the Miller cycle strategy resulted in higher T_m during combustion and hence higher heat loss to the cylinder walls. In addition, the lower compression pressures and temperatures prior to combustion resulted in longer combustion duration as revealed in Figure 5.31. These two effects contributed to the higher fuel consumption for a Miller cycle-only strategy. In the case of the EGR strategy, the variation in ISFC was relatively lower at low load than that at medium load. This was a result of the combination of a higher lambda with lower in-cylinder gas temperatures (see Figure 5.30), which helped minimize heat transfer losses at a lower load. Additionally, a prolonged ignition delay allowed for a higher degree of premixed combustion, which contributed to the improvement in fuel efficiency. As the pressure difference between intake and exhaust manifold was kept constant throughout the experiments, the influence of pumping loss could be negligible in this study.

At 12 bar IMEP, the introduction of EGR and the use of Miller cycle significantly reduced the lambda and slowed down the combustion rate, deteriorating the combustion efficiency. Nevertheless, more than 70% of NOx emission reduction was achieved at 6 and 12 bar

IMEP with the expense of around 1.2% and 2.5% fuel efficiency penalty respectively when compared to baseline condition.

Figure 5.35, 5.36 and 5.37 depict the measured engine-out emissions of NOx, soot, unburned HC, and CO for various EGR rates and ECRs. The plots show the results in net indicated specific values. The use of EGR effectively reduced the NOx formation because of the lower combustion temperatures and in-cylinder oxygen concentration. A Miller cycle strategy produced higher T_m than the baseline at a lower load of 6 bar IMEP, as shown in Figure 5.30. This happened because Miller cycle was less effective in reducing the T_b than the EGR-only strategy, leading to lower capability of NOx abatement.

The smoke emissions demonstrated a different trend from that of NOx emissions when varying the EGR rate and ECR. Figure 5.35 reveals that smoke emissions were less affected by the ECR at 6bar IMEP, although the lambda changed significantly. One of the reasons for this phenomenon is the resulting longer ignition delay owing to the decreased compression pressure and temperature. The relatively more homogeneous mixture helped reduce the formation of soot. Another reason is the increased mean combustion temperatures, which likely improved the oxidation of smoke during diffusion combustion process. This was associated with a sufficiently lean combustion combined with a high concentration of oxygen.

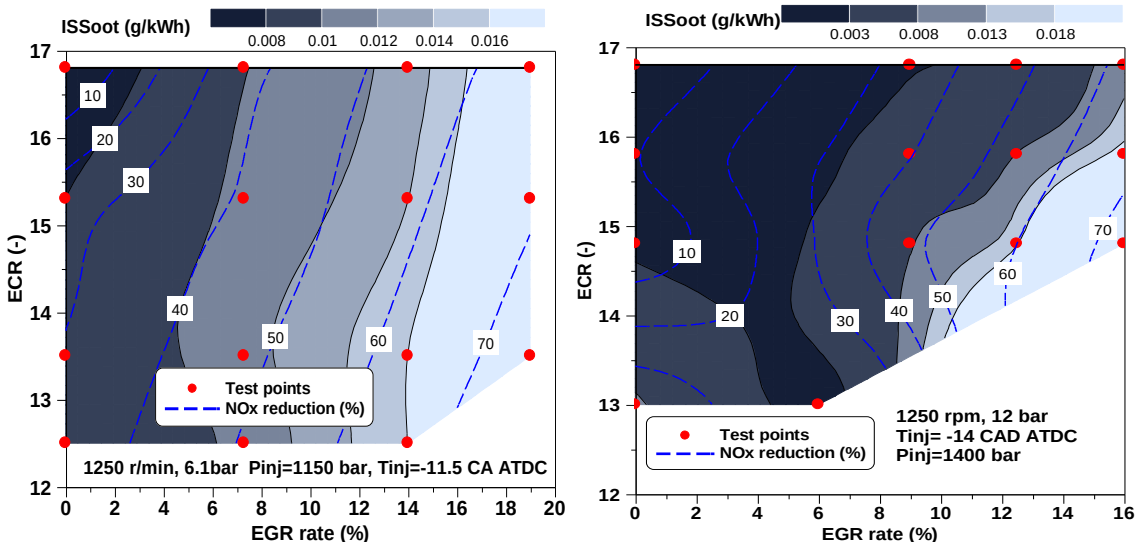

Figure 5.35: The effect of Miller cycle and EGR on soot emissions.

In contrast to a low load operation with Miller cycle, a significant increase in soot emissions was obtained as the IVC timing was delayed at the medium load of 12 bar. This was the result of the lower lambda at this condition. Finally, the soot emissions of two engine loads showed high sensitivities to the use of EGR, in particular when lambda was less than 1.5.

Figure 5.36 shows the CO emissions at low and medium loads. The trends of ISCO for various EGR rates and ECRs are similar to those of soot emissions. The in-cylinder oxygen availability and combustion temperatures played the dominant roles. The use of EGR increased the emissions of CO due to the lower combustion temperatures and oxygen concentration. The variation in ISCO was small with Miller cycle at 6 bar IMEP due to sufficient oxygen concentration and higher combustion temperatures compared to an EGR-only strategy. However, CO emissions increased with delayed IVC timing at 12 bar IMEP owing to the richer combustion.

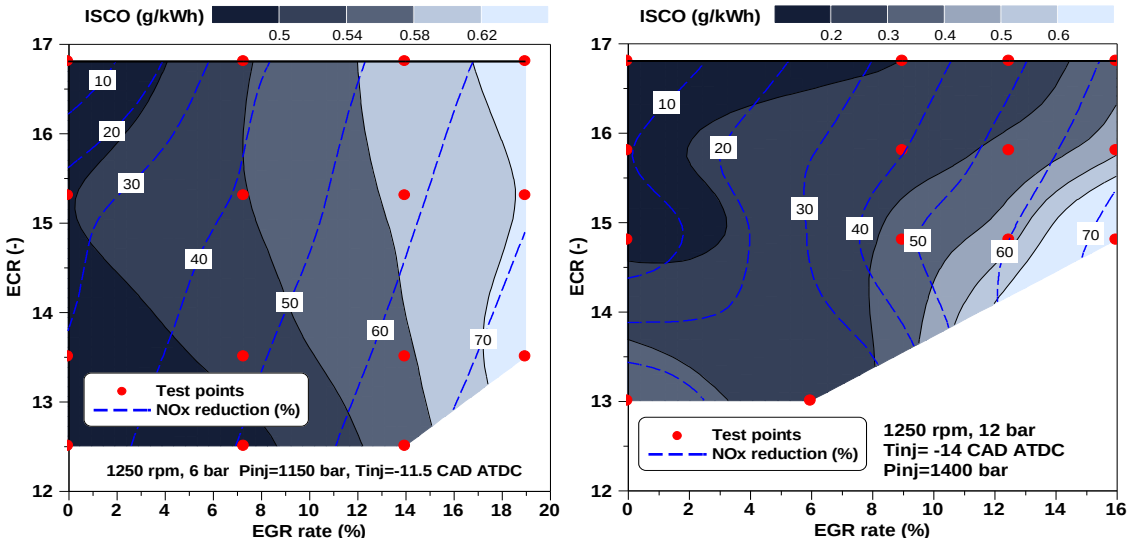

Figure 5.36: The effect of Miller cycle and EGR on CO emissions.

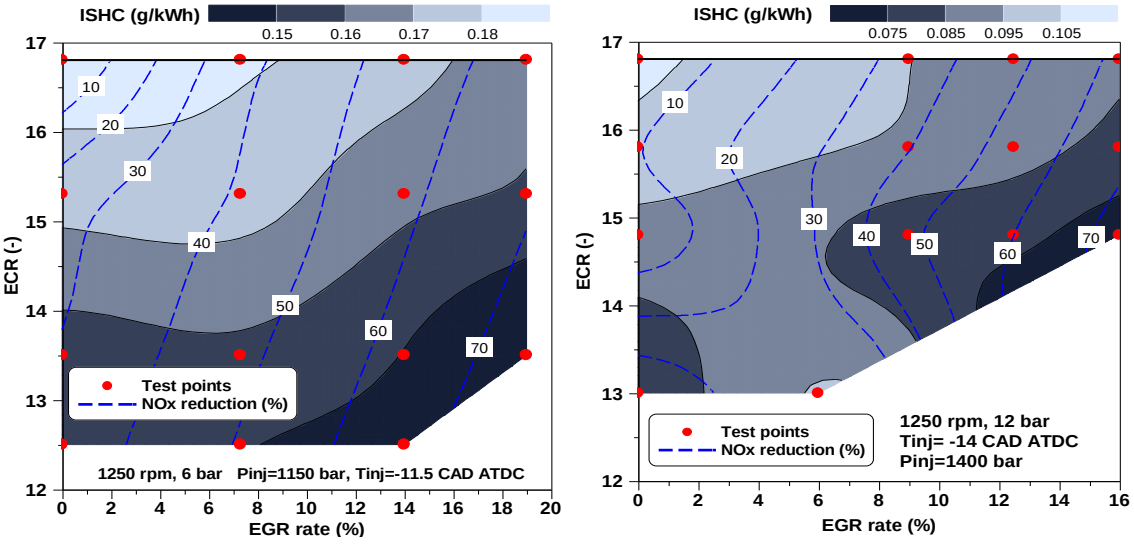

Figure 5.37: The effect of Miller cycle and EGR on HC emissions.

Both EGR and Miller cycle strategies were able to reduce unburned HC emissions, as shown in Figure 5.37. This differs from the majority of the literature, which suggests an

increase in the levels of unburned HC [145,210,211]. The longer ignition delays and higher EGT were likely the major reasons for the decrease in ISHC, as demonstrated by Verschaeren et al. [186] when applying EGR and Miller cycle on a medium speed heavy-duty diesel engine. A later combustion phasing and longer heat release rate led to higher EGTs, which possibly increased the oxidation rates of HC over the expansion stroke.

Figure 5.38 shows the trade-off between ISFC, ISsoot, and ISNOx emissions at low and medium loads. Under the low load operation, an improvement in the ISNOx and ISsoot trade-off was achieved at the expense of a small fuel efficiency penalty when increasing the levels of EGR and with different ECRs. At the 12 bar IMEP, the ISFC was rapidly increased for a Miller cycle strategy as well as when adding more EGR. Since a higher diesel injection pressure could improve the fuel-air mixing process and shorten the combustion duration, an additional experiment was carried out with an increased injection pressure of 1700 bar, as highlighted in Figure 5.38. It can be seen that the trade-off between ISFC, ISNOx, and ISsoot was notably improved when combining a higher injection pressure with EGR and an ECR of 14.8:1. Therefore, the NOx reduction benefit introduced by EGR and Miller cycle can be extended to higher loads with acceptable fuel efficiency and smoke penalties by employing a higher rail pressure. This is supported by the findings of Sjöblom et al. [212] when investigating the combined effects of late IVC timing and EGR at different injection pressures.

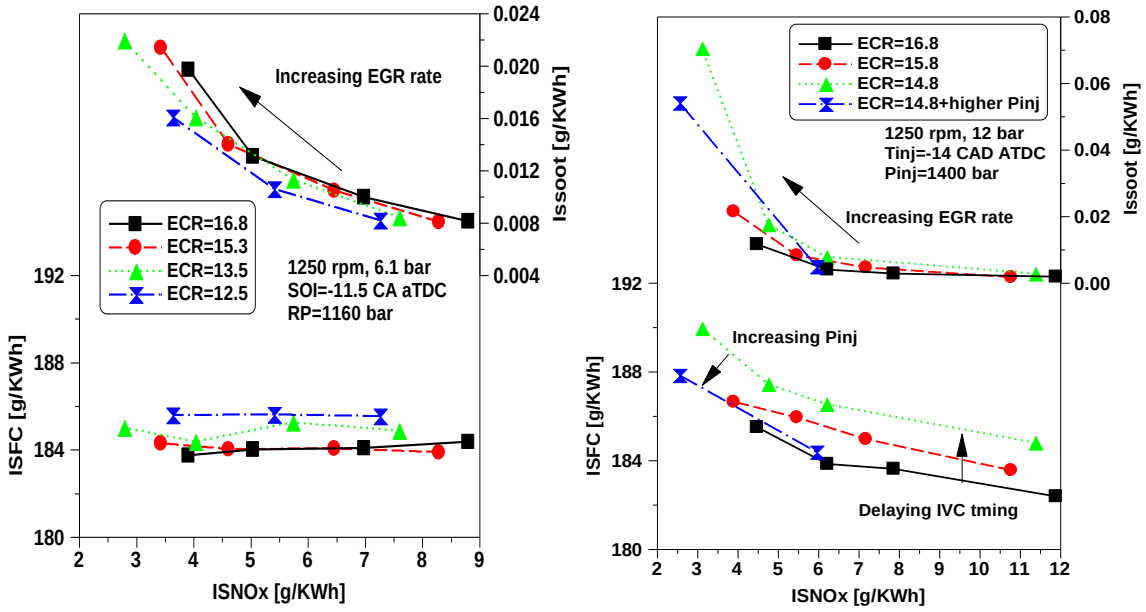

Figure 5.38: The effect of Miller cycle and EGR on the trade-off between ISFC, ISNOx, and ISsoot.

5.4.6 Analysis of the potential benefits of the combined use of Miller Cycle and EGR

This subsection explores the potential of EGR and Miller cycle to reduce engine-out NOx emissions with minimum fuel efficiency penalty. Figure 5.39 shows the "EGR + Miller cycle" and "EGR-only" strategies were compared to the baseline when achieving 64% and 48% NOx reduction at low and medium loads, respectively. The variations in engine performance and emissions were evaluated with constant injection timings and injection pressures.

At 6 bar IMEP, soot and CO emissions increased significantly when achieving 64% lower NOx emissions. Unburned HC emissions were slightly reduced, with the best results for an "EGR + Miller" strategy. The ISFC increased by 0.8% with "EGR-only" and by 1.2% when delaying the IVC with EGR. Lower heat transfer losses partially compensated for a reduction in fuel efficiency caused by the loss of intake fresh air. Overall, the application of EGR with Miller cycle produced lower emissions and higher EGT than the "EGR-only" strategy at the lower engine load. The relatively small fuel efficiency penalty compared to an "EGR-only" strategy at the same NOx reduction level is likely to be offset by a higher SCR conversion efficiency.

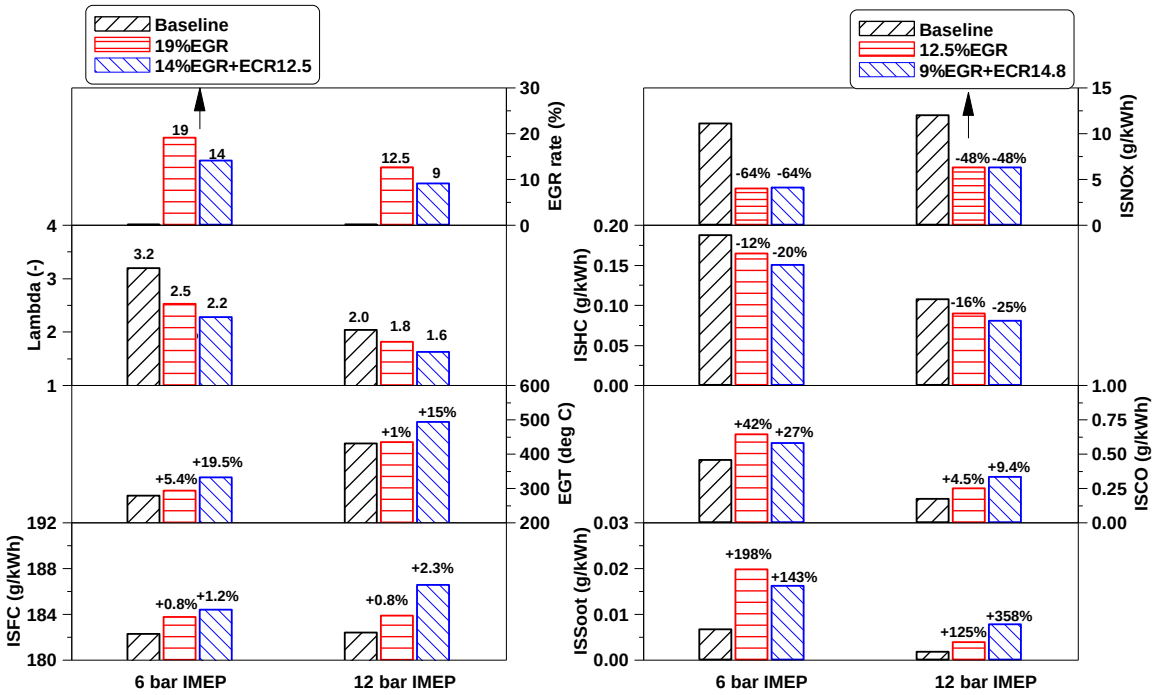

Figure 5.39: Comparison between experimental results for "EGR-only" and "EGR + Miller" strategies.

Similar trends in ISFC and emissions were observed for a constant NOx reduction of 48% at 12 bar IMEP. However, the use of EGR combined with Miller cycle further increased the fuel efficiency penalty as well as soot and CO emissions compared to an “EGR-only” strategy. This was a result of the insufficient in-cylinder mass trapped which led to a significant reduction in lambda. The levels of ISsoot and ISCO could be improved with a higher rail pressure. Nevertheless, the EGT increased by 15% when employing an “EGR + Miller cycle” strategy.

Overall, the combination of Miller cycle with external cooled EGR shows a greater potential to reduce NOx emissions while achieving higher EGTs, in particular at low engine load conditions.

5.5 Exploring the potential of Miller cycle operation with EGR and post injection at low load

The previous section has showed that the use of Miller cycle with external EGR were effective for the EGT and NOx emissions control at low load condition. However, the lower in-cylinder gas temperatures in the burned zone deteriorated the combustion process and slowed down the oxidation of soot and CO emissions, significantly increased the levels of engine-out soot and CO emissions. These results can limit the potential of the “Miller cycle + EGR” strategy for efficient and clean low load engine operation. Although advanced injection timing, higher injection pressure, and higher boost pressure can improve upon this drawback, the EGT can be reduced and the NOx-soot and NOx-CO trade-offs remain. In addition, these strategies may impair the EOC when considering the total fluid consumption including diesel fuel and the estimated urea consumption in the SCR system.

Alternatively, the use of post injections has been demonstrated as an effective means of mitigating soot and CO emissions [213,214]. Therefore, the post injection strategy was investigated in an attempt to improve upon the performance and emissions of the “Miller cycle + EGR” strategy.

5.5.1 Test methodology

The experimental work was carried out at a speed of 1250 r/min and a low engine load of 6 bar IMEP. Table 5.5 depicts the main engine operating conditions for the different combustion control strategies investigated. The ECR was decreased from 16.8 to 12.5 for the Miller cycle cases when delaying the IVC from -174 to -105 CAD ATDC. In the case of combined use Miller cycle and EGR, the in-cylinder air flow mass can be decreased

noticeably, resulting in poor combustion instability and excessive smoke. Therefore, a moderate EGR rate of 15% was employed when the EGR was combined with the Miller cycle. During the experiments, a small pilot injection of 3 mm^3 with a constant dwell time of 1 ms prior to the main injection timing was employed in order to keep the maximum PRR below 20 bar/CAD. Stable engine operation was determined by controlling the COV_IMEP below 3%.

Table 5.5: Engine operating conditions for various IVCs with post injection strategy.

Parameter	Value				
Speed	1250 rpm				
Load	6 bar IMEP				
Injection pressure	1160 bar				
Intake temperature	303 ± 1K				
Testing modes	Baseline	Miller cycle	EGR-only	Miller cycle + EGR	Miller cycle + EGR + Post injection
Intake pressure	1.44 bar	1.44, 1.64, and 1.84 bar	1.44 bar	1.44 bar	1.44 bar
Exhaust pressure	0.10 bar higher than the intake pressure				
IVC timing	-174 CAD ATDC	-95, -105 CAD ATDC	-174 CAD ATDC	-105 CAD ATDC	-120 and -105 CAD ATDC
ECR	16.8	13.5 and 12.5	16.8	13.5	14.5 and 13.5
EGR	0%	0%	15%	15%	15%
Post fuel injection	No	No	No	No	Yes

5.5.2 The optimization of the post injection

Before analysing the potential of the “Miller cycle + EGR + post injection” strategy, the post injection timing and fuel quantity were optimised in order to achieve high efficiency and low engine-out emissions. The optimization was carried out at three IVC timings, including the baseline at -178 CAD ATDC and Miller cycle cases at -120 and -105 CAD ATDC. The main injection timing was held constant at -4 CAD ATDC.

Firstly, the post injection timing was varied between 15 and 24 CAD ATDC while the quantity was held constant at 9 mm^3. Figure 5.40 shows that the soot emissions were sensitive to the post injection timing, decreasing initially and increasing significantly with the most retarded post injection timings. This was likely attributed to the trade-off effect of

post injected fuel on soot formation and oxidation rates in the late combustion phase [213]. Meanwhile, changes in the post injection timing resulted in little impact on NOx emissions. Overall, the post injection timing of 18 CAD ATDC achieved the lowest soot emissions with relatively small decrease in NIE, and thus was selected for the post injection quantity sweep.

Figure 5.41 depicts the optimization of the post injection quantity while maintaining the post injection timing constant at 18 CAD ATDC. An increase in the post injection quantity reduced soot and NOx emissions at the expense of a reduction in the NIE, regardless of the IVC timing. A post injection quantity of 12 mm^3 achieved the optimum trade-off between engine performance and emissions. Therefore, the next subsection explores the potential of the "Miller cycle + EGR + post injection" strategy using a post injection of 12 mm^3 at 18 CAD ATDC.

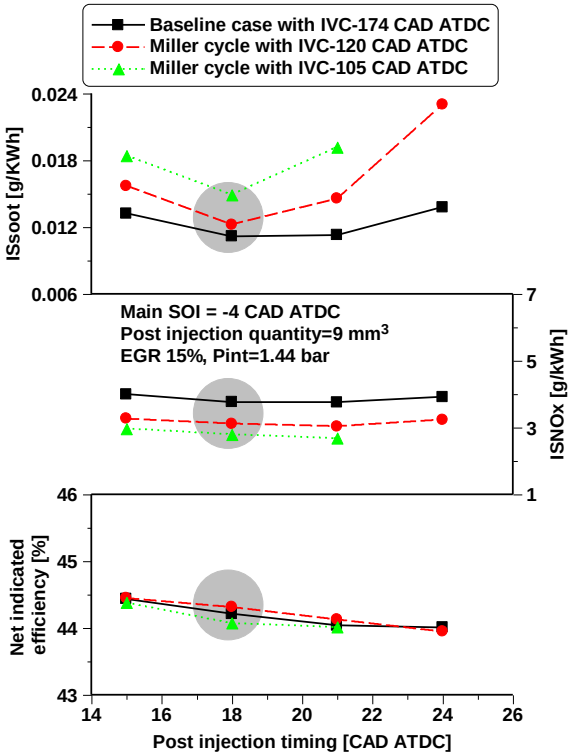

Figure 5.40: Optimization of the post injection timing.

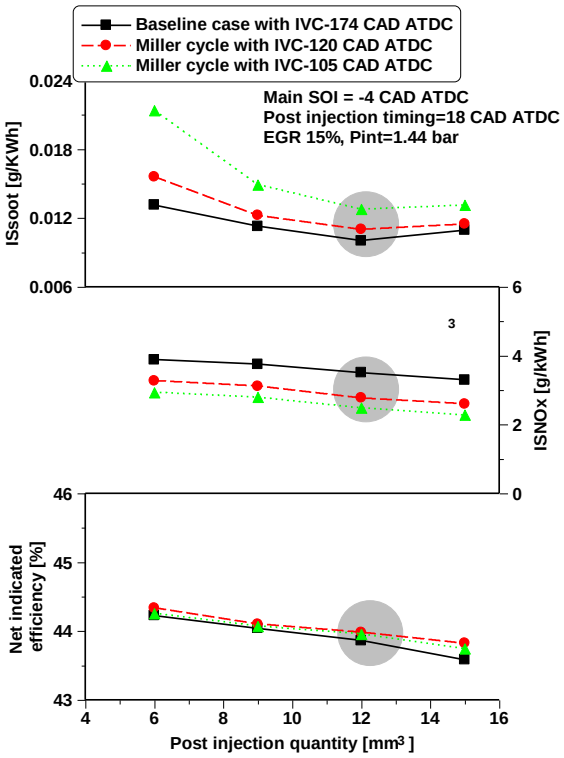

Figure 5.41: Optimization of the post injection quantity.

5.5.3 Combustion characteristics

Figure 5.42 depicts the in-cylinder pressure, HRR, and injector signal for the baseline and Miller cycle cases with and without the optimized post injection strategy. The use of post injection yielded a second and late peak HRR, which represented the combustion of the post injected fuel. The decreased fuel mass in the main injection consequently, lowered the first peak HRR and thus the peak in-cylinder pressure when compared to the baseline cases. Figure 5.43 shows that the post injection strategy also decreased the peak mean in-cylinder gas temperature but increased the average temperature during the late stages of the combustion process. Additionally, it can be seen that the relatively richer mixture of the Miller cycle cases (e.g. lower lambda at a constant P_{int}) shortened the ignition delay of the post injected fuel in comparison with that of the baseline case with a post injection.

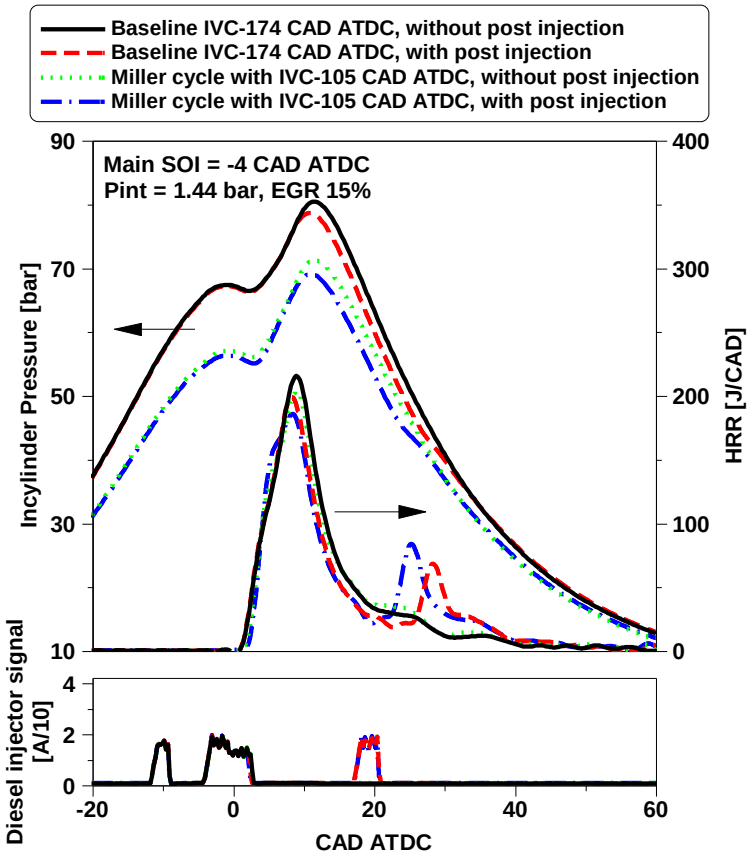

Figure 5.42: In-cylinder pressure, HRR, and diesel injector signal for the baseline and Miller cycle cases with and without post injection.

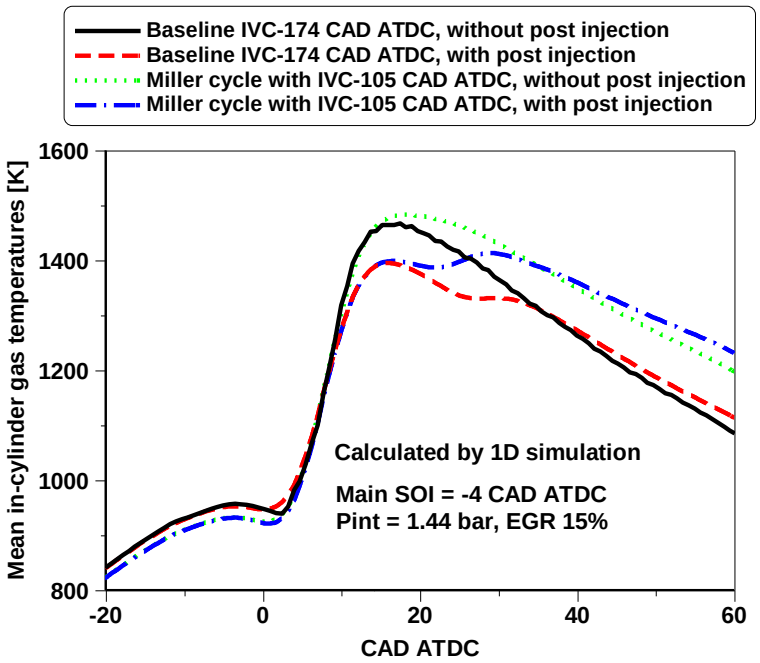

Figure 5.43: Calculated mean in-cylinder gas temperatures for the baseline and Miller cycle cases with and without post injection.

Figure 5.44 compares the resulting heat release characteristics for different IVC timings with and without post injection. The addition of the post injection delayed the CA50 and

CA90 as more fuel was burned during a relatively colder and later combustion phase. As a result, the period of CA50-CA90 was longer for the cases with post injection. These effects contributed to an increase in the combustion duration by up to 5 CAD when compared to the cases without post injection.

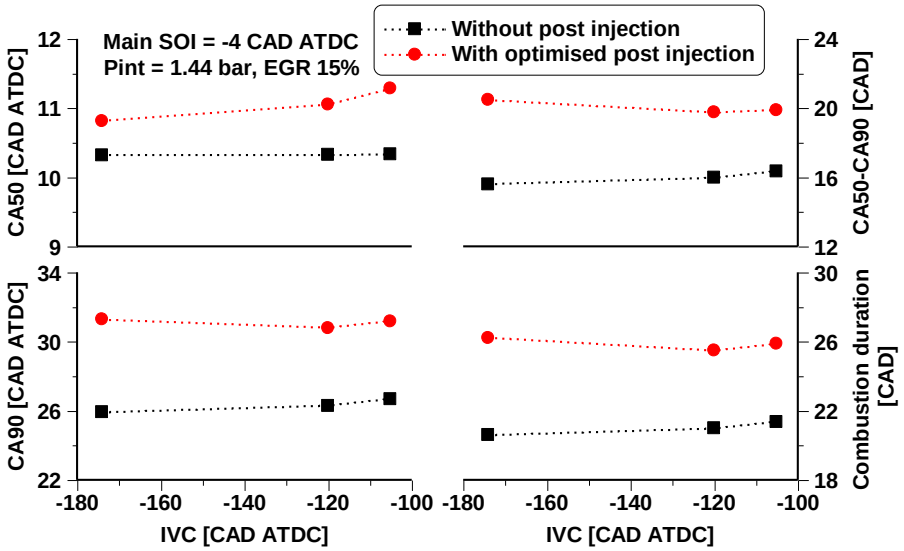

Figure 5.44: The effect of post injection on combustion characteristics.

5.5.4 Engine performance and gaseous emissions

Figure 5.45 shows the lambda was slightly reduced and EGT was increased with the addition of post injection. This was because part of diesel fuel was consumed later in the cycle and consequently a decrease in NIE. Nevertheless, the difference of NIE penalty between the cases with and without post injection was reduced with delayed IVC timing, decreasing from 1.6% at the baseline IVC to below 1% in the Miller cycle with IVC-105 CAD ATDC. This was probably due to the relatively faster heat release of the post injected fuel in the Miller cycle cases.

The emission results showed that soot emissions were significantly reduced by the post injection. The primary reasons for this improvement are likely the shorter injection durations, the enhanced fuel-air mixing, and the increased late combustion temperature achieved with the multiple injections [214]. Meanwhile, the use of a post injection led to a reduction in NOx emissions of 20% on average. This was due to the lower lambda (e.g. less oxygen availability) and most likely the lower burned zone gas temperatures achieved with this injection strategy. The levels of CO showed a similar trend to the soot emissions, and were also reduced with the post injection strategy attributed to the increased late combustion temperatures.

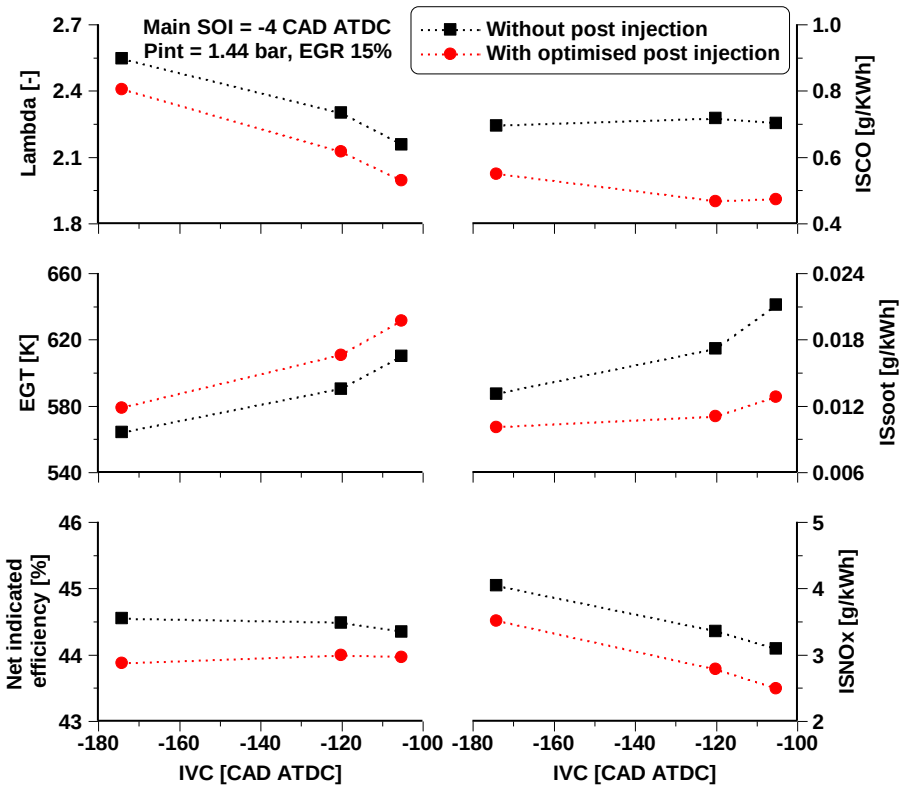

Figure 5.45: The effect of post injection on engine performance and exhaust emissions.

5.5.5 Cost-benefit and overall analysis

In this subsection, the total fluid consumption was calculated by summing up the measured diesel flow rate and aqueous urea solution consumption in an SCR system, as described in subsection 4.5.3, Chapter 4. This allowed for a cost-benefit and overall emissions analysis of the different combustion control strategies.

Figure 5.46 provides an overall assessment of the potential of Miller cycle with EGR and post injection to improve upon the EGT, exhaust emissions, and EOC of a diesel engine operating at 6 bar IMEP. The results of various advanced combustion control strategies are compared to the baseline case using a constant main injection timing of -4 CAD ATDC and P_{int} of 1.44 bar.

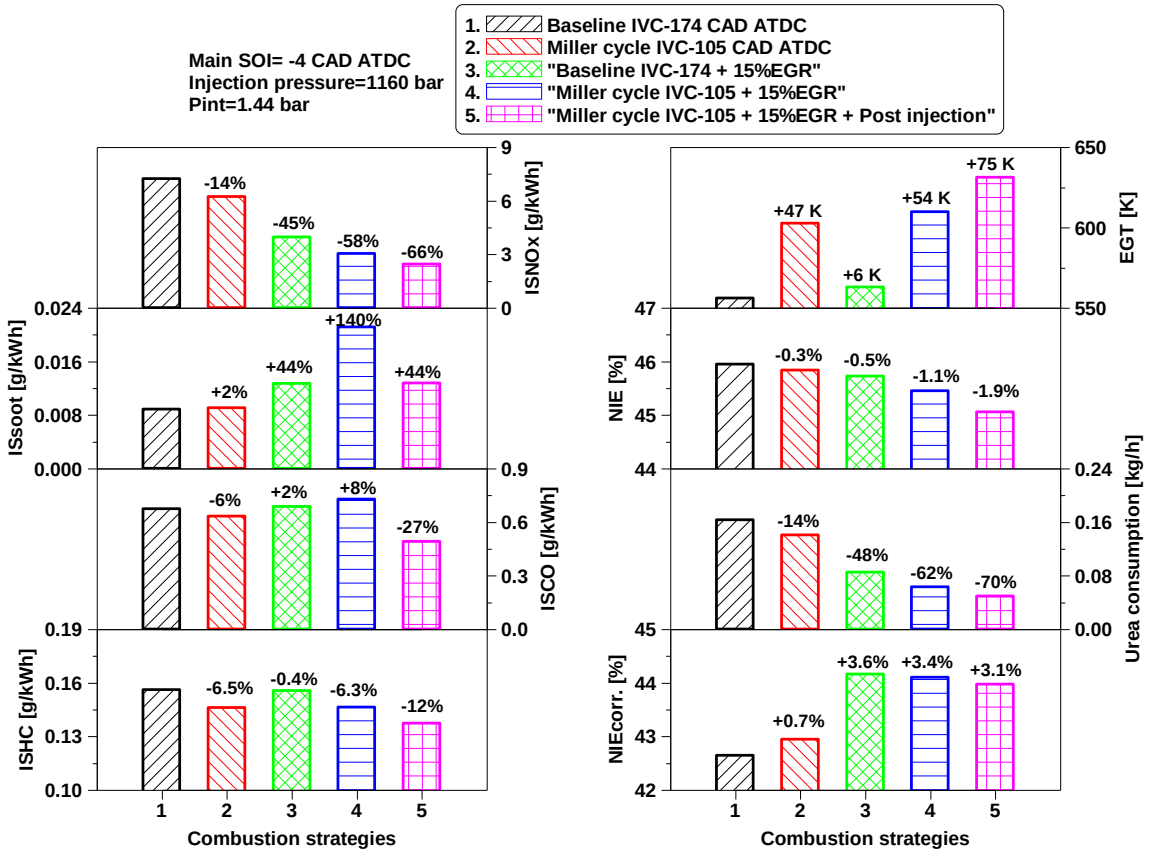

Figure 5.46: Cost-benefit and overall emissions for various combustion control strategies at 6 bar IMEP.

Compared to the baseline case, a “Miller cycle-only” strategy decreased NOx emissions by 14% accompanied with an increase of 47 K in EGT. This was achieved at the expense of a reduction of 0.3% in NIE. The EGR-only strategy achieved a reduction in NOx emissions by 45% but had insignificant impact on the EGT. The combination of a Miller cycle strategy with EGR achieved higher improvement in NOx emissions and EGT, decreasing NOx emissions by 58% and increasing EGT by 54 K in comparison with the baseline case. This significant improvement was obtained with a reduction of 1.1% in NIE. However, the “Miller cycle + EGR” strategy increased soot emissions significantly from 0.009 g/kWh in the baseline case to 0.022 g/kWh and also increased CO emissions by 8%. The introduction of a post injection helped control soot and CO emissions, allowed for further reductions in NOx emissions and increased the EGT by 75 K. It can be also seen that all advanced combustion control strategies achieved relatively lower levels of HC emissions than that of the baseline case. As discussed in subsection 5.5.4, the later and longer combustion process of the “Miller cycle + EGR + post injection” strategy adversely affected the NIE, decreasing it by 1.9% when compared with the baseline engine operation.

Figure 5.46 also revealed that the advanced combustion control strategies helped decrease the urea consumption via lower engine-out NOx emissions. This minimised the total fluid consumption and therefore increased the $NIE_{corr.}$, despite a lower NIE. The highest improvement in $NIE_{corr.}$ of 3.6% was achieved by the EGR-only strategy as a result of the high NOx reduction capability combined with a relatively lower NIE penalty. Alternatively, the “Miller cycle + EGR + post injection” strategy increased the $NIE_{corr.}$ by 3.1% while improving upon EGT as well as soot and CO emissions. Therefore, the combined strategy of “Miller cycle + EGR + post injection” was identified as the most effective means to achieve low EOC and enable exhaust emissions and EGT control.

5.6 Exploring alternative combustion control strategies for light load EGT management

The employment of ATS in modern diesel engines has become indispensable in order to meet the stringent emissions regulations. However, a minimum EGT of approximately 200°C must be reached to initiate the emissions control operations. Light load engine operations usually result in relatively low EGT, which lead to reduced or no exhaust emissions conversion. In this context, this study investigated the use of different combustion control strategies to explore the trade-off between EGT, fuel efficiency, and exhaust emissions at a light load of 2.2 bar IMEP. Strategies including the LIVC strategy, intake throttling, late injection timing, lower injection pressure, as well as iEGR and eEGR were investigated.

The experimental results were divided into three subsections. In the first section, the impact of different control strategies to increase EGT are presented and analysed. This is followed by an analysis and comparison of the most effective strategies attained from the first section. Finally, the combined LIVC with iEGR strategy is investigated for its potential to overcome the negative effect of LIVC strategy on CO and HC emissions.

5.6.1 Test methodology

The study was carried out at a light load of 2.2 bar IMEP, which represents one of typical low EGT operating conditions of a HD drive cycle and is located within the area of the WHSC test cycle, as shown in Figure 5.47. Table 5.6 summaries the engine operating conditions and the matrix of test cases for all strategies.

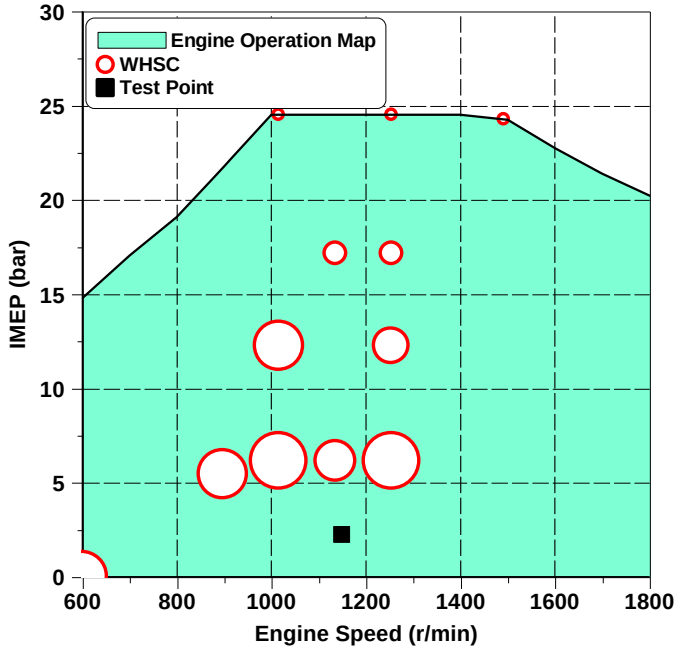

Figure 5.47: Test point and WHSC operation conditions.

Table 5.6: Main operation conditions of various control strategies.

Testing modes	Case number	Speed r/min	Load bar	SOI CAD ATDC	P_{inj} bar	eEGR %	P_{int} bar	P_{exh} bar	2IVC	IVC CAD ATDC	ECR
Baseline	1	1150	2.2	-5.8	515	0	1.15	1.20	off	-178	16.8
LIVC	2			-5.8	515	0	1.15	1.20	off	**-136**	15.3
	3			-5.8	515	0	1.15	1.20	off	**-118**	13.5
	4			-5.8	515	0	1.15	1.20	off	**-107**	12.3
	5			-5.8	515	0	1.15	1.20	off	**-100**	11.4
Intake throttling	6			-5.8	515	0	**1.08**	1.20	off	-172	16.8
	7			-5.8	515	0	**1.03**	1.20	off	-172	16.8
	8			-5.8	515	0	**0.98**	1.20	off	-172	16.8
iEGR	9			-5.8	515	0	1.15	1.20	**on**	-172	16.8
	10			-5.8	515	0	1.15	**1.27**	**on**	-172	16.8
	11			-5.8	515	0	1.15	**1.33**	**on**	-172	16.8
	12			-5.8	515	0	1.15	**1.42**	**on**	-172	16.8
Late SOI	13			**-2**	515	0	1.15	1.20	off	-178	16.8
	14			**1**	515	0	1.15	1.20	off	-178	16.8
	15			**2**	515	0	1.15	1.20	off	-178	16.8
Low P_{inj}	16			-5.8	**360**	0	1.15	1.20	off	-178	16.8
	17			-5.8	**300**	0	1.15	1.20	off	-178	16.8
eEGR	18			-5.8	515	**16**	1.15	1.20	off	-178	16.8
	19			-5.8	515	**31**	1.15	1.20	off	-178	16.8

During the test, the coolant and oil temperatures were kept within at 80 ± 2°C and oil pressure was maintained within 4.0 ± 0.1 bar. The average PRR and COV_IMEP were limited to below 20 bar/CAD and 3%, respectively. The VVA system enables a second

opening event of intake valve (e.g. 2IVO) during the exhaust stroke to trap residual gas. The maximum lift of 2IVO event was 2 mm. Figure 5.48 shows the intake and exhaust valve profiles for the baseline as well as the LIVC and 2IVO events.

In addition, the mean in-cylinder gas temperatures were calculated using the ideal gas state equation

$$PV = mRT_m \tag{5.1}$$

where P and V are the in-cylinder pressure and volume, respectively; m is the mass of charge and R is the specific gas constant.

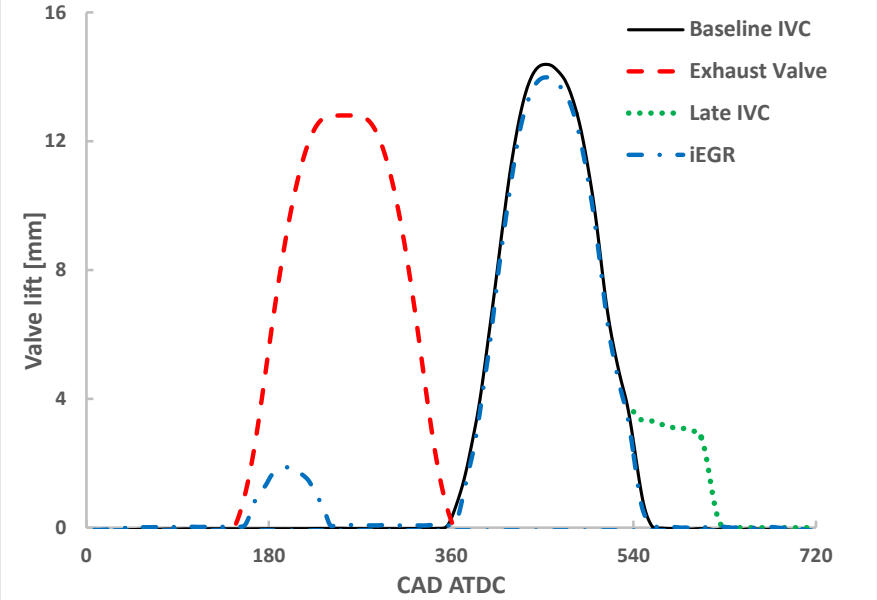

Figure 5.48: Fixed exhaust camshaft timing and variable intake valve lift profiles with VVA.

5.6.2 Evaluation of the effectiveness of various strategies for increasing EGT

In this part, different strategies are explored with respect to their capability to increase EGTs and impact on the relative fuel efficiency penalty, from which the efficient EGT control strategies are selected for further analysis.

Figure 5.49 shows an overview of the variations in fuel consumption versus EGT when different control strategies were applied. The variation value in both ISFC and EGT is defined as the difference between the other test cases and the baseline operation depicted in Table 5.6. It illustrated that the EGT can be effectively increased by LIVC,

intake throttling, or iEGR but much less affected by lowering the injection pressure and eEGR rate. By delaying combustion phase through the late injection timings, higher EGT was observed but with the highest fuel efficiency penalty. These behaviors were supported by Bai et al. [9] carrying out an experimental study at medium and low loads to investigate the effects of injection advance angle and injection pressure on exhaust thermal management. Therefore, strategies including late injection timings, lower injection pressures, and increased eEGR rates have been excluded from further analysis in the next subsection.

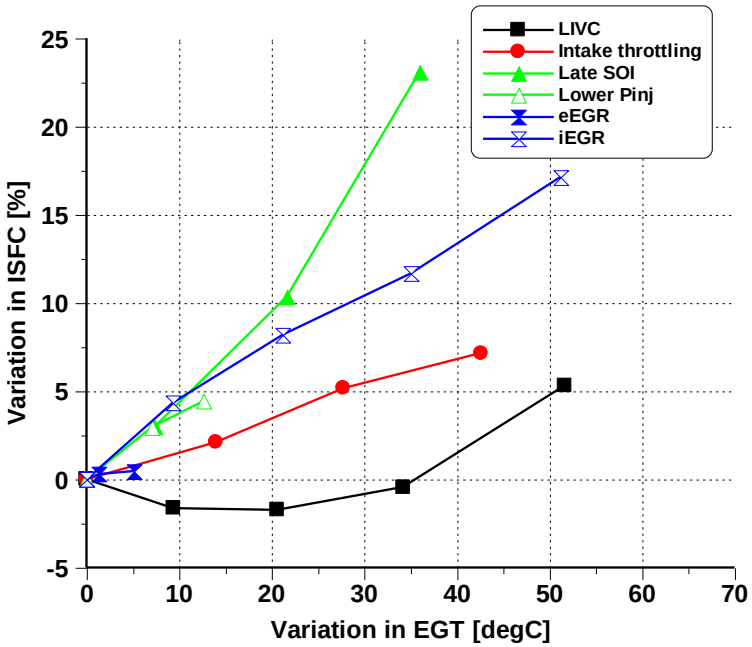

Figure 5.49: Potential of different combustion control strategies in increasing EGT.

5.6.3 Combustion characteristics

In this subsection, the three effective EGT control strategies of LIVC, intake throttling, and iEGR are further analysed and compared to the baseline case.

As shown in Figure 5.48 and Table 5.6, the original valve lift profile was used in a baseline case and the corresponding IVC timing was -178 CAD ATDC. The intake manifold pressure and exhaust back pressure were set to 1.15 bar and 1.25 bar, respectively. The LIVC strategy was run with four different IVC timings from -178 CAD to -100 CAD ATDC. For the intake throttling strategy, the intake air pressure was gradually reduced from 1.15 bar to 0.98 bar while keeping the exhaust pressure constant at 1.20 bar. In the case of iEGR strategy, the intake air pressure was set at 1.15 bar while the exhaust back pressures of 1.27bar, 1.33 bar, and 1.42 bar were performed by using the exhaust back pressure valve in order to trap higher fraction of the residual exhaust gas.

Figure 5.50 shows the in-cylinder pressures of the baseline, Cases 2 and 5 of the LIVC, Cases 6 and 8 of the intake throttling, and Cases 9 and 12 of the iEGR strategies. It can be seen that both LIVC and intake throttling strategies reduced in-cylinder pressures due to the lower ECR and reduced intake air pressure respectively, especially at the Case 5 of LIVC strategy and Case 8 of intake throttling strategy. The use of iEGR strategy via 2IVO event showed less impact on the in-cylinder pressure, even with higher exhaust back pressure of 1.42 bar in Case 12. This behavior was the result of the hot residuals trapped, which increased the in-cylinder gas temperature and hence the compression pressure and temperature. The hot residuals also accelerated the fuel evaporation and combustion process, resulting in a similar in-cylinder pressure curve to that of the baseline case.

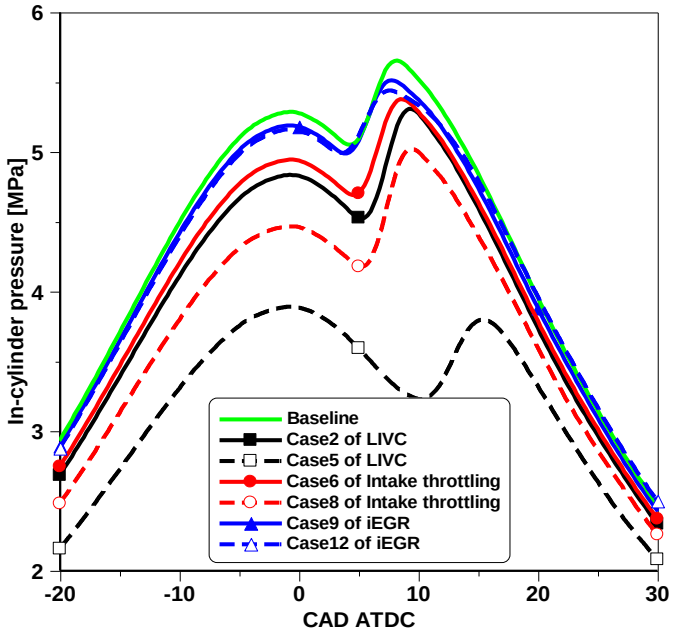

Figure 5.50: In-cylinder pressures for various strategies.

Figure 5.51 shows the heat release rate for all test strategies. The LIVC strategy was characterised by longer ignition delay and higher degree of premixed combustion. The highest peak HRR was obtained in Case 2 of the LIVC strategy, but it declined to the same level of the baseline case when delaying IVC timing to Case 5. This was because the lower in-cylinder temperature and pressure allowed more time for mixture preparation before auto-ignition, and hence higher degree of premixed combustion. The longer ignition delay in Case 5 of the LIVC strategy shifted the combustion process further away from TDC, resulting in lower burned gas temperature and peak HRR. In comparison, the peak HRR increased greatly as the intake throttling strategy was employed from Case 6 to Case 8. This was a result of the reduced in-cylinder charge density caused by the lower intake air pressure, resulting in a higher peak T_m, as shown in the next subsection. Thus, the combustion rate was accelerated with hotter combustion process [24].

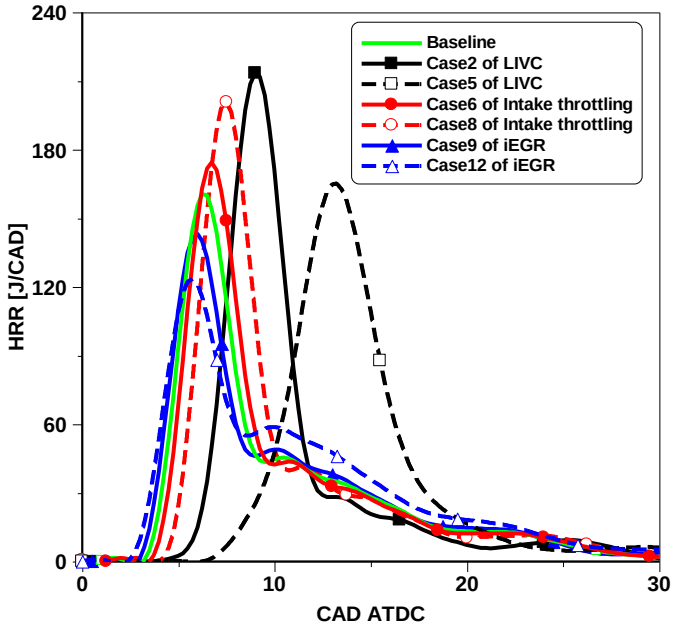

Figure 5.51: Heat release rate for various strategies.

In contrast to the LIVC and intake throttling strategies, the use of iEGR strategy decreased the peak HRR, in particular in Case 12 with higher fraction of the residuals gas. The reason could be explained by the higher in-cylinder charge temperature resulted from the hot residuals. This reduced the ignition delay and caused the combustion happened earlier than a baseline case. Figure 5.52 shows the T_m calculated by the ideal gas state equation. It can be seen that the compression temperature was reduced by using LIVC strategy due to lower ECR. However, it increased with iEGR strategy due to the hot residuals. The highest T_m was achieved in Case 12 of the iEGR strategy due to higher fraction of residuals gas.

In the case of the intake throttling, the peak T_m increased as the intake air pressure was reduced via intake throttling, although the compression temperature is similar to that of the baseline case. For the LIVC strategy, however, the peak T_m increased initially with Case 2 of the LIVC strategy, but dropped as IVC timings were further retarded to Case 5 due to the aggressively reduced compression temperature and pressure and later combustion process.

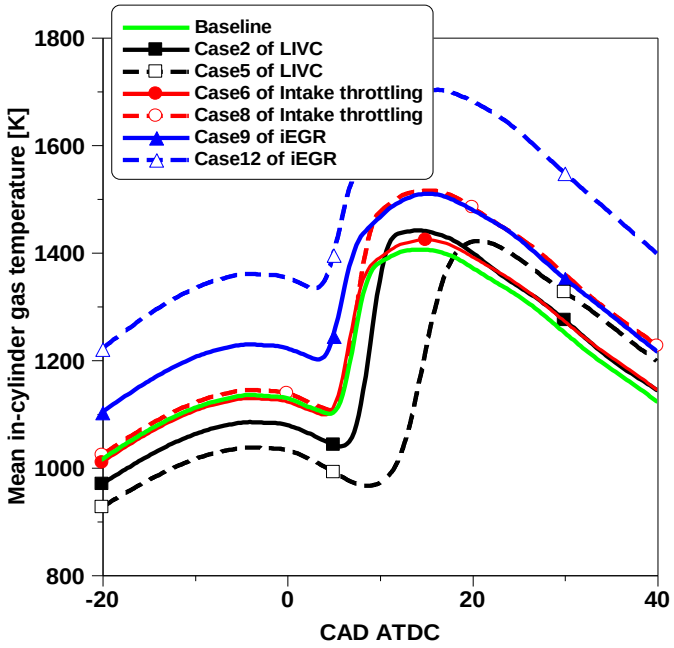

Figure 5.52: Mean In-cylinder gas temperatures for various strategies.

Figure 5.53 shows log P-V diagrams of the baseline case, Case 5 of the LIVC strategy, Case 8 of the intake throttling strategy, and Case 12 of the iEGR strategy at the same injection timing and injection pressure. There was a very small difference in the pumping loop area between the baseline case and LIVC strategy as the intake and exhaust pressures were maintained. However, the iEGR and intake throttling operations were characterised with significantly increased pumping loop areas due to the higher exhaust back pressure and lower intake manifold pressure, respectively.

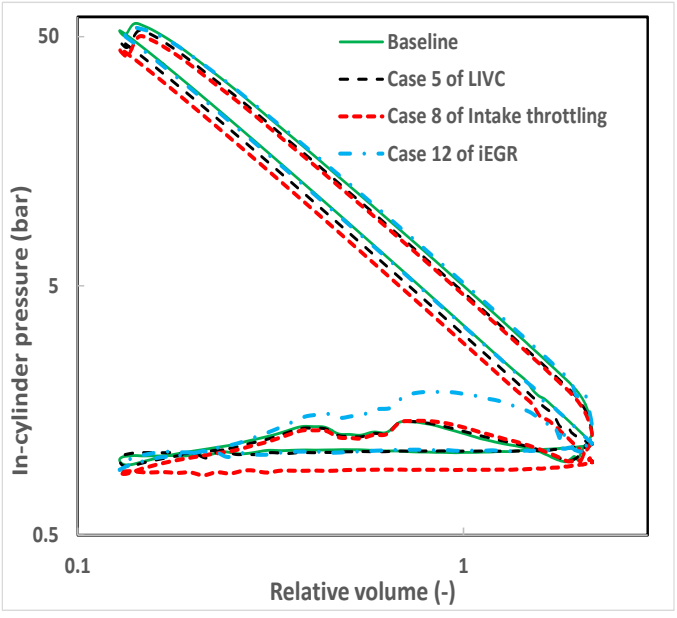

Figure 5.53: Log P-V diagrams of the baseline case, Case 5 of the LIVC strategy, Case 8 of the intake throttling strategy, and Case 12 of the iEGR strategy.

Figure 5.54 shows the combustion characteristics of different strategies versus the variation in EGT. For the LIVC strategy, the reduced ECR increased the ignition delay and lead to the shortest combustion duration. The iEGR strategy was characterised with the shortest ignition delay due to the charge heating effect of the hot residual gas but slowed down the initial heat release rate and increased combustion period because of the dilution effect of residual gas. Finally, as a result of reduced air mass, the intake throttling strategy led to the fastest initial combustion as measured by CA10-CA50 and slightly shorter combustion duration than the iEGR operation.

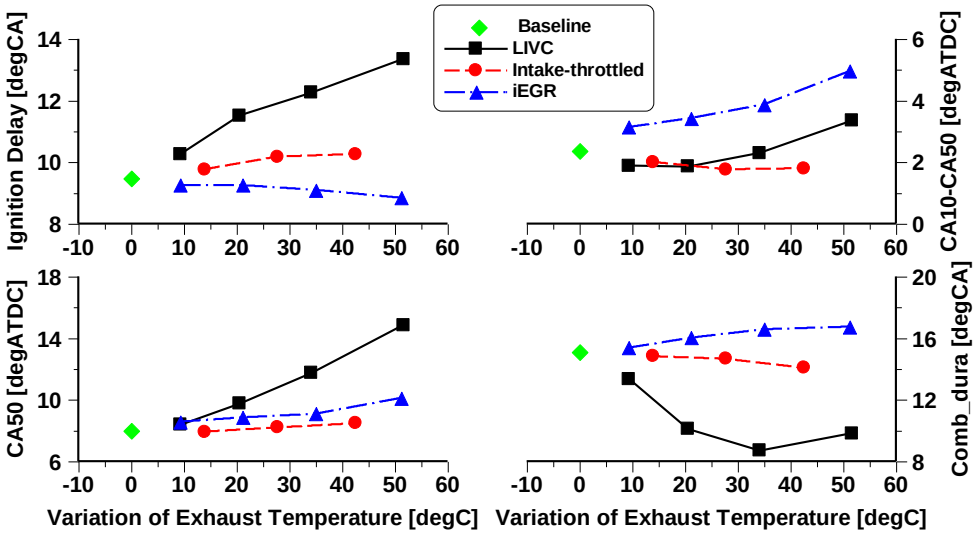

Figure 5.54: Comparison of the combustion characteristics of different strategies.

5.6.4 Engine performance and exhaust emissions

Figure 5.55 shows the lambda of different strategies versus the variation of EGT for the four cases. It can be seen that the EGT increased linearly with a decrease in lambda regardless of the strategy used. The slight deviation of the iEGR operation in the lambda value can be explained by the dilution effect of residual gas.

Figure 5.56 shows the combustion efficiency, PMEP, and variation of fuel consumption of different strategies. The combustion efficiency dropped significantly as the IVC timing was delayed from -178 to -100 CAD ATDC due to the lower compression pressure and the retarded combustion timing, causing the work loss during the combustion stroke. Higher PMEP was found in the strategies of intake throttling and iEGR, which can be explained by the larger pumping loop area in the log P-V diagram as shown in Figure 5.54, and hence higher fuel consumption. The changes in fuel consumption of LIVC strategy was different from others. The fuel consumption increased slightly with the retarded LIVC due to the higher degree of premixed combustion and shorter combustion duration. But as the

IVC timing was further retarded, the fuel consumption went up more rapidly because of the poor combustion efficiency. In order to increase the EGT by 52 °C, the LIVC and iEGR strategies were accompanied by 5.3% and 17% penalties in ISFC, respectively.

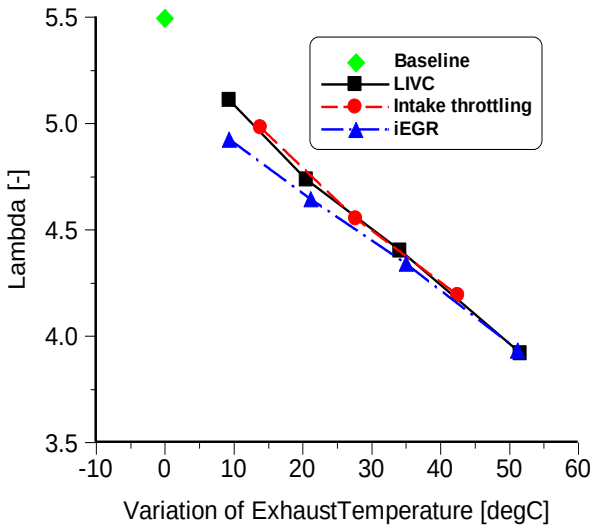

Figure 5.55: Comparison of the lambda at different strategies.

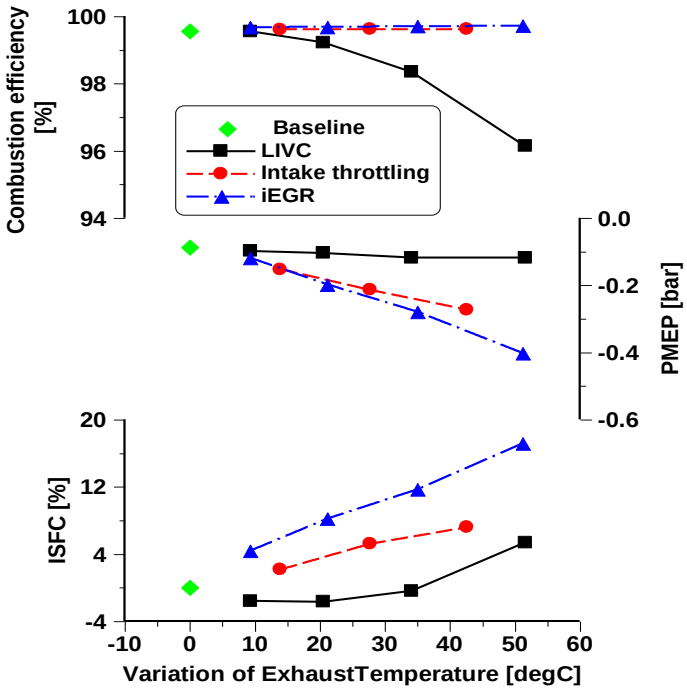

Figure 5.56: Comparison of the combustion efficiency, PMEP, and ISFC at different strategies.

Figure 5.57 shows the engine-out emissions versus the variation of EGT. The use of intake throttling and iEGR strategies had less impact on CO and HC emissions, maintaining as low as the baseline case. However, significant increases in CO and HC emissions were observed in the operation of LIVC strategy when the combustion temperature were much lower because of the lower compression ratio. This was because

the CO and HC emissions are mainly affected by the local oxygen availability during combustion and the combustion temperature. The increased combustion temperature by means of intake throttling and iEGR strategies contributed to the low levels of CO and HC emissions.

The change in soot emissions showed a strong correlation with the variation of the ignition delay. The soot emissions decreased in both LIVC and intake throttling strategies because of the prolonged ignition delay, and it increased by iEGR due to the shorten ignition delay. The NOx emissions demonstrated a different trend from that of soot emissions. With the intake throttling, NOx emissions increased due to the higher combustion temperature but decreased by iEGR due to the higher dilution and heat capacity of residual gas.

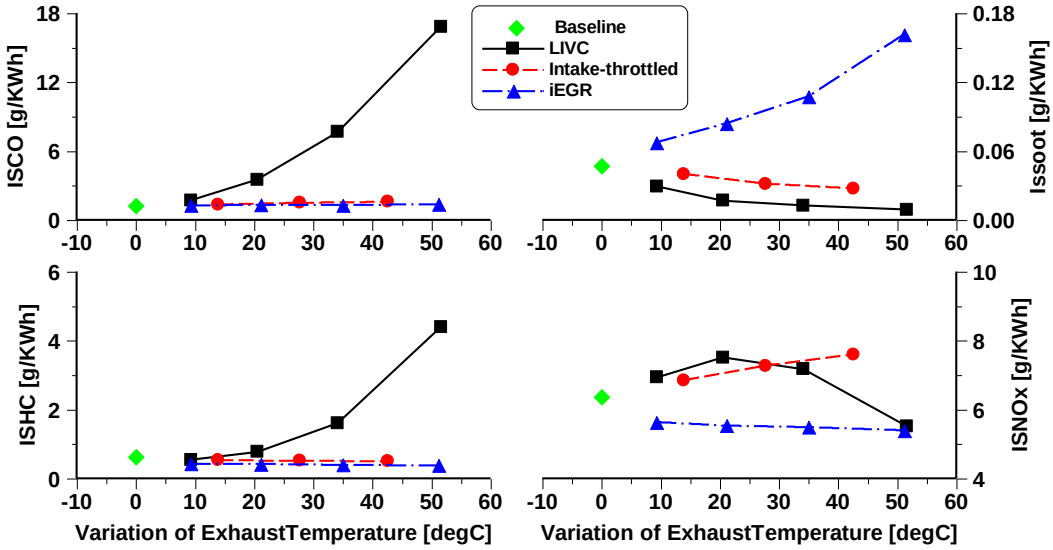

Figure 5.57: Comparison of the indicated specific emissions at different strategies.

Interestingly, the NOx emissions did not change linearly with LIVC strategy. It increased initially due to higher combustion temperature caused by the reduced charge mass, and then decreased when the IVC timing was delayed to beyond -118 CAD ATDC where the combustion took place later and experienced lower combustion temperature and pressure.

5.6.5 Combined effects of LIVC and iEGR

According to the discussion and analysis in the above subsection, the LIVC strategy has been demonstrated as an enabling technology for efficient increase in EGT while maintaining reasonable fuel consumption penalty compared to others. However, a significant increase in CO and HC emissions limit the potential of LIVC strategy. Internal EGR, as analysed in the former section, was an effective means in curbing CO and HC emissions. Therefore, the iEGR strategy was introduced when operating with LIVC strategy in order to offset the negative effects of LIVC on CO and HC emissions.

Figure 5.58 shows that the addition of iEGR to the LIVC operation advanced the combustion timing and increased the peak HRR because the in-cylinder gas temperature was increased by the presence of hot residual gas as shown in Figure 5.59. Both “LIVC-only” and “LIVC + iEGR” operations were characterised with much lower cylinder pressure than the baseline operation.

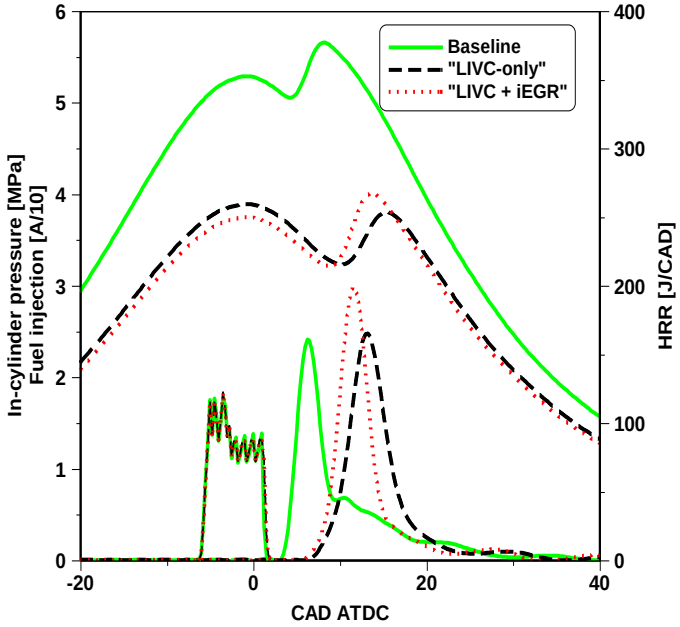

Figure 5.58: In-cylinder pressure, HRR, and injection signal of a baseline case, Case 5 of LIVC strategy, and Case 9 of “LIVC + iEGR” strategy.

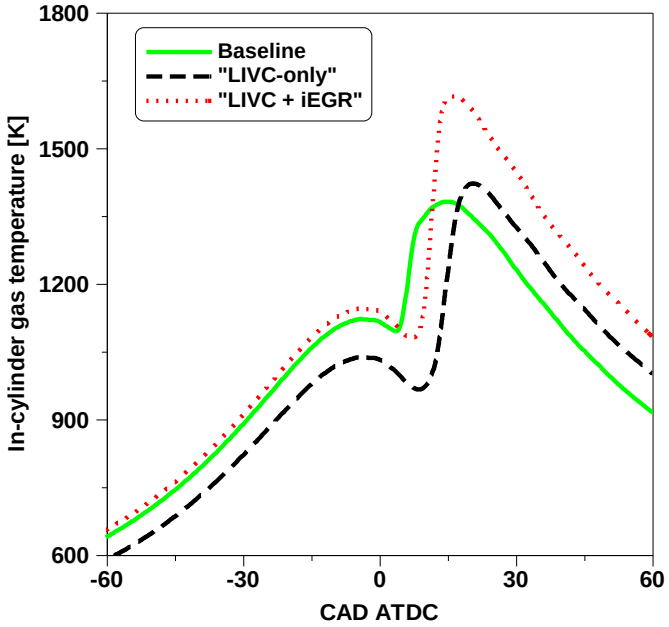

Figure 5.59: Mean in-cylinder gas temperature of a baseline case, Case 5 of LIVC strategy, and Case 9 of “LIVC + iEGR” strategy.

As shown in Figure 5.60, the ignition delay is slightly reduced when combining LIVC with iEGR due to the advanced combustion phasing. The combustion duration of “LIVC + iEGR” strategy became longer initially, and then reduced to a similar level of “LIVC-only” strategy when the IVC timing was further delayed.

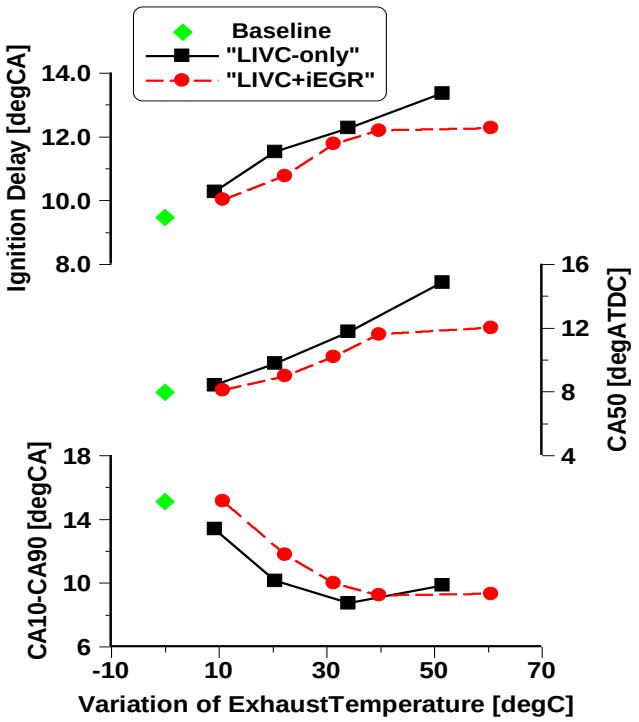

Figure 5.60: Combustion characteristics of a baseline case, Case 5 of LIVC strategy, and Case 9 of “LIVC + iEGR” strategy.

Figure 5.61 shows the relationship between lambda and EGT was the same for “LIVC-only” and “LIVC + iEGR” strategies. The lambda was maintained at a similar level when achieving the same variation in EGT by using LIVC strategies with and without iEGR. Compare to “LIVC-only” strategy, the combustion efficiency was clearly improved by means of “LIVC + iEGR” strategy due to increased combustion temperature. The higher fuel efficiency penalty of the “LIVC + iEGR” strategy with small EGT variation was due to the longer combustion duration. With further delayed IVC timings the combustion efficiency could still be maintained and the fuel consumption penalty decreased. It is noted that an increase in EGT more than 62 °C was obtained with only 4.6% fuel penalty when operating LIVC with iEGR strategy.

As shown in Figure 5.62, the introduction of iEGR reduced both CO and HC emissions, especially when large EGT increase was needed. This was mainly due to the higher in-cylinder combustion temperature, which helped the oxidation of CO and HC emissions. As it did not change the ignition delay clearly, the iEGR had little impact on soot emissions.

The dilution and heat capacity effects of iEGR caused the lower NOx emissions of “LIVC + iEGR” than those of “LIVC-only” in most cases, other than the highest EGT increase operations during which combustion temperature and hence NOx formation were reduced due to the most retarded combustion after TDC.

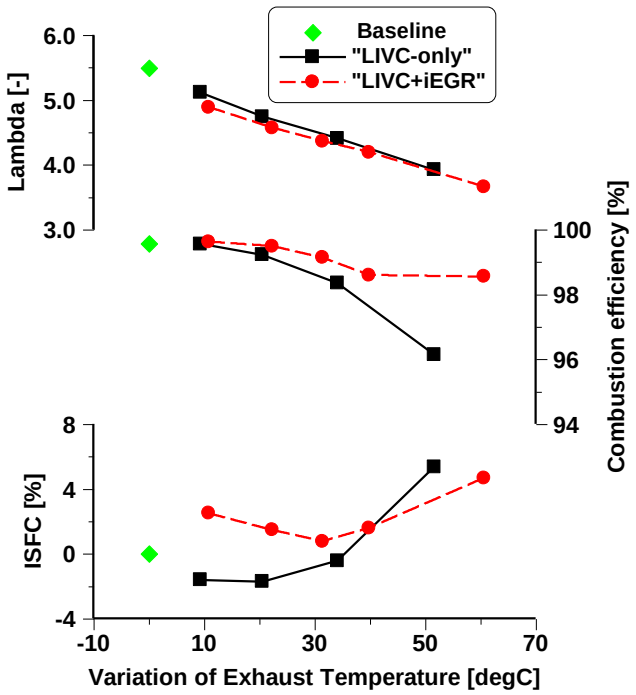

Figure 5.61: Engine performance of a baseline case, Case 5 of LIVC strategy, and Case 9 of “LIVC + iEGR” strategy.

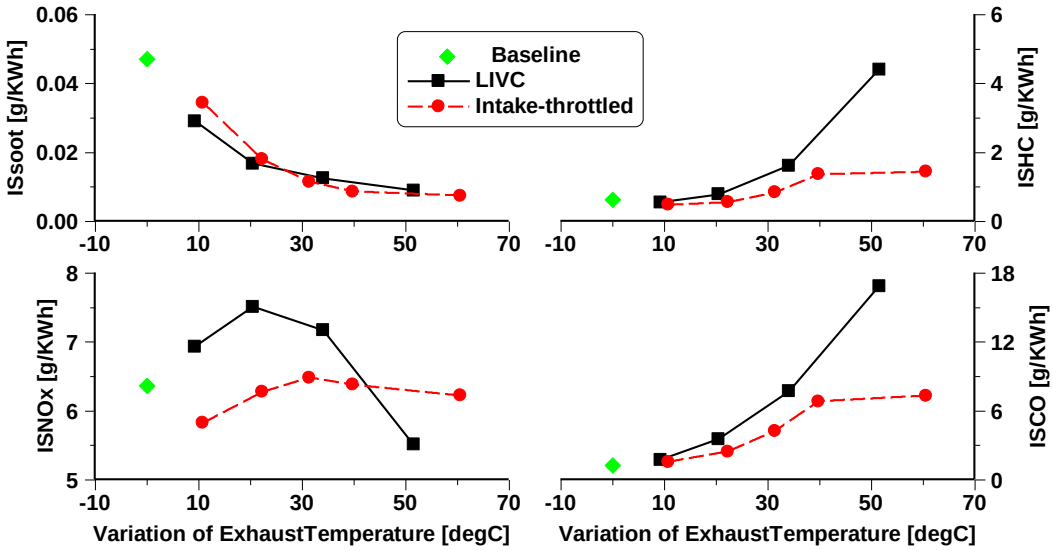

Figure 5.62: Indicated specific emissions of a baseline case, Case 5 of LIVC strategy, and Case 9 of “LIVC + iEGR” strategy.

Figure 5.63 provides an overall assessment of the potential of combined LIVC and iEGR strategy to achieve the optimal trade-off between the EGT, fuel consumption, and

emissions. As shown in Figure 5.63, the results of the optimum “LIVC-only” and “LIVC + iEGR” operations were compared against the baseline operation. It can be seen the “LIVC-only” strategy could increase EGT by 52°C (31%) at the expense of a 5.3% penalty in fuel consumption. By combining LIVC and iEGR, EGT could be increased by 62°C (37%) with 4.6% fuel efficiency penalty and much lower HC and CO emissions than the “LIVC-only” operation. Compared to the baseline operation, the soot emissions were reduced substantially by LIVC operation with or without the iEGR, accompanied with a small decrease in NOx emissions.

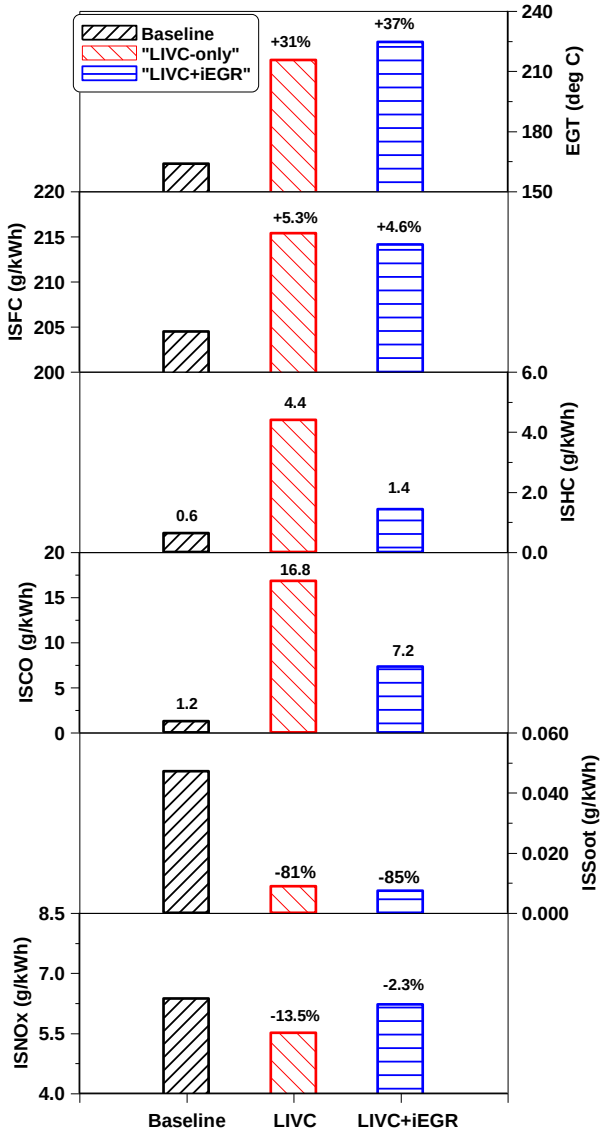

Figure 5.63: Comparison between experimental results for “Case 5 of LIVC” strategy and “Case 5 of LIVC + Case 9 of iEGR” strategy.

Therefore, the combination of LIVC and iEGR was identified as the most effective means amongst the various technologies examined in the current study to raising the EGT with lower engine-out emissions and minimum penalty in fuel consumption.

5.7 Summary

In this chapter, the engine performance, emissions and exhaust gas temperature of the single cylinder HD engine at low and medium loads (between 2.2 and 12 bar IMEP) are presented and discussed. Advanced engine combustion control strategies were explored in order to improve the trade-off between engine efficiency and NOx emissions of the low-medium load Miller cycle operation, while increasing the EGT for rapidly initiate and improve the emissions conversion. In order to gain better understanding of the in-cylinder conditions, a 1D engine model was built to calculate the average in-cylinder gas temperature and burned zone gas temperature. Combustion characteristics, engine performance and exhaust emissions were analysed and discussed. The main findings are summarised below.

i. The Miller cycle (LIVC) was more effective in increasing EGT and reducing NOx emissions than the retarded combustion operation. At low load, the IVC at -110 with CA50 at 12 CAD ATDC allowed for an increase of 70°C in EGT with a fuel penalty of 2.5%, which is not achievable by a late CA50 strategy only. However, the smoke number was more sensitive to the late IVC, which produced slightly higher smoke number than a late CA50 strategy at the same NOx level.
ii. When operating with constant intake pressure, the Miller cycle led to lower in-cylinder mass, producing an adverse impact on smoke number and engine efficiency. However, operating at the same air/fuel ratio as the baseline by means of a higher intake pressure for the Miller cycle operation improved the in-cylinder oxygen availability and accelerate the combustion process, which helped improve upon the performance and emissions of the Miller cycle, especially at the medium load of 12 bar IMEP.
iii. When operating with constant lambda, the Miller cycle strategy enabled simultaneous reduction in NOx and soot emissions while maintaining the engine efficiency the same as the baseline. In addition, the unburn HC emissions were lower by the use of Miller cycle, whether operating with constant intake pressure or lambda. This probably due to the longer ignition delay and higher exhaust gas temperature.
iv. The application of EGR was more effective in reducing NOx emissions than Miller cycle. This was a result of the lower peak combustion temperatures and oxygen concentration attained with EGR, which are the critical conditions to the NOx formation.
v. The combination of Miller cycle and EGR at the low load of 6 bar IMEP resulted in longer ignition delay and reduced the in-cylinder gas temperatures, achieving up

to 70% lower NOx emissions with a low fuel efficiency penalty. At 12 bar IMEP, however, the introduction of EGR with Miller cycle was capable of attaining more than 70% NOx reduction at the expense of higher ISFC penalty and increased emissions of soot and CO.

vi. The “EGR + Miller cycle” strategy allowed for lower NOx emissions with significant higher EGT than an “EGR-only” strategy. The higher EGT attained with the combined strategy at 6 bar IMEP would be preferred for a superior aftertreatment performance and lower vehicle’s tailpipe NOx levels. However, the lower combustion temperatures and lambda adversely affected soot and CO emissions.

vii. The addition of a post injection was effective in minimizing soot and CO emissions of the “Miller cycle + EGR” strategy while achieving lower NOx emissions and higher EGT at low engine load. The improvements, however, were achieved at the expense of a decrease in net indicated fuel conversion efficiency. Overall, the “Miller cycle + EGR + post injection” strategy could reduce NOx emissions by 66% while increasing the EGT and corrected total fluid efficiency by 75°C and 3.1%, respectively.

The results in the exploration of an alternative combustion control strategy for light load EGT management also indicate that

i. Sufficient high EGT could be obtained by means of the LIVC, intake throttling, and iEGR strategies. Reduced diesel injection pressure and external EGR were not effective in increasing EGT. Retarded diesel injection timing could be used to raise EGT but at the expense of high penalty in fuel consumption.

ii. The use of iEGR kept the specific emissions of NOx, HC and CO as low as the baseline case, but resulted in large increase in fuel consumption and higher soot emissions. This was because of the higher pumping work and shorten ignition delay, respectively.

iii. Throttling intake air flow was effective in increasing the EGT by 42°C due to reduced cylinder charge but accompanied with a 7.2% fuel consumption penalty and slightly higher NOx emission.

iv. The application of LIVC enabled an increase in EGT by 52°C and lower NOx and soot emissions with small fuel consumption penalty of 5.3%. However, the lower combustion temperature led to large increase in HC and CO emissions due to a lower combustion efficiency.

v. The combined use of LIVC and iEGR was identified as the most effective means amongst the various technologies examined in the current study, increasing the EGT by 62°C with lower overall engine-out emissions and minimum penalty of 4.6%

in fuel consumption.

Overall, the Miller cycle had been shown as an effective combustion technology for EGT and NOx emissions control at the low-medium load operating conditions. The “Miller cycle + iEGR” strategy at a light load allowed for a higher increase in EGT as well as lower emissions and fuel consumption. The “Miller cycle + EGR + post injection” strategy at low load of 6 bar IMEP enabled simultaneous low levels of NOx and soot emissions with efficient exhaust thermal management. However, a higher intake pressure was required for the Miller cycle operation as the load was increased to medium load of 12 bar IMEP. Additionally, these advanced combustion control strategies helped minimise the total fluid consumption of the low-medium load engine operation.

Chapter 6
Application of the Miller cycle strategy at high engine loads

6.1 Introduction

Diesel engine operation at high load conditions is characterised by higher peak in-cylinder pressure as a result of the higher amount of fuel injection, which restrict the employment of higher intake pressure and injection pressure for the optimisation of engine efficiency. This is especially true at the full engine loads where the maximum engine efficiency is relatively lower attributed to the peak in-cylinder pressure limit. In addition to the limitation of the peak in-cylinder pressure, the relatively higher NOx emission is another challenge for modern turbocharged diesel engines operating at high loads. Miller cycle via LIVC strategy is an effective in-cylinder measure to reduce the peak in-cylinder pressure and NOx emissions by lowering the compression pressure and temperature. However, this can adversely affect the soot emissions and engine efficiency, which heavily depend on the in-cylinder oxygen availability and combustion temperature.

Therefore, investigations were performed on the investigation of combustion control strategies in order to achieve efficient and clean high load engine operation with Miller cycle. The effects of injection timings, injection pressures, intake pressures, and EGR rates on high load Miller cycle operation have been analysed and discussed. The potential of Miller cycle with EGR was also explored at full engine load to improve the NOx emissions and engine efficiency. Additionally, a cost-benefit and overall analysis was carried out by estimating the aqueous urea solution consumption in the SCR system based on the engine-out NOx emissions and the Euro VI NOx limit. This then allowed for the determination of the most effective combustion control strategy in terms of exhaust emissions, fuel conversion efficiency, and engine operational cost.

6.2 Effects of combustion phasing on high load Miller cycle operation

The focus of this section is to assess the effect of SOI on high load Miller cycle operation and optimise the combustion process of all combustion control strategies to achieve the maximum NIE. Experimental works were carried out at a speed of 1250 rpm and a high load of 24 bar IMEP.

6.2.1 Test methodology

Table 6.1 presents the main engine operating conditions for the investigation. A single injection strategy was employed. The SOI was swept up to against the peak in-cylinder pressure limit of 180 bar in order to determine the optimum SOI for the maximum NIE. The injection pressure and EGR rate were held constant at 1700 bar and 15%, respectively. The IVC timing was delayed from -178 to -110 CAD ATDC to realize Miller cycle operation. The stead state condition was quantified by controlling the PRR and COV_IMEP below 30 bar/CAD and 3%, respectively.

Table 6.1: Engine operating conditions for the different IVC timings with a sweep of SOI.

Parameter	Value
Speed	1250 rpm
Load	24 bar IMEP
SOI	Varied between -8 and -15 CAD ATDC
Injection pressure	1700 bar
Intake air temperature	42 ± 1°C
Intake pressure	2.3 bar
Exhaust pressure	2.4 bar
EGR rate	15%
IVC timing	-178, -130, -120 CAD ATDC

6.2.2 Combustion and heat release analysis

Figure 6.1 shows the in-cylinder pressure, HRR, and injector signal for the baseline and Miller cycle operation. The comparison was performed at a constant CA50 and the optimised SOI which attained the maximum NIE. The LIVC timing effectively reduced the in-cylinder pressure and peak HRR at the same SOI due to the decreased ECR. Compared to the Miller cycler operation at low and medium loads, the effect of Miller cycle on ignition delay was relatively smaller at high engine load. This can be explained by a better ignition condition at a higher engine load. A more advanced SOI was obtained in the LIVC timing to achieve the maximum NIE and thus led to an earlier HRR. This can helped improve the fuel conversion efficiency of the Miller cycle operation.

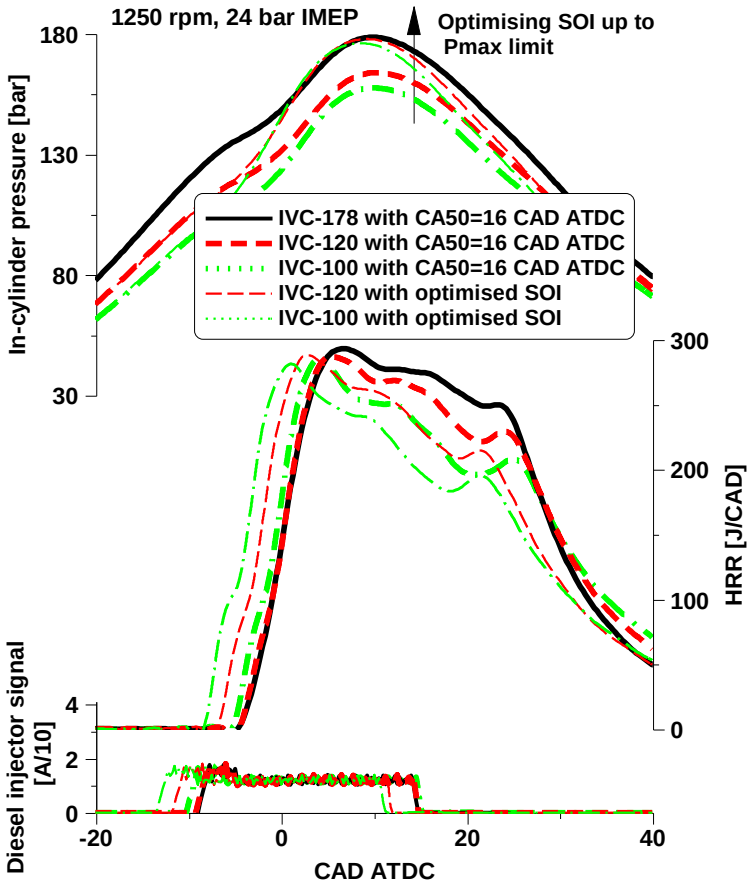

Figure 6.1 In-cylinder pressure, HRR, and injector current signal for the baseline and Miller cycle at a constant CA50 and optimised SOI.

6.2.3 Engine performance and gaseous emissions

Figure 6.2 shows the Miller cycle significantly reduced the peak in-cylinder pressure at a constant CA50. The difference in the peak in-cylinder pressure between the baseline and Miller cycle operation was 30 bar on average. The lambda was reduced significantly by delaying the IVC, decreasing to below 1.2 with the IVC at -100 CAD ATDC. This was the reason for the increase in EGT by approximately 34%. A lower NIE was obtained as the IVC was delayed. This was primarily due to a longer combustion duration and higher heat transfer losses in the Miller cycle operation with the same P_{int} as the baseline. When optimised the combustion process via advancing the SOI, the Miller cycle allowed for an earlier CA50 by 3.5 CAD than that of the baseline case, which helped improve the NIE. As a result, the NIE of Miller cycle with IVC at -120 CAD ATDC was increased to a similar level of the baseline. However, the NIE was significantly lower than the baseline when delayed the IVC to -100 CAD ATDC, despite with a much earlier CA50. This was attributed to the lower lambda and longer combustion duration.

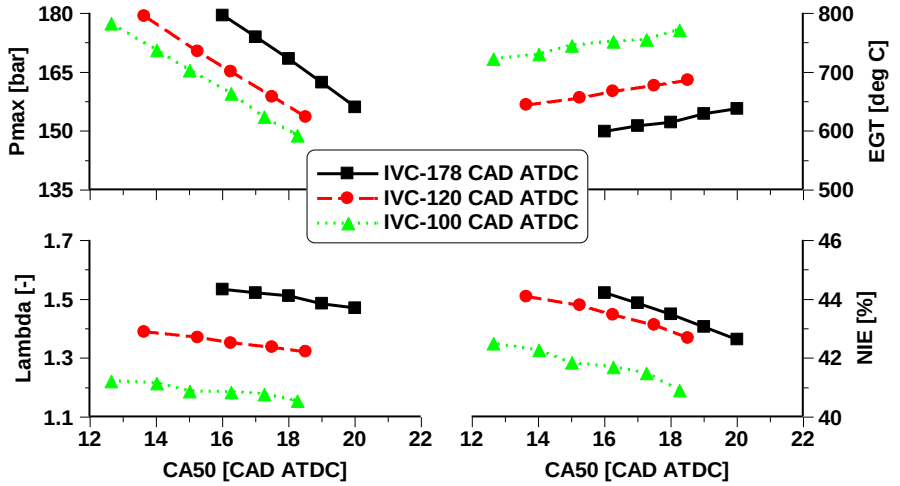

Figure 6.2: Engine performance as a function of CA50 for the baseline and Miller cycle operations.

The data depict in Figure 6.3 is the resulting specific exhaust emissions for the different IVCs. The Miller cycle with IVC at -120 CAD ATDC reduced the NOx emissions by 20% with little impact on soot emissions when comparing at a constant CA50. This was primarily a result of the lower in-cylinder air mass trapped and reduced initial burned zone gas temperature. A higher reduction in NOx emissions by 38% was achieved when the IVC was delayed to -100 CAD ATDC. This was accompanied with excessive soot and CO emissions due to significantly lower lambda and peak in-cylinder combustion temperature. Later CA50 effectively decreased combustion temperatures and therefore NOx emissions of all cases. It can also be seen from Figure 6.3 that the application of Miller cycle decreased unburned HC emissions. This was possibly attributed to the relatively lower lambda and higher average in-cylinder gas temperature, which can improve the oxidation rates of HC emissions during the expansion stroke.

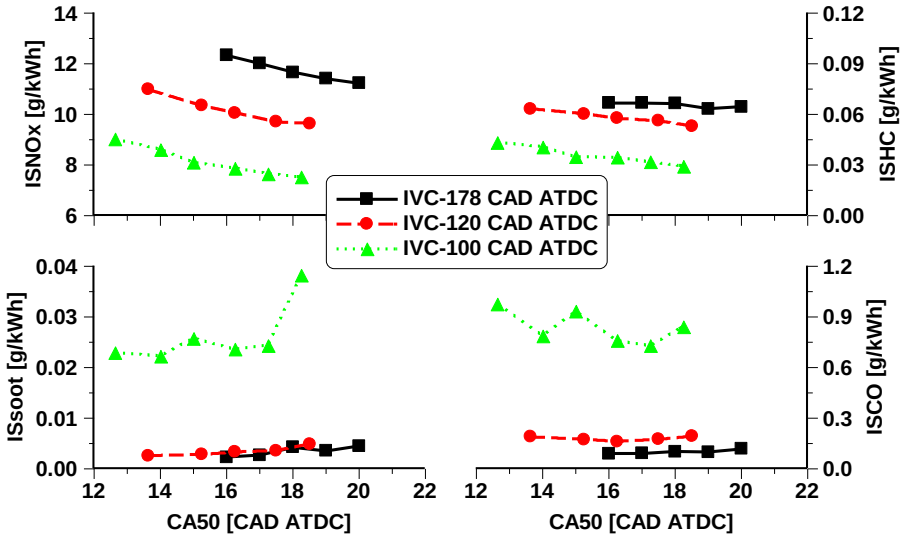

Figure 6.3: Exhaust emissions as a function of CA50 for the baseline and Miller cycle operations.

6.3 Effects of fuel injection pressure on high load Miller cycle operation

The previous section revealed that the combination of Miller cycle and EGR would reduce the NIE and yielded significantly higher soot emissions at high engine loads. However, high injection pressure can be applied to help curb soot emissions and improve engine efficiency. An optimisation was performed to determine the effectiveness of injection pressure for high load Miller cycle operation with EGR. Experimental studies were carried out by varying injection pressures between 1400 and 1800 bar at a speed of 1250 rpm and a high load of 17 bar IMEP.

6.3.1 Test methodology

Table 6.2 summaries the testing conditions for the baseline and Miller cycle operations with 20% EGR. The SOI was swept and optimized up against the in-cylinder pressure limit of 180 bar in order to achieve the maximum NIE. Injection pressure was increased gradually in an attempt to improve engine efficiency and soot emissions. The upper bound of PRR was limited to 30 bar/CAD in order to allow for the employment of higher injection pressure. Stable engine operation was determined by controlling the COV_IMEP below 3%.

Table 6.2: Engine testing conditions

Parameter	Value
Speed	1250 rpm
IMEP	17 bar
SOI	-12 CAD ATDC
Injection pressure	Varied between 1400 and 1800 bar
Intake air temperature	40 ± 1°C
Intake pressure	2.44 bar
Exhaust pressure EGR rate	2.54 bar 20%
Intake valve closing	-178, -130, -120 CAD ATDC

6.3.2 Combustion and heat release analysis

Figure 6.4 shows the in-cylinder pressure, HRR, and injector signal for Miller cycle with IVC at -120 CAD ATDC under different injection pressures. The comparison was performed at a constant SOI of -12 CAD ATDC. The higher injection pressure enabled a better fuel atomization and thus a higher quality of the fuel-air mixture. This led to a faster initiation of combustion and thus shorter ignition delay and combustion period. Consequently, the highest injection pressure of 1800 bar led to the highest peak in-cylinder pressure and peak HRR. It also can be seen that the injection pulse width measured from the injector current signal was reduced as increased injection pressure. This was attributed to the improved combustion process and therefore helped minimise the fuel consumption while producing the same useful work.

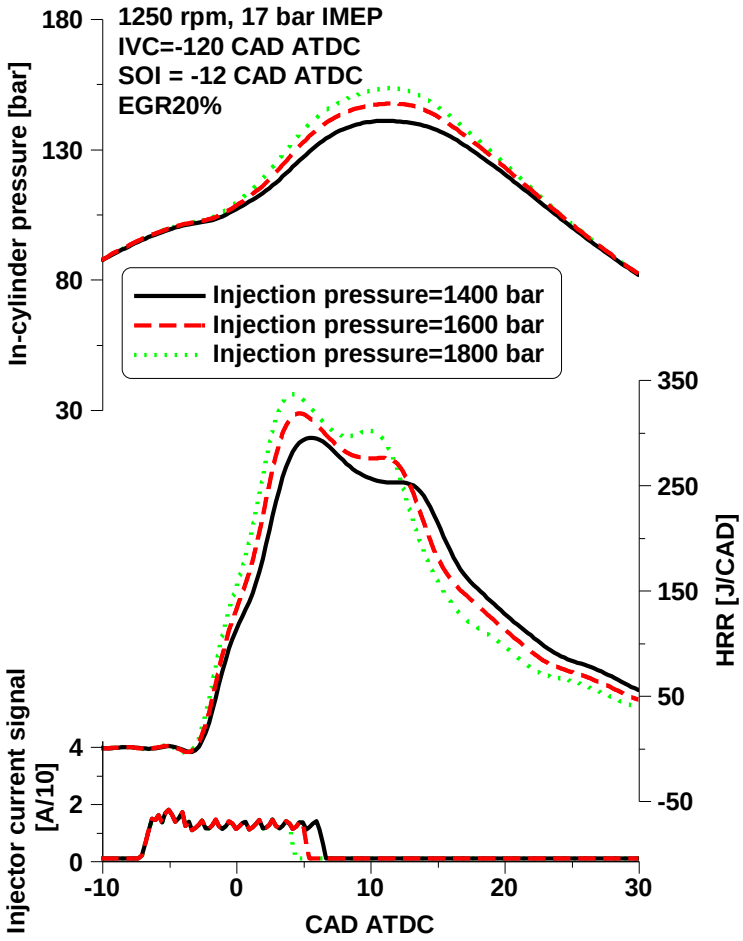

Figure 6.4: Effect of injection pressure on in-cylinder pressure and HRR of the high load Miller cycle operation.

6.3.3 Engine performance and gaseous emissions

Figure 6.5 shows the engine performance parameters for the baseline and Miller cycle operation with different injection pressures. The P_{max} was reduced by the Miller cycle while

was increased by a higher injection pressure. A Miller cycle strategy allowed for the use of a higher injection pressure while maintaining the P_{max} of the baseline case. This helped improve upon NIE and emissions of the Miller cycle. The injection pressure increased the lambda slightly, which was the reason for a reduction in EGT at a given IVC timing. This is to be expected that the LIVC strategy decreased the NIE, which was improved significantly by the use of a higher injection pressure. These improvements were more apparent when operating at the latest IVC of -120 CAD ATDC.

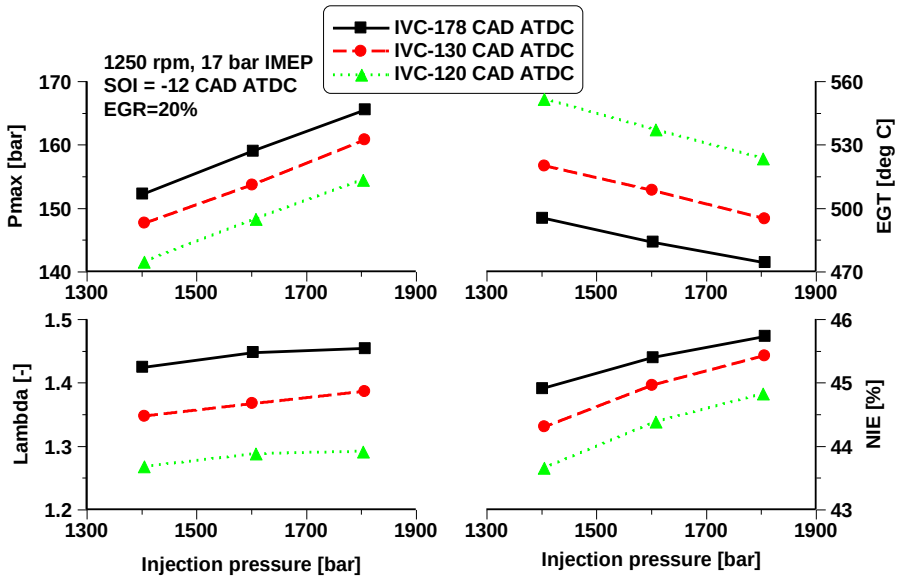

Figure 6.5: The effect of injection pressure on engine performance parameters of the high load Miller cycle operation.

The data depicted in Figure 6.6 is the indicated specific exhaust emissions for the baseline and Miller cycle operation. The Miller cycle effectively reduced the NOx emissions, but led to significantly higher soot and CO emissions. The use of a higher injection pressure improved the fuel-air mixing and accelerated the combustion process and consequently, minimising the soot and CO emissions. These improvements were attained at the expense of the NOx reduction benefit. Nevertheless, the injection pressure had little influence on the unburn HC emissions of the different IVCs.

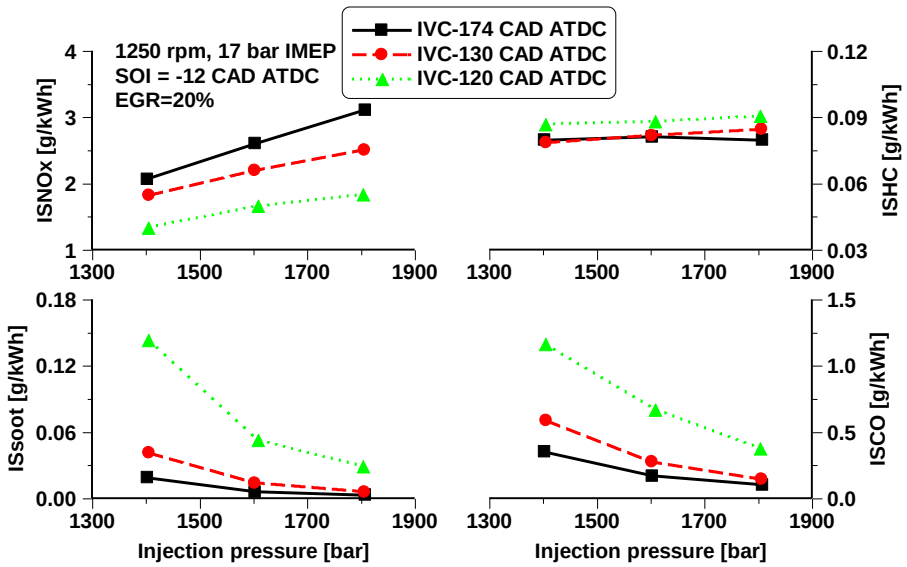

Figure 6.6: The effect of injection pressure on engine emissions of the high load Miller cycle operation.

6.4 Effects of intake pressure on high load Miller cycle operation

Chapter 5 has revealed that the intake pressure had significant influence on the Miller cycle operation at low and medium loads. The NIE and soot emissions were improved simultaneously while maintaining low levels of NOx emissions when the intake pressure was increased. In this section, experimental study was carried out to investigate the effect of intake pressure on engine performance and emissions of a high load Miller cycle operation.

6.4.1 Test methodology

Table 6.3 summaries the engine operating conditions. The experiment was carried out at a speed of 1250 rpm and a high engine load of 17 bar IMEP operating with constant injection pressure of 1400 bar and EGR rate of 15%. The exhaust back pressure was adjusted to maintain a pressure differential of 0.10 bar across the cylinder with higher exhaust back pressure, which allowed for the recirculation of exhaust gas. PRR and COV_IMEP were limited to 30 bar/CAD and 3%, respectively.

Table 6.3: Engine testing conditions.

Parameter	Value
Speed	1250 rpm
IMEP	17 bar
SOI	Varied between -4 and -17.5 CAD ATDC
Injection pressure	1400 bar
Intake air temperature	38 ± 1 K
Intake pressure	Varied between 2.30 bar and 2.65 bar
Exhaust pressure	Maintain 0.10 bar higher than intake pressure
EGR rate	15%
Baseline IVC	-178 CAD ATDC
Miller cycle	-120 CAD ATDC

6.4.2 Combustion and heat release analysis

Figure 6.7 shows the in-cylinder pressure and HRR for the baseline and Miller cycle with constant P_{int} and lambda of the baseline case. Miller cycle operation with a constant P_{int} of 2.3 bar (red dashed line) significantly decreased in-cylinder pressure and peak HRR. This was a result of the lower ECR, which decreased the compression pressure and temperature during the compression stroke.

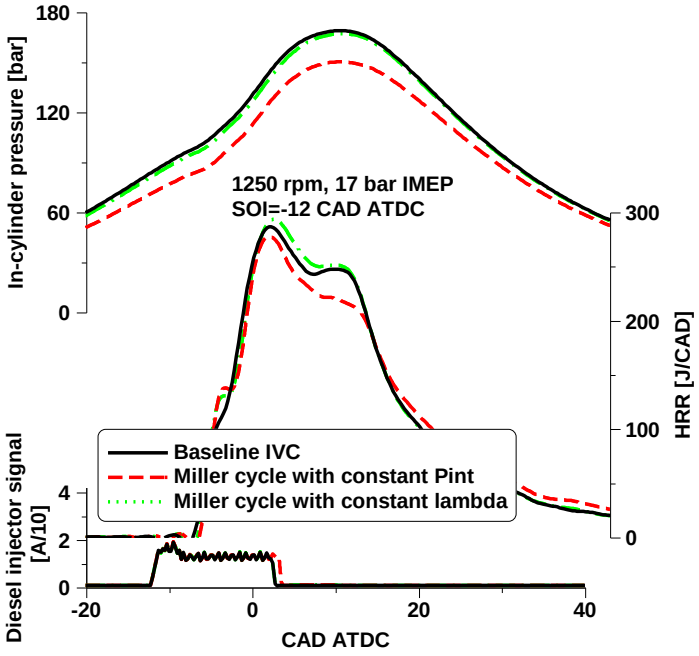

Figure 6.7: In-cylinder pressure, HRR, and injector signal for the baseline and Miller cycle operation.

The formation of a first peak heat release was observed, which represented a higher degree of premixed combustion. A higher P_{int} increased in-cylinder charge density, resulting in relatively higher in-cylinder pressure and peak HRR. The Miller cycle strategy achieved similar in-cylinder pressure and HRR profiles to the baseline case when operating with the same lambda.

Figure 6.8 compares the mean in-cylinder gas temperature of the baseline and Miller cycle cases. The Miller cycle strategy decreased the compressed air temperature due to the LIVC and lower ECR. However, the Miller cycle operating with same P_{int} as the baseline case reduced the in-cylinder mass trapped and thus lower in-cylinder total heat capacity. This resulted in a higher peak T_m, despite a reduction in compressed gas temperature. When operating with the same lambda as the baseline case, the peak T_m was decreased with increased P_{int} and lower than that of the baseline case.

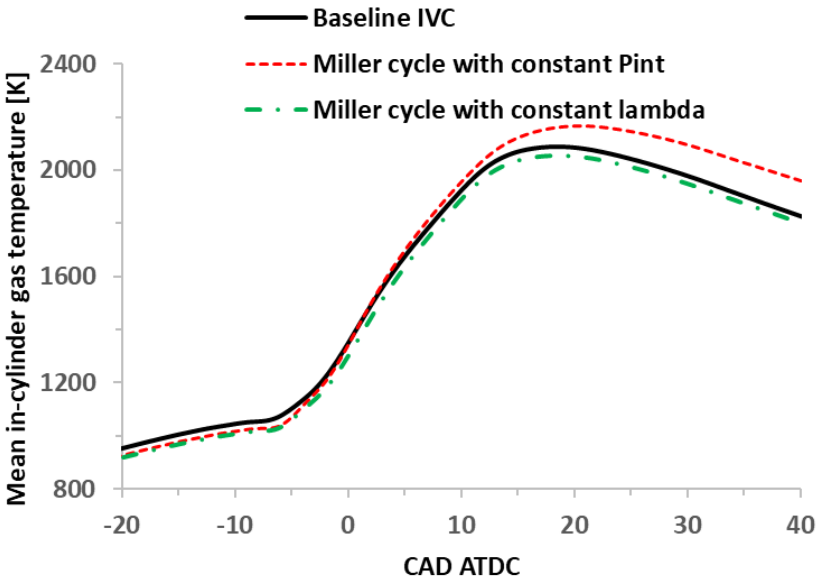

Figure 6.8: Comparison of the mean in-cylinder gas temperature between the baseline and Miller cycle operation.

Figure 6.9 shows the combustion characteristics over a sweep of the injection timing. The lower compressed gas pressure and temperature resulted from Miller cycle increased the ignition delay. The Miller cycle with constant P_{int} delayed the CA90 noticeably due to the later ignition and slowed down combustion process in the late combustion phase. This resulted in a relatively longer period time of CA50-CA90 as well as combustion duration. When operating with same lambda as the baseline case, the higher P_{int} improved the in-cylinder oxygen availability and therefore helped accelerate the combustion process. These effects advanced the CA90 and thus a shorter period time of CA50-CA90, which contributed to a shorter combustion duration. Consequently, the combustion

characteristics of the Miller cycle with constant lambda were similar to that of the baseline operation.

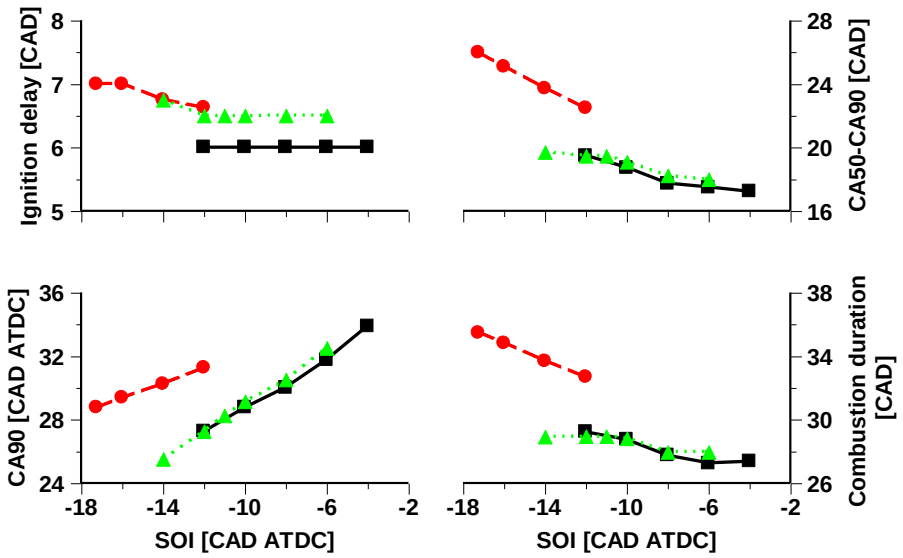

Figure 6.9: Combustion characteristics of the baseline and Miller cycle operating with constant P_{int} and lambda.

6.4.3 Engine performance and exhaust emissions

Figure 6.10 depicts engine performance parameters and net indicated specific emissions of the baseline and Miller cycle cases. The application of Miller cycle with constant P_{int} decreased the lambda noticeably due to lower in-cylinder mass trapped. This was the primary reason for the significant increase in EGT by approximately 90ºC. The Miller cycle displayed higher impact on the combustion process at high engine load than at the low and medium loads, which was suggested by a decrease of 4% in the NIE in comparison with 1% at low and medium loads when operating with a constant P_{int}. This was attributed to the relatively lower in-cylinder oxygen availability (e.g. lower lambda) at high engine load operation. The decreased NIE was the result of slower heat release, longer combustion duration, and higher heat losses to cylinder walls resulted from higher T_m.

The use of a higher P_{int} to maintain the in-cylinder lambda value helped increase the NIE due to the higher in-cylinder oxygen availability, but adversely affected the gains obtained in terms of EGT and NOx emissions. Miller cycle operation with constant lambda achieved an increase of 1.3% in NIE compared to the baseline operation. This was mainly due to the lower T_m as shown in Figure 6.8, which decreased the heat transfer losses. The longer ignition delay of Miller cycle operation with constant lambda increased the degree of premixed combustion as supported by the higher peak HRR, which also helped improve the NIE.

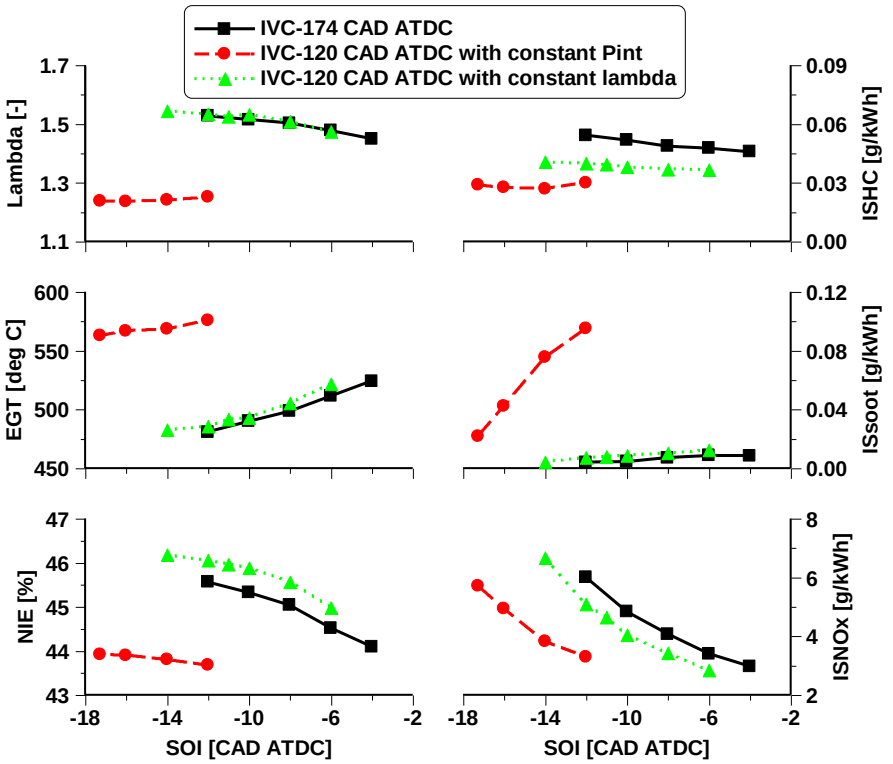

Figure 6.10: Engine performance and exhaust emissions of the baseline and Miller cycle operating with constant P_{int} and lambda.

It can be also seen from Figure 6.10 that Miller cycle with constant P_{int} enabled a reduction in NOx emissions by 45% at the expense of excessive smoke at a constant SOI of -12 CAD ATDC. This was primarily a result of the lower in-cylinder air mass trapped and reduced initial burned zone gas temperature. Additionally, later SOI effectively decreased the combustion temperature and therefore NOx emissions but increased soot emissions. As the P_{int} of the Miller cycle cases was increased, soot emissions were reduced and NOx emissions were increased. As a result, Miller cycle with constant lambda decreased NOx emissions by 20% and had little impact on soot emissions. Moreover, the Miller cycle cases decreased unburned HC emissions, regardless of the intake pressure used, which was similar to the results observed at low and medium load operations. This was also possibly attributed to the relatively lower lambda and higher combustion temperature and exhaust temperature, which can improve the oxidation rates of HC emissions during the expansion stroke.

6.5 Effects of external EGR on high load Miller cycle operation

This section will describe the effect of EGR rate on high load Miller cycle operation. Investigation was performed at an IVC timing of -120 CAD ATDC. The EGR rate was

varied between 0 and 20% in order to determine the optimum EGR rate for achieving the optimum trade-off between exhaust emissions and engine efficiency of the Miller cycle operation.

6.5.1 Test methodology

Table 6.4 depicts the engine operating conditions for the high load Miller cycle operation with EGR. The injection timings were swept to vary the combustion phasing. The injection pressure was held constant at 1400 bar for the EGR rate between 0 and 15%. In the case with an EGR rate of 20%, the in-cylinder air flow mass can be decreased noticeably, which will result in poor combustion instability and excessive smoke. Therefore, a higher injection pressure of 1800 bar was employed when EGR rate was increased to 20%. The PRR and COV_IMEP were limited to 30 bar/CAD and 3%, respectively.

Table 6.4: Engine testing conditions.

Parameter	Value
Speed	1250 rpm
IMEP	17 bar
SOI	swept
Injection pressure	1400 bar, 1800 bar
Intake air temperature	38 ± 1 K
Intake pressure	2.30 bar
Exhaust pressure	2.40 bar
EGR rate	0, 10%, 15%, 20%
Intake valve closure	-120 CAD ATDC

6.5.2 Combustion and heat release analysis

Figure 6.11 shows the in-cylinder pressure and HRR for the Miller cycle operation with different EGR rates at a constant SOI of -12 CAD ATDC. The addition of EGR delayed the SOC mainly due to the lower in-cylinder oxygen concentration (dilution effect) and lower compression temperature because of the lower specific heat values [106]. This increased the degree of premixed combustion and decreased both the peak HRR and peak in-cylinder pressure. EGR rate of 20% with relatively higher injection pressure of 1800 bar resulted in a different HRR profile from others operating with a constant injection pressure of 1400 bar. The use of a higher injection pressure improved the fuel-air mixing and thus accelerated the rate of heat release, resulting in higher peak HRR and peak in-cylinder pressure.

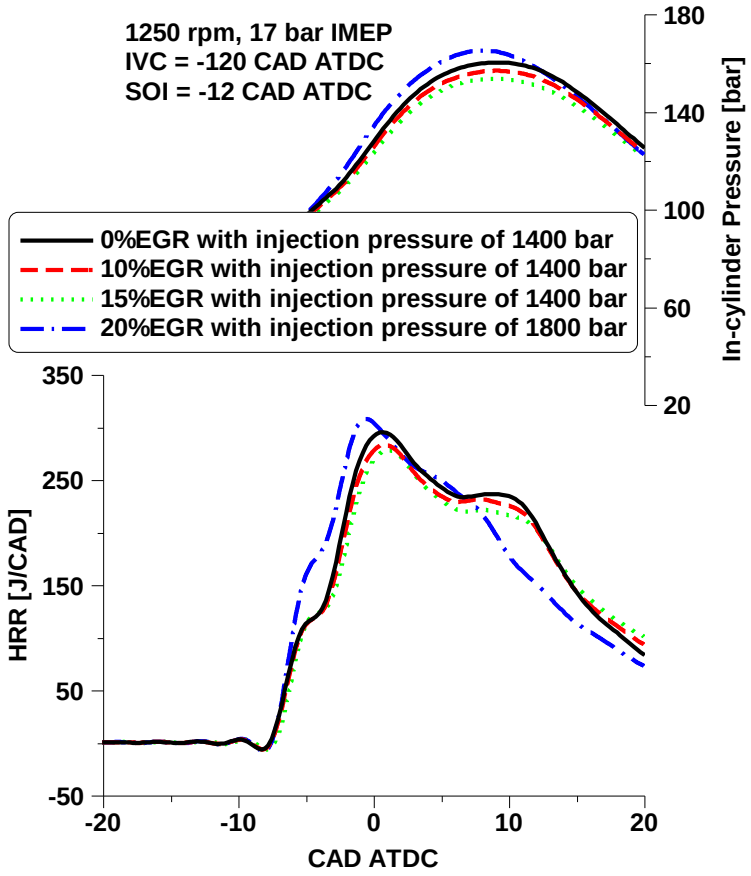

Figure 6.11: In-cylinder pressure and HRR for various EGR rates with a constant SOI.

Figure 6.12 shows the SOI and the resulting heat release characteristics as a function of the CA50. The SOI was advanced as higher EGR rate was introduced. The introduction of EGR resulted in a longer ignition delay due to the thermal and dilution effects, which delayed the SOC. The use of EGR slowed down the diffusion-control combustion process as supported by the longer period of CA50-CA90. This was a result of the later SOC and the lower in-cylinder oxygen concentration. The combination of these effects yielded a longer combustion duration. Overall, the addition of 20% EGR led to the longest combustion duration, despite a relatively higher injection pressure was used.

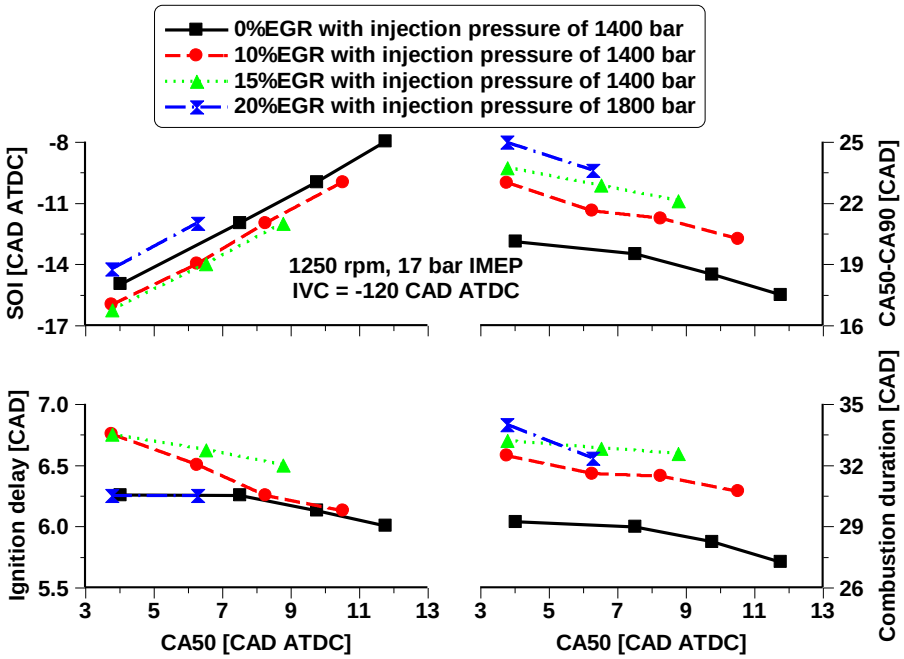

Figure 6.12: Heat release characteristics as a function of CA50 for various EGR rates.

6.5.3 Engine performance and gaseous emissions

Figure 6.13 depicts the engine performance parameters of the Miller cycle with various EGR rates. The use of EGR decreased the lambda noticeably due to the replace of in-cylinder charge with recirculated exhaust gas. The lower lambda as well as the later combustion process as a result of the slowed down diffusion-controlled combustion increased the EGT, particularly in the case with 20% EGR. The addition of 10% EGR had little effect on the combustion efficiency, which is mainly determined by CO and unburn HC emissions. However, the combustion efficiency was gradually reduced with increased EGR rate. The use of 20% EGR led to the lowest combustion efficiency of 99% due to significantly lower lambda and in-cylinder combustion temperature. The NIE exhibited a similar trend to the combustion efficiency, decreased slightly with the addition of 10% EGR while deteriorated rapidly as higher EGR rate was introduced. The lower combustion efficiency and the later and longer combustion duration led to a reduction in the NIE. Overall, Miller cycle operation with an EGR of 20% resulted in the lowest NIE of 42%.

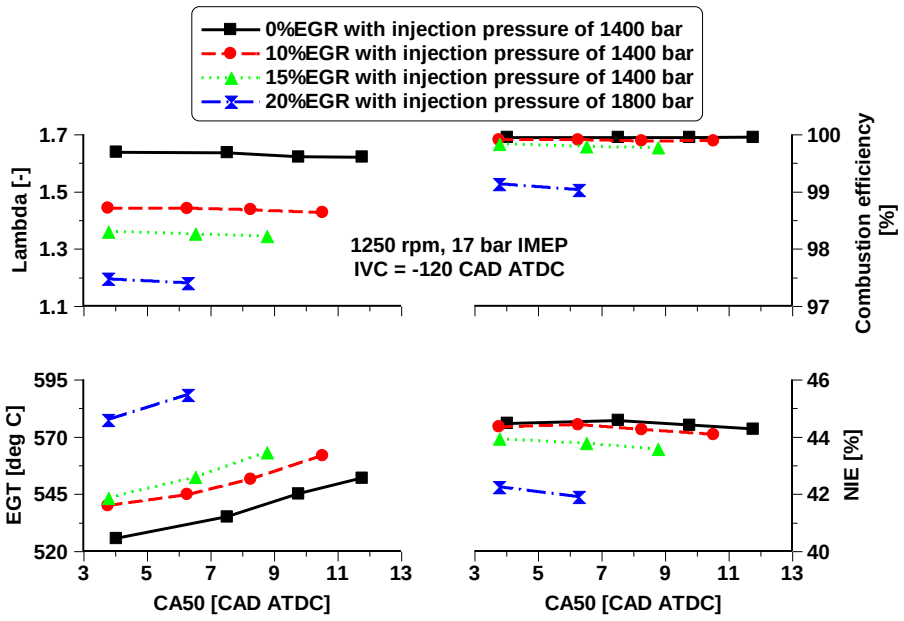

Figure 6.13: Engine performance parameters as a function of CA50 for various EGR rates.

Figure 6.14 shows the net indicated specific emissions for the Miller cycle with various EGR rates. The EGR was effective in curbing NOx emissions at the expense of higher soot emissions. This was due to the lower oxygen availability and in-cylinder gas temperature. At a constant CA50 of 4 CAD ATDC, the use of 10% EGR decreased NOx emissions by 45% while maintaining low level of soot emissions. As the EGR rate was increased, however, the soot emissions were increased noticeably despite a higher NOx emissions reduction. The highest reduction of 85% in NOx emissions was attained with 20% EGR compared to the baseline without EGR. This was achieved at the expense of significantly higher soot emissions, despite a higher injection pressure of 1800 bar was employed. Additionally, a later CA50 strategy effectively decreased the combustion temperatures and therefore NOx emissions.

It can be also seen from Figure 6.14 that the CO emissions exhibited a similar trend to the soot emissions, increasing slightly with lower EGR rates while increasing rapidly as relatively higher EGR rates were introduced. However, the introduction of EGR decreased the unburn HC emissions, especially at higher EGR rates. This was possibly attributed to the relatively lower lambda and higher EGT. The sweep of CA50 demonstrated little impact on CO and HC emissions due to insignificant impact on the lambda value.

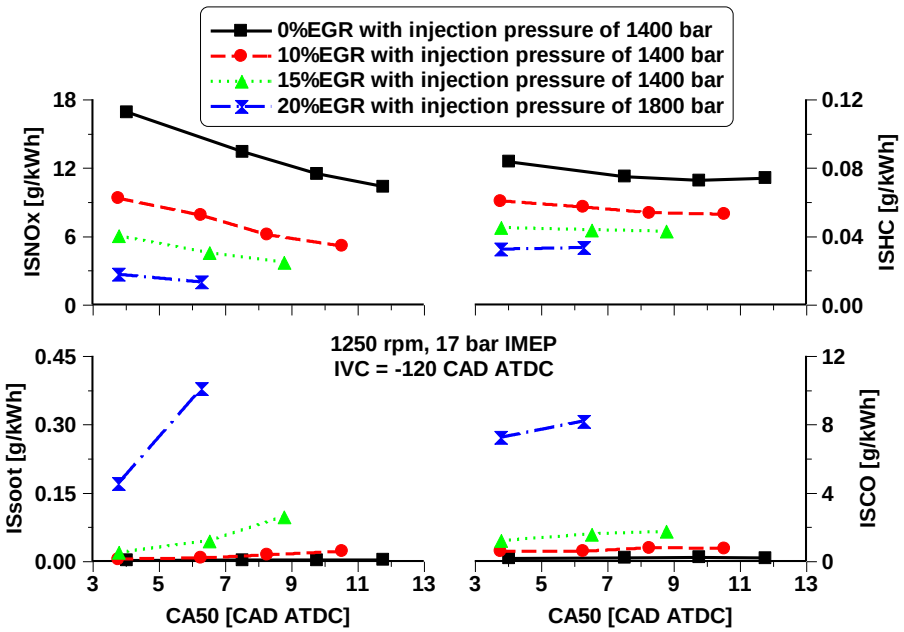

Figure 6.14: Exhaust emissions as a function of CA50 for various EGR rates.

6.6 Exploring the potential of Miller cycle operation with EGR at full engine load

The reduction in NOx emissions from HD diesel engines at high engine loads requires the development of more advanced combustion and control technologies to minimize the EOC. This drives an increased need for highly efficient and clean IC engines. One promising combustion strategy that can curb NOx emissions with a low fuel consumption penalty is to simultaneously reduce the in-cylinder gas temperature and the in-cylinder oxygen concentration. This can be achieved via Miller cycle and EGR, which enables a low EOC by minimizing both the diesel fuel and urea consumptions.

The focus of this subsection is to explore the NOx emissions reduction potential of EGR and Miller cycle with LIVC timing. The effects of Miller cycle and EGR on engine combustion, emissions, and efficiency will be discussed. In the last subsection, the overall exhaust emissions, total fluid consumption, and the $NIE_{corr.}$ will be analysed and compared at the maximum NIE, in order to identify the most effective strategy in terms of EOC.

6.6.1 Test methodology

The experimental investigation was performed at an engine speed of 1250 rpm and a full load of 24 bar IMEP while maintaining intake and exhaust pressures constant. This operating condition is characterized by high peak in-cylinder pressure and combustion temperatures, and hence high NOx formation.

Table 2 summarizes the test conditions for the baseline and Miller cycle operations using 0% and 8%EGR. The SOI was swept and optimized up against the in-cylinder pressure limit of 180 bar in order to achieve the maximum NIE. However, the case of IVC at -114 CAD ATDC with 8%EGR can only be performed with the most advanced SOI as the smoke number was limited to 1 FSN over the test. The injection pressure was held constant at 1800 bar except for the case with an IVC at -114 CAD ATDC and an EGR rate of 8%. In this case, an injection pressure of 2200 bar was used to overcome the combustion instability and excessive smoke. Stable engine operation was determined by controlling the COV_IMEP below 3%.

Table 6.5: Engine testing conditions.

Speed	1250 rpm					
IMEP	24 bar					
Intake Pressure	3.0 bar					
Exhaust Pressure	3.1 bar					
IVC	Baseline		Miller cycle			
	-178 CAD ATDC		-127 CAD ATDC		-114 CAD ATDC	
ECR	16.8		15.9		15.2	
Injection Pressure	1800bar					2200 bar
EGR Rate	0%	8%	0%	8%	0%	8%

The intake and exhaust valve lift profiles used for the baseline and Miller cycle operations are illustrated in Figure 6.15. The IVO timing was set at 367 CAD ATDC while the IVC was delayed from -178 CAD ATDC in the baseline case to -127 and -114 CAD ATDC in the Miller cycle strategies.

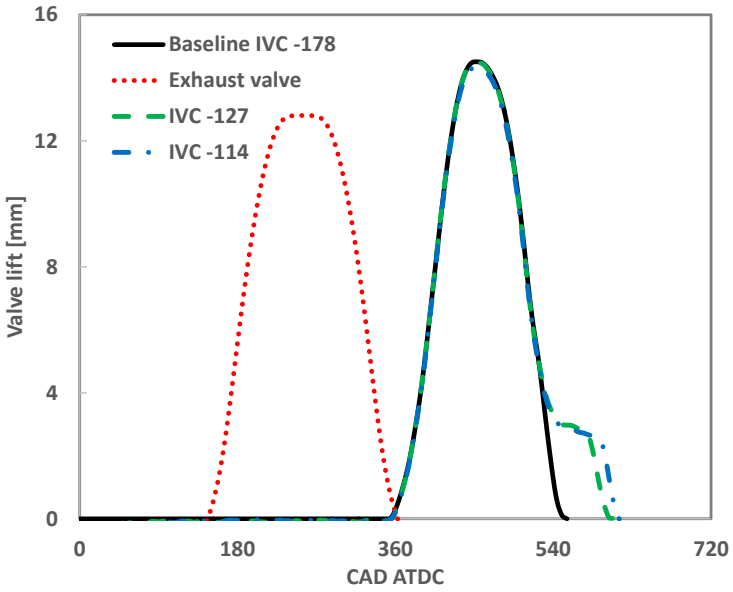

Figure 6.15: Fixed exhaust and variable intake valve lift profiles.

6.6.2 Combustion and heat release analysis

Figure 6.16 shows the in-cylinder pressure and HRR for both the baseline (IVC at -178 CAD ATDC) and the Miller cycle (IVCs at -127 and -114 CAD ATDC) operations with and without EGR. The comparison was performed with a constant SOI at -3 CAD ATDC. Compared to the baseline case, the Miller cycle strategy decreased the compression pressure as a result of the reduction of in-cylinder air flow rate and density. The maximum in-cylinder pressure difference between the baseline and the Miller cycle was approximately 25 bar at the end of compression. The lower compression pressure led to a significant reduction in peak in-cylinder pressure and heat release rate during the combustion process.

The use of EGR with baseline IVC showed less impact on the in-cylinder pressure and peak HRR compared to the Miller cycle strategy, due to the replacement of the fresh air with recirculated exhaust gas instead of reducing the total in-cylinder mass with the Miller cycle strategy. Overall, the combined strategy of Miller cycle and EGR achieved the highest reduction in the P_{max} and the peak HRR due to the reduced in-cylinder air flow caused by the late IVC as well as the dilution effect and higher heat capacity introduced by EGR.

The SOI is an important factor in maximizing engine efficiency and curbing emissions. In order to achieve high NIE, the SOI should be optimized for the main heat release to take place immediately after TDC. Thus, the SOI was swept for various combustion control strategies. The data in Figure 6.17 depicts the sensitivity of maximum in-cylinder pressure

and NIE with respect to SOI at different IVCs with and without EGR. The selected calibrations for different combustion control strategies are denoted with a green circle and will be analysed later on.

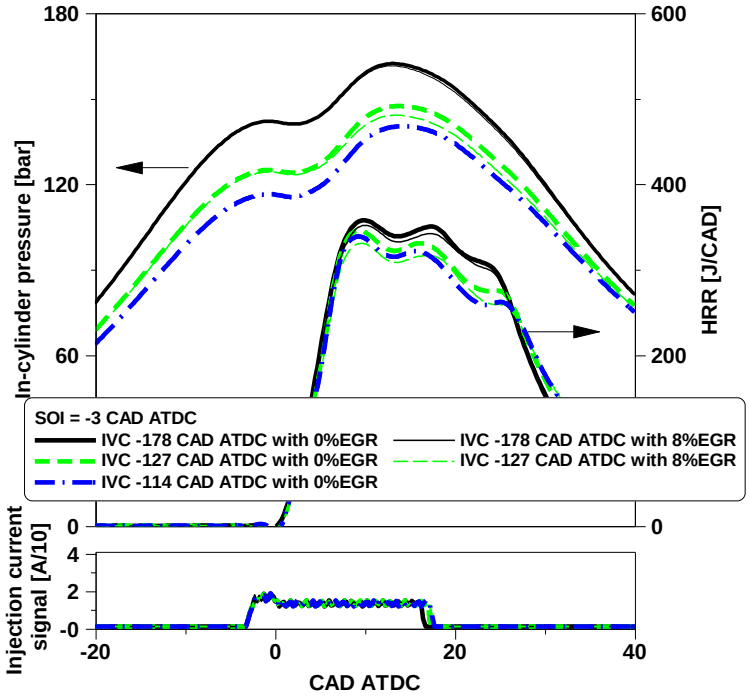

Figure 6.16: The effect of Miller cycle and EGR on in-cylinder pressure and HRR at the same diesel SOI.

As shown in Figure 6.17, the P_{max} and NIE increased linearly as the SOI was advanced for the range of injection timings tested. The maximum NIE were achieved by the most advanced cases, which were limited by the peak in-cylinder pressure of 180 bar. Figure 6.18 depicts the in-cylinder pressures and HRR of various IVCs with and without EGR for the selected calibrations from Figure 6.17. The dilution and higher heat capacity introduced by EGR slowed down the combustion process and slightly reduced the in-cylinder pressure, as depicted in Figure 6.16, allowing for a more advanced SOI to maximize NIE. However, the difference between the optimized (most advanced) diesel SOI with and without EGR of the baseline IVC was less significant than the Miller cycle operation. By delaying IVC, the Miller cycle enabled a more advanced SOI and earlier heat release as a result of the lower ECR. The application of a higher injection pressure in the IVC at -114 CAD ATDC with 8%EGR required retarding CA50 due to the increased P_{max}. Therefore, the earliest heat release was obtained by an IVC at -114 CAD ATDC with no EGR where SOI was the most advanced.

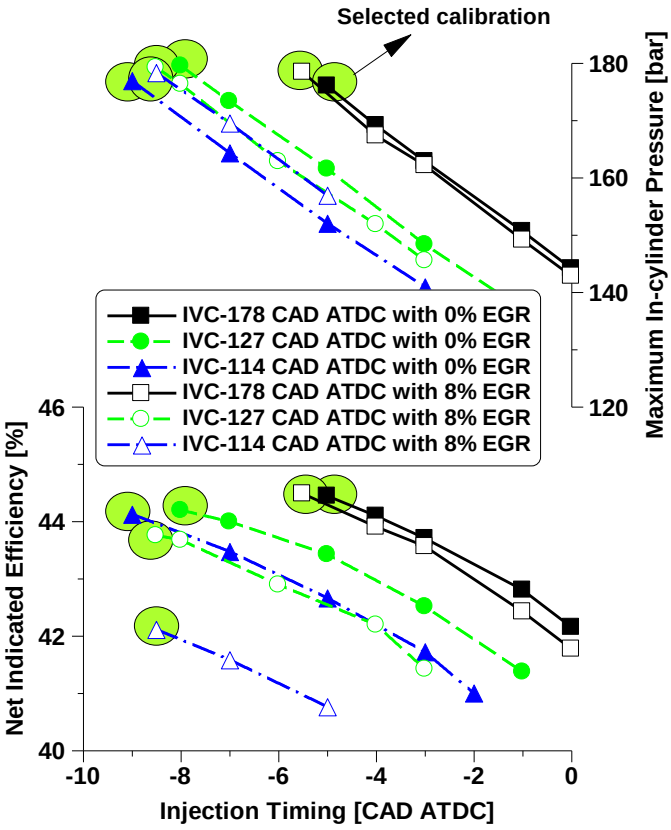

Figure 6.17: P_{max} and NIE vs diesel SOI for various IVC timings with and without EGR.

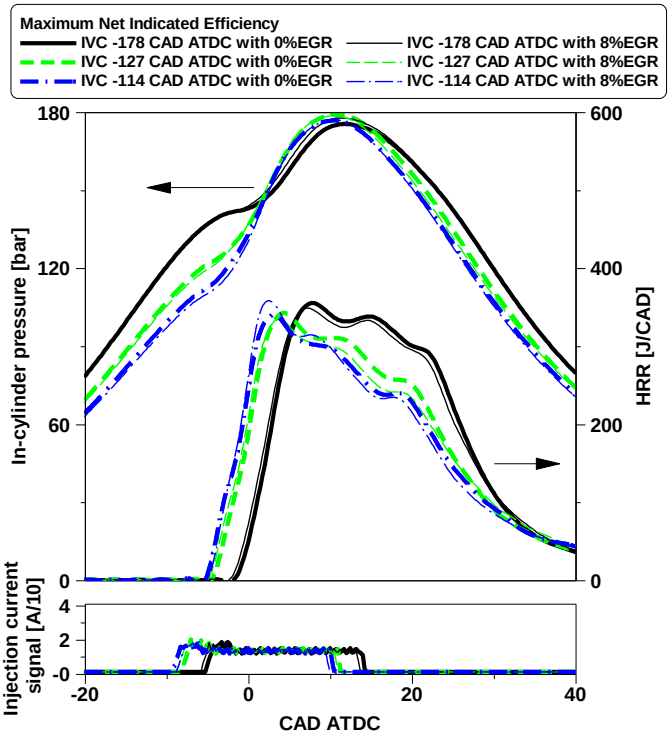

Figure 6.18: The effect of Miller cycle and EGR on in-cylinder pressure and HRR at the optimum SOI.

Figure 6.19 shows the resulting heat release characteristics for the baseline operation with IVC at -178 CAD ATDC and the Miller cycle with IVC at -127 and -114 CAD ATDC. The comparison was performed with a constant SOI at -3 CAD ATDC and the most advanced SOI of the optimum cases, with and without EGR. At full load condition, the changes in ignition delay and the degree of premixed combustion are very marginal with different IVC timings due to the relatively better ignition conditions [164]. A similar trend was observed in this study, the Miller cycle slightly increased the ignition delay by lowering the initial in-cylinder pressure and temperature. The addition of EGR further prolonged the ignition delay when combined with late IVCs. The longer ignition delay in both Miller cycle and EGR strategies led to later CA50, as showed in Figure 6.19. With the maximum efficient cases, the reduction of in-cylinder pressure during the compression stroke allowed for more advanced SOI and earlier CA50 than those attained at constant SOI.

In addition, as a result of the reduced in-cylinder charge and the dilution effect, both Miller cycle and EGR strategies reduced the in-cylinder oxygen availability during the mixing-controlled combustion stage, leading to a slower later combustion process as measured by CA50-CA90. Moreover, the Miller cycle with EGR strategy yielded the longest mixing-controlled combustion process and combustion duration but the earliest combustion phasing measured by CA50.

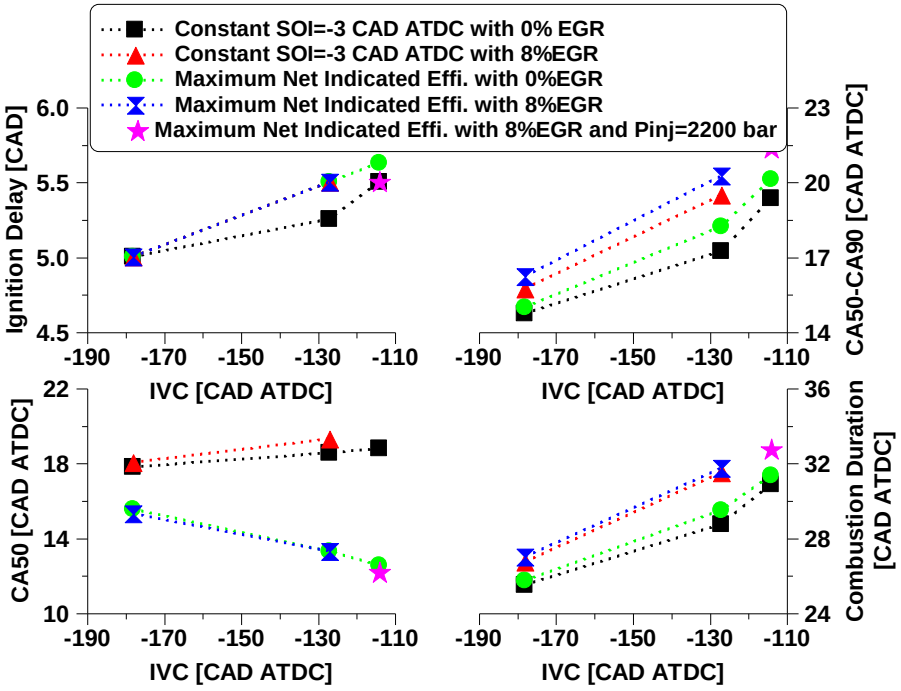

Figure 6.19: The effect of Miller cycle and EGR on the resulting heat release characteristics.

6.6.3 Engine performance and exhaust emissions

Figure 6.20 shows that the use of Miller cycle and EGR significantly reduced the lambda, especially in the cases of EGR with a constant SOI at -3 CAD ATDC. The lowest lambda below 1.2 was measured for the case with an IVC at -114 CAD ATDC and 8% EGR despite the higher injection pressure. The more advanced SOI in the most efficient cases showed higher lambda value than those at a constant SOI as less fuel was burned to maintain the same IMEP when the NIE was increased.

The EGT increased linearly with a decrease in lambda regardless of the strategy used. The Miller cycle led to a notably decrease in lambda, which in turn increased the EGT. The use of EGR presented a little impact on the EGT when operating with the baseline IVC, which can be explained by the dilution and higher heat capacity introduced by EGR, resulting in lower in-cylinder gas temperatures [100]. Besides, the higher lambda value at the baseline IVC with EGR was also the primary reason for the insignificant effect on EGT. However, the addition of EGR showed significant impact on EGT when operating with Miller cycle due to much lower lambda with a delayed IVC.

Figure 6.20 also shows the NIE and fuel consumption of the baseline and the Miller cycle at a constant and optimised SOI for the maximum efficient operations, with and without EGR. It can be seen that the NIE reduced rapidly with delayed IVC while varied slightly in the use of EGR with the baseline IVC. This can be explained by the longer combustion duration in the cases with late IVC timings. Another possible reason is the higher T_m in the Miller cycle due to the reduced total in-cylinder gas heat capacity, resulting in higher heat loss to the cylinder walls. This has been presented in our previous study [209] by using an one-dimensional engine simulation model to calculate the T_m and T_b at 6 bar and 12 bar IMEP. Results revealed that a higher T_m was observed in the Miller cycle strategy while the T_b was reduced due to retarded and slowed down combustion process. As the pressure difference between intake and exhaust manifolds was kept constant during the test, the influence of pumping loss could be negligible.

With the use of EGR and an IVC at -178 CAD ATDC, the NIE decreased slightly at a constant SOI. This was the net result of these two counteracting effects of the prolonged combustion duration and the lower heat transfer loss resulted from higher heat capacity and hence lower combustion temperatures. With late IVCs, the addition of EGR has been observed to notably increase ISFC and thus lower NIE. Without EGR, the NIE was significantly increased in the most efficient cases by advancing the SOI. The high efficiency was maintained when the IVC was delayed from -178 to -114 CAD ATDC. With

EGR, however, the NIE was decreased with late IVC even with the most advanced SOI. In particular, the maximum reduction of NIE by 3.8% in the most efficient cases was obtained when IVC was delayed from -127 to -114 CAD ATDC with 8%EGR, although a higher injection pressure of 2200 bar was applied. As such, the combined effects of the net heat transfer loss and longer combustion duration as well as the late combustion process after TDC accounted for the lower NIE in the combined strategy of Miller cycle with EGR at high engine loads.

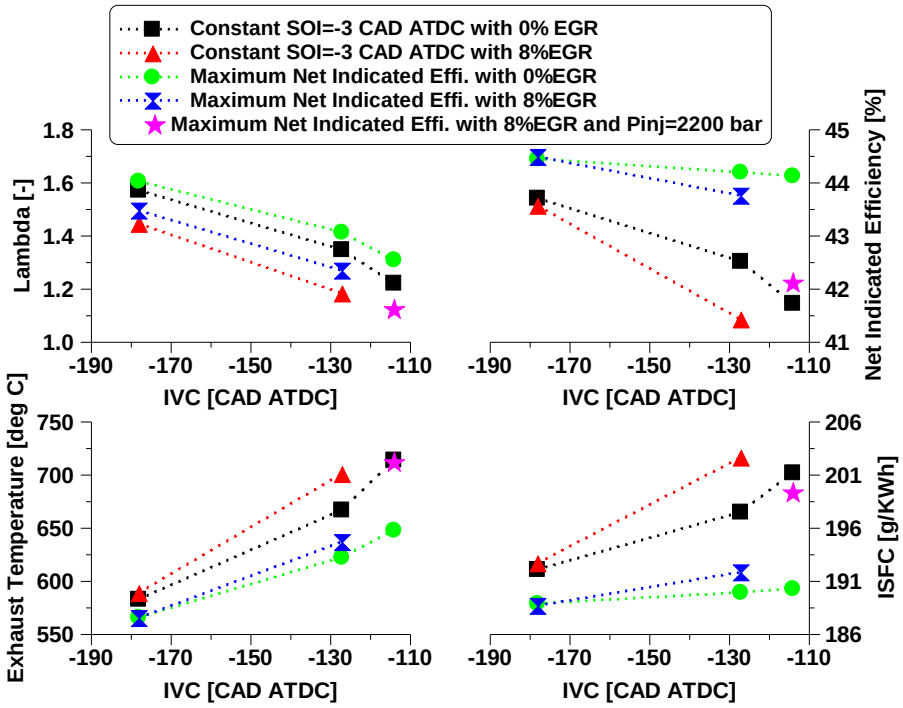

Figure 6.20: The effect of Miller cycle and EGR on lambda and exhaust gas temperatures.

Figure 6.21 depicts the engine-out emissions for various IVC timings with and without EGR shown as the net indicated specific values of NOx, soot, unburned HC and CO. By delaying the IVC, the Miller cycle effectively reduced the NOx emissions primarily due to the lower in-cylinder oxygen availability and flame temperatures. In addition, the lower peak in-cylinder pressure and later combustion phasing were also beneficial to the NOx abatement. The use of EGR was more effective in abating NOx emissions than the Miller cycle strategy attributed to the particular dilution effect and higher heat capacity in decreasing flame temperature. The NOx levels were reduced from 12.8 g/kWh in the baseline to 7.1 g/kW h in the IVC -178 with EGR. The application of Miller cycle with EGR strategy allowed for higher NOx reduction due to relatively lower oxygen availability and in-cylinder gas temperatures, decreasing NOx levels from 12.8 g/kWh to 3.9 g/kWh, approximately by 69%. It is noted that the NOx emissions in the most efficient cases was

slightly higher than that in a constant SOI due to more advanced combustion near TDC and hence higher combustion temperatures.

The soot and CO emissions exhibited a different trend from that of NOx emissions when using Miller cycle and EGR strategies. The soot emissions were less affected by the use of EGR in the IVC of -178 due to a sufficiently high lambda. However, an apparent increase in soot emissions was observed as the IVC was delayed to -114 CAD ATDC attributed to the significantly lower lambda, as shown in Figure 6.20. In the combination of Miller cycle and EGR strategy, the soot emissions increased noticeably and could be improved by advancing the SOI with an IVC at -127 CAD ATDC. However, the lambda dropped lower than 1.2 when the IVC was delayed to -114 CAD ATDC, leading to significantly higher soot emissions. The availability of oxygen in the cylinder played the dominant role on the CO emissions since the combustion temperatures at full load were sufficiently high to maintain a high combustion efficiency, regardless of the strategy used. Likewise, the CO emissions in the Miller cycle and EGR strategies were significantly improved at the most efficient cases, except for the case with IVC at -114 CAD ATDC and 8%EGR. Figure 6.21 also shows that the HC emissions were low in all cases at this operation load. Different from the observed trend of other emissions as shown earlier, the unburned HC showed less sensitivity to the diesel SOI when varying the IVC with or without EGR. Overall, the combination of Miller cycle and EGR achieved the lowest HC emissions, mainly due to the highest fuel/air equivalence ratios and EGT.

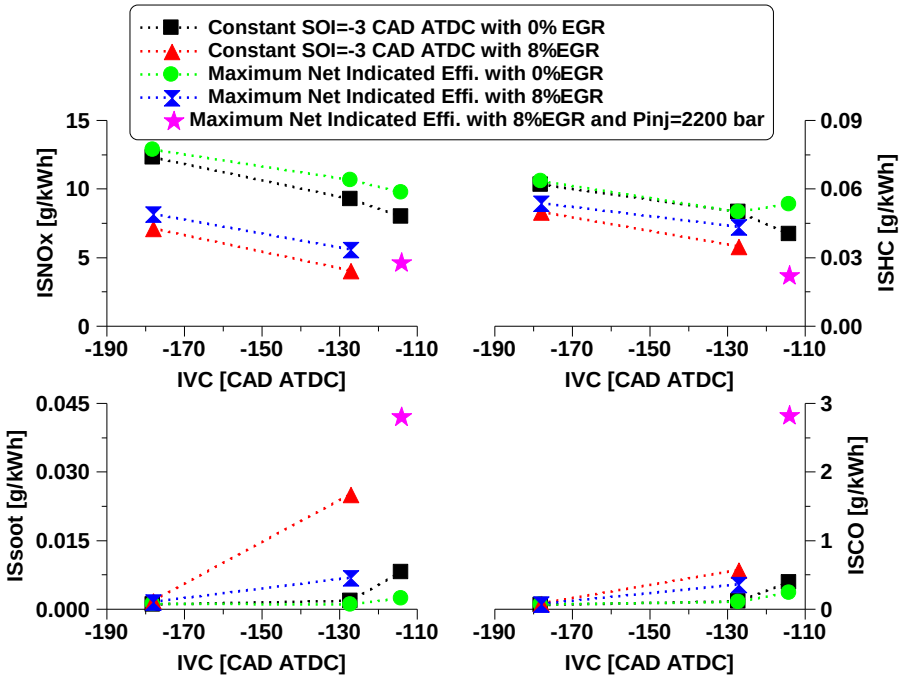

Figure 6.21: The effect of Miller cycle and EGR on engine emissions.

An improvement in the NOx-Soot and NOx-ISFC trade-off relationships was observed when applying Miller cycle and EGR strategies, as shown in Figure 6.22. The Miller cycle strategy alone did not has a great potential in reducing NOx emissions and accompanied with a higher fuel consumption penalty. It can be seen that NOx emissions at IVC -114 with no EGR was reduced by 35% with fuel efficiency penalty of 4% when compared to the baseline case. A higher reduction in NOx emission by 45% with minor fuel efficiency penalty could be obtained by using EGR strategy with IVC at -178 CAD ATDC.

Overall, the introduction of 8% EGR combined with Miller cycle at IVC -127 showed the best trade-off between NOx, ISFC and soot. This can be explained by the high potential of NOx reduction using EGR combined with the high capability in decreasing the peak in-cylinder pressure via delaying IVC. Thus, this strategy allowed for an earlier combustion phasing to minimize fuel efficiency penalty and soot emissions while maintaining lower NOx level benefit achieved by EGR. Additionally, the combined strategy achieved the biggest benefit in NOx abatement, decreasing the NOx levels of the baseline case by 57% and the fuel efficiency by 1.6% while maintaining soot emissions below Euro VI limit of 0.01 g/kWh.

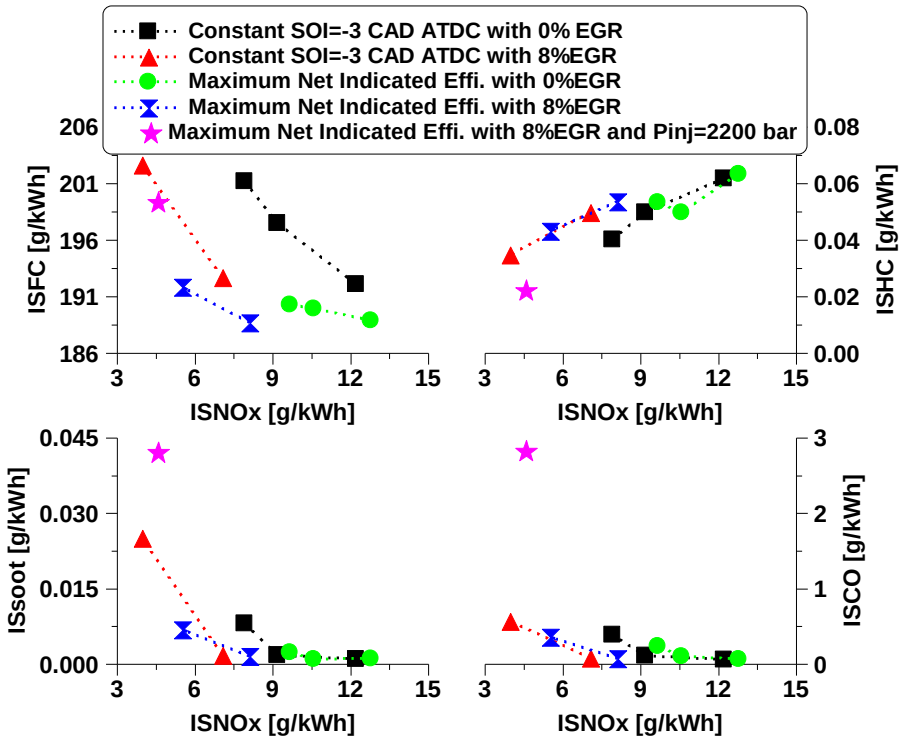

Figure 6.22: The effect of Miller cycle and EGR on NOx, ISFC and ISssot trade-offs.

6.6.4 Estimation of the cost-benefit and overall emissions at the maximum NIE

As described in subsection 4.5.3 of Chapter 4, a urea SCR system was assumed for NOx control in order to estimate the influence of different combustion control strategies on the EOC. Since the EOC is determined by several aspects, such as diesel fuel and aqueous urea solution consumptions, fuel prices, engine efficiency, and engine-out NOx emissions, the EOC might not be the lowest with a high engine efficiency setup. Therefore, an analysis of cost-benefit and overall emissions was carried out at the optimum NIE, in order to determine the best trade-off between the engine efficiency and the engine-out NOx emissions for minimizing the total fluid cost and thus the EOC.

Figure 6.23 shows the diesel fuel flow rate and the required urea consumption to meet Euro VI NOx limit for each case. Both EGR and Miller cycle strategies increased the diesel fuel flow rate as explained previously. Advancing combustion phasing in terms of the most efficient cases resulted in significantly lower diesel fuel flow rate compared to those at a constant SOI. With the use of EGR, the required urea flow rate dropped clearly due to decreased engine-out NOx emissions.

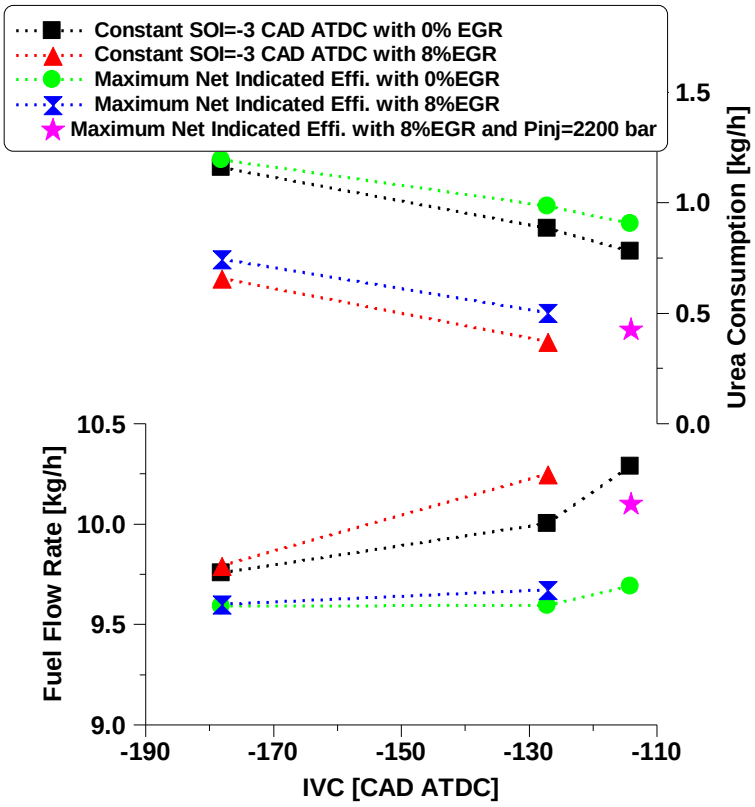

Figure 6.23: Diesel fuel flow rate and the required urea flow rate for various strategies.

Figure 6.24 shows an overall comparison of ISNOx, ISFC, the required urea consumption in the SCR system, as well as the total fluid consumption and the $NIE_{corr.}$. The analysis was carried out with the maximum engine efficiencies in various strategies. The resulting values of IVC at -178 CAD ATDC with no EGR was used as the reference value. As for the case of IVC at -114 CAD ATDC with 8%EGR, a higher injection pressure of 2200 bar was applied to avoid excessive smoke and lower engine efficiency.

The baseline IVC with no EGR led to the lowest $NIE_{corr.}$, although the highest fuel efficiency was achieved. This was a result of the higher urea consumption required in the SCR system due to the higher engine-out NOx emissions, resulting in an increase of the total fluid consumption. Both Miller cycle and EGR strategies showed higher $NIE_{corr.}$ than the baseline mainly attributed to the lower total fluid consumption despite a small fuel efficiency penalty.

It can be seen that the highest $NIE_{corr.}$ of 41.6% was achieved when the IVC was delayed to -127 CAD ATDC with 8% EGR, owing to the significantly lower engine-out NOx emissions. Although the highest reduction of NOx emissions by 64% was obtained when delaying IVC to -114 CAD ATDC with 8%EGR, the fuel efficiency noticeably reduced, leading to lower $NIE_{corr.}$ than IVC at -127 CAD ATDC with 8%EGR. Overall, among these strategies the Miller cycle with IVC at -127 CAD ATDC combined with 8%EGR showed the optimum trade-off between engine-out NOx emissions and engine efficiency, reducing the total fluid consumption by 5.8% and increasing the $NIE_{corr.}$ by 5.3% compared to reference case.

Therefore, the combination of Miller cycle and external cooled EGR strategy at a fixed boost pressure shows a great potential to reduce engine-out NOx emissions with little impact on fuel efficiency, while achieving the lowest total fluid consumption and consequently the highest $NIE_{corr.}$. The results also demonstrate the optimum balance existed between in-cylinder NOx control and aftertreatment NOx control and it is determined by the total fluid consumption and the $NIE_{corr.}$.

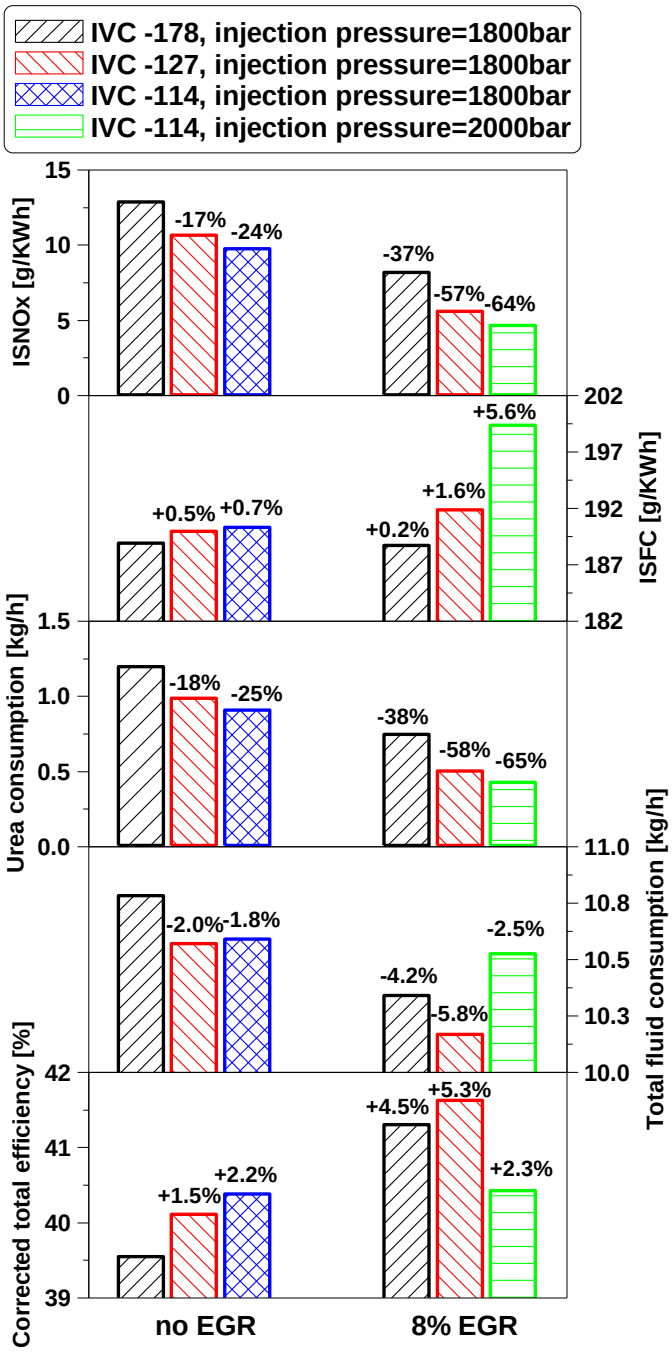

Figure 6.24: Overall evaluation of NOx reduction potential for various combustion strategies.

6.7 Summary

This chapter has presented the experimental results of high load Miller cycle operation and explored the potential of Miller cycle with EGR for emissions control and efficiency improvement at the full engine load. Application of the Miller cycle at high loads is desirable, as it helps to minimise the mechanical and thermal loads as well as improve the trade-off of engine efficiency and NOx emissions and thus lower the total engine operational cost. However, the Miller cycle at high engine loads had adverse effects on

engine efficiency and smoke number due to decreased in-cylinder mass. The influences of combustion phasing, injection pressure, intake pressure, and EGR rate on the Miller cycle combustion process were explored in an attempt to attain high efficient and low emissions engine operation.

The primary findings of the high load Miller cycle operation with different combustion control strategies can be summarised as below:

i. The application of Miller cycle via LIVC lowered the compression pressure and temperature, so that the peak in-cylinder pressure and NOx emissions could be reduced simultaneously at the expense of higher smoke number and lower engine efficiency, when the combustion phasing was kept constant.
ii. Miller cycle allowed the earlier combustion to take place without exceeding the peak in-cylinder pressure limit of 180 bar. The Miller cycle with an earlier combustion phasing achieved low levels of NOx while maintaining the NIE and smoke number similar to that of the baseline.
iii. A higher injection pressure improved the atomization of fuel and enhanced the fuel-air mixing process, allowing for a higher NIE and significantly lower soot emissions. These improvements were attained at the expense of lower NOx reduction.
iv. An increase in the intake pressure effectively increased the in-cylinder oxygen availability and hence improved the combustion process, improving upon the NIE and soot emissions of the Miller cycle combined with EGR strategy. In particular, Miller cycle with constant lambda allowed for simultaneous low levels of NOx and soot emissions while achieving higher NIE than the baseline operation.
v. The introduction of EGR was effective in reducing the NOx emissions, decreasing the NOx level by 45% at an EGR rate of 10% while introducing little impact on the NIE and soot emissions. However, a higher EGR could deteriorated the engine efficiency and yielded excessive smoke attributed to the significantly lower in-cylinder oxygen availability. Therefore, the EGR rate should be optimized properly when operating with Miller cycle.

The results of exploring the potential of Miller cycle operation with EGR at full load also reveal that

i. The use of EGR was more effective in minimizing NOx emissions than the Miller cycle strategy while maintaining a similar engine efficiency to that of baseline case. This was a result of lower average and flame combustion temperatures as well as oxygen concentration introduced from EGR, which are critical to the NOx formation

and the lower combustion temperature is beneficial to the heat losses reduction.

ii. For a certain intake pressure, a greater potential in reducing peak in-cylinder pressure by Miller cycle combined with the higher NOx reduction potential of EGR produced the best NOx-ISFC and NOx-soot trade-offs with optimized SOI.

iii. The Miller cycle with IVC -127 CAD ATDC combined with 8% EGR was effective in reducing engine-out NOx emissions by approximately 57% with negligible impact on the fuel efficiency compared to the baseline IVC with no EGR, while maintaining the soot emissions below Euro VI limit. This improvement notably minimized the required urea consumption in the SCR system and thus achieved the highest $NIE_{corr.}$.

iv. There is an optimum balance between in-cylinder NOx control and aftertreatment NOx control to obtain the lowest total engine operational cost, which could be achieved by the optimization of Miller cycle and EGR strategies. A reduction in the total fluid consumption by 5.8% was achieved via this combined strategy in the full load of 24 bar IMEP and speed of 1250 rpm with a constant intake pressure of 3 bar.

The above results have demonstrated that the Miller cycle with LIVC strategy allowed for the use of more advanced combustion control strategies to enable high efficiency as well as low NOx and soot emissions at high engine load operation. Nevertheless, combustion control parameters such as the CA50, injection pressure, intake pressure, EGR rate, as well as IVC timing need to be carefully optimised to minimise the EOC of Miller cycle operation.

Chapter 7
Exploring the potential of Miller cycle with and without EGR for maximum efficiency and minimum exhaust emissions

7.1 Introduction

The previous chapters have presented the results of Miller cycle operation from low to full engine loads separately. In this chapter, Miller cycle operation with different emission control and fuel efficiency technologies will be shown and compared to the baseline case at the maximum $NIE_{corr.}$ at a steady-state engine speed of 1250 rpm and engine loads between 25% and 100% of full load. Furthermore, the cycle-averaged results calculated over the WHSC test cycle will be presented and discussed. Finally, the potentials of Miller cycle with EGR (SCR + EGR) and without EGR (SCR-only) to meet the Euro VI emission regulation are assessed at different NOx aftertreatment efficiencies. The aim of the investigation is to explore Miller cycle based cost-effective emission control and fuel efficiency technologies that could be suitable for the “SCR-only” and “SCR + EGR” technical routes for future HD diesel engines.

7.2 Test procedure

In this chapter, the effects of Miller cycle combined with different combustion technologies such as EGR and boost pressure on engine performance and exhaust emissions, as well as total EOC were evaluated over the WHSC test cycle.

Figure 7.1 shows the location of the WHSC test points over a HD diesel engine operation map. There are 13 modes in the WHSC test cycle (red circles), which consist of five speeds (25%, 35%, 45%, 55%, and 75%, which are abbreviated as A, B, C, D, and E, respectively) and four engine loads (25%, 50%, 70%, and 100%), as well as two idle modes at the beginning and the end of test cycle. The size of the circle represents the weighting factor. A bigger size indicates a higher relative weighting of the engine operation conditions over the WHSC cycle.

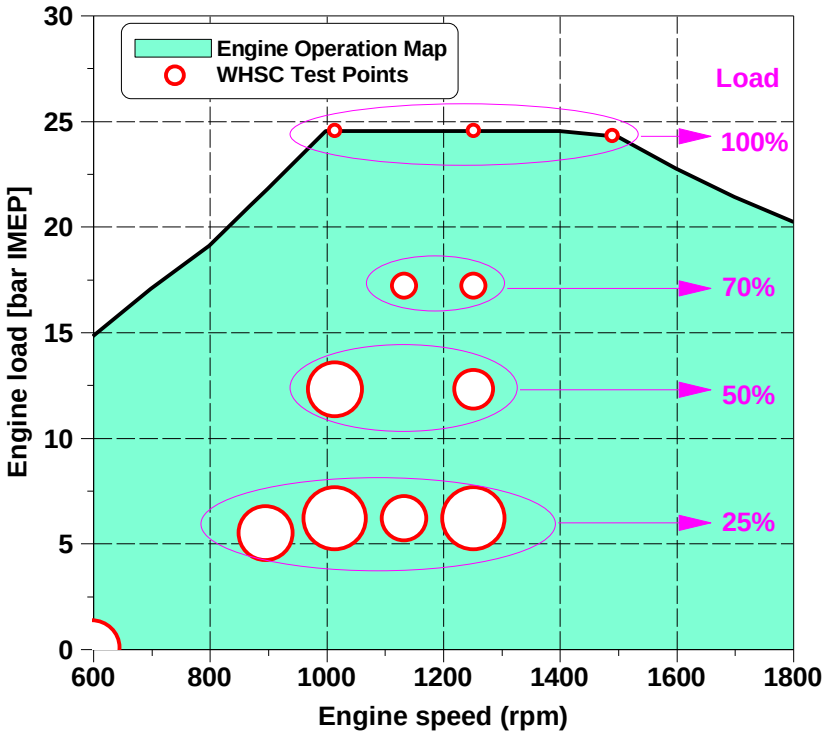

Figure 7.1: The WHSC operation conditions over an estimated HD diesel engine speed-load map.

Table 7.1 summarises the engine operating conditions for the different combustion control strategies investigated between 25% and 100% of full engine loads. The intake pressure (P_{int}) set point of the baseline operation was taken from a corresponding multi-cylinder HD diesel engine, which complies with the Euro V emission regulations. The exhaust pressures were adjusted to provide a constant pressure differential of 0.10 bar above the intake pressure, in order to simulate the actual engine operation with a turbocharger and realize the required EGR rate. An analysis of operating with constant lambda and constant P_{int} was carried out on the Miller cycle operation (using the respective set points from the baseline engine operation) to help evaluate the potential of the technology.

With regard to the operations with EGR, the EGR rate was kept constant for all combustion control strategy at a given load. An EGR rate of 15% was used between 25% and 70% engine loads, and was decreased to 8% at 100% engine load. The moderate EGR rates were used in this study to avoid the combustion instability, excessive smoke, poor fuel efficiency, as well as to minimise the demand on the boosting system when operating the engine with Miller cycle and EGR. These were also the reasons for the relatively earlier IVC timings used in the cases with EGR when compared to a Miller cycle operation without EGR. The IVC timings of EGR cases were varied from -100 to -130 CAD ATDC and they were from -92 to -120 CAD ATDC for cases without EGR as the engine load increased.

Table 7.1: Test conditions for baseline and Miller cycle with and without EGR from low to full engine loads.

Engine load	Rail Pressure	EGR	Exhaust pressure	Baseline operation		Miller cycle operation			
						Intake pressure		IVC	
				Intake pressure	IVC	Constant P_{int}	Constant lambda	Without EGR	With EGR
% of full load	bar	%	bar	bar	CAD ATDC	bar	bar	CAD ATDC	CAD ATDC
25	1150	0 and 15	0.10 bar higher than the intake pressure	1.44	-178	1.44	2.10	-92	-100
50	1400	0 and 15		1.74	-178	1.74	2.35	-100	-110
70	1500	0 and 15		2.30	-178	2.30	2.70	-110	-120
100	1800	0 and 8		2.70	-178	2.70	3.10	-120	-130

During the experiments, a small pilot injection of 3 mm^3 with a constant dwell time of 1 ms prior to the main injection timing was employed for both 25% and 50% engine load conditions in order to keep the maximum PRR below 30 bar/CAD. The coolant and oil temperatures were kept within 85 ± 2°C. Oil pressure was maintained within 4.0 ± 0.1 bar. The maximum in-cylinder pressure was limited to 180 bar. Stable engine operation was determined by controlling the COV_IMEP below 3%.

7.3 Miller cycle operation with and without EGR

In this subsection, Miller cycle operation with and without EGR using constant P_{int} and a constant lambda as those of the baseline cases were investigated in order to analyse the effect of Miller cycle on engine performance, exhaust emissions, and total EOC over the engine loads. The results were analysed and comparisons were made with the baseline operations at 1250 rpm over a range of loads from 25% to 100% of full engine load. Diesel injections were optimised for the maximum $NIE_{corr.}$.

7.3.1 Analysis of the in-cylinder pressure and heat release rate

Figure 7.2 shows the in-cylinder pressure, HRR, and diesel injector signal for cases attained the maximum $NIE_{corr.}$ at 50% of full engine load. The Miller cycle operation without EGR and with a constant P_{int} of 1.74 bar as the baseline operation was characterised by lower in-cylinder pressure and peak HRR. This was due to the later initiation of the compression process resulted from the LIVC and hence lower in-cylinder compressed pressure and temperature. The use of EGR allowed for a more advanced diesel SOI to achieve the maximum $NIE_{corr.}$ when compared to the cases without EGR. This enabled an earlier SOC, consequently increasing the peak in-cylinder pressures of the optimum cases. When operating with constant lambda by increasing the intake pressure, Miller cycle with

and without EGR achieved relatively higher peak HRR, although a later main SOI than that with constant P_{int}.

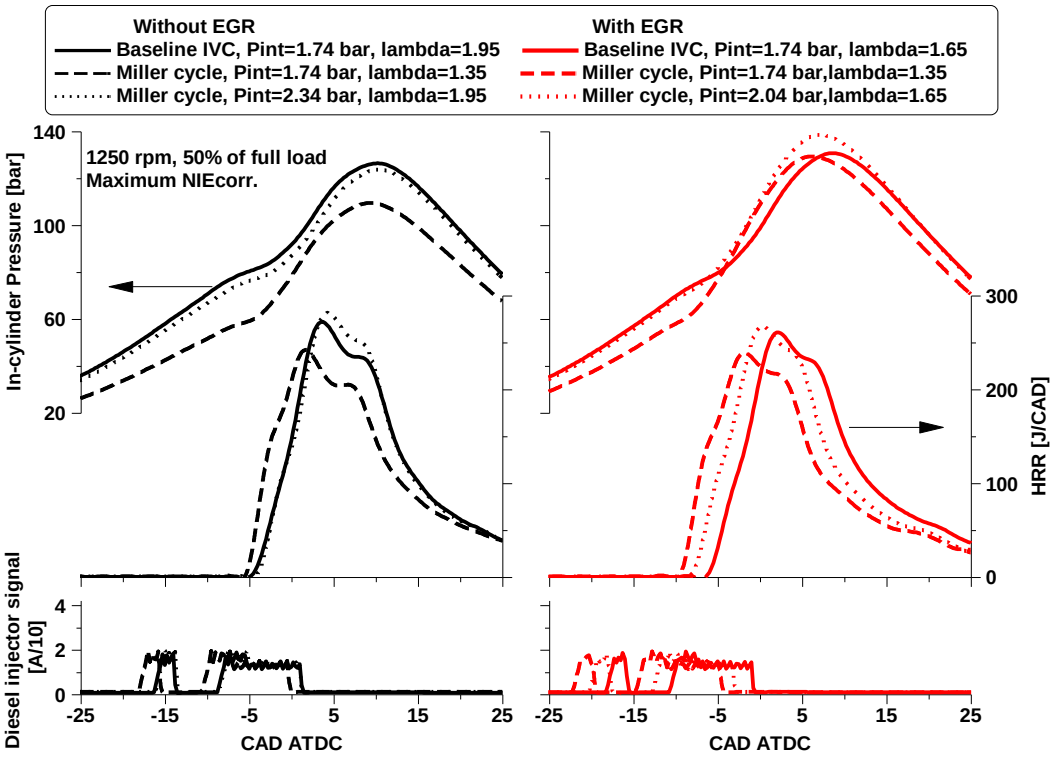

Figure 7.2: In-cylinder pressure, HRR, and diesel injector signal for the baseline and Miller cycle cases with the maximum $NIE_{corr.}$.

Figure 7.3 depicts the in-cylinder pressure, HRR, and diesel injector signal for cases with same engine-out NOx levels. The NOx emissions were controlled at 8.0 g/kWh for cases without EGR and 4.0 g/kWh for those with EGR. This was attributed to the limited capability in reducing NOx emissions by Miller cycle alone compared to the EGR strategy. Miller cycle allowed for an earlier main SOI to achieve similar NOx levels to that of the baseline case. This was attributed to the lower peak combustion temperature and in-cylinder oxygen availability. In particular, the LIVC significantly advanced the main SOI for the cases with EGR thanks to the relatively lower in-cylinder oxygen concentration and thus the NOx emissions. As a result, the P_{max} was higher than that of the baseline case. A higher P_{int} improved the in-cylinder oxygen availability, which helped accelerate the combustion rate and consequently higher peak HRR.

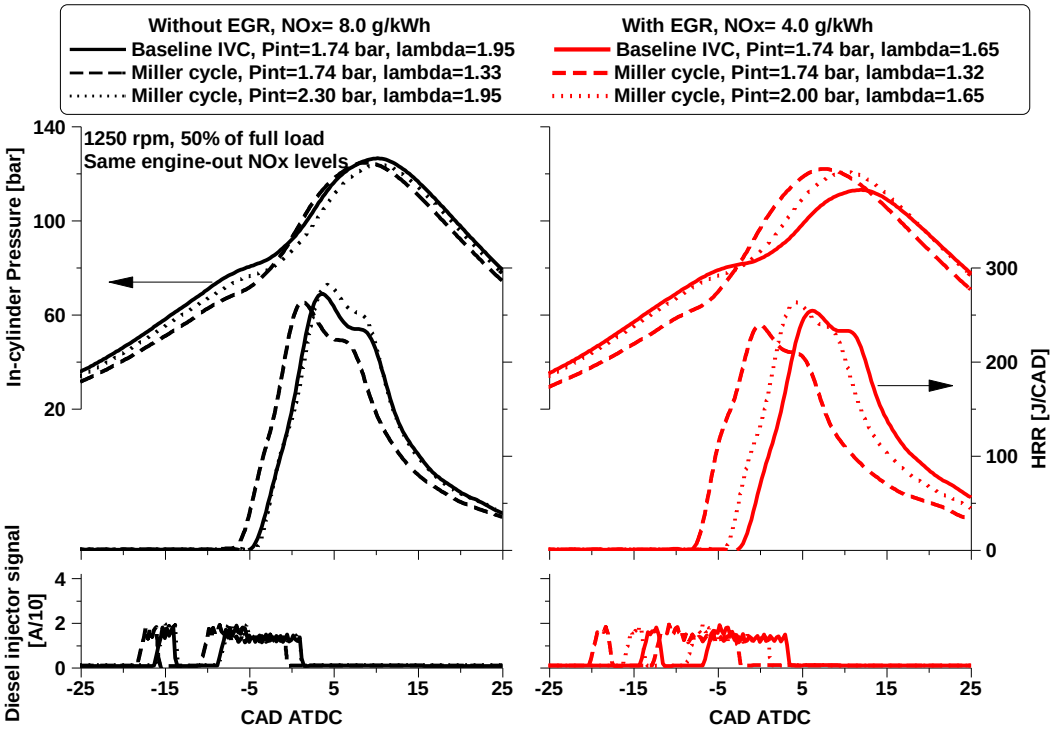

Figure 7.3: In-cylinder pressure, HRR, and diesel injector signal for the baseline and Miller cycle cases with the same engine-out NOx levels.

7.3.2 Combustion characteristics

Figure 7.4 shows the main SOI and the resulting combustion characteristics for the baseline and Miller cycle cases that attained the maximum $NIE_{corr.}$. The Miller cycle with constant P_{int} of the baseline cases allowed for more advanced main SOI, particularly in the cases with EGR. At 100% of full load, the optimisation of SOI was constrained by the P_{max} of 180 bar. The Miller cycle and EGR strategies increased the ignition delay in most cases. This was attributed to the lower compression pressures and in-cylinder oxygen availability, as well as the advanced SOI. The PRR was kept below 30 bar/CAD for all cases.

The optimum CA50 was initially advanced from low to medium loads likely due to the longer period CA10-CA90 and lower heat transfer losses, and then was delayed at high engine loads attributed to the limit of peak in-cylinder pressure. This trend became more obvious for the cases with EGR. The reduced in-cylinder oxygen availability via the use of Miller cycle and EGR slowed down the rate of heat release, leading to a later CA90 and longer period of CA10-CA90. A higher P_{int} improved the in-cylinder oxygen availability and accelerated the combustion process of Miller cycle with and without EGR. This advanced the CA90 and yielded shorter CA50-CA90 period and combustion duration when operating with a constant lambda.

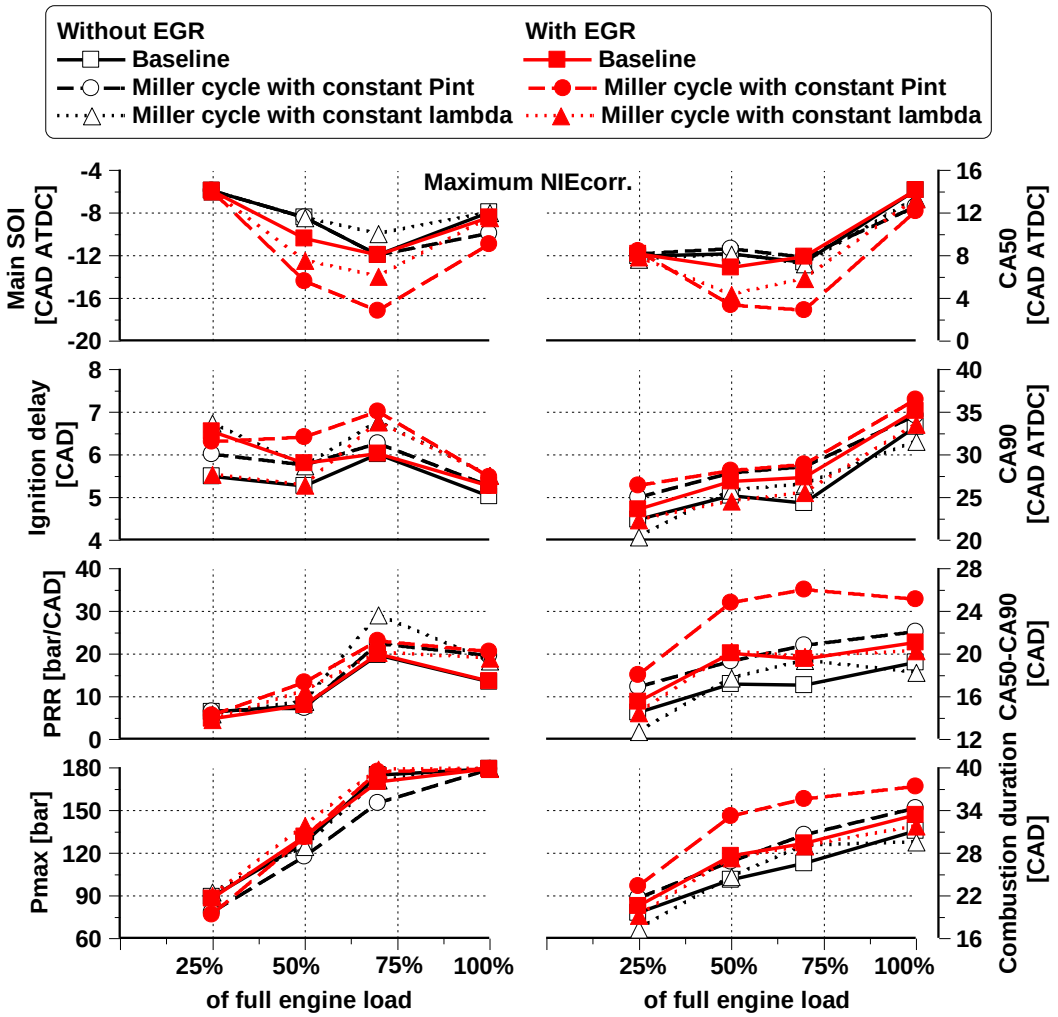

Figure 7.4: Injection timing and combustion characteristics of the baseline and Miller cycle cases with maximum $NIE_{corr.}$.

7.3.3 Engine performance, exhaust emissions, and fuel efficiency

Figure 7.5 shows the engine performance parameters and net indicated specific emissions for the baseline and Miller cycle cases with and without EGR. Miller cycle with a constant P_{int} decreased the lambda due to a reduction in the in-cylinder mass trapped, particularly with EGR. This was the primary reason for an increase in EGT. However, the "EGR-only" strategy showed little impact on the EGT due to the replacement of air with the recirculated exhaust gas and lower combustion temperatures.

Compared to the baseline engine operations, Miller cycle with and without EGR decreased the NIE at a constant P_{int}. This was a result of the later combustion process and longer combustion duration, as well as the higher average in-cylinder gas temperatures, as presented in our previous work [209]. The reduction in NIE is associated with an increase in heat losses. By using a higher P_{int} to improve the in-cylinder oxygen

availability, however, the NIE of Miller cycle was improved and was slightly higher than that of the baseline operation when operating with a constant lambda.

When considering the urea consumption in the SCR system, the total EOC is related to the $NIE_{corr.}$, which will be determined by the engine-out NOx emissions and the fuel conversion efficiency. As shown in the bottom left of Figure 7.5, the engine operations with EGR achieved higher maximum $NIE_{corr.}$ than those cases without EGR over the sweep of engine loads as a result of the lower NOx emissions. When operating without EGR, the maximum $NIE_{corr.}$ of Miller cycle with constant P_{int} was comparable to that of the baseline. When operating with EGR, Miller cycle strategy significantly reduced the maximum $NIE_{corr.}$. However, by increasing P_{int} and keeping the lambda constant helped to improve the trade-off between NOx emissions and NIE, increasing the $NIE_{corr.}$ of the Miller cycle strategy.

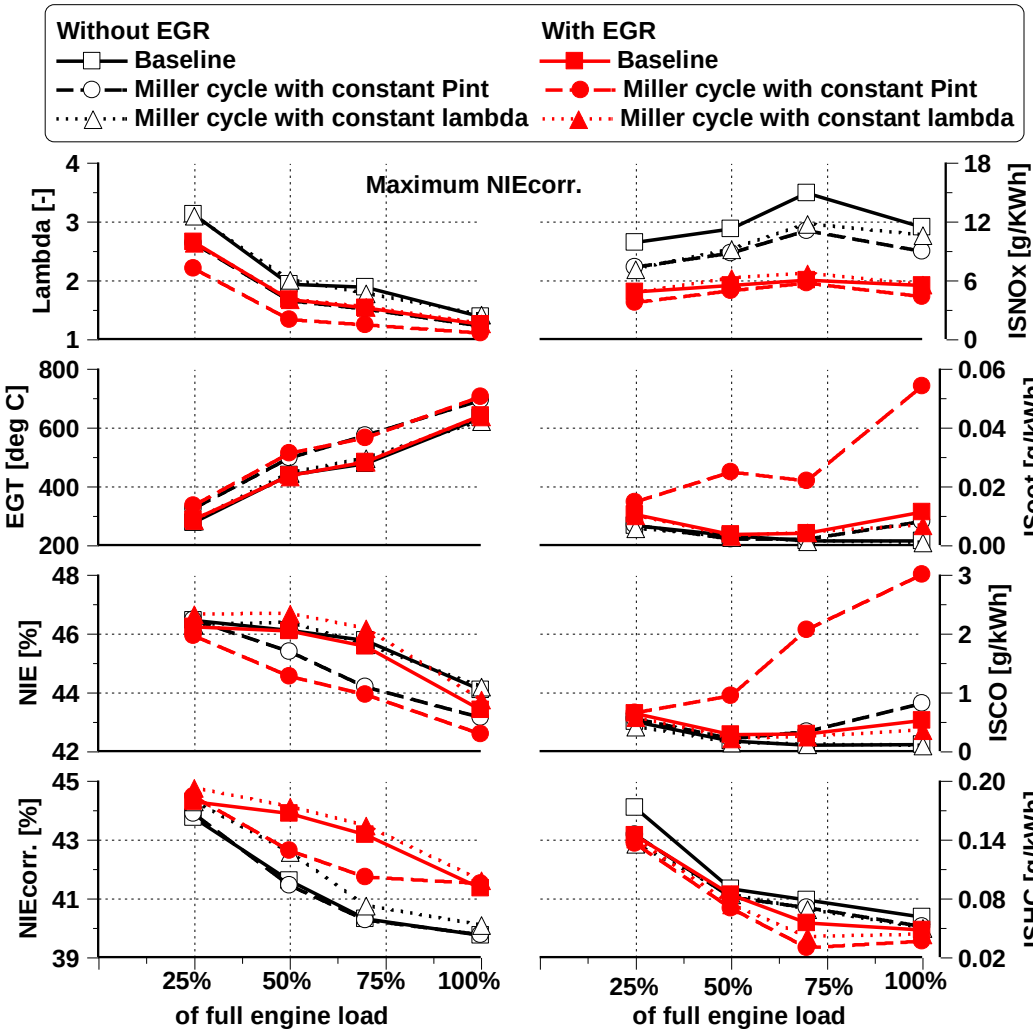

Figure 7.5: Engine performance, emissions, and fuel efficiency of the baseline and Miller cycle cases with maximum $NIE_{corr.}$.

It can be also seen from Figure 7.5 the engine-out emissions of NOx, soot, unburned HC, and CO. The NOx emissions were increased between 25% and 70% of full engine load but then decreased at 100% of full engine load. This was likely due to the increased combustion temperature from 25% to 70% of full engine load. The NOx reduction at full engine load was associated with the significantly lower lambda value. The use of EGR was more effective in minimizing engine-out NOx emissions than Miller cycle in all cases. The “Miller cycle + EGR” strategy with constant P_{int} achieved low NOx levels but yielded excessive smoke, particularly at high engine loads. Soot emissions were reduced when operating with the same lambda of the baseline cases and were maintained below the Euro VI limit of 0.01 g/kWh at 50% and 70% of full engine load. Therefore, the use of high boost pressures is a key enabler for achieving simultaneous low NOx and soot emissions when operating Miller cycle and EGR, especially at high engine loads.

The observed trend of CO emissions was similar to that of soot emissions. This was mainly because the in-cylinder oxygen concentration played an important role on the CO and soot formations. Miller cycle and EGR strategies showed little impact on CO emissions except when they were combined. The use of a higher P_{int} between medium and full engine loads helped to curb CO emissions from the Miller cycle operating with EGR. Finally, Figure 7.5 revealed that all advanced combustion control strategies decreased HC emissions compared to the baseline cases. Overall, the lowest levels of HC emissions were achieved by the “Miller cycle + EGR” strategy with constant P_{int}. This could be linked to the use of more advanced diesel injections and higher average in-cylinder gas temperature at lower lambda [215].

7.3.4 Analysis of the potential benefit of Miller cycle with and without EGR at the same engine-out NOx levels

This subsection explores the potential of Miller cycle for emissions control and efficiency improvements at the same engine-out NOx levels for cases with and without EGR. Figure 7.6 shows the engine-out emissions and fuel efficiency of the baseline and Miller cycle operations with and without EGR at the same engine-out NOx emissions.

The cases with EGR achieved lower levels of NOx emissions and relatively higher NIE in comparison with those without EGR due to the higher NOx reduction capability and the earlier CA50 resulted from the use of EGR. These improvements were achieved at the expense of higher soot and CO emissions, especially for the “Miller cycle + EGR” strategy with constant P_{int}. When operating without EGR, the Miller cycle cases with constant P_{int} allowed for earlier CA50, which helped improve the fuel conversion efficiency and thus

the NIE. When operating with EGR, however, the Miller cycle strategy decreased the NIE compared to the baseline cases, despite an advanced CA50. This was attributed to the relatively lower in-cylinder oxygen availability when applying Miller cycle and EGR with constant P_{int}. The NIE was increased noticeably when Miller cycle operating with constant lambda, whether with or without EGR. It can be also seen that all advanced combustion control strategies achieved relatively lower levels of HC emissions than that of the baseline cases.

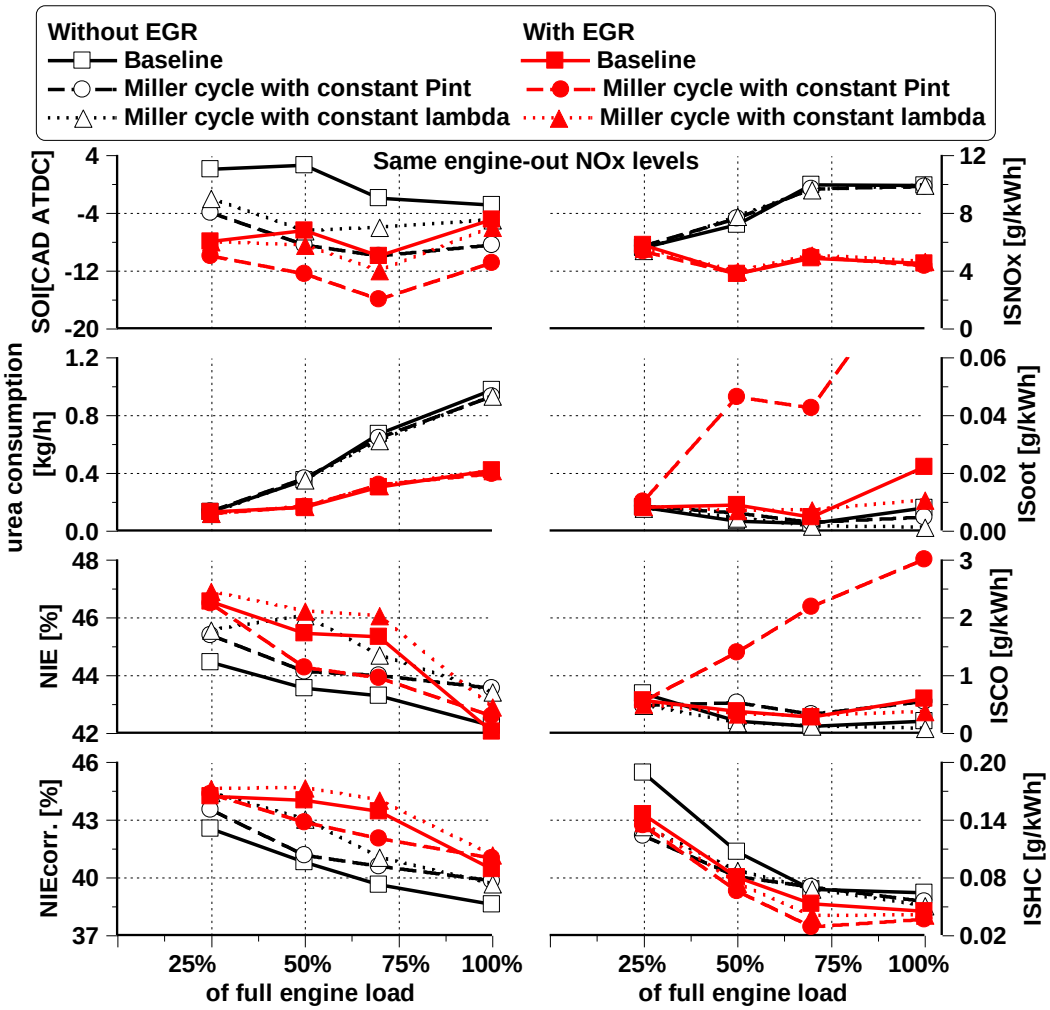

Figure 7.6: Comparison of the baseline and Miller cycle cases at the same engine-out NOx levels when operating the engine with and without EGR.

Figure 7.6 also shows that the engine operations with EGR achieved higher $NIE_{corr.}$ than those without EGR. This was due to the lower engine-out NOx levels and relatively higher NIE. Similar to the observed trend of NIE, the $NIE_{corr.}$ was increased in the Miller cycle operations without EGR and was reduced when operating with EGR. A higher P_{int} helped improve the $NIE_{corr.}$ of Miller cycle with and without EGR. Overall, the "Miller cycle + EGR" strategy with constant lambda achieved the highest NIE and $NIE_{corr.}$ while achieving simultaneous low levels of soot and HC emissions at all engine loads.

7.4 Analysis of Miller cycle operation with and without EGR over the WHSC test cycle

The purpose of this subsection is to analyse and compare the cycle-averaged performance, emissions, and total EOC of different combustion control strategies over the WHSC test cycle. The diesel SOI was varied at each combustion control strategy in order to obtain the different cycle-averaged NOx emissions.

7.4.1 Cycle-averaged engine exhaust emissions at different engine-out NOx levels

Figure 7.7 shows the exhaust emissions as a function of different cycle-averaged NOx emissions over the WHSC test cycle for the baseline and Miller cycle operations with and without EGR. The diesel SOI was varied in order to achieve different engine-out and thus cycle-average NOx emissions for all strategies investigated.

The cycle-averaged soot emissions of all combustion control strategies increased with the reduction in cycle-averaged NOx emissions. The baseline operation without EGR showed little impact on soot emissions when the NOx emissions were controlled at approximately 10 g/kWh or higher. Further reduction in the NOx emissions by delaying the SOI resulted in higher soot emissions. Miller cycle operation without EGR produced less soot emissions than the baseline cases at the NOx level of 8 g/kWh. This was a result of more advanced diesel injections, which helped improve the air/fuel mixing. However, the soot emissions increased linearly as the cycle-averaged NOx emissions decreased to below 6.5 g/kWh.

EGR is required to achieve cycle-averaged NOx emissions lower than 6 g/kWh. The results indicated that the use of EGR was effective in reducing NOx emissions while producing slightly higher soot emissions. However, the combination of Miller cycle and EGR at a constant P_{int} produced excessive soot emissions due to the lower lambda at such conditions. This was overcome by increasing intake pressure and was maintained below Euro VI soot limits, as denoted with a red dash line in Figure 7.7. As a result, simultaneous low levels of soot and NOx emissions were obtained when the engine was operated with the same lambda as the baseline case with EGR.

The data in Figure 7.7 also shows the cycle-averaged CO emissions, which increased with the reduction in cycle-averaged NOx emissions. Similar to the impact on soot emissions, the SOI in the baseline operations had little impact on the CO emissions.

However, the use of late SOI in the Miller cycle operation with a constant P_{int} increased the CO emissions, particularly when using EGR. This drawback was overcome when operating with a higher P_{int}. Different from the soot and CO emissions, HC emissions decreased with a reduction in NOx emissions for all advanced combustion control strategies. These improvements were relatively higher in the Miller cycle cases. Overall, the cycle-averaged CO and HC emissions of all cases were maintained within the Euro VI limits. It should be also noted that CO and HC emissions are not the primary issues in conventional diesel engines. This is due to the fact that HD diesel engines are equipped with a diesel oxidation catalyst (DOC) which can effectively reduce CO and unburnt HC emissions from the engine exhaust gases when the exhaust temperatures were held between 200 and 450℃ [216].

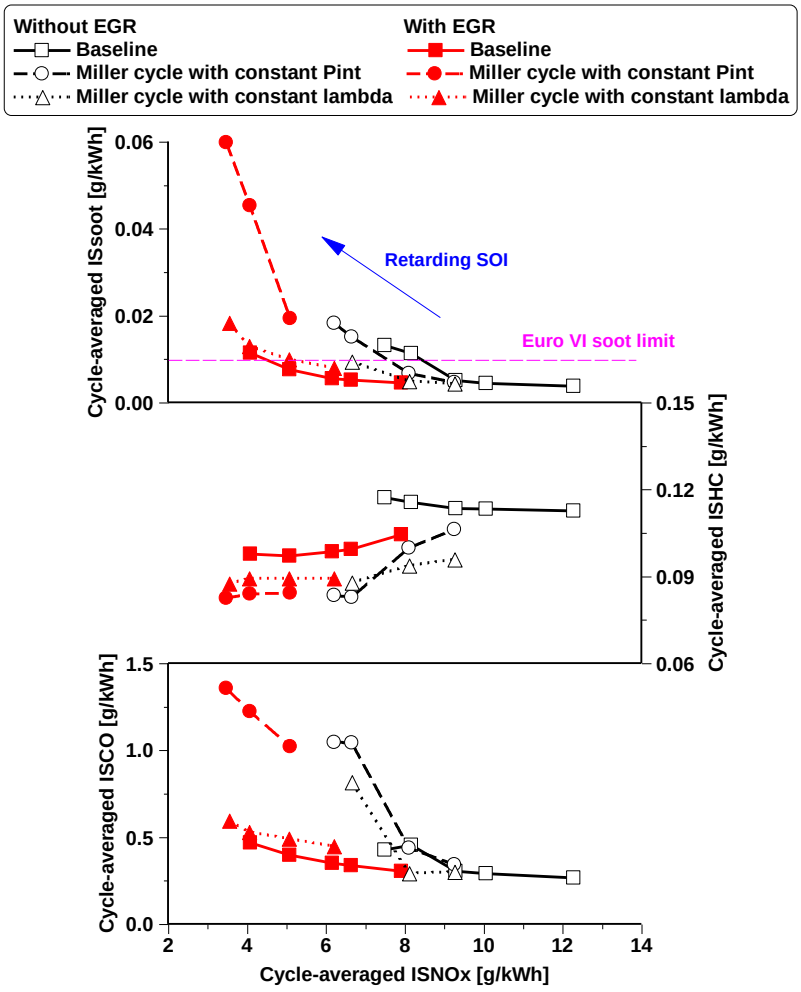

Figure 7.7: Cycle-averaged exhaust emissions for baseline and Miller cycle cases over the WHSC test cycle.

7.4.2 Analysis of cycle-averaged performance and potential of different technical routes

Figure 7.8 depicts the cycle-averaged performance as a function of various cycle-averaged NOx emissions for all combustion control strategies. The EGT increased with the reduction in the cycle-averaged NOx emissions. This was due to the use of Miller cycle, EGR, and late SOI for NOx control, which decreased the in-cylinder air mass trapped and/or delayed the combustion process. The highest increase in EGT of approximately 140℃ was achieved by the "Miller cycle-only" strategy. The addition of EGR in the Miller cycle operation had little impact on the EGT, despite the lower lambda.

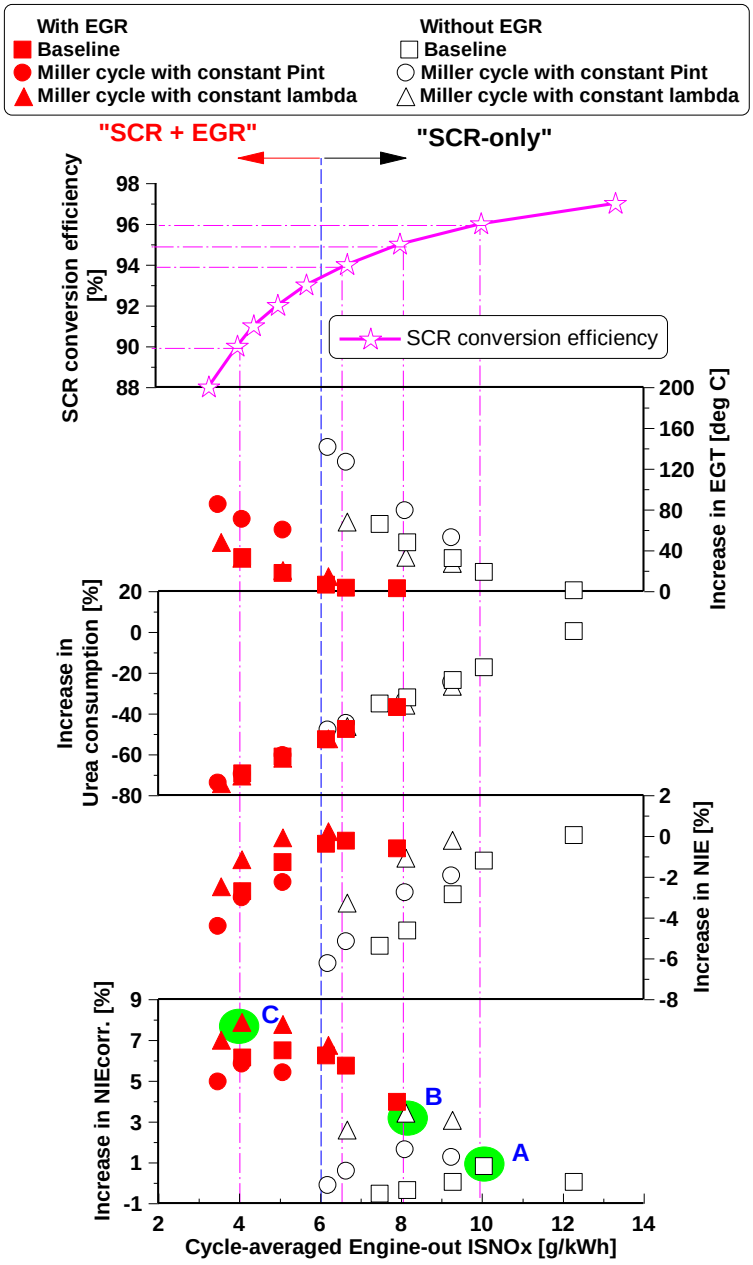

Figure 7.8: Potential of the proposed "SCR-only" and "SCR + EGR" technical routes to meet the Euro VI NOx limit (0.4 g/kWh) over the WHSC test cycle. A) Optimum baseline

engine operation without EGR; B) Optimum “Miller cycle-only” strategy with constant lambda; C) Optimum “Miller cycle + EGR” strategy with constant lambda.

In addition, all combustion control strategies yielded lower NIE when reducing the cycle-averaged NOx emissions. The baseline operations achieved lower NOx emissions via a retarded SOI, reducing the NOx emissions by 39% with a penalty of 6% in NIE. Compared to the baseline without EGR, the “Miller cycle-only” strategy achieved a reduction in NOx emissions of 49% with the same NIE penalty of 6%. The NIE penalty could be reduced to 3% while preserving the NOx reduction benefit by increasing the P_{int} and maintaining the same lambda of the baseline engine operation. The “EGR-only” strategy reduced the NOx emissions by 67% with a NIE penalty of 2.7%. Alternatively, the “Miller cycle + EGR” strategy with the same lambda as the baseline cases with EGR reduced NOx emissions by up to 71%. This was achieved with the same NIE penalty of 2.7% measured in the “EGR-only” strategy.

Furthermore, the SCR conversion efficiency was used to calculate the urea consumption and the $NIE_{corr.}$ of the engine operation, in order to fully evaluate the potential of these different combustion control strategies to meet different engine-out NOx levels over the WHSC test cycle. It can be seen from Figure 7.8 the cycle-averaged urea consumption in the SCR system as a function of cycle-averaged engine-out NOx emissions. The advanced combustion control strategies helped decrease the urea consumption via lower engine-out NOx emissions. This could minimise the cycle-averaged total fluid consumption and therefore increased the $NIE_{corr.}$. The “Miller cycle + EGR” strategy with a constant lambda attained the highest $NIE_{corr.}$ over the WHSC, increasing the cycle-averaged engine efficiency by up to 8% in comparison with the baseline without EGR.

Finally, Figure 7.8 demonstrates the potential of different combustion control strategies to meet the Euro VI emission regulations. It should be noted that the proposed “SCR + EGR” and “SCR-only” technical routes represent the combustion control strategy with and without using EGR, respectively. The results demonstrated that the baseline case without EGR was adequate for the cycle-averaged engine-out NOx emissions of 10 g/kWh and would require an overall SCR conversion efficiency of 96% with a penalty on the NIE by 1.5%. In addition, the optimum $NIE_{corr.}$ of the baseline engine operation was achieved at this cycle-averaged engine-out NOx level of 10 g/kWh, as denoted by point “A” in the bottom of Figure 7.8. When the cycle-averaged engine-out NOx emissions was required to be lower than 10 g/kWh, the Miller cycle without EGR strategy was preferable when operating with a constant lambda of the baseline case without EGR. This strategy enabled a relatively lower penalty of 3.3% on the NIE and an increase of 2.6% in the $NIE_{corr.}$ at the NOx level of 6.5 g/kWh. Besides, the EGT was increased by 68℃ and the minimum

required SCR conversion efficiency was reduced to 93.5%. It should be also noted that the optimum $NIE_{corr.}$ of "Miller cycle-only" strategy was improved up to 3.5% when controlling the NOx level at 8 g/kWh, as denoted by point "B" in Figure 7.8. Therefore, the "Miller cycle-only" strategy with a constant lambda of the baseline case without EGR was determined as the most effective means for the "SCR-only" technical route, achieving lower EOC, higher EGT, and lower soot emissions when the engine-out NOx emissions were to be held between 6 and 10 g/kWh.

When the cycle-averaged engine-out NOx emissions were required to be controlled below 6 g/kWh, however, the "Miller cycle-only" strategy resulted in a penalty of 6.3% on NIE and adversely affected the $NIE_{corr.}$. Therefore, the introduction of EGR was necessary owing to its high NOx reduction capability and relatively lower penalty on the fuel conversion efficiency. Particularly, the "Miller cycle +EGR" strategy with constant P_{int} could decrease the cycle-averaged engine-out NOx emissions from 12.3 g/kWh in the baseline operation without EGR to 3.4 g/kWh while increasing upon the $NIE_{corr.}$ of 4.9%, despite a reduction in NIE of approximately 4.6%. Meanwhile, this lower cycle-averaged engine-out NOx emissions allowed for a reduction in the minimum required SCR conversion efficiency down to 88%, which can significantly minimize the catalyst volumes and thus can simplify the SCR system [217]. However, this strategy increased cycle-averaged soot emissions to up to 0.06 g/kWh as a result of the lower lambda, which was significantly higher than the Euro VI limit of 0.01 g/kWh (seen in Figure 7.7). These results can limit the potential of the "Miller cycle + EGR" strategy for efficient and clean engine operation.

Preferably, a more efficient Miller cycle operation with EGR was achieved by keeping the lambda the same as the baseline operation with EGR via a higher P_{int}. The cycle-averaged soot emissions were significant reduced and were controlled within the Euro VI limit at most cases, except for the cases with cycle-averaged engine-out NOx emissions below 4 g/kWh, as shown in Figure 7.7. Meanwhile, the penalty on the NIE was notably minimized and the $NIE_{corr.}$ was significantly increased while maintaining low levels of NOx emissions. Overall, the "Miller cycle + EGR" strategy with a constant lambda achieved the highest improvement in the $NIE_{corr.}$ of 8% when controlling the cycle-averaged engine-out NOx emissions at 4 g/kWh, as denoted by point "C" in Figure 7.8. This was accompanied with an increase in EGT by 40℃ and a lower minimum required SCR conversion efficiency of 90% when compared to the baseline engine operation without EGR. Therefore, the "Miller cycle + EGR" strategy with a higher P_{int} was identified as the most effective

means for the “SCR + EGR” technical route, achieving low EOC while simultaneously enabling low cycle-averaged exhaust emissions.

7.5 Summary

This chapter investigated the effect of Miller cycle with and without EGR on the combustion characteristics, exhaust emissions, and performance of a HD diesel engine over the WHSC tests cycle. Miller cycle, EGR, and multiple injections were achieved by means of a VVA system, a high-pressure loop cooled EGR, and a common rail fuel injection system, respectively. A comparison was performed between the baseline and Miller cycle operations with and without EGR attained the maximum $NIE_{corr.}$ from low to full engine loads. Experimental analysis of cycle-averaged results of the different combustion control strategies were carried out in order to demonstrate their potential to meet the Euro VI NOx limit. The aim of the research was to explore a cost-effective emission control and fuel efficiency technology based on the “SCR-only” and “SCR + EGR” technical routes for the future HD diesel engines. The primary findings can be summarised as below.

1. At the optimum efficiency and without taking into account the urea consumption in the SCR system, Miller cycle with and without EGR decreased the NIE at the same intake pressure as the baseline operation. By increasing the boost pressure to keep the lambda same as the baseline, the NIE of Miller cycle operation was improved and comparable to that of the baseline operation at all engine loads.
2. At the same engine-out NOx emissions and without taking into account the urea consumption in the SCR system, the NIE was increased by the Miller cycle operation without EGR. When combining the use of the Miller cycle and EGR with a constant P_{int} as the baseline case with EGR, the NIE decreased. By increasing the boost pressure to keep the same lambda as the baseline case, the NIE of Miller cycle operation was improved and even slightly higher than that of the baseline operation at all engine loads.
3. When considering the total fluid consumption (e.g. fuel and urea), the baseline engine operations with EGR achieved higher $NIE_{corr.}$ and hence lower total fluid consumption than the baseline cases without EGR at the expense of higher soot and CO emissions. Particularly, the “Miller cycle + EGR” strategy with constant lambda achieved the highest NIE and $NIE_{corr.}$ while achieving simultaneous low levels of exhaust emissions from low to full engine loads.
4. The cycle-averaged results over the WHSC test cycle showed that all advanced combustion control strategies enabled a reduction in the cycle-averaged NOx

emissions and higher EGT. These improvements were attained at the expense of lower NIE and higher soot and CO emissions. However, higher $NIE_{corr.}$ could be achieved via lower urea consumption in the SCR system, especially when operating with a higher intake pressure.

5. The “Miller cycle-only” strategy with constant intake pressure achieved a reduction in the cycle-averaged engine-out NOx emissions of 49% at the expense of a penalty on NIE of 6%. When increasing the intake pressure to maintain the same lambda of the baseline operation without EGR, the “Miller cycle-only” strategy enabled a relatively lower penalty of 3.3% on the NIE and increased the $NIE_{corr.}$ by 2.6% at the cycle-averaged engine-out NOx level of 6.5 g/kWh. In the meantime, the cycle-averaged EGT was increased by 68℃.
6. The “Miller cycle + EGR” strategy with constant intake pressure could decreased the cycled-average engine-out NOx emissions from 12.3 g/kWh in the baseline operation without EGR to 3.4 g/kWh, but adversely affected soot emissions and NIE. The use of a higher intake pressure to maintain the same lambda of the baseline operation with EGR enabled a “Miller cycle + EGR” strategy achieving the highest improvement of approximately 8% in the $NIE_{corr.}$ while elevating the EGT by 40℃ and controlling the NOx levels at 4 g/kWh. Meanwhile, the highly boosted strategy helped increase the NIE and curb soot emissions.
7. Overall, the “Miller cycle-only” and “Miller cycle+ EGR” strategies with the same lambda as the baseline operations were identified as the most effective emission control and fuel efficiency technologies for the “SCR-only” and “SCR + EGR” technical routes accordingly. Moreover, the minimum required SCR conversion efficiency was reduced from 96% in the baseline engine operation to 93.5% in the “Miller cycle-only” strategy and 90% in the “Miller cycle+ EGR” strategy when they were combined with a highly boosted strategy.

Chapter 8
Conclusions and future work

8.1 Conclusions

This work was conducted with the primary aim of optimising fuel injection and exploring VVA-based advanced combustion control strategy to maximise engine efficiency and minimise engine-out emissions in a single cylinder heavy-duty diesel engine, in an attempt to explore a cost-effective emission control and fuel efficiency technology for the future HD diesel engines.

Following the review of the overall research background related to this work and a detail description of the experimental setup and test methodology that were taken for data analysis, different injector geometry parameters and engine combustion control strategies were investigated. Alternative control strategies were explored to address the major issues of low EGT at low engine loads and high mechanical and thermal loads at high engine loads, as well as the problematic soot and NOx emissions over the HD diesel engine speed-load map. Moreover, a cost-efficient analysis exhibited significant potential to increase the total engine efficiency between 6 and 24 bar IMEP by means of Miller cycle, especially with EGR and higher boost pressure. Ultimately, analysis of cycle-averaged results of the different combustion control strategies over the WHSC test cycle were carried out as well as their potential to meet Euro VI NOx limit. The “SCR-only” and “SCR + EGR” technical routes based on Miller cycle for the future HD diesel engines were evaluated along with the required SCR conversion efficiencies. The investigation of the influence of injector nozzle design on engine performance and emissions has led to the following main findings.

- The injectors with Ks-hole shape nozzles helped to reduce soot emissions and fuel consumption compared to the cyl-hole shape injector due to better fuel atomization quality and longer spray tip penetration resulted from higher discharge coefficient. The lower fuel mass flow rate injector reduced the NOx and soot emissions at most test points due to improved fuel atomization quality and a shorter spray tip penetration, which reduced the possibility of the liquid spray impinging on the walls. However, soot emissions and fuel consumption were increased at higher engine load due to longer period of fuel injection and therefore allowed less time for mixing.
- The injector tip protrusion exhibited a strong effect on the interaction between the

fuel spray and combustion bowl. The bigger spray angle with a deeper tip protrusion presented better trade-off relationships of NOx-soot and NOx-ISFC. In addition, the injection pressure and injection timing also showed important impact on the injector geometry optimization as the injection timing could change the spray targeting position in the piston bowl and the injection pressure exhibited important impact on the spray penetration.

- Injector with the biggest spray cone angle obtained the highest fuel efficiency while the injector with the smallest spray cone angle produced the lowest level of NOx. Ultimately, a cost-benefit analysis showed that injector with the smallest spray angle of 146º coupled with a washer thickness of 2 mm attained the highest total engine efficiency. Overall, the investigation of injector geometry structure demonstrated that injector parameters including nozzle hole shape, fuel flow rate and spray cone angle had great potential to improve the trade-off between engine efficiency and exhaust emissions.

Investigations of advanced combustion control strategies, such as Miller cycle, internal and external EGR, and higher boost pressure were explored over the WHSC test cycle and the relevant conclusions can be summarised as follows.

- At the light load of 2.2 bar IMEP, the application of Miller cycle enabled an increase in EGT by 52°C and lower NOx and soot emissions with a fuel consumption penalty of 5.3%. However, the resulting lower combustion temperature and later combustion process led to a significant increase in HC and CO emissions. This can be overcome by the combined use of LIVC and iEGR, which was identified as the most effective means amongst the various technologies examined in this study, increasing the EGT by 62°C and reducing soot emissions by 87% at the expense of fuel consumption penalty by 4.6%. The higher EGT attained with the combined strategy would be preferred for a superior aftertreatment performance and lower vehicle's tailpipe NOx levels.
- At 6 bar IMEP, Miller cycle was more effective in increasing EGT and reducing NOx emissions than a late CA50 strategy. The "EGR + Miller cycle" strategy resulted in a longer ignition delay and reduced the peak in-cylinder gas temperatures, achieving up to 70% lower NOx emissions with a low fuel efficiency penalty and reasonable levels of smoke. Furthermore, the addition of a post injection was effective in minimizing soot and CO emissions of the "Miller cycle + EGR" strategy while achieving lower NOx emissions and higher EGT.
- As the engine load increased to 12 bar IMEP, however, Miller cycle with constant intake pressure led to lower in-cylinder mass, incurring an adversely impact on

smoke number and engine efficiency. Particularly, the introduction of EGR with Miller cycle was capable of attaining more than 70% NOx reduction at the expense of higher ISFC penalty and increased emissions of soot and CO. This required higher intake pressure to maintain the in-cylinder air/fuel ratio. In addition, the unburn HC emissions were always lower in the Miller cycle operation. This was probably due to the lower lambda value and higher average in-cylinder gas temperature.

- The engine efficiency was restricted by the in-cylinder pressure when the engine load reached 17 bar IMEP. The application of Miller cycle was able to simultaneously reduce the peak in-cylinder pressure and NOx emissions at the expense of higher smoke number and lower engine efficiency. An increased intake pressure showed higher impact on the Miller cycle operation than a higher injection pressure and advanced SOI owing to the significantly lower in-cylinder air mass. The introduction of EGR presented huge sensitivity for the NOx emissions, decreasing the NOx level by 65% at an EGR rate of 15% with optimized injection timing while introducing little impact on the NIE and soot emissions. However, the efficiency apparently decreased as the EGR rate was increased to 20% attributed to the significantly lower in-cylinder oxygen availability.
- The result of the Miller cycle operation with EGR at full load revealed that earlier combustion phasing and higher injection pressure were beneficial to the improvement of engine efficiency and soot emissions for the Miller cycle operation. For a given intake pressure, the greater effect on reducing peak in-cylinder pressure by means of Miller cycle combined with the higher NOx reduction potential of EGR produced the best NOx-ISFC and NOx-soot trade-offs. Consequently, this improvement notably minimized the required urea consumption in the SCR system and thus achieved a higher total engine efficiency.
- According to the cycle-averaged results calculated over the WHSC test cycle, different combustion and engine control technologies could be adopted with and without EGR to meet Euro VI NOx limit were explored. A conventional baseline engine operation with a high SCR efficiency of 96% was adequate to meet the NOx emissions limit of 10 g/kWh. Miller cycle operation without EGR (Miller cycle-only) can decrease the NOx levels further to 6.5 g/kWh with less total fluid consumption of fuel and urea and reduced SCR efficiency to 93.5%. The Miller cycle operation with EGR and highly boosted strategy could lower the WHSC cycle-averaged engine-out NOx levels to 4.0 g/kWh, decrease the total fluid consumption by 8% and reduce the required SCR conversion efficiency down to 90%.

Therefore, this study has presented a promising cost-effective emission control and fuel efficiency technology based on the “SCR-only” and “SCR + EGR” technical routes for the future HD diesel engines. Figure 8.1 shows the overview of the optimum combustion control strategies with the application of Miller cycle over the whole engine operation map.

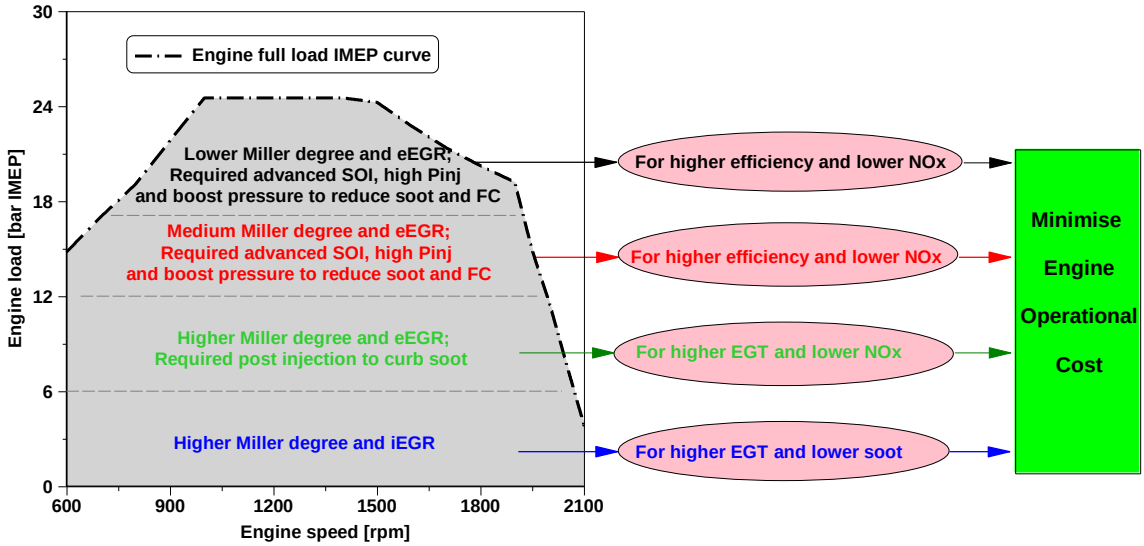

Figure 8.1: Optimum combustion strategies with the application of Miller cycle over the HD diesel engine operation map.

8.2 Recommendations for future work

From the results presented in this study, it can be seen the engine combustion system used in this work could be further optimised. Moreover, the impact of applying Miller cycle on the turbocharger and aftertreatment systems is not clear as this investigation is carried out on a single cylinder external supercharged engine instead of a multi-cylinder turbocharged engine. Therefore, there is scope for further improvement and understanding of the Miller cycle operation. The following are some relevant recommendations to be considered:

- Potential improvements to engine performance and exhaust emissions can be obtained if the piston bowl can be further optimised.
- A three-dimensional computational fluid dynamics modelling for fuel spray analysis in the injector geometry optimization investigation can help the understanding of the spray-bowl and spray-wall interaction.
- To explore the potential of Miller cycle in practical application in terms of the actual engine efficiency and emissions benefit, experimental investigation on a multi-cylinder turbocharged diesel engine is essential.

- A variable valve actuation system is required for the introduction of late intake valve closing and intake valve re-opening strategies, as the preferred Miller cycle degree for different engine operating conditions is different and also a fixed intake camshaft profile would likely balance engine performance at high speed and fuel economy at low speed [174].
- The application of Miller cycle technology to the HD diesel engines facing challenges such as the resulting hugely different thermodynamics and the durability required. Thus, more research on transient speed and load conditions is required to ensure the transient respond ability and the reliability of the constant switching variable valve actuation device.
- The resulting higher exhaust gas temperature but lower exhaust gas mass flow rates from the utilization of Miller cycle strategy could affect the operation performance of turbocharger and aftertreatment systems, which need to be studied.
- Finally, one-dimensional thermodynamic simulation for single-cylinder and multi-cylinder models will be required in order to better understand the effect and demand on air handling system when using Miller cycle and EGR over the WHSC test cycle, as the boosting system has been demonstrated as a key enabler for introducing the Miller cycle strategy and EGR on a HD diesel engine and it exhibited notable impact on the NIE as well as the total engine operational cost.

List of references

1. ExxonMobil, “2017 Outlook for Energy,” 27–28, 2017.
2. US Energy Information Administration (EIA), “Global Transportation Energy Consumption : Examination of Scenarios to 2040 using ITEDD,” (September), 2017.
3. 2018 BP Energy Outlook, 2018.
4. Pachauri, R.K., “Climate Change 2014 Synthesis Report,” *Russ. Fed. Hoesung Lee (Republic Korea) Scott B. Power N.H. Ravindranath* 167, 2014, doi:10.1017/CBO9781107415324.
5. International Organization of Motor Vehicle Manufacturers, “Climate Change and CO2 Brochure,” 9, 2008.
6. The, I.N., States, U., and Change, C., “Climate change indicator in the united states,” 2016.
7. SMMT, “New Car CO 2 Report 2018,” 2018.
8. Mock, P., “2020 – 2030 CO 2 standards for new cars and light-commercial vehicles in the European Union,” (November), 2016.
9. G20, “G20 Energy Efficiency Leading Programme,” 2016.
10. Gravel, R., “Freight Mobility and SuperTruck,” 2016.
11. Miller, J.D. and Façanha, C., “The state of clean transport policy - A 2014 synthesis of vehicle and fuel policy developments,” *ICCT Rep.* 73, 2014.
12. Delgado, O. and Lutsey, N., “The U.S. SuperTruck Program,” (June), 2014.
13. Heywood J.B, “Internal Combustion Engine Fundamentals,” ISBN 007028637X, 1988.
14. Jääskeläinen, H. and Majewski, W.A., “Engine Technology Evolution: Heavy-Duty Diesels,” *DieselNet Technol. Guid.* 10–12, 2014.
15. DieselNet, “EU Heavy-Duty Truck and Bus Engines - Emission Standards,” (2000):1–7, 2014.
16. Regulation No 49 – uniform provisions concerning the measures to be taken against the emission of gaseous and particulate pollutants from compression-ignition engines and positive ignition engines for use in vehicles. Off J Eur Union, 2013.
17. Delivery, U., Haul, L., Delivery, R., and Reduction, M., “FACT SHEET : EUROPE HEAVY-DUTY VEHICLES : BASELINE AND POTENTIAL FOR THE 2020 – 2030 TIMEFRAME,” (July), 2017.
18. Standards, E., “DieselNet : Emission Standards United States : Heavy- Duty Onroad Engines,” 1–8, 2018.
19. Posada, F., Chambliss, S., and Blumberg, K., “Costs of emission reduction

technologies for heavy-duty diesel vehicles," (February), 2016.

20. Update, P., "UNITED STATES EFFICIENCY AND GREENHOUSE GAS EMISSION REGULATIONS FOR MODEL YEAR 2018-2027 HEAVY-DUTY VEHICLES , ENGINES , AND TRAILERS," (June 2015), 2018.
21. Delgado, O., Rodríguez, F., and Muncrief, R., "Fuel Efficiency Technology in European Heavy-Duty Vehicles: Baseline and Potential for the 2020-2030 Time Frame," *ICCT White Pap.* (July), 2017.
22. ICCT, "Impacts of World-Class Vehicle Efficiency and Emissions Regulations in Select G20 Countries," *ICCT - Int. Counc. Clean Transp.* (January):17, 2017.
23. Haagen- Smit, a. J., "Chemistry and Physiology of Los Angeles Smog," *Air Pollut.* 44(6):1342–1346, 1950.
24. Goldstone, M.E., "Review of evidence on health aspects of air pollution - REVIHAAP project," *Air Qual. Clim. Chang.* 49(2):35, 2015.
25. Kittelson, D.B., "Engines and nanoparticles: A review," *J. Aerosol Sci.* 29(5–6):575–588, 1998, doi:10.1016/S0021-8502(97)10037-4.
26. Stone, R., "Introduction to Internal Combustion Engines," *J. Chem. Inf. Model.* 53:160, 1989, doi:10.1017/CBO9781107415324.004.
27. Han, Z., Uludogan, A., Hampson, G.J., and Reitz, R.D., "Mechanism of Soot and NOx Emission Reduction Using Multiple-injection in a Diesel Engine," (412), 1996, doi:10.4271/960633.
28. Boulter, P.G., Borken-Kleefeld, J., and Ntziachristos, L., "The Evolution and Control of NOx Emissions from Road Transport in Europe," *Hdb Env Chem* (July):31–54, 2012, doi:10.1007/698.
29. Buckendale, L.R., Stanton, D.W., and Stanton, D.W., "Systematic Development of Highly Efficient and Clean Engines to Meet Future Commercial Vehicle Greenhouse Gas Regulations," *SAE Int.* 2013-01-2421, 2013, doi:10.4271/2013-01-2421.
30. Desantes, J.M., Benajes, J., García, A., and Monsalve-Serrano, J., "The role of the in-cylinder gas temperature and oxygen concentration over low load reactivity controlled compression ignition combustion efficiency," *Energy* 78(x):854–868, 2014, doi:10.1016/j.energy.2014.10.080.
31. Prasad, B.V.V.S.U., Sharma, C.S., Anand, T.N.C., and Ravikrishna, R. V., "High swirl-inducing piston bowls in small diesel engines for emission reduction," *Appl. Energy* 88(7):2355–2367, 2011, doi:10.1016/j.apenergy.2010.12.068.
32. Ehleskog, M., Gjirja, S., and Denbratt, I., "Effects of Variable Inlet Valve Timing and Swirl Ratio on Combustion and Emissions in a Heavy Duty Diesel Engine," *SAE Tech. Pap.* 01(1719), 2012, doi:10.4271/2012-01-1719.
33. Yoo, D., Song, J., Kim, Y., Jung, W., and Kim, D., "Fuel Consumption Improvement

of 2.4L ULPC Diesel Engine by Optimizing the Combustion System; Nozzle, Swirl Ratio and Piston Bowl Geometry," 2015, doi:10.4271/2015-01-0785.

34. Quazi, M.A., Singh, S.K., and Jadhao, M., "Effect of piston bowl shape, swirl ratio and spray angle on combustion and emission in off road diesel engine," *SAE Tech. Pap.*, 2015, doi:10.4271/2015-26-0142.
35. Shi, Y. and Reitz, R.D., "Optimization study of the effects of bowl geometry, spray targeting, and swirl ratio for a heavy-duty diesel engine operated at low and high load," *Int. J. Engine Res.* 9(4):325–346, 2008, doi:10.1243/14680874JER00808.
36. Genzale, C.L., Reitz, R.D., and Wickman, D.D., "A Computational Investigation into the Effects of Spray Targeting, Bowl Geometry and Swirl Ratio for Low-Temperature Combustion in a Heavy-Duty Diesel Engine," 2007(724):776–790, 2007, doi:10.4271/2007-01-0119.
37. Fridriksson, H.S., Tuner, M., Andersson, O., Sunden, B., Persson, H., and Ljungqvist, M., "Effect of Piston Bowl Shape and Swirl Ratio on Engine Heat Transfer in a Light-Duty Diesel Engine," *SAE Techinical Pap. 2014-01-1141*, 2014, doi:10.4271/2014-01-1141.
38. Kook, S., Bae, C., Miles, P.C., Choi, D., Bergin, M., and Reitz, R.D., "The Effect of Swirl Ratio and Fuel Injection Parameters on CO Emission and Fuel Conversion Efficiency for High-Dilution, Low-Temperature Combustion in an Automotive Diesel Engine," 2006(724), 2006, doi:10.4271/2006-01-0197.
39. Mccracken, M.E. and Abraham, J., "Swirl-Spray Interactions in a Diesel Engine," 2001(724), 2001, doi:10.4271/2001-01-0996.
40. Lee, J., Lee, S., Kim, J., and Kim, D., "Bowl Shape Design Optimization for Engine-Out PM Reduction in Heavy Duty Diesel Engine," 2015, doi:10.4271/2015-01-0789.
41. Risi, A. De, Donateo, T., Laforgia, D., and Dipartimento, L., "Optimization of the Combustion Chamber of Direct Injection Diesel Engines," *Society* (724), 2003.
42. Dolak, J.G., Shi, Y., and Reitz, R., "A computational investigation of stepped-bowl piston geometry for a light duty engine operating at low load," *SAE Tech. Pap.* 1–31, 2010, doi:10.4271/2010-01-1263.
43. Cao, L., Bhave, A., Su, H., Mosbach, S., Kraft, M., Dris, A., and McDavid, R.M., "Influence of Injection Timing and Piston Bowl Geometry on PCCI Combustion and Emissions," *SAE Tech. Pap. 2009-01-1102* 2(1):1–14, 2009, doi:10.4271/2009-01-1102.
44. Splitter, D., Wissink, M., Kokjohn, S., and Reitz, R., "Effect of Compression Ratio and Piston Geometry on RCCI Load Limits and Efficiency," *SAE Tech. Pap. 2012-01-0383* (x), 2012, doi:10.4271/2012-01-0383.
45. Desantes, J.M., Payri, R., Salvador, F.J., and Soare, V., "Study of the influence of geometrical and injection parameters on Diesel Sprays characteristics in isothermal

conditions," *SAE Pap. 2005-01-0913* 2005(724), 2005, doi:10.4271/2005-01-0913.

46. Bergstrand, P., Persson, F., Forsth, M., and Denbratt, I., "A study of the influence of nozzle orifice geometries on fuel evaporation using laser-induced exciplex fluorescence," *SAE Trans.* 112(4):1264–1275, 2003, doi:10.4271/2003-01-1836.
47. Karra, P.K. and Kong, S.-C., "Experimental Study on Effects of Nozzle Hole Geometry on Achieving Low Diesel Engine Emissions," *J. Eng. Gas Turbines Power* 132(2):022802, 2010, doi:10.1115/1.3124791.
48. Bergstrand, P. and Denbratt, I., "Diesel combustion with reduced nozzle orifice diameter," *SAE Tech. Pap. 2001-01-2010* (724), 2001, doi:10.4271/2001-01-2010.
49. Benajes, J., Molina, S., Rudder, K. De, Maroteaux, D., and Hadj Hamouda, H. Ben, "The use of micro-orifice nozzles and swirl in a small HSDI engine operating at a late split-injection LTC regime," *Proc. Inst. Mech. Eng. Part D J. Automob. Eng.* 220(12):1807–1817, 2006, doi:10.1243/09544070JAUTO383.
50. Kang, S., Cho, W., Bae, C., and Kim, Y., "Influence of the Injector Geometry at 250 MPa Injection in a Light-Duty Diesel Engine," 2017, doi:10.4271/2017-01-0693.Copyright.
51. Kim, B. and Yoon, W., "Effect of the injector nozzle hole diameter and number on the spray characteristics and the combustion performance in medium-speed diesel marine engines," *SAE Tech. Pap.* (724), 2005, doi:10.4271/2005-01-3853.
52. Brusiani, F., Bianchi, G.M., Falfari, S., Onorati, A., Lucchini, T., Gioia, R. Di, Marelli, M., and Spa, P., "Influence of Cylindrical , k , and ks Diesel Nozzle Shape on the Injector Internal Flow Field and on the Emerging Spray Characteristics ks-Hole Geometry Experimental," *SAE Tech. Pap.* (1), 2014, doi:10.4271/2014-01-1428.Copyright.
53. Som, S., Ramirez, A.I., Longman, D.E., and Aggarwal, S.K., "Effect of nozzle orifice geometry on spray, combustion, and emission characteristics under diesel engine conditions," *Fuel* 90(3):1267–1276, 2011, doi:10.1016/j.fuel.2010.10.048.
54. Brusiani, F., Bianchi, G.M., Gioia, R. Di, Marelli, M., and Spa, P., "Experimental Characterization of the Geometrical Shape of ks- hole and Comparison of its Fluid Dynamic Performance Respect to Cylindrical and k-hole Layouts," (1):1553–1565, 2013, doi:10.4271/2013-24-0008.
55. Benajes, J., Pastor, J. V., Payri, R., and Plazas, a. H., "Analysis of the Influence of Diesel Nozzle Geometry in the Injection Rate Characteristic," *J. Fluids Eng.* 126(January):63, 2004, doi:10.1115/1.1637636.
56. Desantes, J.M., Arrègle, J., López, J.J., and Hermens, S., "Experimental characterization of outlet flow for different diesel nozzle geometries," 2005, doi:10.4271/2005-01-2120.
57. Kim, K., Jung, Y., Kim, D., and Bae, C., "Effect of a conical nozzle orifice on the

combustion and emissions in a direct- injection compression ignition engine under low-load conditions," *Int. J. Engine Res.* 17(3):1468087415573799-, 2015, doi:10.1177/1468087415573799.

58. Diwakar, R., Diwakar, R., Singh, S., and Singh, S., "Importance of Spray-Bowl Interaction in a DI Diesel Engine Operating under PCCI Combustion Mode," *SAE 2009-01-0711*, 2009, doi:10.4271/2009-01-0711.
59. Vanegas, a, Vanegas, A., Won, H., Won, H., Peters, N., and Peters, N., "Influence of the Nozzle Spray Angle on Pollutant Formation and Combustion Efficiency for a PCCI Diesel Engine," *SAE*, 2009, doi:10.4271/2009-01-1445.
60. Lechner, G., Jacobs, T., and Chryssakis, C., "Evaluation of a narrow spray cone angle, advanced injection timing strategy to achieve partially premixed compression ignition combustion in a diesel engine," *SAE 2005-01-0167* 2005(x), 2005, doi:10.4271/2005-01-0167.
61. Jia, M., Peng, Z., Xie, M., and Stobart, R., "Evaluation of Spray/Wall Interaction Models under the Conditions Related to Diesel HCCI Engines," 1(1):993–1008, 2008, doi:10.4271/2008-01-1632.
62. Siewert, R.M., "Spray Angle and Rail Pressure Study for Low NOx Diesel Combustion," *SAE Pap. 2007-01-0122* 2007(724):776–790, 2007, doi:10.4271/2007-01-0122.
63. Niemi, S., Törnvall, J., Laurén, M., and Nousiainen, P., "Optimization of some injection parameters in a common-rail non-road diesel engine," *SAE Tech. Pap.* 4970, 2009, doi:10.4271/2009-01-1833.
64. Fang, T., Coverdill, R., and Lee, C., "Smokeless combustion within a small-bore HSDI diesel engine using a narrow angle injector," *SAE 2007-01-0203* 2007(724):776–790, 2007, doi:10.4271/2007-01-0203.
65. Mobasheri, R. and Peng, Z., "A Computational Investigation into the Effects of Included Spray Angle on Heavy-Duty Diesel Engine Operating Parameters," 2012, doi:10.4271/2012-01-1714.
66. Yu, H., Li, D., Liang, X., Shu, G., Wang, Y., Wang, X., and Dong, L., "Numerical Investigation of the Effect of Spray Cone Angle on Mixture Formation and CO / Soot Emissions in an Early Injection HCCI Diesel Engine," *2015-01-1070* 2015-01-1070, 2015, doi:10.4271/2015-01-1070.Copyright.
67. Wang, X., Huang, Z., Zhang, W., Kuti, O.A., and Nishida, K., "Effects of ultra-high injection pressure and micro-hole nozzle on flame structure and soot formation of impinging diesel spray," *Appl. Energy* 88(5):1620–1628, 2011, doi:10.1016/j.apenergy.2010.11.035.
68. Han, S. and Bae, C., "The Influence of Fuel Injection Pressure and Intake Pressure on Conventional and Low Temperature Diesel Combustion," *SAE Int.* 2012-01-

1721, 2012, doi:10.4271/2012-01-1721.

69. Needham, D., “Dynamic rate shaping – one diesel common-rail injector for all combustion strategies,” 1–23.
70. Palanisamy, M., Lorch, J., Truemner, R.J., and Baldwin, B., “Combustion Characteristics of a 3000 Bar Diesel Fuel System on a Single Cylinder Research Engine,” *SAE 2015-01-2798* 8(2):2015-01-2798, 2015, doi:10.4271/2015-01-2798.
71. Fang, T. and Coverdill, R., “Effects of Injection Pressure on Low-sooting Combustion in an Optical HSDI Diesel Engine Using a Narrow Angle Injector,” *SAE Tech. Pap.*, 2010, doi:10.4271/2010-01-0339.
72. Kiplimo, R., Tomita, E., Kawahara, N., Zhou, S., and Yokobe, S., “Effects of Injection Pressure , Timing and EGR on Combustion and Emissions Characteristics of Diesel PCCI Engine,” *SAE Pap.* (2011-01-1769):714–727, 2011, doi:10.4271/2011-01-1769.
73. Zhang, G., Qiao, X., Miao, X., Hong, J., and Zheng, J., “Effects of highly dispersed spray nozzle on fuel injection characteristics and emissions of heavy-duty diesel engine,” *Fuel* 102:666–673, 2012, doi:10.1016/j.fuel.2012.07.053.
74. Chen, P.C., Wang, W.C., Roberts, W.L., and Fang, T., “Spray and atomization of diesel fuel and its alternatives from a single-hole injector using a common rail fuel injection system,” *Fuel* 103(x):850–861, 2013, doi:10.1016/j.fuel.2012.08.013.
75. Rusly, A., Le, M.K., and Kook, S., “Effect of Injection Pressure on Transient Behaviour of Wall-Interacting Jet Flame Base in an Automotive-Size Diesel Engine,” *SAE Int. J. Fuels Lubr.* 6(3):2013-01-2536, 2013, doi:10.4271/2013-01-2536.
76. Le, M.K. and Kook, S., “Injection Pressure Effects on the Flame Development in a Light-Duty Optical Diesel Engine,” *SAE Int. J. Engines* 8(2):609–624, 2015, doi:10.4271/2015-01-0791.
77. Çelikten, I., “An experimental investigation of the effect of the injection pressure on engine performance and exhaust emission in indirect injection diesel engines,” *Appl. Therm. Eng.* 23(16):2051–2060, 2003, doi:10.1016/S1359-4311(03)00171-6.
78. Morgan, R., Banks, A., Auld, A., and Heikal, M., “The Benefits of High Injection Pressure on Future Heavy Duty Engine Performance,” (x), 2015, doi:10.4271/2015-24-2441.Copyright.
79. Zhao, H., “Advanced Direct Injection Combustion Engine Technologies and Development - Volume 2: Diesel Engines,” ISBN 9781855737426, 2009, doi:10.1533/9781845697457.
80. Charlton, S., “Developing Diesel Engines to Meet Ultra-Low Emission Standards,” *Tech. Pap.* (2005-11-01):42, 2005, doi:10.4271/2005-01-3628.
81. Serrano J R, Arnau F J, D. V, “ANALYSIS OF THE CAPABILITIES OF A TWO-STAGE TURBOCHARGING SYSTEM TO FULFIL THE US2007 ANTI-

POLLUTION DIRECTIVE FOR HEAVY DUTY DIESEL ENGINES," *Int. J. …* 9(3):277–288, 2008, doi:10.1007/s12239.

82. Plianos, A. and Stobart, R., "Modeling and Control of Diesel Engines Equipped with aTwo-Stage Turbo-System," *SAE Tech. Pap. 2008-01-1018* 2008(724), 2008, doi:2008-01-1018.
83. Kang, J., Lee, J., Song, H., and Lee, D., "Enhancing Power Density with Two-Stage Turbochargers," *SAE Tech. Pap. 2012-01-0709*, 2012, doi:10.4271/2012-01-0709.
84. Mattarelli, E., Rinaldini, C.A., Mazza, A., and Oliva, M., "Development of a 2-Stage Supercharging System for a HSDI Diesel Engine," *SAE Tech. Pap. 2009-01-2757* 4970, 2009, doi:10.4271/2009-01-2757.
85. Zhao, C., Yu, G., Yang, J., Bai, M., and Shang, F., "Achievement of Diesel Low Temperature Combustion through Higher Boost and EGR Control Coupled with Miller Cycle," (x), 2015, doi:10.4271/2015-01-0383.
86. Millo, F., Mallamo, F., and Mego, G.G., "The Potential of Dual Stage Turbocharging and Miller Cycle for HD Diesel Engines," 2005(724), 2005, doi:10.4271/2005-01-0221.
87. Moraal, P. and Kolmanovsky, I., "Turbocharger Modeling for Automotive Control Applications," (724), 1999, doi:10.4271/1999-01-0908.
88. Liu, J., Wang, H., Zheng, Z., Zou, Z., and Yao, M., "Effects of Different Turbocharging Systems on Performance in a HD Diesel Engine with Different Emission Control Technical Routes," *SAE Tech. Pap.*, 2016, doi:10.4271/2016-01-2185.
89. Keidel, S., Wetzel, P., Biller, B., and Birckett-FEV, A., "Diesel Engine Fuel Economy Improvement Enabled by Supercharging and Downspeeding," *SAE Tech. Pap.* 483–493, 2012, doi:10.4271/2012-01-1941.
90. https://www.dieselnet.com/tech/air_turbo_vgt.php.
91. Galindo, J., Serrano, J.R., Climent, H., and Varnier, O., "Impact of two-stage turbocharging architectures on pumping losses of automotive engines based on an analytical model," *Energy Convers. Manag.* 51(10):1958–1969, 2010, doi:10.1016/j.enconman.2010.02.028.
92. Leek, V., Ekberg, K., and Eriksson, L., "Development and Usage of a Continuously Differentiable Heavy Duty Diesel Engine Model Equipped with VGT and EGR," *Sae Tech. Pap. 2017-01-0611*, 2017, doi:10.4271/2017-01-0611.
93. Mao, B., Yao, M., Zheng, Z., and Liu, H., "Effects of Dual Loop EGR and Variable Geometry Turbocharger on Performance and Emissions of a Diesel Engine," 2016, doi:10.4271/2016-01-2340.
94. Xue, X. and Rutledge, J., "Potentials of Electrical Assist and Variable Geometry Turbocharging System for Heavy-Duty Diesel Engine Downsizing," *SAE Tech. Pap.*

2017–March(March):ADIENT; et al.; HITACHI; Mentor Automotive; OMRON;, 2017, doi:10.4271/2017-01-1035.

95. Costall, A., Ivanov, R., and Langley, T., “Electric turbo assist: efficient rapid boost for heavy duty diesel engines,” *Proceedings of the Conference on Thermo and Fluid Dynamic Processes in Direct Injection Engines*, 1–18, 2012.
96. Ibaraki, S., Yamashita, Y., Sumida, K., Ogita, H., and Jinnai, Y., “Development of the ‘Hybrid Turbo’ an Electrically Assisted Turbocharger,” *Mitsubishi Heavy Ind. Tech. Rev.* 43(3):1–5, 2006, doi:10.4271/2002-01-0378.
97. Hiroshi Uchida, T., “Trend of Turbocharging Technologies,” *R&D Rev. Toyota CRDL* 41(3):1–8, 2006.
98. Terdich, N., “IMPACT OF ELECTRICALLY ASSISTED TURBOCHARGING ON THE TRANSIENT RESPONSE OF AN OFF-HIGHWAY DIESEL ENGINE,” PhD Thesis, Imperial College London, 2015.
99. https://www.dieselnet.com/tech/engine_egr_sys.php.
100. Ladommatos, N., Abdelhalim, S.M., Zhao, H., and Hu, Z., “The Dilution , Chemical , and Thermal Effects of Exhaust Gas Recirculation on Diesel Engine Emissions - Part 4 : Effects of Carbon Dioxide and Water Vapour,” (412), 1997.
101. Maiboom, A., Tauzia, X., and Hétet, J.-F., “Experimental study of various effects of exhaust gas recirculation (EGR) on combustion and emissions of an automotive direct injection diesel engine,” *Energy* 33(1):22–34, 2008, doi:10.1016/j.energy.2007.08.010.
102. Millo, F., Giacominetto, P.F., and Bernardi, M.G., “Analysis of different exhaust gas recirculation architectures for passenger car Diesel engines,” *Appl. Energy* 98:79–91, 2012, doi:10.1016/j.apenergy.2012.02.081.
103. Shi, L., Cui, Y., Deng, K., Peng, H., and Chen, Y., “Study of low emission homogeneous charge compression ignition (HCCI) engine using combined internal and external exhaust gas recirculation (EGR),” *Energy* 31(14):2329–2340, 2006, doi:10.1016/j.energy.2005.12.005.
104. Gan, S., Ng, H.K., and Pang, K.M., “Homogeneous Charge Compression Ignition (HCCI) combustion: Implementation and effects on pollutants in direct injection diesel engines,” *Appl. Energy* 88(3):559–567, 2011, doi:10.1016/j.apenergy.2010.09.005.
105. Zhao, H., Xie, H., and Peng, Z., “Effect of recycled burned gases on homogeneous charge compression ignition combustion,” *Combust. Sci. Technol.* 177(10):1863–1882, 2005, doi:10.1080/00102200590970258.
106. Asad, U. and Zheng, M., “Exhaust gas recirculation for advanced diesel combustion cycles,” *Appl. Energy* 123:242–252, 2014, doi:10.1016/j.apenergy.2014.02.073.
107. Ladommatos, N., Abdelhalim, S., and Zhao, H., “The effects of exhaust gas

recirculation on diesel combustion and emissions," *Int. J. Engine Res.* 1(1):107–126, 2000, doi:10.1243/1468087001545290.

108. Tomazic, D. and Pfeifer, A., "Cooled EGR – A Must or an Option for 2002 / 04 Reprinted From : Compression Ignition Combustion and In-Cylinder Diesel Particulates and NOx Control," *SAE Int.* (SAE 2002-01-00962), 2002.
109. Schwoerer, J., Dodi, S., Fox, M., Huang, S., and Yang, Z., "Internal EGR Systems for NOx Emission Reduction in Heavy-Duty Diesel Engines," *SAE Tech. Pap.* (724), 2004, doi:10.4271/2004-01-1315.
110. Dittrich, P.A., Peter, F., Huber, G., and Kuehn, M., "Thermodynamic potentials of a fully variable valve actuation system for passenger-car diesel engines," *SAE Tech. Pap.*, 2010, doi:2010-01-1199.
111. Balaji, J., M. V., G.P., Rao, L.N., Bandaru, B., and Ramesh, A., "Modelling and Experimental Study of Internal EGR System for NOx Control on an Off-Road Diesel Engine," *SAE Technical Paper*, 2014, doi:10.4271/2014-01-2645.
112. Dahodwala, M., Joshi, S., Koehler, E.W., and Frank, M., "Investigation of Diesel and CNG Combustion in a Dual Fuel Regime and as an Enabler to Achieve RCCI Combustion," *SAE 2014 World Congr.* 2014-01-13(2014-01-1308):1308–2014, 2014, doi:10.4271/2014-01-1308.
113. Pedrozo, V.B., May, I., Lanzanova, T.D.M., and Zhao, H., "Potential of internal EGR and throttled operation for low load extension of ethanol–diesel dual-fuel reactivity controlled compression ignition combustion on a heavy-duty engine," *Fuel* 179:391–405, 2016, doi:10.1016/j.fuel.2016.03.090.
114. Guan, W., Zhao, H., Ban, Z., and Lin, T., "Exploring alternative combustion control strategies for low-load exhaust gas temperature management of a heavy-duty diesel engine," *Int. J. Engine Res.* 146808741875558, 2018, doi:10.1177/1468087418755586.
115. Korfer, T., Busch, H., Kolbeck, A., Severin, C., Schnorbus, T., and Honardar, S., "Advanced Thermal Management for Modern Diesel Engines - Optimized Synergy between Engine Hardware and Software Intelligence," *Proc. Asme Intern. Combust. Engine Div. Spring Tech. Conf. 2012* 415–430, 2012, doi:10.1115/ICES2012-81003.
116. Baratta, M., Finesso, R., Misul, D., and Spessa, E., "Comparison between Internal and External EGR Performance on a Heavy Duty Diesel Engine by Means of a Refined 1D Fluid-Dynamic Engine Model," *SAE Int. J. Engines* 8(5):1977–1992, 2015, doi:10.4271/2015-24-2389.
117. Dallmann, T. and Menon, A., "Technology Pathways for Diesel Engines Used in Non-Road Vehicles and Equipment," *ICCT White Pap.* (September), 2016.
118. Williams, M. and Minjares, R., "A technical summary of Euro 6/VI vehicle emission

standards," *ICCT Brief. Pap.* (June), 2016.

119. Johnson, T. V., "Review of Vehicular Emissions Trends," *SAE Int. J. Engines* 8(3), 2015, doi:10.4271/2015-01-0993.
120. Johnson, T., "Vehicular Emissions in Review," *SAE Int. J. Engines* 6(Ld):699–715, 2017, doi:10.4271/2013-01-0538.
121. McKinley, T. and Alleyne, A., "Adaptive Model Predictive Control of an SCR Catalytic Converter System for Automotive Applications," *IEEE Trans. Control Syst. Technol.* 20(6):1533–1547, 2012, doi:10.1109/TCST.2011.2169494.
122. Chatterjee, S., Naseri, M., and Li, J., "Heavy Duty Diesel Engine Emission Control to Meet BS VI Regulations," *SAE Tech. Pap.* (x), 2017, doi:10.4271/2017-26-0125.
123. Kamm, S., Schraml, S., and MAN Truck & Bus AG, "Future Requirements & Challenges on Aftertreatment of Heavy Duty Diesel Engines Future Requirements & Challenges," *Present. SAE 2016 Heavy-Duty Diesel Emiss. Control Symp.*, 2016.
124. Pischinger, S., Korfer, T., Wiartalla, A., Schnitzler, J., Tomazic, D., and Tatur, M., "Combined particulate matter and NOx aftertreatment systems for stringent emission standards.," *SAE Tech. Pap. 2007-01-1128* 2007(724), 2007, doi:10.4271/2007-01-1128.
125. Charlton, S., Dollmeyer, T., and Grana, T., "Meeting the US Heavy-Duty EPA 2010 Standards and Providing Increased Value for the Customer," *SAE Int. J. Commer. Veh.* 3(1):101–110, 2010, doi:10.4271/2010-01-1934.
126. Schär, C.M., Onder, C.H., and Geering, H.P., "Control of an SCR catalytic converter system for a mobile heavy-duty application," *IEEE Trans. Control Syst. Technol.* 14(4):641–653, 2006, doi:10.1109/TCST.2006.876634.
127. Shead, L. and Steffen, T., "The State of the Art in Selective Catalytic Reduction Control Zakwan Skaf," 2014, doi:10.4271/2014-01-1533.Copyright.
128. Gmbh, F.E. V, Bhardwaj, O.P., Blanco, D., Krishnamurthy, K., and Holderbaum, B., "Optimization of Engine Efficiency and Diesel Aftertreatment System Architecture Using an Integrated System Simulation Approach Regeneration in Emerging Markets," (x), 2016, doi:10.4271/2016-28-0227.Copyright.
129. López-De Jesús, Y.M., Chigada, P.I., Watling, T.C., Arulraj, K., Thorén, A., Greenham, N., and Markatou, P., "NOx and PM Reduction from Diesel Exhaust Using Vanadia SCRF®," *SAE Int. J. Engines* 9(2):1247–1257, 2016, doi:10.4271/2016-01-0914.
130. Johnson, T. and Joshi, A., "Review of Vehicle Engine Efficiency and Emissions," 2017, doi:10.4271/2017-01-0907.
131. Ando, R., Hihara, T., Banno, Y., Nagata, M., and Corp, N.E.C., "Detailed Mechanism of S Poisoning and De-Sulfation Treatment of Cu-SCR Catalyst," *SAE Tech. Pap.* No. 2017-0, 2017, doi:10.4271/2017-01-0944.Copyright.

132. Lewander, M., Ekholm, K., Johansson, B., Tunestål, P., Milovanovic, N., Keeler, N., Harcombe, T., and Bergstrand, P., “Investigation of the Combustion Characteristics with Focus on Partially Premixed Combustion in a Heavy Duty Engine,” *SAE Int. J. Fuels Lubr.* 1(1):1063–1074, 2008, doi:10.4271/2008-01-1658.
133. Lewander, M., Johansson, B., Keeler, N., Tullis, S., and Milovanovic, N., “Evaluation of the Operating Range of Partially Premixed Combustion in a Multi Cylinder Heavy Duty Engine with Extensive EGR Magnus Lewander,” *SAE Tech. Pap.* (2009-01-1127), 2009, doi:10.4271/2009-01-1127.
134. Doosje, E., Willems, F., Baert, R., and Dijk, M. Van, “Experimental Study into a Hybrid PCCI / CI Concept for Next-Generation Heavy-Duty Diesel Engines,” *SAE Tech. Pap. 2012-01-1114* (x), 2012, doi:10.4271/2012-01-1114.
135. Asad, U., Zheng, M., Ting, D.S.-K., and Tjong, J., “Implementation Challenges and Solutions for Homogeneous Charge Compression Ignition Combustion in Diesel Engines,” *J. Eng. Gas Turbines Power* 137(October 2015):1–10, 2015, doi:10.1115/1.4030091.
136. M, M.P. and Krishnasamy, A., “A Comparison of Different Low Temperature Combustion Strategies in a Small Single Cylinder Diesel Engine under Low Load Conditions,” 2018, doi:10.4271/2017-01-2363.Copyright.
137. Hardy, W.L. and Reitz, R.D., “A Study of the Effects of High EGR , High Equivalence Ratio , and Mixing Time on Emissions Levels in a Heavy-Duty Diesel Engine for PCCI Combustion,” *Engineering* 2006(724):2006-01-0026, 2006, doi:10.4271/2006-01-0026.
138. Lianhao Yin, Gabriel Ingesson, Sam Shamun, Per Tunestål, Rolf Johansson, and Bengt Johansson, “Sensitivity Analysis of Partially Premixed Combustion (PPC) for Control Purposes,” *SAE Techcnical Pap.* (2015-1–884), 2015, doi:10.4271/2015-01-0884.
139. Minato, A., Tanaka, T., and Nishimura, T., “Investigation of Premixed Lean Diesel Combustion with Ultra High Pressure Injection Reprinted From : Compression Ignition Combustion Processes 2005,” *Engineering* 2005(724), 2005, doi:10.4271/2005-01-0914.
140. Kimura, S., Kimura, S., Aoki, O., Aoki, O., Ogawa, H., Ogawa, H., Muranaka, S., Muranaka, S., Enomoto, Y., and Enomoto, Y., “New combustion concept for ultra-clean and high-efficiency small DI diesel engines,” *SAE Pap. 1999-01-3681* 3pp(724):01-3681, 1999, doi:10.4271/1999-01-3681.
141. Hasegawa, R. and Yanagihara, H., “HCCI Combustion in DI Diesel Engine,” 2003, doi:10.4271/2003-01-0745.
142. Kitabatake, R., Shimazaki, N., and Nishimura, T., “Expansion of Premixed Compression Ignition Combustion Region by Supercharging Operation and Lower

Compression," (724):7–14, 2013.

143. Beatrice, C. and Guido, C., "Benefits and drawbacks of compression ratio reduction in PCCI combustion application in an advanced LD diesel engine Future Targets and Technology Pathways for PC Diesel Engines," *Source* 2(August):4–7, 2008, doi:10.4271/2009-01-1447.
144. Nevin, R.M., Sun, Y., D, M. a G., and Reitz, R.D., "PCCI Investigation Using Variable Intake Valve Closing in a Heavy Duty Diesel Engine," *SAE Tech. Pap.* 2007(724):776-0790, 2011, doi:10.4271/2007-01-0903.
145. Jia, M., Xie, M., Wang, T., and Peng, Z., "The effect of injection timing and intake valve close timing on performance and emissions of diesel PCCI engine with a full engine cycle CFD simulation," *Appl. Energy* 88(9):2967–2975, 2011, doi:10.1016/j.apenergy.2011.03.024.
146. Jia, M., Li, Y., Xie, M., Wang, T., Wang, H., and Reitz, R.D., "The Potential of High-load Extension by Using Late Intake Valve Closing for a Diesel Premixed Charge Compression Ignition (PCCI) Engine," *Phys. Procedia* 66(x):33–36, 2015, doi:10.1016/j.egypro.2015.02.018.
147. Jia, M., Li, Y., Xie, M., and Wang, T., "Numerical evaluation of the potential of late intake valve closing strategy for diesel PCCI (premixed charge compression ignition) engine in a wide speed and load range," *Energy* 51(x):203–215, 2013, doi:10.1016/j.energy.2012.12.041.
148. Kulkarni, A.M., Stricker, K.C., Blum, A., and Shaver, G.M., "PCCI Control Authority of a Modern Diesel Engine Outfitted With Flexible Intake Valve Actuation," *J. Dyn. Syst. Meas. Control* 132(5):051009, 2010, doi:10.1115/1.4002106.
149. J. Atkinson, "Gas Engine," USA Patent 336505, 1886.
150. J. Atkinson, "Gas Engine," USA Patent 367496, 1887.
151. R. Miller, "High-Pressure Supercharging System," USA Patent 2670595, 1954.
152. R. Miller, "High Expansion, Spark Ignited, Gas Burning, Internal Combustion Engines," USA Patent 2773490, 1956.
153. Miller, R., "Supercharged Engine," US Patent 2817322 A, 1957.
154. R. Miller, "Supercharge and internally cooling for high output," *ASME Trans.* 69:453–464, 1947.
155. https://en.m.wikipedia.org/wiki/Miller_cycle.
156. Zhao, H., "Advanced Direct Injection Combustion Engine Technologies and Development - Volume 1: Gasoline and Gas Engines," ISBN 9781845697327, 2010, doi:10.1533/9781845697457.
157. Cornell, S.O., Leman, S.A., "Engine valve actuation system (Caterpillar)," US Patent 7,004,122, 2006.
158. Boretti, A. and Scalzo, J., "Exploring the advantages of atkinson effects in variable

compression ratio turbo GDI engines," *SAE 2011 World Congr. Exhib.*, 2011, doi:10.4271/2011-01-0367.

159. Benajes, J., Molina, S., Novella, R., and Belarte, E., "Evaluation of massive exhaust gas recirculation and Miller cycle strategies for mixing-controlled low temperature combustion in a heavy duty diesel engine," *Energy* 71:355–366, 2014, doi:10.1016/j.energy.2014.04.083.
160. Wan, Y. and Du, A., "Reducing part load pumping loss and improving thermal efficiency through high compression ratio over-expanded cycle," *SAE Tech. Pap.* 2013-01-1744, 2013, doi:10.4271/2013-01-1744.
161. Zhao, J., "Research and application of over-expansion cycle (Atkinson and Miller) engines ??? A review," *Appl. Energy* 185:300–319, 2017, doi:10.1016/j.apenergy.2016.10.063.
162. Neher, D., Scholl, F., Deinert, M., Kettner, M., Schwarz, D., Klaissle, M., and Olavarría, B.G., "Miller / Atkinson Valve Timing as Full Load Concept for a Naturally Aspirated Cogeneration Engine," 2016.
163. Li, T., Zheng, B., and Yin, T., "Fuel conversion efficiency improvements in a highly boosted spark-ignition engine with ultra-expansion cycle," *Energy Convers. Manag.* 103:448–458, 2015, doi:10.1016/j.enconman.2015.06.078.
164. Kovács, D. and Eilts, P., "Potentials of the Miller Cycle on HD Diesel Engines Regarding Performance Increase and Reduction of Emissions," *SAE Tech. Pap.*, 2015, doi:10.4271/2015-24-2440.
165. Codan, E. and Vlaskos, I., "Turbocharging medium speed diesel engines with extreme Miller timing," *Proc. 9th Turbocharging Conf. Dresden, Ger. Sept.* 23–24, 2004.
166. Honda Worldwide | Technology Picture Book | EXlink, http://world.honda.com/powerproducts-technology/exlink/, Sep. 2017.
167. I. Hirose, H. Kudo, T. Kihara, M. Yamakawa, and M.H., "MAZDA SKYACTIV-G 2.0L Gasoline Engine," 1st Aachen Colloquium China 2011, 2011.
168. Goto, T., Hatamura, K., Takizawa, S., Hayama, N., Abe, H., and Kanesaka, H., "Development of V6 Miller Cycle Gasoline Engine," (41 2), 1994, doi:10.4271/940198.
169. Fukuzawa, Y., Shimoda, H., and Kakuhama, Y., "Development of high efficiency Miller cycle gas engine," *Tech. Rev.* 38(3):146–150, 2001.
170. Doug Woodyard, "Pounder's Marine Diesel Engines and Gas Turbines," 9th Editio, Butterworth-Heinemann, 2009.
171. https://www.dieselnet.com/tech/engine_miller-cycle.php.
172. He, X., Durrett, R.P., and Sun, Z., "Late intake valve closing as an emissions control strategy at Tier 2 Bin 5 engine-out NOx level," *SAE Tech. Pap.* 01(0637):2008-01–

0637, 2008, doi:10.4271/2008-01-0637.

173. J. BENAJES , S. MOLINA, R.N. and M.R., “IMPROVING POLLUTANT EMISSIONS IN DIESEL ENGINES FOR HEAVY-DUTY TRANSPORTATION USING RETARDED INTAKE VALVE CLOSING STRATEGIES,” *Int. J. …* 13(2):293–300, 2012, doi:10.1007/s12239.
174. Bruce Morey, “IAV brings variable valvetrains to heavy duty,” *SAE Int. United States*, 2017.
175. Molina, S., García, A., Monsalve-Serrano, J., and Estepa, D., “Miller cycle for improved efficiency, load range and emissions in a heavy-duty engine running under reactivity controlled compression ignition combustion,” *Appl. Therm. Eng.* 136(December 2017):161–168, 2018, doi:10.1016/j.applthermaleng.2018.02.106.
176. Osborne, R., Downes, T., O’Brien, S., Pendlebury, K., and Christie, M., “A Miller Cycle Engine without Compromise - The Magma Concept,” *SAE Int. J. Engines* 10(3):2017-01–0642, 2017, doi:10.4271/2017-01-0642.
177. He, Y., Liu, J., Zhu, B., and Sun, D., “Development of a Miller cycle engine with single-stage boosting and cooled external exhaust gas recirculation,” *Proc. Inst. Mech. Eng. Part D J. Automob. Eng.*, 2016, doi:10.1177/0954407016662567.
178. Al-Hasan, N., Beer, J., Ehrhard, J., Lorenz, T., and Stump, L., “Charging Technologies for CO_2 Optimization by Millerization,” 2015, doi:10.4271/2015-01-1250.
179. Kudo, M., Shinagawa, T., Matsubara, W., Hikichi, K., and Spray, F., “The New Inline 4 Cylinder 1 . 2L Turbocharged Direct Injection Gasoline Engine,” (May):20155293, 2015, doi:10.4271/2015-01-1268.Copyright.
180. Taylor, J., Fraser, N., Dingelstadt, R., and Hoffmann, H., “Benefits of Late Inlet Valve Timing Strategies Afforded Through the Use of Intake Cam In Cam Applied to a Gasoline Turbocharged Downsized Engine,” 2011, doi:10.4271/2011-01-0360.
181. Rinaldini, C.A., Mattarelli, E., and Golovitchev, V.I., “Potential of the Miller cycle on a HSDI diesel automotive engine,” *Appl. Energy* 112(x):102–119, 2013, doi:10.1016/j.apenergy.2013.05.056.
182. Wang, Y., Zeng, S., Huang, J., He, Y., Huang, X., Lin, L., and Li, S., “Experimental Investigation of Applying Miller Cycle to Reduce NO_x Emission From Diesel Engine,” *Proc. Inst. Mech. Eng. Part A J. Power Energy* 219(8):631–638, 2006, doi:10.1243/095765005X31289.
183. Wu, B., Zhan, Q., Yu, X., Lv, G., Nie, X., and Liu, S., “Effects of Miller cycle and variable geometry turbocharger on combustion and emissions in steady and transient cold process,” *Appl. Therm. Eng.* 118(x):621–629, 2017, doi:10.1016/j.applthermaleng.2017.02.074.
184. Gonca, G., Sahin, B., Parlak, A., Ust, Y., Ayhan, V., Cesur, İ., and Boru, B.,

"Theoretical and experimental investigation of the Miller cycle diesel engine in terms of performance and emission parameters," *Appl. Energy* 138:11–20, 2015, doi:10.1016/j.apenergy.2014.10.043.

185. Gonca, G., Sahin, B., Parlak, A., Ayhan, V., Cesur, I., and Koksal, S., "Application of the Miller cycle and turbo charging into a diesel engine to improve performance and decrease NO emissions," *Energy* 93:795–800, 2015, doi:10.1016/j.energy.2015.08.032.
186. Verschaeren, R., Schaepdryver, W., Serruys, T., Bastiaen, M., Vervaeke, L., and Verhelst, S., "Experimental study of NOx reduction on a medium speed heavy duty diesel engine by the application of EGR (exhaust gas recirculation) and Miller timing," *Energy* 76(x):614–621, 2014, doi:10.1016/j.energy.2014.08.059.
187. Benajes, J., Serrano, J.R., Molina, S., and Novella, R., "Potential of Atkinson cycle combined with EGR for pollutant control in a HD diesel engine," *Energy Convers. Manag.* 50(1):174–183, 2009, doi:10.1016/j.enconman.2008.08.034.
188. Ratzberger, R., Kraxner, T., Pramhas, J., Hadl, K., Eichlseder, H., and Buergler, L., "Evaluation of Valve Train Variability in Diesel Engines," *SAE Int. J. Engines* 8(5):2015-24–2532, 2015, doi:10.4271/2015-24-2532.
189. Garg, A., Magee, M., Ding, C., Roberts, L., Shaver, G., Koeberlein, E., Shute, R., Koeberlein, D., McCarthy, J., and Nielsen, D., "Fuel-efficient exhaust thermal management using cylinder throttling via intake valve closing timing modulation," *Proc. Inst. Mech. Eng. Part D J. Automob. Eng.* 230(4):470–478, 2016, doi:10.1177/0954407015586896.
190. Ojeda, W. De, "Effect of variable valve timing on diesel combustion characteristics," *SAE Pap.*, 2010, doi:2010-01-1124.
191. Roberts, L., Magee, M., Shaver, G., Garg, A., McCarthy, J., Koeberlein, E., Holloway, E., Shute, R., Koeberlein, D., and Nielsen, D., "Modeling the impact of early exhaust valve opening on exhaust aftertreatment thermal management and efficiency for compression ignition engines," *Int. J. Engine Res.* 16(6):773–794, 2015, doi:10.1177/1468087414551616.
192. Modiyani, R., Kocher, L., Alstine, D.G. Van, Koeberlein, E., Stricker, K., Meckl, P., and Shaver, G., "Effect of intake valve closure modulation on effective compression ratio and gas exchange in turbocharged multi-cylinder engines utilizing EGR," *Int. J. Engine Res.* 12(6):617–631, 2011, doi:10.1177/1468087411415180.
193. Scania, "Six new engines added to Scania's Euro 6 Range," https://www.scania.com/group/en/wp-%0Acontent/uploads/sites/2/2017/06/p17067en-six-new-engines-added-to- scanias-euro-6-range, 2017.
194. Kim, J. and Bae, C., "An investigation on the effects of late intake valve closing and exhaust gas recirculation in a single-cylinder research diesel engine in the low-load

condition," *Proc. Inst. Mech. Eng. Part D J. Automob. Eng.* 230(6):771–787, 2015, doi:10.1177/0954407015595149.

195. Schwoerer, J., Kumar, K., Ruggiero, B., and Swanbon, B., "Lost-Motion VVA Systems for Enabling Next Generation Diesel Engine Efficiency and After-Treatment Optimization," *SAE Tech. Pap.* 01(1189), 2010, doi:10.4271/2010-01-1189.
196. Zhang, Y., "Experimental investigation of CAI combustion in a two-stroke poppet valve DI engine," (October), 2014.
197. Zhao H; Ladommatos N., "Engine combustion instrumentation and diagnostics," SAE International, 2001.
198. Calculation of Uncertainty of Measurement for Diesel Engine ESC Test Emissions, 2013.
199. AVL., "AVL 415SE Smoke Meter," *Prod. Guid. Graz, Austria;*, 2013.
200. https://www.dieselnet.com/standards/cycles/esc.php.
201. Pedrozo, V.B., May, I., and Zhao, H., "Exploring the mid-load potential of ethanol-diesel dual-fuel combustion with and without EGR," *Appl. Energy* 193:263–275, 2017, doi:10.1016/j.apenergy.2017.02.043.
202. Hanson, R., Ickes, A., and Wallner, T., "Comparison of RCCI Operation with and without EGR over the Full Operating Map of a Heavy-Duty Diesel Engine," *SAE Tech. Pap.* (x), 2016, doi:10.4271/2016-01-0794.
203. Johnson, T. V, "Diesel Emissions in Review," *SAE Int. J. Engines* 4(1):143–157, 2011, doi:10.4271/2011-01-0304.
204. Ickes, A., Hanson, R., and Wallner, T., "Impact of Effective Compression Ratio on Gasoline- Diesel Dual-Fuel Combustion in a Heavy-Duty Engine Using Variable Valve Actuation," 2015.
205. Modiyani, R., Kocher, L., Alstine, D.G. Van, Koeberlein, E., Stricker, K., Meckl, P., and Shaver, G., "Effect of intake valve closure modulation on effective compression ratio and gas exchange in turbocharged multi-cylinder engines utilizing EGR," *Int. J. Engine Res.* 12(6):617–631, 2011, doi:10.1177/1468087411415180.
206. Stricker, K., Kocher, L., Koeberlein, E., Alstine, D. Van, and Shaver, G.M., "Estimation of effective compression ratio for engines utilizing flexible intake valve actuation," *Proc. Inst. Mech. Eng. Part D J. Automob. Eng.* 226(8):1001–1015, 2012, doi:10.1177/0954407012438024.
207. He, X., Durrett, R.P., and Sun, Z., "Late intake valve closing as an emissions control strategy at Tier 2 Bin 5 engine-out NOx level," *SAE Tech. Pap.* 01(0637):2008-01–0637, 2008, doi:10.4271/2008-01-0637.
208. Lambert, C., Hammerle, R., and Mcgill, R., "Technical Advantages of Urea SCR for Light-Duty and Heavy-Duty Diesel Vehicle Applications Reprinted From : Diesel

Exhaust Emission Control," *SAE Tech. Pap.* (724), 2004, doi:10.4271/2004-01-1292.

209. Guan, W., Pedrozo, V., Zhao, H., Ban, Z., and Lin, T., "Investigation of EGR and Miller Cycle for NOx Emissions and Exhaust Temperature Control of a Heavy-Duty Diesel Engine," *SAE Tech. Pap.*, 2017, doi:10.4271/2017-01-2227.
210. Bression, G., Pacaud, P., Soleri, D., Cessou, J., Doradoux, L., and Guerrassi, N., "Comparative study in LTC combustion between a short HP EGR loop without cooler and a Variable Lift and Duration system," 2005.
211. Murata, Y., Kusaka, J., Daisho, Y., Kawano, D., Suzuki, H., Ishii, H., and Goto, Y., "Miller-PCCI Combustion in an HSDI Diesel Engine with VVT," *SAE Int. J. Engines* 1(1):444–456, 2008, doi:10.4271/2008-01-0644.
212. Sjöblom, J., "Combined Effects of Late IVC and EGR on Low-load Diesel Combustion," *SAE Tech. Pap.* 01(2878), 2014, doi:10.4271/2014-01-2878.
213. Bobba, M., Musculus, M., and Neel, W., "Effect of Post Injections on In-Cylinder and Exhaust Soot for Low-Temperature Combustion in a Heavy- Duty Diesel Engine," *SAE Int J Engines* 3(1):496–516, 2010, doi:10.4271/2010-01-0612.
214. O'Connor, J. and Musculus, M.P.B., "Post Injections for Soot Reduction in Diesel Engines: A Review of Current Understanding," *SAE Int. J. Engines* 6(1):400–421, 2013, doi:10.4271/2013-01-0917.
215. Guan, W., Pedrozo, V., Zhao, H., Ban, Z., and Lin, T., "Exploring the NOx Reduction Potential of Miller Cycle and EGR on a HD Diesel Engine Operating at Full Load," *SAE Tech. Pap.* 2018–April:1–12, 2018, doi:10.4271/2018-01-0243.
216. Gehrke, S., Kovács, D., Eilts, P., Rempel, A., and Eckert, P., "Investigation of VVA-Based Exhaust Management Strategies by Means of a HD Single Cylinder Research Engine and Rapid Prototyping Systems," *SAE Tech. Pap.* 01(0587):47–61, 2013, doi:10.4271/2013-01-0587.
217. Chi, J.N., "Control Challenges for Optimal NOx Conversion Efficiency from SCR Aftertreatment Systems," *SAE Tech. Pap.*, 2009, doi:10.4271/2009-01-0905.

Appendix A – Test cell measurement devices

Variable	Device	Manufacturer	Measurement range	Linearity/Accuracy
Speed	AG 150 Dynamometer	Froude Hofmann	0-8000 rpm	± 1 rpm
Torque	AG 150 Dynamometer	Froude Hofmann	0-500 Nm	± 0.25% of FS
Diesel flow rate (supply)	Proline promass 83A DN01	Endress+Hauser	0-20 kg/h	± 0.10% of reading
Diesel flow rate (return)	Proline promass 83A DN02	Endress+Hauser	0-100 kg/h	± 0.10% of reading
Intake air mass flow rate	Proline t-mass 65F	Endress+Hauser	0-910 kg/h	± 1.5% of reading
In-cylinder pressure	Piezoelectric pressure sensor Type 6125C	Kistler	0-300 bar	≤ ± 0.4% of FS
Intake and exhaust pressures	Piezoresistive pressure sensor Type 4049A	Kistler	0-10 bar	≤ ± 0.5% of FS
Oil pressure	Pressure transducer UNIK 5000	GE	0-10 bar	< ± 0.2% FS
Temperature	Thermocouple K Type	RS	233-1473K	≤ ± 2.5 K
Intake valve lift	S-DVRT-24 Displacement Sensor	LORD MicroStrain	0-24 mm	± 1.0% of reading using straight line
Smoke number	415SE	AVL	0-10 FSN	-
Fuel injector current signal	Current Probe PR30	LEM	0-20A	± 2 mA

Appendix B – Camshaft design

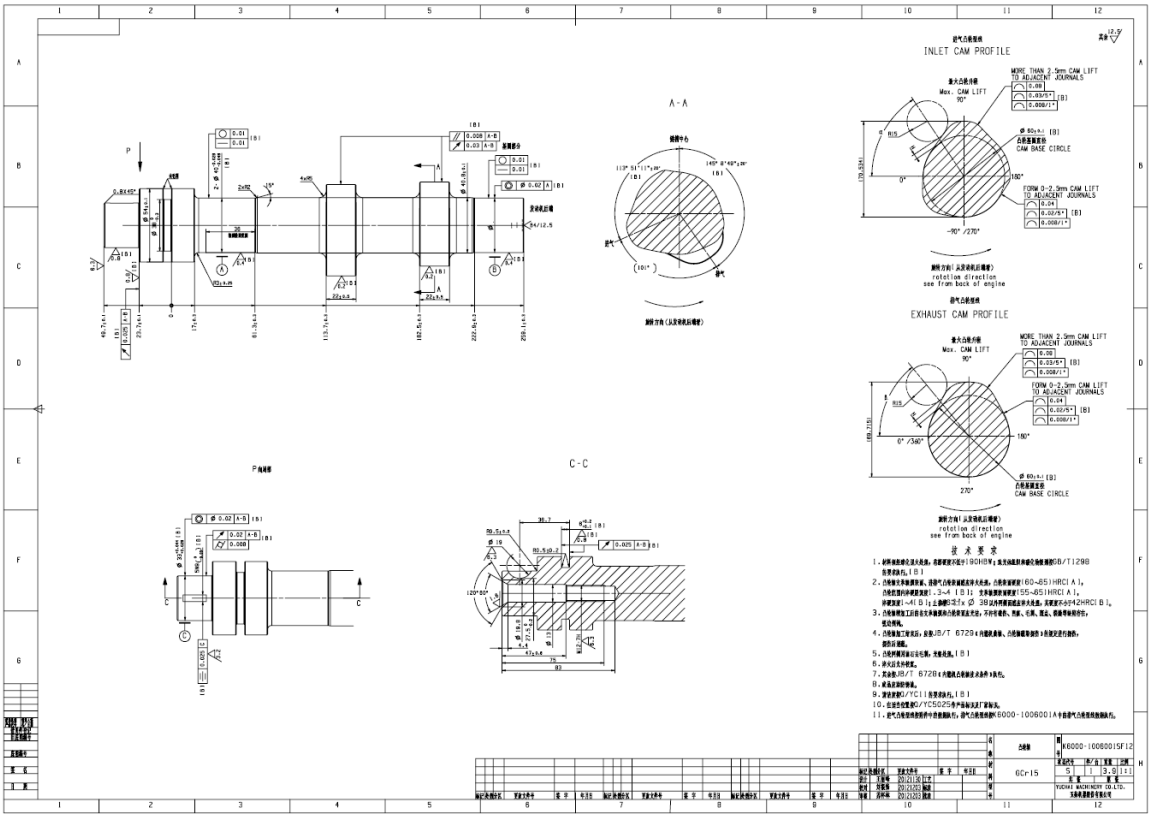

Appendix C – Fuel mass flow meter calibration

Endress+Hauser
People for Process Automation

Flow Calibration with Adjustment

10528369-2693828

40637498 Purchase order number	FCP-10 Calibration rig
GB-3004776180-10 / Endress+Hauser Flowtec AG Order N°/Manufacturer	4 kg/hr (≙ 100%) Calibrated full scale
83A01-15J5/0 Order code	Service interface Calibrated output
PROMASS 83 A DN01 / 1/24" Transmitter/Sensor	0.66174 Calibration factor
EC0F2102000 Serial N°	-14 Zero point
– Tag N°	22.1 °C Water temperature

Flow [%]	Flow [kg/hr]	Duration [s]	m target [kg]	m meas. [kg]	Δ o.r.* [%]	Outp.** [mA]
24.9	0.997	30.0	0.00832	0.00832	0.00	7.99
24.9	0.997	30.1	0.00833	0.00833	0.00	7.99
99.2	3.97	30.1	0.03313	0.03313	0.00	19.87
99.2	3.97	30.1	0.03313	0.03313	0.00	19.87
-	-	-	-	-	-	-
-	-	-	-	-	-	-
-	-	-	-	-	-	-
-	-	-	-	-	-	-
-	-	-	-	-	-	-
-	-	-	-	-	-	-

*o.r.: of rate
**Calculated value (4 - 20 mA)

Measured error % o.r.

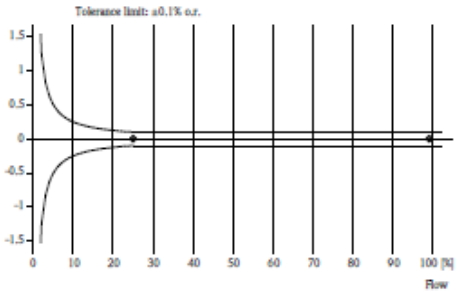

For detailed data concerning output specifications of the unit under test, see Technical Information (TI), chapter Performance characteristics.

Traceability to the national standard for all test instruments used for the calibration is guaranteed.

Endress+Hauser Flowtec operates ISO/IEC 17025 accredited calibration facilities in Reinach (CH), Cernay (FR), Greenwood (USA), Aurangabad (IN) and Suzhou (CN).

27.12.2011
Date of calibration

Endress+Hauser Flowtec AG
Kägenstrasse 7 / Rue de l'Europe 35
CH-4153 Reinach / F-68700 Cernay

C. Altermatt
Operator

Certified acc. to
ISO 9001

Appendix D – Diesel fuel specification

PHILLIPS 66 LIMITED / JET :- UK MARKETING SPECIFICATION

SULPHUR FREE (MAXIMUM 10 PPM) GAS OIL TO BS 2869:2010-PART 1: CLASS A2

PROPERTY & UNITS	LIMIT		TEST METHOD Note (1)
Appearance		Free from visible water and sediment	Visual
Colour		Red	Visual
Odour		Merchantable	
Density @ 15C (kg/m3)	Typical Range	820.0 - 875.0	BS EN ISO 3675 / 12185
Cold Filter Plugging Point			BS EN 116
Winter C (Note 2)	Max	-12	
Summer C (Note 2)	Max	-4	
Cloud Point			ASTM D2500 / IP219
Winter C (Note 2)	Max	-2	
Summer C (Note 2)	Max	+3	
Flash Point (PMCC) C	Min	56	BS EN ISO 2719
Cetane Number / DCN	Min	45.0 (Note 5)	BS EN ISO 5165 / BS 2000-498
or Cetane Index	Min	45.0 (Note 5)	BS EN ISO 4264
Kinematic viscosity mm2/s @ 40C	Min - max	2.00 - 5.00	BS EN ISO 3104
Sulphur content (mg/kg)			
At point of manufacture	Max	10 (Note 8)	BS EN ISO 20846 / 20884
At point of distribution to end user	Max	20 (Note 8)	
Copper Corrosion (3 Hr @ 50C)	Class	1	BS EN ISO 2160
Carbon Residue (micro) :-			
Residue wt% on 10% Bottoms	Max	0.30	BS EN ISO 10370
Ash content % (m/m)	Max	0.01	BS EN ISO 6245
Particulate content (mg/kg)	Max	24	IP 415
Water content (mg/kg)	Max	200	BS EN ISO 12937
Distillation C			BS EN ISO 3405
% Vol Rec @ 350C	Min	85	
% Vol Rec @ 250C	Max	65	
50% Vol Recovered (Note 3)	Range	240 - 340	
Strong Acid Number (mgKOH/g)		Zero	BS ISO 6618
Lubricity (wear scar dia, micron)	Max	460	BS 2000 - 450
Oxidation stability			
0.0% - 7.0% FAME g/m3 (Note 6)	Max	25	BS 2000-388
2.0% - 7.0% FAME h	Min	20	BS EN 15751
FAME content (%v/v) (Note7)	Max	7.0	BS EN 14078

Notes.

1) Latest Test Methods or technical equivalent used

2) Unless otherwise advised the following seasonal dates apply ex refinery or import terminal:-
Summer : 16 March - 15 October inc
Winter : 16 October - 15 March inc
Winter : 01 November - 15 March inc for delivery from terminals

3) 50 % evaporated is an HMRC requirement.

4) Product will be marked with HMR&C statutory marker

5) May contain an ignition improver in which case
(i) the carbon residue test is not valid and
(ii) the cetane number minimum will apply.

6) This test applies to all fuels, additional Rancimat only applies to those fuels containing > 2.00% FAME

7) FAME must meet BS EN 14214

8) 10/20 ppm sulphur limits applicable from 1 January 2011

THIS SPECIFICATION IS ACCURATE AT THE DATE OF ISSUE, AND SUPERSEDES ALL PREVIOUS ISSUES.

PQ Issue 6 : July 2012